Rheological investigation of manufacturability and injectability of highly concentrated monoclonal antibody formulations

Inauguraldissertation

zur

Erlangung der Würde eines Doktors der Philosophie
vorgelegt der
Philosophisch-Naturwissenschaftlichen Fakultät
der Universität Basel

von

Andrea Martina Allmendinger
aus Ludwigsburg, Deutschland

Basel, 2014

Genehmigt von der Philosophisch-Naturwissenschaftlichen Fakultät

auf Antrag von:

– Prof. Dr. Jörg Huwyler

– Prof. Dr. Wolfgang Friess

Basel, den 14. Oktober 2014

Prof. Dr. Jörg Schibler

Dekan

Gutta cavat lapidem.

Steter Tropfen höhlt den Stein.

Ovid.
(43 v.Chr. – 17 n. Chr.)

Für meine Eltern

Danksagung (Acknowledgment)

Summary

Highly concentrated protein therapeutics offer a convenient way for subcutaneous (sc) drug administration by the patient him-/herself or a healthcare professional. As the therapy e.g. with monoclonal antibodies requires quite high doses in the range of mg per kg body weight, the development of highly concentrated protein formulations is needed due to the limited injection volume, generally considered being $1 - 2\,\mathrm{mL}$ for sc administration. The development of highly concentrated formulations exceeding $50 - 100\,\mathrm{mg/mL}$ poses several challenges including chemical and physical stability (e.g. aggregation) as well as solution viscosity. Thereby, the increase in viscosity observed with higher protein concentration may cause severe limitations during product development as well as processing and drug administration. These limitations are defined by the flow rate/injection rate depending on the applied pressure which is needed during manufacture (fill-finish), in particular during filtration, and drug administration.

The focus of this work was to investigate the rheological behavior of protein solutions at high protein concentrations. The main objective was to obtain a profound understanding of two critical, hydrodynamic processes for highly concentrated protein solutions, which were drug administration and filtration, and to elucidate the role of viscosity with regard to potential limitations.

The current work provides a detailed overview on product characteristics of ten commercially available, highly concentrated protein therapeutics (Chapter 1). This technical overview summarizes formulation properties like viscosity and number of visible and sub-visible particles, physico-chemical properties like pH and osmolality as well as injection device characteristics, such as device dimensions. The analysis of marketed products revealed significant differences between the products. The current benchmark for maximum protein concentration and of viscosity was identified as a liquid formulation at a protein concentration of $200\,\mathrm{mg/mL}$ with a dynamic viscosity of 102 mPas (20°C). This product, which is provided in a pre-filled syringe, also exhibits the largest inner needle diameter of 25 G compared to other commercial products using 27 G needle for the injection device.

In the following (Chapter 2), advantages and limitations of different methods for viscosity determination of protein formulations are discussed. Moreover, a high-throughput method to measure viscosity was established. This method uses a capillary electrophoresis instrumentation without operation of the electrical field. The established method has the advantage of being automated offering the possibility for high-throughput by use of low sample amounts in the microliter range at the same time. (Allmendinger *et al.*, J Pharm Biomed Anal, 99 (2014) 51-58)

Based on these studies, the present work investigated and characterized the subcutaneous drug administration process of highly concentrated protein formulations providing quantitative *in vitro* (Chapter 3) and *in vivo* data (Göttingen minipigs) of injection forces (Chapter 4).

Chapter 3 describes in detail the establishment of an *in silico* model to predict injection forces depending on syringe and needle dimensions, solution viscosity, and injection rate. Importantly, this model accounts for shear thinning behavior (non-Newtonian flow behavior) of highly concentrated protein solutions, which leads to lower effective injection forces than expected from current literature models. (Allmendinger *et al.*, Eu J Pharm Biopharm, 87 (2014) 318-328)

To address the *in vivo* situation, Chapter 4 investigates and quantifies the contribution of the subcutaneous tissue backpressure and specifically reports the additional influence of body temperature on injection forces, which was found to compensate the tissue backpressure to some parts. Overall, an extended model, which addresses the injection force as a function of viscosity, volumetric flow/injection

rate, needle/device dimensions, shear-thinning behavior, sc backpressure, and body temperature, was developed to predict injection forces representative for the *in vivo* situation. This knowledge is of key importance for the development of combination products (e.g. autoinjectors or pre-filled syringes) as a detailed understanding of injection forces depending on various parameters is required. It may be also supportive for the definition of limits during the evaluation, planning, and design phase during the development of injection devices. (Allmendinger *et al.*, submitted to J Control Release, 2014)

Besides drug administration, filtration was investigated as another critical hydrodynamic process for highly concentrated protein formulations, depending on formulation composition and filter material (Chapter 5). For both processes, filtration and drug administration, shear thinning behavior was found for some of the products depending on viscosity and protein concentration, shear rate, and formulation composition.

Within the present work it was shown, that the two investigated hydrodynamic processes, filtration and drug administration by injection, are two highly complex processes which are influenced by various factors. Thereby, the final limiting parameter for the injection process is given by the user capability of the patient population. However, the needle inner diameter was shown to have major influence on injection forces. It is related to injection forces by the power of four compared to other parameters like viscosity, injection rate, and contribution of sc backpressure being directly proportional. For the filtration process, the final limiting parameter may be discussed controversially. The study showed that the filtration pressure is mainly defined by the pore size distribution of the filter material, which was furthermore found to trigger the rheological behavior at high protein concentrations dependent on filtration rate. Moreover, literature data reported that the influence of filtration pressure on product quality might not be the limiting parameter during filtration. For the formulations previously tested, the shear stress exposure during manufacture was not considered important for final product quality, however only tested up to a protein concentration of 100 mg/mL. More important causes of aggregation were suggested to be the presence of air-bubbles, adsorption to solid surfaces, or contamination by particulates. Nevertheless, the stability of formulations showing pronounced shear-thinning behavior at high shear rates, which is most likely only the case for higher protein concentrations than previously tested, needs further experiments and has to be evaluated on a case-by-case basis dependent on product and process characteristics. (Allmendinger *et al.*, submitted to J Pharm Sci, 2014)

With respect to viscosity, the current work has demonstrated for both processes, drug administration and filtration, that the potential limitation defined by the proportional increase in pressure based on Newtonian flow behavior was overestimated due to the presence of shear-thinning behavior which was shown for highly concentrated protein formulations.

Zusammenfassung

Subkutane Injektionen stellen für den Patienten einen angenehmeren Weg der parenteralen Medikamentenverabreichung dar, da sie dem Patienten die Möglichkeit geben, das Medikament selbst zu injizieren oder durch medizinisches Fachpersonal zu Hause verabreichen lassen zu können. Da die Therapie mit beispielsweise monoklonalen Antikörpern in der Regel relativ hohe therapeutische Dosen im Bereich von mehreren Milligramm pro Kilogramm Körpergewicht benötigt und das Injektionsvolumen für subkutane Verabreichung oftmals auf ungefähr $1-2$ mL begrenzt wird, besteht die Notwendigkeit hochkonzentrierte Proteinformulierungen zu entwickeln. Die Entwicklung von hochkonzentrierten Formulierungen die eine Proteinkonzentration von $50-100$ mg/mL überschreiten führt dabei zu Herausforderungen im Hinblick auf chemische und physikalische Stabilität, wie beispielsweise Aggregation, sowie erhöhte Viskosität der Formulierung. Der Viskositätsanstieg, der mit höherer Proteinkonzentration beobachtet wird, kann dabei zu starken Limitationen während der Produktentwicklung, der Herstellung und der Injektion selbst führen. Diese Limitationen sind durch die begrenzte Flussrate/Injektionsrate definiert, die abhängig vom ausgeübten Druck ist, der während der Herstellung (Fertigabfüllung), vor allem während der Filtration, und während der Medikamentenverabreichung durch Injektion ausgeübt wird.

Der Fokus dieser Arbeit lag darauf, das rheologische Verhalten von Proteinlösungen bei hohen Proteinkonzentrationen zu untersuchen. Das Hauptziel war es ein tiefgehendes Verständnis sowohl des Injektionsprozesses/der Medikamentenverabreichung als auch der Filtration zu erlangen, und den Einfluss der Viskosiät in Bezug auf potentielle Grenzen/Limitationen aufzuzeigen.

Zu Anfang gibt die vorliegende Arbeit einen detaillierten Überblick über die Eigenschaften von zehn sich derzeit auf dem Markt befindenden konzentrierten Proteintherapeutika (Kapitel 1). Der technische Überblick beinhaltet die Charakterisierung von Formulierungseigenschaften wie z.B. Viskosität und Anzahl sichtbarer und subvisueller Partikel, physiko-chemische Eigenschaften, wie pH und Osmolalität, sowie die Charakterisierung von Eigenschaften des Injektionshilfsmittels. Die Charakterisierung der Marktprodukte zeigte signifikante Unterschiede zwischen den Produkten. Die höchste Proteinkonzentration und Viskosität wurde dabei für eine Flüssigformulierung mit 200 mg/mL und 102 mPas (20°C) bestimmt. Dieses Produkt, das als Fertigspritze auf dem Markt ist, hat unter anderem den grössten Nadelinnendurchmesser von 25 G im Vergleich zu anderen Marktprodukten, die eine 27 G Nadel für die Fertigspritzen verwenden.

Im darauffolgenden Kapitel werden die Vorteile und Grenzen verschiedenster Methoden, die zur Messung der Viskosität von Proteinformulierungen eingesetzt werden, diskutiert (Kapitel 2). Desweiteren wurde eine Hochdurchsatzmethode zur Bestimmung der Viskosität entwickelt. Dieser Ansatz verwendet zur Probenmessung ein Kapillarelektrophorese-Instrument, jedoch ohne das elektrische Feld zu nutzen, und hat den Vorteil einer automatisierten Methode. Damit bietet sie die Möglichkeit eines hohen Durchsatzes bei gleichzeitiger Verwendung kleiner Probenmengen im Bereich von einigen Mikrolitern. (Allmendinger *et al.*, J Pharm Biomed Anal, 99 (2014) 51-58)

Basierend auf diesen beiden Studien untersucht und charakterisiert die vorliegende Arbeit den Injektionsprozess von hochkonzentrierten Proteinformulierungen zur subkutanen Verabreichung. Dazu wurden quantitative Daten von Injektionskräften sowohl *in vitro* (Kapitel 3) als auch *in vivo* (Göttingen Minischwein) erhoben (Kapitel 4). Im Detail beschreibt Kapitel 3 die Etablierung eines *in silico* Models zur Vorhersage von Injektionskräften abhängig von Spritzen- und Nadelkonfiguration, Viskosität der Lösung und Injektionsrate. Besonders wichtig ist dabei, dass das Model für scherverdünnendes Fliessverhal-

ten (nicht Newton'sches Fliessverhalten) anwendbar ist. Es wurde gezeigt, dass hochkonzentrierte Proteinlösungen scherverdünnendes Fliessverhalten während des Injektionsprozesses/bei hohen Scherraten zeigen können, das zu niedrigeren Injektionskräften führt als von bisherigen Modellen in der Literatur vorhergesagt. (Allmendinger *et al.*, Eu J Pharm Biopharm, 87 (2014) 318-328)

Um die *in vivo* Situation abzudecken wird in Kapitel 4 der Beitrag des subkutanen Gewebegegendrucks untersucht und quantifiziert. Im Besonderen wurde der zusätzliche Einfluss der Körpertemperatur zu Injektionskräften aufgezeigt, der den Beitrag des Gewebegegendrucks zu Teilen aufhebt. Insgesamt konnte ein erweitertes Model zur Vorhersage von Injektionskräften entwickelt werden, das repräsentativ für die tatsächliche *in vivo* Situation im Tier ist. Das Model beschreibt die Injektionskraft als Funktion der Viskosität, des Volumenstroms/der Injektions-rate, der Nadel- und Device-Dimensionen, abhängig von scherverdünnendem Verhalten, dem subkutanen Gewebegegendruck, und der Körpertemperatur. Diese Daten sind von grundlegender Bedeutung für die Entwicklung von Kombinationsprodukten (z.B. Autoinjektoren oder Fertigspritzen), da diese ein grundlegendes Verständnis von Injektionskräften abhängig von verschiedenen Parametern benötigt. Gleichzeitig kann es für die Festlegung der Grenzen während der Evaluierungs-, Planungs- und Designphase während der Entwicklung der Kombinationsprodukte dienen. (Allmendinger *et al.*, eingereicht bei J Control Release, 2014)

Neben dem Injektionsprozess wurde die Filtration als weiterer kritischer hydrodynamischer Prozess für hochkonzentrierte Proteinformulierungen abhängig von Filtermaterial und Formulierungszusammensetzung untersucht (Kapitel 5). Bei beiden Prozessen, sowohl Filtration als auch während des Injektionsprozesses, wurde für einige Produkte scherverdünnendes Verhalten beobachtet, das abhängig von Viskosität und Proteinkonzentration, Scherrate und Formulierungszusammensetzung war. Innerhalb dieser Arbeit wurde gezeigt, dass die beiden untersuchten hydrodynamischen Prozesse der Filtration und Injektion zwei hochkomplexe Prozesse darstellen, die von verschiedensten Faktoren beeinflusst werden. Der eigentliche limitierende Faktor des Injektionsprozesses stellt dabei die Leistungsfähigkeit (Kraftaufwand) der Patientenpopulation dar. Desweiteren konnte gezeigt werden, dass der Innendurchmesser der Injektionsnadel den grössten Einfluss auf die Injektionskraft darstellt, da er mit der vierten Potenz eingeht im Vergleich zu anderen Parametern wie Viskosität, Injektionsrate und der Beitrag des Gewebegegendrucks, die direkt proportional zur Injektionskraft sind.

Für die Filtration kann der limitierende Faktor kontrovers diskutiert werden. Innerhalb dieser Arbeit wurde gezeigt, dass der Filtrationsdruck vor allem durch die Verteilung der Porengrösse des Filtermaterials beeinflusst wird, die auch das rheologische Verhalten bei hohen Proteinkonzentrationen abhängig von der Filtrationsrate bestimmt. Dabei wurde in der Literatur berichtet, dass der Einfluss des Filtrationsdruckes auf die Produktqualität nicht der limitierende Faktor während der Filtration sein könnte, da für die getesteten Formulierungen der Scherstress während der Herstellung nicht bestimmend für die finale Produktqualität war. Wichtigere Ursachen für Aggregation während der Herstellung könnten Luftblasen, Adsorption an feste Oberflächen oder Partikelkontamination darstellen. Dabei wurde allerdings lediglich bis zu einer Proteinkonzentration von 100 mg/mL getestet. Deshalb benötigt es weitergehender Experimente um die Stabilität von Formulierungen mit scherverdünnendem Verhalten zu untersuchen, das in den meisten Fällen in der Regel bei höheren Proteinkonzentrationen auftreten wird, als bisher getestet. Die Produktstabilität muss von Fall zu Fall für jedes Produkt einzeln abhängig von Produktcharateristika und Prozess evaluiert werden. (Allmendinger *et al.*, eingereicht bei J Pharm Sci, 2014)

Mit Bezug auf die Viskosität konnte innerhalb dieser Arbeit für beide Prozesse, der Injektion und der Filtration, gezeigt werden, dass durch das scherverdünnende Verhalten, das für einige hochkonzentrierte Proteinformulierungen gezeigt werden konnte, die potentiellen Limitationen durch den proportionalen Anstieg des Druckes basierend auf Newtonschem Fliessverhalten, überschätzt wurden.

Table of Contents

Table of Abbreviations

AI	Autoinjector
ArgHCl	Arginine-hydrochloride
B	Bevel
CE	Capillary electrophoresis
DIN-EN-ISO	Deutsche Industrienorm, European Norm, International Standards Organization
CPT	Commercial product / protein therapeutic
DLS	Dynamic light scattering
EMA	European Medicines Agency
Eq.	Equation
FDA	Food and Drug administration
Fig.	Figure
FTU	Formazin turbidity units
G	Gauge
His/His-HCl	Histidine/histidine-hydrochloride
HMW	High molecular weight species
HS	Hard sphere
id	Intradermal
iCE	Isoelectric capillary electrophoresis
IEC	Ionic exchange chromatography
IgG	Immunglobulin G
im	Intramuscular
iv	Intravenous
L	Lyophilisate
LMW	Low molecular weight species
mAb	Monoclonal antibody
Mr	Relative molecular mass
Mw	Molecular weight
NaCit	Sodium citrate
NaCl	Sodium chloride
NaOH	Sodium hydroxide

PES	Polyethersulfone
PFS	Pre-filled syringe
Ph.Eur.	European Pharmacopeia
pI	Isoelectric point
PIL	Patient information leaflet
PPI	Protein-protein interaction
PS	Polysorbate
PVDF	Polyvinylidene difluoride
PTFE	Polyvinylidene tetrafluoride
QC	Quality control
RAB	Restricted access barrier
RNS	Rigid needle shield
Rp	Receptor
RSD	Residual sum of squares
RSS	Relative standard deviation
SANS	Small-angle neutron scattering
SAXS	Small-angle X-ray scattering
sc	Subcutanous
sd	Standard deviation
SEC / SE-HPLC	Size exclusion (high-performance liquid) chromatography
SPC	Summary of product characteristics
TNF	Tumor necrosis factor
TRIS	Tris(hydroxymethyl)-aminomethan/ Trometamol
USP	United States Pharmacopeia
UV	Ultraviolet spectra
vDW	Van-der-Waals forces
w/v%	Weight per volume percentage
w/w%	Weight per weight percentage

Introduction

Highly concentrated protein formulations

The biotechnological sector is one of the fastest growing segments within the pharmaceutical market with sales of over \$163 billion worldwide in 2012 and an expected growth of the total global market of 9% annually over the next several years. [1-4] Technical innovations like genetic engineering have led to a rapid development especially in the field of monoclonal antibody-based (mAb) products. [4, 5] They reached global sales of \$51.5 billion in 2012 and are expected to reach \$89.9 billion in 2017 constituting the largest biopharmaceutical product category besides vaccines from a sales point of view (Figure 1). [3]
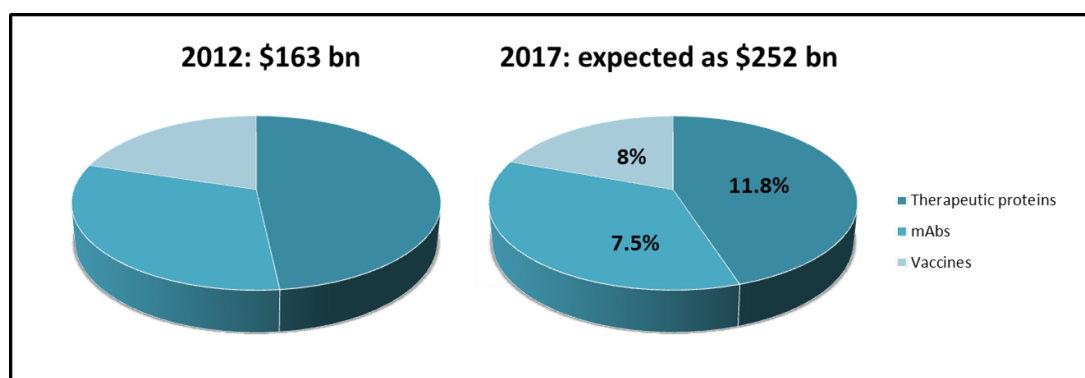
Figure 1: Global sales of biotechnological sector for 2012 and expected sales including annual growth rate until 2017 divided into therapeutic segments. [3]

Biotherapeutics cover a broad range of indications including cancer treatment as well as autoimmune and inflammatory diseases to name only the largest groups. [4] In most cases, patients receive their treatment at the hospital where the drug is administered intravenously usually over several hours. A more convenient way for the patient is the possibility for home-treatment or ambulant, shorter administration by sc injection, especially for those indications requiring frequent dosing, for chronic diseases like rheumatoid arthritis or even for cancer therapies. Formulations which are applicable using the subcutaneous (sc) route of injection may allow the patient to administer the drug by him/herself or receive injections by a healthcare professional. The injection volume for sc drug administration is currently considered to be limited to $1-2$ mL and mAb treatment requires high therapeutic doses in the rage of mg per kg bodyweight. [6-9] This generates the need to develop highly concentrated formulations exceeding the 100 mg/mL applicable for sc use.

For a more convenient and safe drug administration, concentrated protein formulations are developed as combination products especially in cases where convenience of self-administration is required. These are e.g. injection devices like pre-filled syringes, autoinjectors, or injection pumps. Picture 1 shows three examples of combination products which are currently approved by EMA and FDA. These examples are Actemra sc® which is approved as a pre-filled syringe with a safety device (A), Herceptin sc Single-injection-device® (B), and the Humira® Pen (C).

The development of highly concentrated formulations exceeding the $50-100$ mg/mL poses several
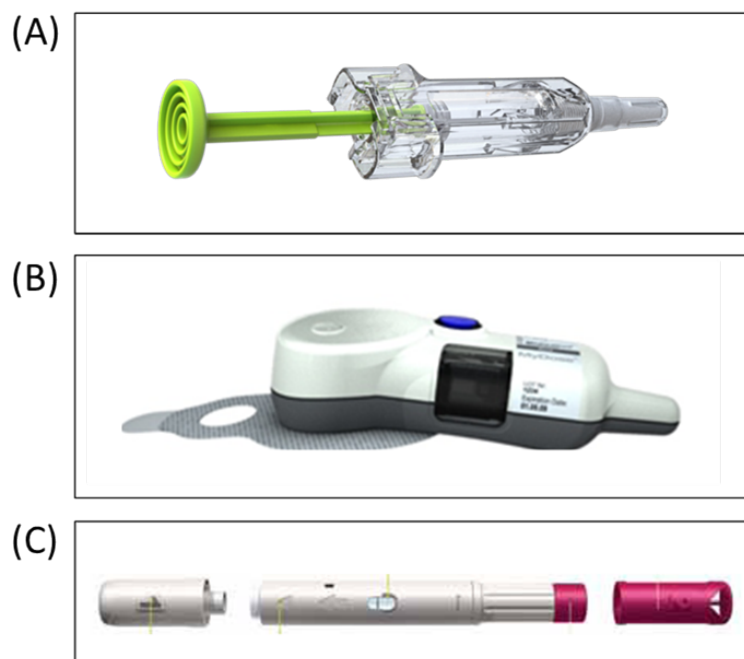
Picture 1: (A) Actemra sc ® pre-filled syringe, (B) Herceptin sc Single-Injection device®, (C) Humira® Pen [10]. Pictures (A) and (B) were obtained from Roche internal websites.

challenges, including chemical, and physical stability (e.g. aggregation), as well as solution viscosity. [11-13] In particular, the increase in viscosity with higher protein concentration may cause limitations during product development and processing, which may occur during manufacture (filtration, pumping, filling) as well as during drug administration (injectability). [6, 8, 11, 12] These limitations arise due to an increase in pressure/force which is needed for manufacturing or injection of the sample in a defined (injection) time. The increase in pressure is triggered by (elevated) viscosity and the smallest orifice diameter of the process (law of Hagen-Poiseuille). [14, 15] For drug administration, this is the inner diameter of the injection needle that is critical, which is e.g. 0.21 mm for a 27 G needle (0.19 – 0.24 mm according to DIN EN ISO 7864:1993). A 27 G needle is used for most of the marketed products for sc injection as outlined later in this work. An overview of the commercial manufacturing process of protein therapeutics will be provided in the following.

Fill-finish manufacturing process of protein solutions

Parenterally administered protein formulations are typically formulated and manufactured as either liquid formulation in a vial, pre-filled syringe, or cartridge in an injection device, or as a lyophilisate in a vial or dual-chamber syringe. Figure 2 provides an overview of a typical fill-finish process of a liquid formulation. After thawing of the usually frozen API bulk solution (active pharmaceutical ingredient), the solution is transferred into a compounding vessel. In the compounding vessel, the solution is

homogenized and additional excipients can be added, as required. After a bioburden reduction filtration using a 0.22 μm filter into a holding tank, the formulation is sterile-filtered through a 0.22 μm filter prior or during filling. Filling into primary packaging material such as glass vials is performed in class A environment (isolator or RAB = restricted access barrier) using e.g. peristaltic pumps. A surge tank might be included into the fill-finish process serving for venting. After filling, the vials are stoppered and further transported for capping. For lyophilisates, vials are only stoppered partially and then transported and loaded to the lyophilizer. After subsequent lyophilization and stoppering in the lyophilizer, vials are unloaded and capped.

The fill-finish process of a sterile solution includes several hydrodynamic processes which are driven by the applied pressure during the respective process steps. The applied pressure defines the flow rate which is directly proportional to viscosity and the smallest passage diameter during the process, which are the pores of the sterile filters with a nominal pores size of 0.22 μm.
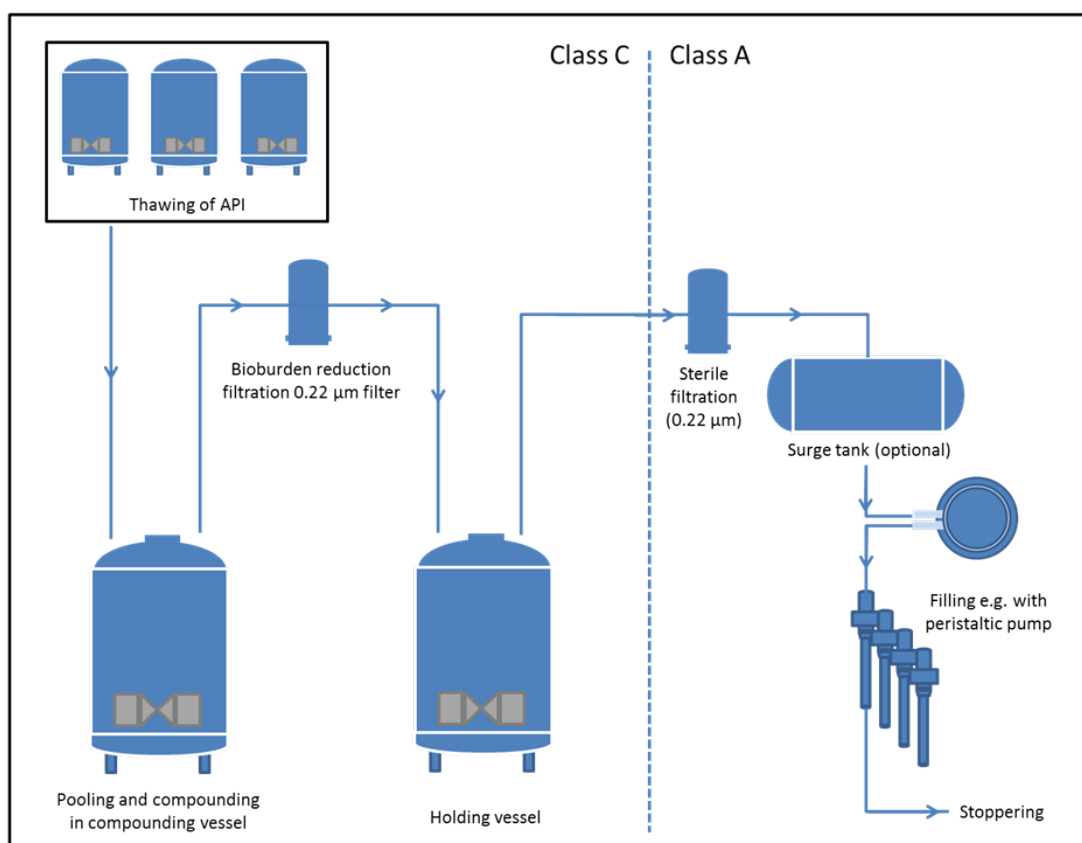
Figure 2: Typical fill-finish process of a liquid formulation. API = active pharmaceutical ingredient.

Viscosity of highly concentrated protein solutions

Viscosity of concentrated protein solutions is governed by multiple factors including, but not limited to protein concentration [16, 17], temperature [18-22], formulation pH, and solution composition [23-25]. Dynamic viscosity increases in an exponential fashion at higher protein concentration and is governed by two factors. This is on the one hand volume exclusion which is based on the increase in volume fraction of the protein as well as of the excipients, leading to crowding of the molecules. [26-28] On the other hand, viscosity is governed by protein-protein interactions (PPI). PPIs are manifold in nature and dependent on the intermolecular distance (r) and therefore protein concentration. [23] The interplay of volume exclusion and PPIs can be described by the potential of mean force W_{22} between two molecules dependent on the intermolecular distance as follows [29-31]:

$$W_{22}(r) = W_{HS}(r) + W_q(r) + W_\mu(r) + W_{VdW}(r) + W_{osmotic}(r)$$

$$with\, W_q(r) + W_\mu(r)$$

$$= W_{q-q}(r) + W_{q-\mu}(r) + W_{q-i\mu}(r) + W_{\mu-\mu}(r) + W_{\mu-i\mu}(r)$$

The negative derivative of W_{22}, which is $-\partial W(r)/\partial r$, is equal to the force between two protein molecules and is averaged over all possible orientations and configurations of the molecule. [32] The main contribution to the potential of mean force is derived from the hard-sphere potential (HS), which accounts for volume exclusion of the protein molecules, as well as electrostatic interactions (q). Both are repulsive in nature and were shown to dominate at low protein concentrations dependent on formulation composition/ at low salt conditions. [24] Attractive forces might be also present at low protein concentrations but are considered as negligible at large intermolecular distances (low salt conditions). At high protein concentrations and conclusively smaller inter-molecular distance, Van der Waals forces (VdW) and dipole/induced dipole ($\mu/i\mu$) potentials as well as the combination of $\mu/i\mu$ and q potentials increase, which are attractive in nature. Moreover, the osmotic/excluded-volume effect $W_{osmotic}$ of added salt contributes to the attractive potential at high protein concentrations, but becomes only predominant at salt concentrations >1 M. [33]

The relative contribution of the potentials changes with protein concentration and formulation composition. Figure 3 shows the mean force potential as a function of the intermolecular distance indicating that the sum of all potentials, i.e. attractive and repulsive interactions, govern the interaction potential and therefore viscosity behavior at small intermolecular distances. [23, 24, 31]

Besides the non-specific contributions, also specific interactions like hydrogen-bonding or interactions driven by local geometry may contribute to the interaction potential in some cases as reported by Kanai *et al.* in 2007 and Yadav *et al.* in 2009 for a specific mAb. [34, 35]

 The importance of electrostatic PPIs for the viscosity behavior of mAbs was recently investigated by Yadav and colleagues. [36] Especially the distribution of surface charge was shown to play an essential role and governs viscosity behavior. The viscosity of concentrated mAb formulations can be reduced by the addition of chaotropic cations or anions like e.g. Hofmeister salts [34]. The increase of ionic strength likely leads to shielding of the electronic surface charges which leads to a decrease in viscosity for most protein formulations. [23] This is explained by the potential of mean force as the molecular charge of the protein is shielded by the ions and therefore the contribution of electrostatic PPIs to the repulsive
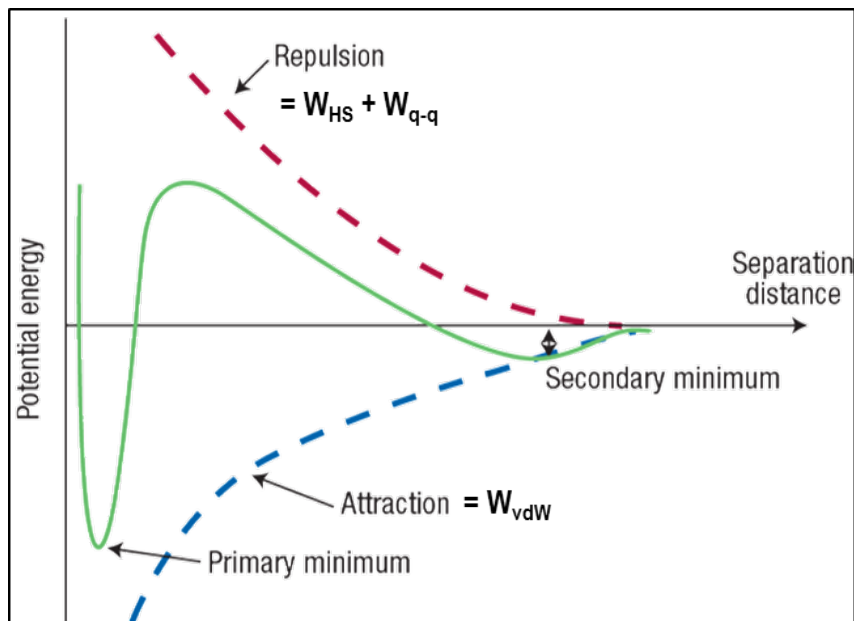
Figure 3: Interaction potential energy as a function of intermolecular distance. The green line (repulsive potential) is obtained by adding hard-core (W_{HS}) and screened coulombic (W_{q-q}) potential. The blue line represents Van der Waals potentials (W_{vdW}; attractive). The interplay of these potentials is historically known as DLVO theory. The values of minima and maxima as well as their position depend on the solution characteristics. (From Malescio, *Nature Materials 2*, 501-503, August 2003)[31]

interaction potential decreases. [16, 37] Viscosity lowering excipients for protein formulations were studied intensively in the past. Du and co-workers have recently reported that hydrophobic salts significantly lowered the viscosity of concentrated bovine serum albumin and γ-globulin solutions. [38] Guo *et al.* have previously proposed that cations/anions being hydrophobic, bulky, and aliphatic in nature were most effective to reduce viscosity of mAb formulations. [39] Promising candidates for lowering viscosity of highly concentrated mAb formulation are currently amino acid derivatives like arginine salts as reported by Liu and co-workers. [40]

Viscosity of protein solutions is exponentially dependent on protein concentration and can be described mathematically using the modified Mooney equation [41]:

$$\eta = \eta_0 \cdot e^{\dfrac{c \cdot [\eta]}{1 - c \cdot [\eta] \cdot k/\nu}}$$

The dynamic viscosity η (mPas) is described as the product of placebo viscosity η_0 (mPas) multiplied by an exponential term consisting of the product of protein concentration c (g/L) and intrinsic viscosity $[\eta]$ which is equal to 6.3 mL/g for monoclonal antibodies [42], as well as the fraction of a crowding factor divided by a form factor k/ν accounting for the dependence of viscosity on size and shape of the protein. These two parameters are both dimensionless and obtained by fitting of the Mooney equation to the experimental data. The Mooney equation was recently applied to several mAb formulations to describe the concentration dependence of viscosity. However, deviation in experimental data from the model were ascribed to PPIs and protein-solvent interaction, as the Mooney equation describes the concentration

dependence of dynamic viscosity of dispersed hard-sphere, non-interacting molecules only accounting for volume exclusion. [17, 34, 37]

A direct measure of the protein-protein pair potential is the osmotic second virial coefficient, B_{22} (also termed A_2), which can be analytically quantified by various methods. B_{22} is thereby related to the potential of mean force W_{22} by the molar mass of the protein as described by Hill and colleagues in 1957. [29, 43] The most commonly used methods are static light scattering [44-46], analytical ultracentrifugation [37, 47], membrane osmometry [48-50], self-interaction chromatography [51, 52], and dynamic light scattering [25, 44, 53]. However, these methods measure at low protein concentrations and are thus limited in the application to protein concentrations exceeding 50 mg/mL. At high protein concentrations, the second term of the virial equation is no longer sufficient to describe PPIs, as higher interactions between three or more molecules contribute to the overall interaction potential. [17] Nevertheless, correlation of the second virial coefficient A_2 with viscosity at high protein concentration was intensively studied in the past revealing quantitative relation of viscosity and attractive PPIs for some mAb formulations. [25, 54] Methods applicable at high protein concentrations are limited and include small-angle X-ray scattering (SAXS) [55, 56] as well as small-angle neutron scattering (SANS) [57-59]. Saluja and co-workers have recently used characterization of elastic properties by the storage modulus G as a measure for PPIs at high protein concentrations. [60-62] They also showed that G correlated qualitatively with viscosity in their studies.

Viscosity at high protein concentrations is governed by higher order interactions as outlined. Recently published data suggested the formation of transient mAb networks, so-called clusters, due to reversible self-association. [36, 37, 63-66] Wayne *et al.* proposed that only small anisotropic PPIs between surfaces are required to initiate cluster formation. They found that the size of clusters was directly correlated to solution viscosity. [63] Yadav and colleagues reported that the charge distribution on the mAb surface plays an essential role during self-association. [36] The formation of clusters with increasing volume fraction is a commonly known phenomenon observed in polymer chemistry. [67] Thereby, the formation of higher order structures leads among others to non-ideal solution and flow behavior at high shear rates. [67, 68] Thus, non-ideal/ non-Newtonian flow behavior would be of high relevance during drug administration as well as filtration of highly concentrated protein formulations and will be investigated within this work.

References (Introduction)

1. Research and Markets, Biopharmaceuticals - A Global Market Overview, published July 2013 (11. September 2014).

2. A. Hiller, Fast Growth Foreseen for Protein Therapeutics, BioMarket Trends, 29 (2009) 153-155.

3. BCC Research, Biologic Therapeutic Drugs: Technologies and Global Markets (2012-2017), in: Biotechnology, BCC Research, 2013.

4. G. Walsh, Pharmaceutical biotechnology products approved within the European Union, Eu J Pharm Biopharm, 55 (2003) 3-10.

5. P.A. Scolnik, mAbs: a business perspective, MAbs, 1 (2009) 179-184.

6. R.J. Harris, S.J. Shire, C. Winter, Commercial manufacturing scale formulation and analytical characterization of therapeutic recombinant antibodies, Drug Develop Res, 61 (2004) 137-154.

7. O. Shpilberg, C. Jackisch, Subcutaneous administration of rituximab (MabThera) and trastuzumab (Herceptin) using hyaluronidase, Br J Cancer, 109 (2013) 1556-1561.

8. S.J. Shire, Z. Shahrokh, J. Liu, Challenges in the development of high protein concentration formulations, J Pharm Sci, 93 (2004) 1390-1402.

9. N.W. Warne, Development of high concentration protein biopharmaceuticals: the use of platform approaches in formulation development, Eu J Pharm Biopharm, 78 (2011) 208-212.

10. A. Kivitz, O.G. Segurado, HUMIRA pen: a novel autoinjection device for subcutaneous injection of the fully human monoclonal antibody adalimumab, Expert Rev Med Devices, 4 (2007) 109-116.

11. S.J. Shire, Formulation and manufacturability of biologics, Curr Opin Biotech, 20 (2009) 708-714.

12. J. Jezek, M. Rides, B. Derham, J. Moore, E. Cerasoli, R. Simler, B. Perez-Ramirez, Viscosity of concentrated therapeutic protein compositions, Adv Drug Deliv Rev, 63 (2011) 1107-1117.

13. M.C. Manning, D.K. Chou, B.M. Murphy, R.W. Payne, D.S. Katayama, Stability of protein pharmaceuticals: an update, Pharm Res, 27 (2010) 544-575.

14. G.H.L. Hagen, Über die Bewegung des Wassers in engen zylindrischen Röhren., Poggendorfs Annalen der Physik und Chemie, 46 (1939) 423-442.

15. J.L.M. Poiseuille, Recherches experimentales sur le mouvement des liquides dans les tubes de tres petits diametres, C.R. Acad. Sci., 11 (1840) 1041-1048.

16. B.A. Salinas, H.A. Sathish, S.M. Bishop, N. Harn, J.F. Carpenter, T.W. Randolph, Understanding and Modulating Opalescence and Viscosity in a Monoclonal Antibody Formulation, J Pharm Sci, 99 (2010) 82-93.

17. S. Yadav, S.J. Shire, D.S. Kalonia, Factors Affecting the Viscosity in High Concentration Solutions of Different Monoclonal Antibodies, J Pharm Sci, 99 (2010) 4812-4829.

18. K. Monkos, Concentration and temperature dependence of viscosity in lysozyme aqueous solutions, Biochim Biophys Acta, 1339 (1997) 304-310.

19. K. Monkos, On the hydrodynamics and temperature dependence of the solution conformation of human serum albumin from viscometry approach, Bba-Proteins Proteom, 1700 (2004) 27-34.

20. K. Monkos, Viscosity analysis of the temperature dependence of the solution conformation of ovalbumin, Biophys Chem, 85 (2000) 7-16.

21. K. Monkos, Viscosity of bovine serum albumin aqueous solutions as a function of temperature and concentration, Int J Biol Macromol, 18 (1996) 61-68.

22. K. Monkos, B. Turczynski, A comparative study on viscosity of human, bovine and pig IgG immunoglobulins in aqueous solutions, Int J Biol Macromol, 26 (1999) 155-159.

23. R. Chari, K. Jerath, A.V. Badkar, D.S. Kalonia, Long- and Short-Range Electrostatic Interactions Affect the Rheology of Highly Concentrated Antibody Solutions, Pharm Res, 26 (2009) 2607-2618.

24. S. Yadav, S.J. Shire, D.S. Kalonia, Viscosity Analysis of High Concentration Bovine Serum Albumin Aqueous Solutions, Pharm Res, 28 (2011) 1973-1983.

25. S. Yadav, S.J. Shire, D.S. Kalonia, Viscosity behavior of high-concentration monoclonal antibody solutions: correlation with interaction parameter and electroviscous effects, J Pharm Sci, 101 (2012) 998-1011.

26. T. Laue, Proximity energies: a framework for understanding concentrated solutions, J Mol Recognit, 25 (2012) 165-173.

27. A.P. Minton, Macromolecular crowding, Curr Biol, 16 (2006) R269-271.

28. A.P. Minton, Influence of excluded volume upon macromolecular structure and associations in 'crowded' media, Curr Opin Biotechnol, 8 (1997) 65-69.

29. R.A. Curtis, J.M. Prausnitz, H.W. Blanch, Protein-protein and protein-salt interactions in aqueous protein solutions containing concentrated electrolytes, Biotechnol Bioeng, 57 (1998) 11-21.

30. A. Saluja, D.S. Kalonia, Nature and consequences of protein-protein interactions in high protein concentration solutions, Int J Pharm, 358 (2008) 1-15.

31. G. Malescio, Intermolecular potentials–past, present, future, Nat Mater, 2 (2003) 501-503.

32. W.G.M. McMillan Jr., Joseph E. , The Statistical Thermodynamics of Multicomponent Systems J Chem Phys, 13 (1945) 276-305.

33. V. Vlachy, J.M. Prausnitz, Donnan Equilibrium - Hypernetted-Chain Study of One-Component and Multicomponent Models for Aqueous Polyelectrolyte Solutions, J Phys Chem, 96 (1992) 6465-6469.

34. S. Kanai, J. Liu, T.W. Patapoff, S.J. Shire, Reversible self-association of a concentrated monoclonal antibody solution mediated by Fab-Fab interaction that impacts solution viscosity, J Pharm Sci, 97 (2008) 4219-4227.

35. S. Yadav, J. Liu, S.J. Shire, D.S. Kalonia, Specific interactions in high concentration antibody solutions resulting in high viscosity, J Pharm Sci, 99 (2010) 1152-1168.

36. S. Yadav, T.M. Laue, D.S. Kalonia, S.N. Singh, S.J. Shire, The influence of charge distribution on self-association and viscosity behavior of monoclonal antibody solutions, Mol Pharm, 9 (2012) 791-802.

37. J. Liu, M.D. Nguyen, J.D. Andya, S.J. Shire, Reversible self-association increases the viscosity of a concentrated monoclonal antibody in aqueous solution, J Pharm Sci, 94 (2005) 1928-1940.

38. W. Du, A.M. Klibanov, Hydrophobic salts markedly diminish viscosity of concentrated protein solutions, Biotechnol Bioeng, 108 (2011) 632-636.

39. Z. Guo, A. Chen, R.A. Nassar, B. Helk, C. Mueller, Y. Tang, K. Gupta, A.M. Klibanov, Structure-Activity Relationship for Hydrophobic Salts as Viscosity-Lowering Excipients for Concentrated Solutions of Monoclonal Antibodies, Pharm Res, (2012).

40. J. Liu, S.J. Shire, Patent: Reduced-viscosity concentrated protein formulations, WO 2002030463 A2 (2002).

41. M. Mooney, The viscosity of a concentrated suspension of spherical particles, J Colloid Sci, 6 (1951) 162-170.

42. J.W. Mehl, J.L. Oncley, R. Simha, Viscosity and the Shape of Protein Molecules, Science, 92 (1940) 132-133.

43. T.L. Hill, Theory of Solutions., J Am Chem Soc, 79 (1957) 4885-4890.

44. C. Lehermayr, H.C. Mahler, K. Mader, S. Fischer, Assessment of net charge and protein-protein interactions of different monoclonal antibodies, J Pharm Sci, (2011).

45. A. Saluja, A.V. Badkar, D.L. Zeng, S. Nema, D.S. Kalonia, Ultrasonic Storage Modulus as a Novel Parameter for Analyzing Protein-Protein Interactions in High Protein Concentration Solutions: Correlation with Static and Dynamic Light Scattering Measurements, Biophys J, 92 (2007) 234-244.

46. K. Demoruelle, B. Guo, S. Kao, H.M. McDonald, D.B. Nikic, S.C. Holman, W.W. Wilson, Correlation between the osmotic second virial coefficient and solubility for equine serum albumin and ovalbumin, Acta Crystallogr D Biol Crystallogr, 58 (2002) 1544-1548.

47. S.E. Harding, A.J. Rowe, Insight into protein-protein interactions from analytical ultracentrifugation, Biochem Soc T, 38 (2010) 901-907.

48. V.L. Vilker, C.K. Colton, K.A. Smith, The Osmotic-Pressure of Concentrated Protein Solutions - Effect of Concentration and Ph in Saline Solutions of Bovine Serum-Albumin, J Colloid Interf Sci, 79 (1981) 548-566.

49. Y.U. Moon, C.O. Anderson, H.W. Blanch, J.M. Prausnitz, Osmotic pressures and second virial coefficients for aqueous saline solutions of lysozyme, Fluid Phase Equilibr, 168 (2000) 229-239.

50. S. Ruppert, S.I. Sandler, A.M. Lenhoff, Correlation between the osmotic second virial coefficient and the solubility of proteins, Biotechnol Prog, 17 (2001) 182-187.

51. P.M. Tessier, A.M. Lenhoff, S.I. Sandler, Rapid measurement of protein osmotic second virial coefficients by self-interaction chromatography, Biophys J, 82 (2002) 1620-1631.

52. S.Y. Patro, T.M. Przybycien, Self-interaction chromatography: A tool for the study of protein-protein interactions in bioprocessing environments, Biotechnol Bioeng, 52 (1996) 193-203.

53. S. Yadav, T.M. Scherer, S.J. Shire, D.S. Kalonia, Use of dynamic light scattering to determine second virial coefficient in a semidilute concentration regime, Anal Biochem, 411 (2011) 292-296.

54. S. Saito, J. Hasegawa, N. Kobayashi, N. Kishi, S. Uchiyama, K. Fukui, Behavior of Monoclonal Antibodies: Relation Between the Second Virial Coefficient (B-2) at Low Concentrations and Aggregation Propensity and Viscosity at High Concentrations, Pharm Res, 29 (2012) 397-410.

55. F.J. Zhang, M.W.A. Skoda, R.M.J. Jacobs, R.A. Martin, C.M. Martin, F. Schreiber, Protein interactions studied by SAXS: Effect of ionic strength and protein concentration for BSA in aqueous solutions, J Phys Chem B, 111 (2007) 251-259.

56. J. Narayanan, X.Y. Liu, Protein interactions in undersaturated and supersaturated solutions: A study using light and x-ray scattering, Biophys J, 84 (2003) 523-532.

57. O.D. Velev, E.W. Kaler, A.M. Lenhoff, Protein interactions in solution characterized by light and neutron scattering: comparison of lysozyme and chymotrypsinogen, Biophys J, 75 (1998) 2682-2697.

58. Y. Liu, E. Fratini, P. Baglioni, W.R. Chen, S.H. Chen, Effective long-range attraction between protein molecules in solutions studied by small angle neutron scattering - art. no. 118402, Phys Rev Lett, 95 (2005).

59. E.J. Yearley, I.E. Zarraga, S.J. Shire, T.M. Scherer, Y. Gokarn, N.J. Wagner, Y. Liu, Small-angle neutron scattering characterization of monoclonal antibody conformations and interactions at high concentrations, Biophys J, 105 (2013) 720-731.

60. A. Saluja, A.V. Badkar, D.L. Zeng, S. Nema, D.S. Kalonia, Application of high-frequency rheology measurements for analyzing protein-protein interactions in high protein concentration solutions using a model monoclonal antibody (IgG2), J Pharm Sci, 95 (2006) 1967-1983.

61. A. Saluja, D.S. Kalonia, Application of ultrasonic shear rheometer to characterize rheological properties of high protein concentration solutions at microliter volume, J Pharm Sci, 94 (2005) 1161-1168.

62. A.R. Patel, B.A. Kerwin, S.R. Kanapuram, Viscoelastic Characterization of High Concentration Antibody Formulations Using Quartz Crystal Microbalance with Dissipation Monitoring, J Pharm Sci, 98 (2009) 3108-3116.

63. W.G. Lilyestrom, S. Yadav, S.J. Shire, T.M. Scherer, Monoclonal Antibody Self-Association, Cluster Formation, and Rheology at High Concentrations, J Phys Chem B, 94 (2005) 1928-1940.

64. A. Chaudhri, I.E. Zarraga, T.J. Kamerzell, J.P. Brandt, T.W. Patapoff, S.J. Shire, G.A. Voth, Coarse-Grained Modeling of the Self-Association of Therapeutic Monoclonal Antibodies, J Phys Chem B, 116 (2012) 8045-8057.

65. A. Chaudhri, I.E. Zarraga, S. Yadav, T.W. Patapoff, S.J. Shire, G.A. Voth, The role of amino acid sequence in the self-association of therapeutic monoclonal antibodies: insights from coarse-grained modeling, J Phys Chem B, 117 (2013) 1269-1279.

66. T.M. Scherer, J. Liu, S.J. Shire, A.P. Minton, Intermolecular interactions of IgG_1 monoclonal antibodies at high concentrations characterized by light scattering, J Phys Chem B, 114 (2010) 12948-12957.

67. A.Y. Bai Xu, Mitchell A. Winnik, Kayvan Sadeghy-Dalivand, David F. James, Richard Jenkins, David Bassett, Viscoelastic Properties in Water of Comb Associative Polymers Based On Poly(ethylene oxide), Langmuir, 13 (1997) 6903-6911.

68. M.T. Hernandez, J. Pellicer, J. Delegido, M. Dolz, Rheological characterization of easy-to-disperse (ETD) Carbopol hydrogels, J Disper Sci Technol, 19 (1998) 31-42.

Scope

The increasing demand for subcutaneous formulations of protein therapeutics results in the increasing request for highly concentrated formulations exceeding 50 – 100 mg/mL. However, severe limitations are given by the rheological behavior during product development as well as during processing and drug administration. The elevated viscosity at high protein concentrations leads to an increase in pressure/ resulting force required to manufacture, especially filter, or administer the protein solution.

The focus of this work is to investigate the rheological behavior of protein solutions at high protein concentrations. The main objective is to obtain a profound understanding of the drug administration as well as of the filtration process and to elucidate the role of viscosity with regard to potential limitations. The present work provides an overview of commercially available highly concentrated protein formulations for subcutaneous or intramuscular administration as well as of methods used for viscosity characterization with establishment of a high-throughput method for viscosity determination. Based on these studies, the present work targets to investigate and characterize in detail the two outlined hydrodynamic processes which are filtration as well as the injection process for highly concentrated mAb formulations.

In detail, ten commercial highly concentrated biotherapeutics were investigated to provide a technical overview of commercial protein products and to summarize requirements defined by the European Pharmacopoeia (**Chapter 1**). The products were characterized for formulation, packaging as well as for injection forces and device components, and served as a benchmark for the subsequent studies.

Succeeding the depiction of landscape of commercial products, an automated high-throughput method was developed to measure dynamic viscosity using capillary electrophoresis equipment, due to the limited number of commercially available methods suitable to measure viscosity of protein formulations. **Chapter 2** reports the development of this method as well as the application to protein therapeutics. Based on these preliminary studies, injectability and filtration of highly concentrated protein formulations were investigated in **Chapter 3, 4,** and **5**.

Injection forces of a monoclonal antibody at maximum protein concentration feasible (250 mg/mL) as well as of different commercial products were investigated in **Chapter 3**. A mathematical *in silico* model was established for prediction of injection forces applicable for Newtonian solutions and especially extended for non-Newtonian fluids. The model was experimentally verified (*in vitro*) by use of surrogate samples (Carbopol gels) and applied to injection force measurements of the protein samples.

For a complete and comprehensive picture of parameters contributing to injection forces based on **Chapter 3** representative for the *in vivo* situation, the potential influence of the backpressure of the sc tissue layer to injection forces was investigated in Göttingen minipigs (*in vivo*) dependent on viscosity, injection rate, and injection volume. The minipigs received injections of a surrogate solution (dextran) into the *plica inguinalis* by use of an instrumental set-up built for this purpose (**Chapter 4**).

To complete the work, filtration of different mAb formulations was investigated in a lab-scale set-up (**Chapter 5**) as the second hydrodynamic process. Filtration forces were determined dependent on filter material, protein concentration, and viscosity, and differences were linked to filter resistance, pore size distribution, and formulation composition.

Chapter 1

Technical overview

– Characterization of commercial protein therapeutics for subcutaneous and intramuscular administration

Research Document Repository Hoffmann-La Roche, 2013
Technical Report

Authors:
Andrea Allmendinger

Stefan Fischer
Hanns-Christian Mahler
Edward Schwarb
Robert Mueller

The following study provides a technical overview of highly concentrated biotech therapeutics for subcutaneous or intramuscular use currently approved by the European Medicines Agency. Ten different commercial products were characterized in terms of formulation properties like osmolality, pH, turbidity, color, viscosity, number of visible and sub-visible particles, level of soluble aggregates and fragments as well as for forces required for simulated administration (glide force, removal of needle cover). A summary of device characteristics (e.g. needle dimensions), patient Information for correct administration (e.g. equilibration time, injection angle), and secondary packaging are provided. Additionally, requirements of the European Pharmacopoeia for protein therapeutics for subcutaneous and intramuscular administration are outlined.

1.1 Introduction

In 2012, nine highly concentrated (>50 mg/mL) biotech therapeutics were approved by the EMA for intramuscular (im) or subcutaneous (sc) injection. They have been launched as either liquid and/or lyophilized formulation resulting in 12 different formulations on the market. [1] Stelara®, Ilaris®, Prolia®, Humira®, Simponi®, and Cimzia® were approved as liquid formulations; Enbrel®, Xolair®, and Synagis® are available as liquid and lyophilized formulations. Five of these highly concentrated biotech products were commercialized in 2009 and 2010 alone, which are Stelara®, Ilaris®, Prolia®, Simponi®, and Cimzia®, showing the rapid development of this expanding market. [2] A number of criteria for biotech products are defined in the Pharmacopeias. The following enumeration lists the applicable Monographs:

- Clarity and degree of opalescence of liquids (Ph. Eur. 2.2.1.) [3]

- Degree of coloration of liquids (Ph. Eur. 2.2.2.) [4]

- Osmolality (Ph. Eur. 2.2.35.) [5]

- Test for extractable volume of parenteral preparations (Ph. Eur. 2.9.17.) [6]

- Particulate contamination: sub-visible particles (Ph. Eur. 2.9.19.) [7]

- Particulate contamination: visible particles (Ph. Eur. 2.9.20.) [8]

- Monograph: Monoclonal antibodies for human use (Ph. Eur. 2031.) [9]

- Monograph: Parenteral preparations (Ph. Eur. 0520.) [10]

A number of routinely performed analytics for characterization of highly concentrated protein formulations is not defined in the Pharmacopeia, including viscosity to name only one example. Thus, the characterization of formulation as well as the investigation of device properties of currently marketed high-concentration products is desirable in order to benchmark internal development programs.

The following study provides a technical overview of highly concentrated protein therapeutics currently approved by the EMA (European Medicines Agency). Ten different products were characterized in terms of osmolality, pH, turbidity, color, viscosity, number of visible and sub-visible particles, level of soluble aggregates and fragments as well as for forces required for simulated administration (glide force, removal of needle cover). A summary of device characteristics (e.g. needle dimensions), patient Information for correct administration (e.g. equilibration time, injection angle), and secondary packaging are provided, and requirements of the European Pharmacopoeia for protein therapeutics for subcutaneous and intramuscular administration are summarized.

Picture 1: Liquid formulations provided as prefilled syringes. Cimzia®, Humira®, Simponi®, Enbrel®, Prolia® (from left to right). Picture 2: Liquid formulations provided as auto-injectors. Simponi Smartject®, Humira®, and Enbrel MyClic® (from above to below). Picture 4 to 6: Enbrel®, Xolair®, Raptiva®, Synagis® lyophilisate.

1.2 Product information

Ten highly concentrated protein therapeutics were investigated in this study, comprising concentrations between 50 to 200 mg/mL. Table 1.1 summarizes the date of approval, manufacturer, indication, active pharmaceutical ingredient, IgG subtype, target, route of administration, and formulation of the products. Eight out of ten investigated formulations are currently (2012) approved for the European market. One investigated product (Raptiva®) was withdrawn after the start of this study, in 2008. The Roche product, Actemra sc®, was close to market launch.

As active ingredient, the investigated products contain therapeutic monoclonal antibodies of the isotype $IgG_{1\kappa}$ (Simponi®, Humira®, Actemra sc®, Raptiva®, Synagis®, Xolair®) or IgG_2 (Prolia®). Enbrel® contains a fusion protein with a conjugated Fc-fragment, and Cimzia® contains a pegylated Fab-fragment. Solely five products are approved for rheumatoid arthritis (Cimzia®, Enbrel®, Simponi®, Humira®, and Actemra sc®). Prolia® is approved for bone loss and osteoporosis, Synagis® for respiratory-synctial-virus, Raptiva® for plaque psoriasis, and Xolair for persistent allergic asthma. The route of administration is either im (Synagis®) or sc injection (all other products).

Six products were obtained as liquid formulations (Prolia®, Cimzia®, Enbrel®, Simponi®, Humira®, and Actemra sc®). These products were provided as prefilled syringes (PFS) and are shown in Picture 1. Picture 2 shows the liquid formulations which are also available as autoinjectors. These are Enbrel®, Simponi®, and Humira®. As lyophilisates, Enbrel®, Raptiva®, Synagis®, and Xolair® were obtained, as shown in Picture 3 – 6

1.3 Materials and Methods

1.3.1 Materials

Cimzia® 200 mg (UCB GmbH, Brussels, BE) (lot: 35613, expiry date: 03.12., date of testing: 07.11.), Prolia® 60 mg (Amgen Europe B.V., Breda, NL) (lot: 1026050A, expiry date: 04.12., date of testing: 07.11.), Simponi® 50 mg (Essex Pharma, Leiden, NL) (lot: 10L041AD01 and 10L041AL, expiry date: 11.11., date of testing: 07.11.), Humira® 40 mg (Abbott Laboratories Ltd, Maidenhead, UK) (lot: 9611OXD07, expiry date: 11.12., date of testing: 07.11.) and Enbrel® 50 (Wyeth Europe Ltd, Maidenhead, UK) (lot: F20467, expiry date: 06.12., date of testing: 07.11.) were purchased as prefilled syringes. Actemra sc® 180 mg (prefilled syringe) was kindly provided by F. Hoffmann-La Roche Ltd (Basel, CH). Enbrel MyClic® prefilled pen 50 mg (Wyeth Europe Ltd, Maidenhead, UK) (lot: E12839, expiry date: 03.11.), Simponi Smartject® 50 mg (Essex Pharma, Leiden, NL) (lot: 09D101.AF, expiry date: 05.10.) and Humira® 40 mg prefilled pen (Abbott Laboratories Ltd, Maidenhead, UK) (lot: 6005812, expiry date: 07.11.) were obtained as autoinjector. Enbrel® 50 mg (Wyeth Europe Ltd, Maidenhead, UK) (expiry date: 06.09., date of testing: 03.08.), Raptiva® 100 mg (Merck Serono Europe Ltd., Rome, IT) (expiry date: 08.09., date of testing: 03.08.), Synagis® 100 mg (Abbott Laboratories Ltd, Maidenhead, UK) (expiry date: 09.09., date of testing: 03.08.) and Xolair® 150 mg (Novartis Europharm Ltd., West Sussex, UK) (expiry date: 07.10., date of testing: 03.08.) were purchased as lyophilisates. All samples were kept at 2 to 8°C until use and are referred to as CPTs (=commercial protein therapeutics) in the following.

Information on manufacturer, indication, active pharmaceutical ingredient, IgG subtype, target, route of administration, formulation, device characteristics, primary and secondary packaging, room equilibration time, reconstitution time for lyophilisates, holding time and extractable volume were compiled from the Summary of Product Characteristics (SPC) and the Patient Information leaflets (PIL). Dates of approval were acquired from the European commissions website, referring to the European approval numbers of the product. [1]

1.3.2 Methods

Visual inspection

Visible particles were detected by visual inspection using (1) a black-and-white panel as outlined in Ph. Eur. 2.9.20. [12], (2) an Optima I 1351 lamp (Simplex PR Apparate, Berlin, DE), (3) a Seidenader V 90-T instrument (Seidenader Maschinenbau GmbH, Markt Schwaben, DE), and (4) a VHX digital microscope VH-S30K (Keyence, Urdorf, CH).

The Optima lamp was equipped with a twofold magnifying glass and two polarization filters. Light passed from the back through the sample, originating from an opal glass lamp. The Seidenader instrument was equipped with a magnifying glass, with the light passing through the bottom, the side, and top of the sample. The samples were set in rotation by rollers, and particles were detected by the reflected light due to the Tyndall effect. The digital microscope consisted of a 10-times magnifier and also allowed hands-free inspection by a speed control unit AXU-D40-CX (Oriental Motor Europe GmbH, Stuttgart, DE). The sample was illuminated from the side. As prefilled syringes could not be set in rotation under the digital microscope, samples were transferred under laminar air flow into washed, particle-free 11 mm

glass tubes (Hach Lange GmbH, Dsseldorf, DE). They were left at 5°C prior to analysis until all visible air bubbles were removed from the sample. As a negative control, 10 mL ampoules of *Aqua ad iniectabilia* Fresenius (Fresenius Kabi AG, Stans, CH) were prepared in the same way.

The number of visible particles was classified into (1) free of particles (internal standard: 0 particles), (2) practically free of particles (internal standard: $0 - \leq 2$ particles), (3) several/few particles (internal standard: $>2 - \leq 7$ particles), and (4) many particles (internal standard: >7 particles).

Turbidity (opalescence) and color

Sample preparation was performed by transferring the samples under laminar air flow into washed, particle-free 11 mm glass tubes (Hach Lange GmbH, Dsseldorf, DE). They were left at 5°C prior to analysis until all visible air bubbles were removed from the sample.

Turbidity was measured as outlined in Ph. Eur. 2.2.1. [3] using a Hach 2100AN turbidimeter (Hach Company, Loveland, Co) in the ratio mode. The results were reported in Formazin turbidity units (FTU), as the instrument was calibrated against formazin reference suspensions. Results were classified into five subclasses: clear ($0 - 3$ FTU), slightly opalescent ($3 - 6$ FTU), opalescent ($6 - 18$ FTU), strong opalescent ($18 - 30$ FTU), and very strong opalescent (>30 FTU).

The color of the samples was measured with a Dr. Lange LICO 200 colorimeter (Hach Lange GmbH, Rheineck, CH) with automatic selection of color scale.

Light obscuration

Quantification of sub-visible particles was performed under laminar air flow by light obscuration based on the method described in Ph. Eur. 2.9.19. [13] The method was adapted to reduced sample volumes using a HIAC/ROYCO 9703 Liquid Syringe Sampler 3000A with a HRLD-150 sensor. 1.2 mL of sample were used for three measurements at a fill and ejection rate of 10 mL/min. From the second and the third injection, a mean value was obtained using the PharmSpec v1.4 software (Skan AG, Allschwill, CH). The amount of sub-visible particles was reported as cumulative counts/mL for particle sizes ≥ 2 μm, ≥ 5 μm, ≥ 10 μm, ≥ 25 μm, and ≥ 50 μm.

Digital fluid imaging

Sub-visible particles were characterized by high-speed digital fluid imaging using a Benchtop FlowCam® VII instrument (Fluid Imaging Technologies, Yarmouth, Me). The FlowCam® was equipped with a 100 μm flow cell, a digital camera with a resolution of 1280 x 960 pixels, and an objective with 10-times magnification. The instrument was placed under a laminar air flow bench. 0.8 mL of sample were analyzed with a flow rate of 0.15 mL/min, taking 20 colored frames per second, which resulted in a maximal sample efficiency of 30%. Prior to analysis, samples were prepared by emptying the prefilled syringe at a constant velocity of 342 mm/min (0.5 mL/10 s) using a TA.XT2i Texture Analyzer (Stable Microsystems, Surrey, UK). Samples were then pipetted into the FlowCam® and analysis was started 2.5 min after excertion of the syringe, thus standardizing the preparation procedure. Images were captured when sample flowed through the flow cell, which was centered in the field of view. Each individual particle was extracted by the VisualSpreadsheet V2.4.10 software (Fluid Imaging Technologies, Yarmouth, Me) and quantified as

counts/mL. By visually inspection of the pictures, the particles were manually classified into silicone oil droplets, air bubbles, amorphous particles including protein aggregates, and unidentified counts. They were reported as relative counts/mL referring to the total particle count/mL.

Size exclusion high performance liquid chromatography (SE-HPLC)

SE-HPLC was performed using a TSK G3000 SWXL, 7.8 x 300 mm column (Tosoh Bioscience, Stuttgart, DE) on an Alliance 2695 HPLC instrument (Waters Corporation, Baden-Daettwil, CH). The HPLC system was equipped with a 2487 UV detector (Waters Corporation, Baden-Daettwil, CH). Detection occured at a wavelength of 280 nm. The mobile phase consisted of 200 mM K_2HPO_4/KH_2PO_4 and 250 mM KCl (pH 7.0). The measurement was run with a flow rate of 0.5 mL/min at 25°C and a loading volume of 15 μL. Prior to injection, samples were diluted to 10 mg/mL with mobile phase and stored at 5°C in the auto sampler. Species were classified into monomer, low molecular weights (fragmentation and degradation products; LMW) and high molecular weights (dimers and higher soluble oligomers; HMW). The percentage of peak area relative to the total peak area was reported using the Empower 2 Chromatography Data System software (Waters Corporation, Baden-Daettwil, CH).

Osmolality and pH

The osmolality was measured by freezing point depression based on Ph. Eur. 2.2.35. [5] using a Gonotec Osmomat 030 cryoscopic osmometer (Huslab GmbH, Ostermundingen, CH) and by vapor pressure elevation using a Wescor VP osmometer (Wescor, Logan, Ut). The pH value was determined potentiometrically using a Methrom biotrode glass electrode that was connected to a Methrom 781 pH-meter (Metrohm Schweiz AG, Zofingen, CH). The measurements were performed at room temperature.

Imaged capillary electrophoresis (iCE)

The isoelectric point was determined by use of isoelectric focusing performed on an iCE280-iEF-Analyzer (Convergent Bioscience, Toronto, CA). It was connected to a Prince micro injector auto sampler. Measurements were performed at 8°C with a focusing period of 1 min at 1 V followed by 7 min at 3000 V using a fluorocarbon-coated cartridge (d = 50 μm; Convergent Bioscience, Toronto, CAN). Prior to injection, the samples were diluted to 0.07 mg/mL with water and then diluted 1:1 with the mobile phase. It consisted of 1% methylcellulose (Convergent Bioscience, Toronto, CAN), two carrier ampholytes pH 3 – 10 and pH 8 – 10.5 (GE Healthcare, Uppsala, S), two pI marker pH 4.65 and pH 9.5 (Convergent Bioscience, Toronto, CAN), and water. The electrodes were placed into a mixture of 0.1 M NaOH and 0.1% methylcellulose (cathode) and 0.08 M H_3PO_4 in 0.1% methylcellulose (anode) (Convergent Bioscience, Toronto, CAN). Detection occured at 280 nm by a UV CCD imaging camera (CCD = charge-coupled device sensor). Determination of the main peak was performed using the ICE280CFR software 2.3. (Convergent Bioscience, Toronto, CAN) and it was defined as the isoelectric point.

Viscosity measurement

Dynamic viscosity was measured at 5°C, 10°C, 15°C, 20°C, and 25°C using a MCR 301 cone and plate rheometer (Anton Paar AG Switzerland, Zofingen, CH) and the Rheoplus/32 V3.40 software (Anton Paar AG Switzerland, Zofingen, CH). The rheometer was equipped with a measuring cone with an angle of 5°C and a diameter of 50 or 25 mm (Anton Paar AG Switzerland, Zofingen, CH). After one minute

equilibration time at a shear rate of 10 s^{-1}, the shear rate was increased from 100 up to 2000 s^{-1} during one minute. The dynamic viscosity was then determined as an average value of six data points measured at a shear rate of 2000 s^{-1} during 15 s. To obtain a complete shear rate profile, the shear rate was again decreased from 2000 to 100 s^{-1} during one minute.

Force measurements

All force measurements were performed at 25°C on a force testing instrument with a 500 N force sensor (Zwick GmbHandCoKG, Ulm, DE). Data analysis was performed with the Test Xpert II V2.2 software (Zwick GmbHandCoKG, Ulm, DE).

Removing of needle cover of prefilled syringes
The needle cover (also known as RNS = rigid needle shield) was pulled off of the prefilled syringe at a constant velocity of 3 mm/s and the maximal force was determined. 3 mm/s is thereby a reference speed and does not represent user behavior.

Injectability from a generic plastic syringe
To compare liquid and lyophilized formulations, a generic set-up was chosen to test the injection forces of the products. The samples were transferred into a 1 mL BD Plastipak^{TM} syringe (BD, Madrid, ES) and a BD Microlance^{TM}3 27 G needle ($\frac{3}{4}''$, Luer) (BD, Drogheda, IE) was attached. The needle diameter was chosen based on the needle size of the commercial prefilled syringes for CPT 1 and CPT 3–6, which is 27 G. The generic syringes were emptied at a constant velocity of 342 mm/min which corresponds to a volumetric flow of 1 mL/10 s and the maximal force of the injection force was determined. A volumetric flow of 1 mL/10 s was chosen representing a commonly accepted speed which is relevant for the end-user, and which is also used for QC testing. For the product CPT 2, a Sterican$^{®}$ 25 G 1″ needle (B. Braun, Melsungen, DE) was used as it was not possible to inject the product through a 27 G needle without damage of the set-up.

Injectability from the original primary container
The prefilled syringes were emptied at a constant injection speed of 342 mm/min and the maximal force was determined from the injection force profile. The speed of 342 mm/min corresponds to a volumetric flow of 0.5 mL/10 s for all prefilled syringes. This speed, which is smaller than the one used for the generic set-up, was chosen to ensure that the forces from all prefilled syringes can be compared.

Needle dimensions and head space of prefilled syringes

External needle diameter, needle length, bevel of the needle and head space of prefilled syringes were determined using a digimatic caliper CD-15CXR (Mitutoyo America Corporation, Chicago, Il) and a Leica MZ 12 microscope (Leica Microsystems AG, Heerbrugg, CH).

Density and extractable volume

Prefilled syringes were weighed before and after expelling of the product (N = 3). The density was measured at 20°C by using a DMA38 density meter (Anton Paar AG Switzerland, Zofingen, CH) (N = 2). As outlined in Ph. Eur. 2.9.17., the extractable volume was calculated from the mass of the liquid divided by the density. [14] For prefilled syringes with a nominal volume of less than 3 mL the European Pharmacopoeia demands five containers to be tested. In this study we investigated only three.

Reconstitution time

The reconstitution time of lyophilisates was measured with a Zyliss® Switzerland digital timer (DKB Household Switzerland AG, Zrich, CH) and was defined as the time between addition of liquid and complete dissolution without shaking.

1.4 Result summary

Appearance of the product: Visible particles, turbidity, and color

Visible particles were analyzed using (1) a black-and-white panel as outlined in Ph. Eur. 2.9.20. [12], (2) an Optima lamp, (3) a Seidenader instrument, and (4) a VHX digital microscope. Table 1.2 summarizes the visible particle count for the different methods. Except for CPT 3 PFS, all products were characterized as 'free of particles' when analyzed by the black-and-white panel or using the Optima lamp. CPT 3 PFS showed in average two particles per container and was therefore classified as 'practically free of particles'. For CPT 9 lyophilisate (L), detection of visible particles by visual inspection was difficult due to the presence of air bubbles and foam formation at the surface of the liquid.

Referring to the European Pharmacopeia, the Monograph of monoclonal antibodies requires products to contain no visible particles unless otherwise authorized/justified. [15] The Monograph of parenteral preparations which applies for CPT 2 and CPT 3 requires the products to be only 'practically free of particles'. [10]

In addition, the products were inspected visually using a Seidenader instrument and a digital microscope. The literature describes the human eye as able to resolve objects slightly smaller than approximately $80 \, \mu$m. [16] With a magnifying lens, automated handling, inspector training, and interdependent with the number and type of particles, the limit of detection can even extend to $25 \, \mu$m. [17] The Seidenader instrument and the digital microscope are therefore two more sensitive inspection methods compared to the black-and-white panel which is the required method by the European Pharmacopoeia. Using the Seidenader instrument, visible particles were detected in CPT 3 PFS and CPT 5 PFS. These products were therefore classified to contain 'many particles'.

Figure 1.1 shows the turbidity and the color of the investigated products. The color of the products was almost colorless or slightly brownish. The European Pharmacopoeia used to require monoclonal antibody formulations to be colorless or slightly yellow and to be clear or slightly opalescent. [10, 15] Up to date, this criterion is defined specifically to the product.

The turbidity lay between 1.5 ±<0.1 FTU (CPT 2 PFS) and 17.2 ±0.8 FTU (CPT 5 PFS). The products were therefore classified into clear (three products), slightly opalescent (two products), and opalescent (five products). The turbidity depends on various factors including but not limited to formulation components (buffer, ionic strength, excipients, and pH), temperature, type of antibody, and especially to protein concentration. [18-20]

Sub-visible particles

Sub-visible particles were analyzed by light obscuration. Figure 1.2 shows the sub-visible particle counts $\geq 10 \, \mu$m and $\geq 25 \, \mu$m. For particles larger or equal to $10 \, \mu$m, the cumulative counts/mL lay between 7 ±7 counts/mL (CPT 8 L) and 1280 ±340 counts/mL (CPT 3 PFS). For particles larger or equal to

Product (Date of approval)	Manufacturer	Indication	API	IgG subtype	Target	Galenics	Concentration [mg/mL]	Route of administration	Formulation
Prolia (05/2010)	Amgen	bone loss; osteoporosis	Denosumab	Human IgG$_2$	RankL	Liquid	60	sc	Sodium acetate buffer; 0.01% Polysorbate 20; Sorbitol E420
Cimzia (10/2009)	UCB Pharma	rheumatoid arthritis	Certolizumab-Pegol	Pegylated humanized Fab-Fragment	TNF α	Liquid	200	sc	Sodium acetate buffer; NaCl
Enbrel (PFS: 09/2006 AI: 07/2009 L: 04/2005)	Wyeth	rheumatoid arthritis; psoriasis-arthritis; ankylosing spondylitis; psoriasis	Etanercept	Fusion protein of hFc and extracellular domain of TNFRp2-75	TNF α	Liquid / Lyophilisate	50	sc	Sodium phosphate buffer; Sucrose; NaCl; Arginine-HCl; / TRIS buffer; Sucrose; Mannitol
Simponi (10/2009)	Essex Pharma	rheumatoid arthritis; psoriasis-arthritis; ankylosing spondylitis	Golimumab	Human IgG$_1$κ	TNF α	Liquid	100	sc	L-Histidine buffer; 0.02% Polysorbate 80; Sorbitol E420
Humira (PFS: 09/2003 AI: 11/2006)	Abbott	rheumatoid arthritis; psoriasis-arthritis; ankylosing spondylitis; psoriasis; juvenile idiopathic arthritis; Crohn's desease	Adalimumab	Human IgG$_1$κ	TNF α	Liquid	50	sc	Sodium phosphate and Sodium citrate buffer; 0.1% Polysorbate 80; Mannitol; NaCl; NaOH
Actemra close to market launch	Roche	rheumatoid arthritis	Tocilizumab	Humanized IgG$_1$κ	s/m-Il6-Rp	Liquid	180	sc	L-Histidine buffer; Methionine; Arginine-HCl; 0.02% Polysorbate 80
Raptiva 2004 *withdrawn 2009	Serono Pharma	plaque psoriasis	Efalizumab	Humanized IgG$_1$κ	CD11a	Lyophilisate	100	sc	L-Histidine buffer; 0.2% Polysorbate 20; Sucrose
Synagis (08/1999)	Abbott	virial respiratory tract desease (RSV = respiratory-synctial-virus)	Palivizumab	Humanized IgG$_1$κ	F protein hRSV	Lyophilisate	100	im	L-Histidine buffer; Glycine; Mannitol
Xolair (10/2005)	Novartis	persistent allergic asthma	Omalizumab	Humanized IgG$_1$κ	IgE	Lyophilisate	125	sc	L-Histidine buffer; 0.04% Polysorbate 20; Sucrose

Table 1.1: Summary of product information including date of approval, manufacturer, indication, active pharmaceutical ingredient (API), IgG subtype, target, route of administration and formulation. (PFS = prefilled syringe; AI = autoinjector; L = lyophilisate) * Raptiva was taken off the market in 2009 as 'the benefits (. . .) no longer outweigh(ed) its risks, because of safety concerns, including the occurrence of progressive multifocal leukoencephalopathy'. [11]

Product	Black/white panel	Optima	Seidenader	Digital microscope
CPT 1 PFS	Free of particles	Free of particles	Free of particles	Free of particles
CPT 2 PFS	Free of particles	Free of particles	Free of particles	Free of particles
CPT 3 PFS	Practically free of particles	Practically free of particles	Many particles	Many particles
CPT 4 PFS	Free of particles	Free of particles	Free of particles	Free of particles
CPT 5 PFS	Free of particles	Free of particles	Many particles	Many particles
CPT 6 PFS	Free of particles	Free of particles	Free of particles	Free of particles
CPT 7 L	Not determined	Not determined	Free of particles	Free of particles
CPT 8 L	Not determined	Not determined	Free of particles	Free of particles
CPT 9 L*				
CPT 10 L	Not determined	Not determined	Free of particles	Free of particles

Table 1.2: Visible particle count analyzed by visual inspection using the black-and-white panel (Ph. Eur. 2.9.20.), the Optima lamp, the Seidenader instrument, and the digital microscope. Measurements were performed as triplicates. The number of visible particles were classified into (1) free of particles, (2) practically free of particles, (3) several particles, and (4) many particles. (PFS = prefilled syringe; L = lyophilisate, *difficult to determine due to foam formation and many air bubbles.)

25μm the cumulative counts/mL varied between $0 \pm <1$ counts/mL (CPT 8 L) and 65 ± 19 counts/mL (CPT 3 PFS). The sub-visible particle count of particle sizes $\geq 2 \mu$m, $\geq 5 \mu$m, and $\geq 50 \mu$m is reported in Table 1.3. Referring to the European Pharmacopoeia, less than 6000 cumulative counts per container is required for particles equal to or bigger than 10μm, and 600 cumulative counts/mL for particles equal to or bigger than 25μm. [13] For all tested products, the sub-visible particle count was found far below this threshold. Up to date (2012), there is no requirement by the European Pharmacopoeia concerning smaller particle sizes.

For the liquid products, sub-visible particles were further characterized using digital fluid imaging. The particles were classified into four subpopulations: These were silicone oil droplets, air bubbles, amorphous particles including protein aggregates, and unidentified counts. Figure 1.3 shows the relative particle count of each subclass for particle sizes $\geq 10 \mu$m and $\geq 25 \mu$m. Corresponding numbers are presented in Table 1.10 in the appendix. Representative pictures of each product and subclass are displayed in Table 1.4. Amorphous particles, which may include protein aggregates and other particles, varied between 0.1 $\pm 0.1\%$ (CPT 1 PFS) and 69.4 $\pm 14.0\%$ (CPT 3 PFS) for particles equal to/bigger than 10μm and between 0.1 $\pm 0.2\%$ (CPT 5 PFS) and 79.9 $\pm 14.8\%$ (CPT 3 PFS) for particles bigger than/equal to 25μm. For silicone oil droplets the range was quantified as 13.9 $\pm 1.1\%$ (CPT 2 PFS) to 86.1 $\pm 3.2\%$ (CPT 5 PFS) ($\geq 10 \mu$m) and 8.8 $\pm 3.6\%$ (CPT 2 PFS) to 99.7 $\pm 0.5\%$ (CPT 5 PFS) ($\geq 25 \mu$m). Air bubbles were found to vary between 2.3 $\pm 1.0\%$ (CPT 3 PFS) and 24.7 $\pm 11.5\%$ (CPT 2) ($\geq 10 \mu$m) and between <0.1 $\pm <0.1\%$ (CPT 1 PFS) and 34.2 $\pm 17.8\%$ (CPT 2 PFS) ($\geq 25 \mu$m). Only a small number of particles could not be identified. For particles bigger than 10μm, this subclass varied between 0.1 $\pm 0.1\%$ (CPT 5 PFS) and 7.5 $\pm 10.4\%$ (CPT 6 PFS), and for particles equal to/bigger than 25μm between no counts (5 products) and 7.1 $\pm 12.2\%$ (CPT 6 PFS).

The European Pharmacopoeia stipulates a limit for the overall amount of sub-visible particles $\geq 10 \mu$m
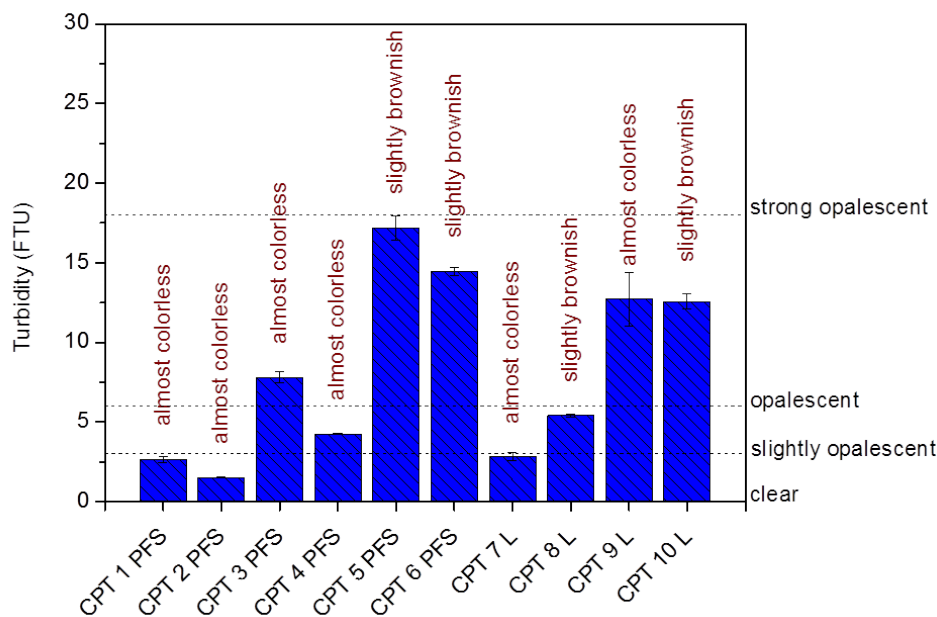
Figure 1.1: Turbidity and color of the investigated products. Measurements were performed as triplicates. The average and standard deviation of the mean are reported. (PFS = prefilled syringe; L = lyophilisate)

and $\geq 25\,\mu$m measured by light obscuration. However, in some cases it may be relevant to differentiate between silicone oil droplets and air bubbles in contrast to amorphous particles including protein aggregates given the regulatory concern on the latter being immunogenic. [21-24]

Quantification of the sub-visible particles/mL of each class was carried out with reference to the total sub-visible particle count/mL in %. However, it should be considered that the absolute amount of sub-visible particles differs among the products. Furthermore, it should be taken into account that the absolute counts of sub-visible particles measured by light obscuration cannot be directly compared to the absolute count obtained by digital fluid imaging, as translucent and irregular shaped particles might be missed by the light obscuration method.

Monomer content, soluble aggregates, and fragments

Monomer, soluble aggregates, and fragments were analyzed by size exclusion chromatography using a generic method for all products. Species were classified into monomer, low molecular weights consisting of fragmentation and degradation products, and high molecular weights comprising dimers and higher soluble oligomers. Table 1.5 shows the monomer content, low molecular weights, and high molecular weights for each product. The relative peak area of monomers as the active ingredient varied between 95.8 $\pm$0.1 (CPT 7 L) and 99.8 $\pm$<0.1% (CPT 4 PFS, CPT 8 L). Dimers and higher soluble oligomers are present to a very low extent in all products (0.2 $\pm$<0.1% for CPT 4 PFS, CPT 5 PFS, and CPT 8 L to 2.3 $\pm$<0.1% for CPT 3 PFS) and fragmentation and degradation product levels are even lower (<0.1 $\pm$0.1% for CPT 1 PFS, CPT 2 PFS, CPT 4 PFS, CPT 5 PFS, CPT 8 L and CPT 10 L to 2.6 $\pm$0.1% for CPT 7 L). Figure 1.4 shows the chromatogram of CPT 1 and CPT 3 as a representative example.
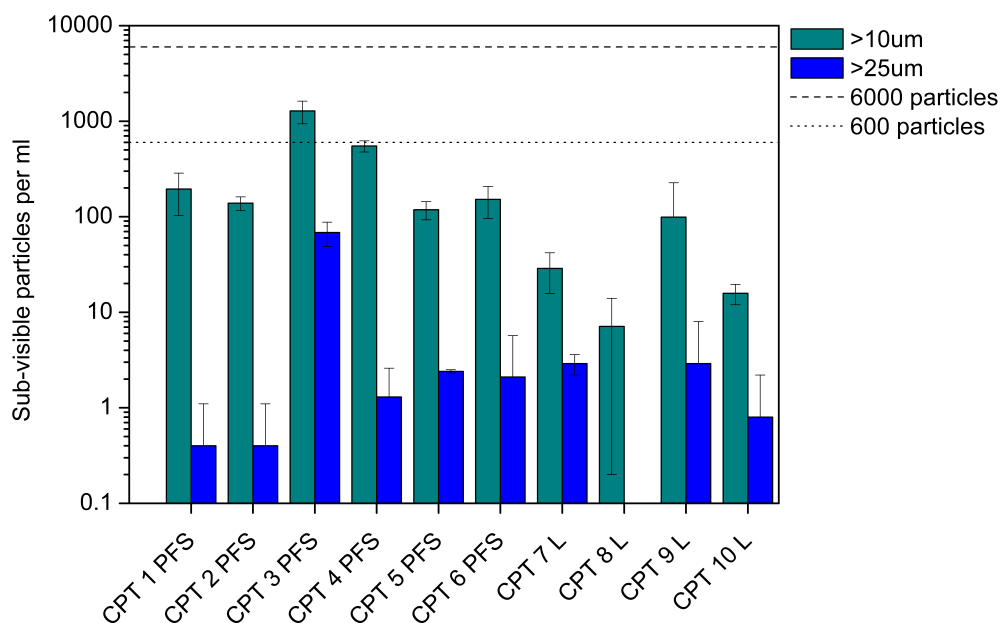
Figure 1.2: Sub-visible particles $\geq 10\,\mu$m and $\geq 25\,\mu$m measured by light obscuration. Sub-visible particles are presented as cumulative counts/mL. Measurements were performed as triplicates. The average and standard deviation of the mean are reported. The dotted line represents the threshold defined by the European Pharmacopeia per container for particles $\geq 10\,\mu$m (6000 counts) and $\geq 25\,\mu$m (600 counts). The data is also summarized in Table 1.3 including particle sizes $\geq 2\,\mu$m, $\geq 5\,\mu$m, and $\geq 50\,\mu$m. (PFS = prefilled syringe; L = lyophilisate)

pH, isoelectric point, and osmolality

The pH value and the isoelectric point of the investigated products are reported in Table 1.6. The isoelectric point was determined by isoelectric focusing. The pH values lie between 4.7 $\pm<$0.1 (CPT 2 PFS) and 7.4 $\pm$0.1 (CPT 7 L). The isoelectric points varied between 5.2 $\pm<$0.1 (CPT 3 PFS/L) and 9.2 $\pm<$0.1 (CPT 6 PFS). The isoelectric point of CPT 8 L, CPT 9 L, and CPT 10 L was not determined. Based on these results, the difference between the isoelectric point and the pH value was calculated. The biggest difference was found for CPT 2 PFS, with 3.6 units, and the smallest was found for CPT 3 PFS with a formulation pH of only 1 unit away from the isoelectric point. The consideration of the difference between the formulation pH and the isoelectric point of the active ingredient is essential as proteins may aggregate close to the isoelectric point due to lack of repulsive charges. [25] Nevertheless, it is crucial to find a compromise for the pH of the formulation to increase physical as well as chemical stability and take into account physiological compatibility at the same time. Thereby, a formulation pH far below or above isohydric conditions (pH 7.4) may lead to pain during injection or to damage of endothelial tissue. [26-29] However, during intravenous injection, pain was only reported at pH values exceeding 10.5 (11) and below a pH of 3 (4). For other extravascular routes such as intramuscular or subcutaneous injection,

Product	$\geq 2\,\mu$m	$\geq 5\,\mu$m	$\geq 10\,\mu$m	$\geq 25\,\mu$m	$\geq 50\,\mu$m
CPT 1 PFS	6861 ±809	1495 ±339	195 ±92	0 ±1	0 ±<1
CPT 2 PFS	2439 ±361	500 ±24	139 ±23	0 ±1	0 ±<1
CPT 3 PFS	25128 ±1931	6329 ±1023	1280 ±340	65 ±19	3 ±1
CPT 4 PFS	18881 ±265	4460 ±220	550 ±73	1 ±1	0 ±<1
CPT 5 PFS	4478 ±486	1220 ±91	118 ±26	2 ±1	1 ±1
CPT 6 PFS	11535 ±1740	1442 ±137	152 ±56	2 ±4	0 ±<1
CPT 7 L	2091 ±1453	353 ±225	29 ±13	3 ±<1	0 ±1
CPT 8 L	664 ±191	59 ±12	7 ±7	0 ±<1	0 ±<1
CPT 9 L	13081 ±3035	1122 ±581	99 ±128	3 ±5	0 ±<1
CPT 10 L	4692 ±726	385 ±73	16 ±4	0 ±1	0 ±1

Table 1.3: Sub-visible particles $\geq 2\,\mu$m, $\geq 5\,\mu$m, $\geq 10\,\mu$m, $\geq 25\,\mu$m, and $\geq 50\,\mu$m measured by light obscuration. Sub-visible particles are presented as cumulative counts/mL. Measurements were performed as triplicates. The average and standard deviation of the mean (sd) are reported. (PFS = prefilled syringe; L = lyophilisate)

the range is even smaller with approximately a pH of 4 up to 9. Tolerance maxima are reached at a pH of 2 and 13, respectively. [26, 27, 30] Even more important than the pH value itself is the buffer capacity of the formulation. If the buffer capacity of the formulation is much higher than the one of the human blood system (carbonate, phosphate, hemoglobin, and albumin buffer), the formulation cannot be neutralized by the intrinsic buffer system. This may lead to disruption of the pH homoeostasis and among others to damage of the endothelial tissue as outlined.

The osmolality was measured by freezing point depression and is summarized in Table 1.6. The osmolality of the products was determined between 295 ±<0.1 (CPT 7 L) and 466 ±7.6 mOsm/kg (CPT 9 L). However, cryoscopic artifacts may occur during freezing point depression measurements due to high viscosity or suspended particles. [31, 32] For this reason, the osmolality of CPT 2 PFS was determined additionally by vapor pressure elevation as it showed elevated viscosity of 102.3 ±0.7 mPas during viscosity characterization. The osmolality of CPT 2 PFS was found as 451 ±4.0 mOsm/kg measured by freezing point depression and only 334 ±1.5 mOsm/kg by vapor pressure elevation. This indicates that cryoscopic artifacts influence the result during measurement of freezing point depression for the product CPT 2. Parentally administered pharmaceuticals are tried to be formulated close to isotonic conditions corresponding to an osmolality of 295 mOsm/kg. Formulations below or above these conditions may lead to pain during injection and even tissue damage may occur. However, pain was only reported during intravenous injection if osmolality exceeded 3 Osm/kg. [26-29]

Dynamic viscosity

Dynamic viscosity of the products was measured by plate/cone rheometry at 5°C, 10°C, 15°C, 20°C, and 25°C and is reported in Table 1.7. The viscosity of CPT 7 L, CPT 8 L, and CPT 10 L was only measured at 20°C due to sample shortage. Dynamic viscosity of the products was found to lie between
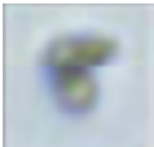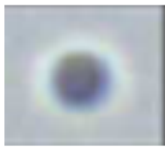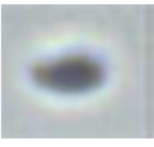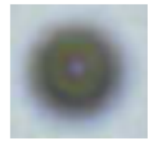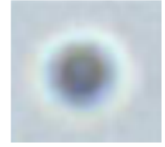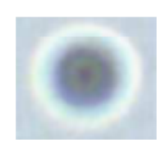
Product	Amor-phous	Silicone oil	Air bubble	Unidentified
CPT 1 PFS				
CPT 2 PFS				
CPT 3 PFS				
CPT 4 PFS				
CPT 5 PFS				
CPT 6 PFS				

Table 1.4: Representative pictures of sub-visible particles of the products purchased as prefilled syringes (PFS) measured by digital fluid imaging. The sub-visible particles were classified into silicone oil droplets, air bubbles, unidentified particles, and amorphous particles (size range of examples $15 - 25\,\mu$m).
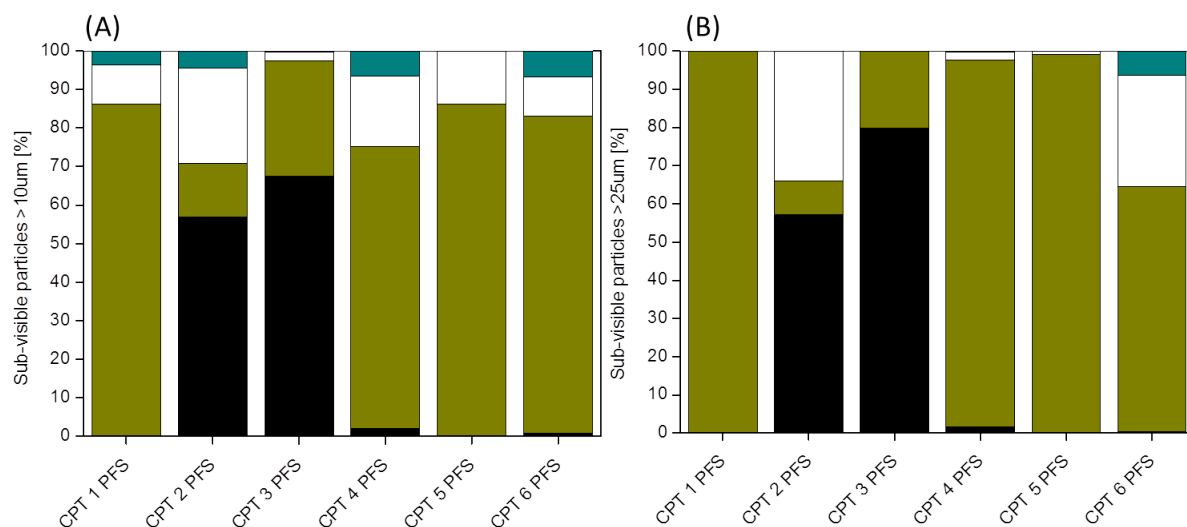
Figure 1.3: Characterization of sub-visible particles of the products purchased as prefilled syringes measured by digital fluid imaging. Sub-visible particles are classified into 4 classes with either a particle size of (A) $\geq 10\,\mu$m or (B) $\geq 25\,\mu$m: amorphous sub-visible particles including protein aggregates (black), silicone oil droplets (green), air bubbles (white), and unidentified particles (blue). Quantification of the sub-visible particles/mL of each class was carried out with reference to the total sub-visible particle count/mL in %. Measurements were performed as triplicates and the average is reported. (PFS = prefilled syringe)

1.6 $\pm$<0.1 (CPT 5 PFS) and 10.8 $\pm$0.2 mPas (CPT 6 PFS) measured at 20°C. Two products showed elevated viscosity with 102.3 $\pm$0.7 mPas (CPT 2 PFS) and 86.4 $\pm$4.1 mPas (CPT 10 L).

 Table 1.7 shows that the viscosity is temperature dependent with increasing viscosity at lower temperatures. This temperature dependence is of great importance as an increase in temperature and therefore decrease in viscosity can be used to facilitate manufacturing of the product (filtering, pumping) if product stability is warranted. [33] Furthermore, during storage of the product at 2 to 8°C, the product has a higher viscosity compared to its viscosity at room temperature. As injection forces are directly dependent on viscosity, lower viscosities are desired to reduce injection forces and facilitate injection. This is one of the reasons why the product should be equilibrated to the desired target temperature before administration according to the related instructions.

 Figure 1.5 shows the dynamic viscosity as a function of shear rate between 100 and 2000 s^{-1} for CPT 10 L and CPT 3 PFS as representative example. CPT 3 PFS showed constant viscosity over the whole shear rate range indicating Newtonian behavior. The other products exhibited this behavior, too. CPT 10 in the contrary showed reversible shear thinning when the shear rate was increased/decreased to/from 2000 s^{-1}.

During drug administration, shear rates in the range of 100 000 – 200 000 s^{-1} depending on the inner diameter of the needle may occur. [34, 35] If fluids exhibit non-Newtonian flow behavior at high shear rates, this may lead to reduced forces during injection compared to solutions with Newtonian flow behavior. However, further experiments have to be performed to confirm the rheological behavior of the products at these shear rates which is subject of ongoing research.

Product	Monomer [%]±sd	HMW [%]±sd	LMW [%]±sd
CPT 1 PFS	99.4 ±<0.1	0.6 ±<0.1	<0.1 ±<0.1
CPT 2 PFS	98.3 ±0.2	1.7 ±0.2	<0.1 ±<0.1
CPT 3 PFS	96.4 ±0.1	2.3 ±<0.1	1.3 ±0.1
CPT 4 PFS	99.8 ±<0.1	0.2 ±<0.1	<0.1 ±<0.1
CPT 5 PFS	99.7 ±<0.1	0.2 ±<0.1	<0.1 ±<0.1
CPT 6 PFS	99.4 ±<0.1	0.6 ±<0.1	0.1 ±<0.1
CPT 7 L	95.8 ±0.1	1.6 ±<0.1	2.6 ±0.1
CPT 8 L	99.8 ±<0.1	0.2 ±<0.1	<0.1 ±<0.1
CPT 9 L	99.5 ±0.1	0.5 ±0.1	0.4 ±<0.1
CPT 10 L	99.6 ±0.1	0.4 ±<0.1	<0.1 ±<0.1

Table 1.5: Soluble species measured by SE-HPLC. They were classified as monomer, high molecular weights (HMW) and low molecular weights (LMW). The percentage of peak area relative to the total peak area is reported. Measurements were performed as triplicates. The average and standard deviation of the mean are reported. (PFS = prefilled syringe; L = lyophilisate)

Injectability and removal of needle cover

Injectability of the products into air was tested with a generic device system to compare liquid formulations as well as the lyophilisates. The injection force can be differentiated into the break loose force of the plunger and the subsequent glide force. In our experiment, the maximal injection force at 25°C was determined and was found to correspond to the glide force for all products. The data are presented in Table 1.8. The glide force at a volumetric flow of 1 mL/10 s lie between 3.1 ±0.1 N (CPT 1 PFS) and 21.9 ±0.5 N (CPT 10 L). For CPT 2 PFS, the injection force through a 27 G needle could not be determined without damage of the system due to its highly viscous content. By replacing the 27 G needle with a 25 G needle, which is the needle diameter used for the original PFS, the maximum force was reduced and the glide force determined as 10.7 ±1.2 N.

To evaluate forces experienced by the patient during the application process, injection forces were analyzed by use of the original primary container as well as forces to remove the needle cover, also known as rigid needle shield (RNS). The corresponding data are summarized in Table 1.8. The glide force varied between 3.7 ±0.1 N (CPT 5 PFS) and 39.9 ±1.8 N (CPT 2 PFS) at a volumetric flow of 0.5 mL/10 s. This flow, which is smaller than the one used for the generic set-up, was chosen to ensure that the forces from all prefilled syringes could be compared including CPT 2 PFS. The constant test speed was chosen for standardized injection although not entirely representing end-user behavior as patients are known to make speed compensation based upon resistive force, capability, and own preference.

The maximal force to remove the needle cover was found between 5.4 ±1.2 N (CPT 4 PFS) and 15.8 ±2.1 N (CPT 6 PFS). As an example, Figure 1.6 shows the injection force profile into air for CPT 3 PFS as a function of distance (A) and the force profile of the removal of the needle cover for CPT 1 PFS (B). In the injection force profile, the force was differentiated into the break loose and the glide force.
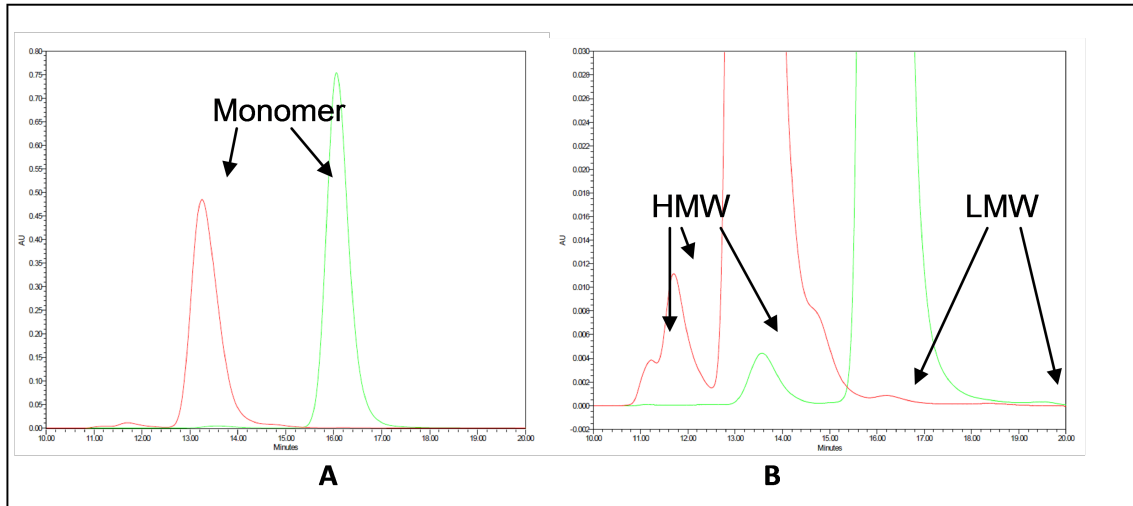
Figure 1.4: Representative chromatogram of CPT 3 PFS (red) and CPT 1 PFS (green) measured by SE-HPLC. Species were classified as monomer, high molecular weights (HMW) and low molecular weights (LMW). (A) unzoomed (B) zoomed in. (PFS = prefilled syringe)
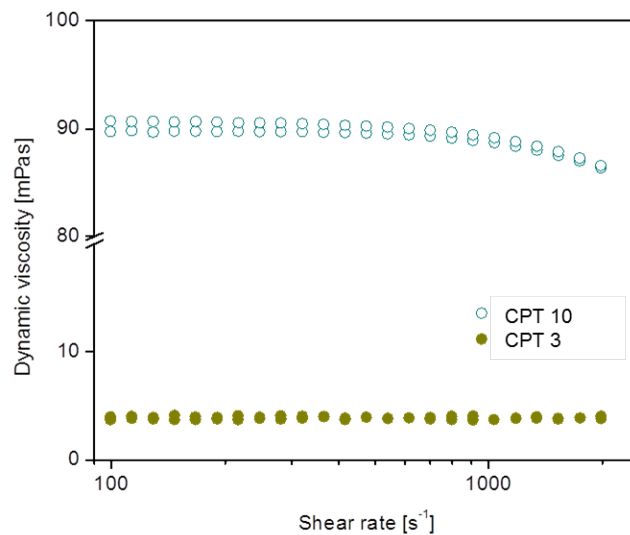
Figure 1.5: Dynamic viscosity as a function of shear rate at 20°C. CPT 3 PFS shows Newtonian behavior with a constant viscosity; CPT 10 L shows reversible shear thinning (Non-Newtonian behavior) with increasing shear rate to $2000\,\mathrm{s}^{-1}$. (PFS = prefilled syringe; L = lyophilisate)

Product	pH ±sd	Isoelectric point ±sd	Difference between pH and isoelectric point	Osmolality [mOsm/kg] ±sd (Freezing point)
CPT 1 PFS	5.2 ±<0.1	8.1 ±0.1	2.9	311.3 ±1.5
CPT 2 PFS	4.7 ±<0.1	8.3 ±0.1	3.6	451.7 ±4.0 (Vapor pressure: 334.0 ±1.5)
CPT 3 PFS	6.2 ±<0.1	5.2 ±<0.1	-1.0	311.7 ±0.6
CPT 4 PFS	5.6 ±<0.1	8.5 ±<0.1	2.9	295.0 ±<0.1
CPT 5 PFS	5.2 ±<0.1	8.3 ±0.1	3.1	307.0 ±1.0
CPT 6 PFS	6.1 ±<0.1	9.2 ±0.1	3.1	312.3 ±4.7
CPT 7 L	7.4 ±0.1	5.2 ±<0.1	-2.2	273.7 ±8.5
CPT 8 L	6.1 ±<0.1	-	-	366.0 ±7.0
CPT 9 L	6.1 ±<0.1	-	-	466.0 ±7.6
CPT 10 L	6.2 ±<0.1	-	-	374.7 ±7.4

Table 1.6: pH, isoelectric point, difference between pH and isoelectric point, and osmolality of the investigated products. Measurements were performed as triplicates. The average and standard deviation of the mean are reported. (PFS = prefilled syringe; L = lyophilisate).

Device charaterization

Picture 1 to 6 shows the primary packaging of the liquid formulations provided as pre-filled syringes. Cimzia PFS, Enbrel PFS, and Humira PFS show a special accessory attached to the prefilled syringe. This accessory supports the index and the middle finger to facilitate injection. Simponi PFS and Prolia PFS consist of the prefilled syringe and a safety device that covers the needle after injection. Cimzia PFS shows additionally a special ring-shaped needle cover that simplifies preparation of the device which facilitates injection for patients with rheumatoid arthritis (indication of Cimzia) with limited mobility. [36]

Picture 2 shows the autoinjectors of Enbrel, Simponi, and Humira being even more appealing/convenient to the patient compared to prefilled syringes. For autoinjectors, the injection process is initiated by a mechanical process driven by a strained spring. Interestingly, the activation button of Simponi Smartject® is located at the side of the autoinjector compared to the other two devices having the activation button on the top. Therefore, the Smartject® autoinjector uses the grip force for activation which is higher than the force exerted solely by the thumb.

The injection forces are influenced by different parameters. These are besides the product viscosity the inner diameter and the length of the needle, the inner diameter of the syringe, and the frictional forces occurring at the contact area between stopper and syringe barrel. The frictional forces are thereby influenced be the thickness and viscosity of the lubricant layer (silicon oil) and by the injection speed. [35] Table 1.9 summarizes the syringe and needle type/dimensions of the products. All liquid formulations are filled into 1 mL glass syringes with staked-in needle from different manufacturers (BD and Ompi). Five out of six prefilled syringes are equipped with a 27 G $\frac{1}{2}$ inch needle and only CPT 2 PFS with a 25 G $\frac{1}{2}$ inch needle.

Product	5°C	0°C	15°C	20°C	25°C
CPT 1 PFS	3.0 ±0.1	2.8 ±<0.1	2.4 ±0.1	2.0 ±0.1	1.9 ±<0.1
CPT 2 PFS	213.2 ±1.4	161.0 ±2.6	128.9 ±1.8	102.3 ±0.7	91.8 ±<0.1
CPT 3 PFS	6.4 ±0.1	5.8 ±0.1	4.7 ±0.1	3.7 ±<0.1	3.6 ±0.1
CPT 4 PFS	5.1 ±0.3	4.4 ±0.1	3.8 ± < 0.1	3.0 ±<0.1	2.9 ±<0.1
CPT 5 PFS	3.0 ±<0.1	2.4 ±<0.1	2.0 ±<0.1	1.6 ±<0.1	1.6 ±<0.1
CPT 6 PFS	16.8 ±<0.1	13.8 ±0.2	12.0 ±0.7	10.8 ±0.2	9.6 ±<0.1
CPT 7 L	-	-	-	5.4 ±0.4	-
CPT 8 L	-	-	-	3.5 ±0.1	-
CPT 9 L	4.7 ±0.2	4.4 ±0.1	3.6 ±<0.1	3.5 ±0.1	2.9 ±<0.1
CPT 10 L	-	-	-	86.4 ±4.1	-

Table 1.7: Dynamic viscosity of the investigated products (mPas) at a shear rate of $2000\,\mathrm{s}^{-1}$ at different temperatures (5°C, 10°C, 15°C, 20°C, and 25°C). Measurements were performed as triplicates. The average and standard deviation of the mean are reported. (PFS = prefilled syringe; L = lyophilisate)

As already outlined, CPT 2 showed a high viscosity of 102.3 ±0.7 mPas measured at 20°C. Therefore, it was not feasible to inject the solution through a 27 G needle. With regard to needle dimensions, it was not determined whether the needles had a normal or a thin wall. For the lyophilisates, a separate needle was included only for CPT 3 and CPT 8. These were a 27 G and 25 G $\frac{1}{2}$ inch needle, respectively. For CPT 10 L there is an explicit recommendation on the packaging insert that a 25 G needle should be used due to the high viscosity of the product.

Picture 7 shows the needle tips of the prefilled syringes investigated under the light microscope. The needle tip of CPT 1 PFS, CPT 3 PFS, CPT 4 PFS, and CPT 5 PFS was characterized to show 5 bevels; CPT 2 PFS and CPT 6 PFS are equipped with a needle of three bevels. The number of bevels may directly influence the compliance of the patient as a higher number of bevels is considered to lead to less pain during injection. [37]

A requirement by the European Pharmacopoeia is the test for extractable volume which was investigated in this study for the prefilled syringes. The European Pharmacopoeia requires in the Monograph for Extractable Volume 2.9.17. that the measured volume must be 'not less than the nominal volume'. [14] Figure 1.7 shows the measured extractable volume in comparison to the volume as written on the product. The measured extractable volume varied between 1% underfill (CPT 3 PFS and CPT 5 PFS) up to 8% overfill (CPT 4 PFS). However, there is no statistical significant difference between measured and labeled extractable volume for CPT 3 PFS and CPT 5 PFS (tested by student-t-test with $\alpha = 0.05$ and 2 degrees of freedom). If underfill occurs, the question arises if the target dose can be provided to the patient. An overfill on the other side might be a severe safety issue. However, this depends on the safety data.
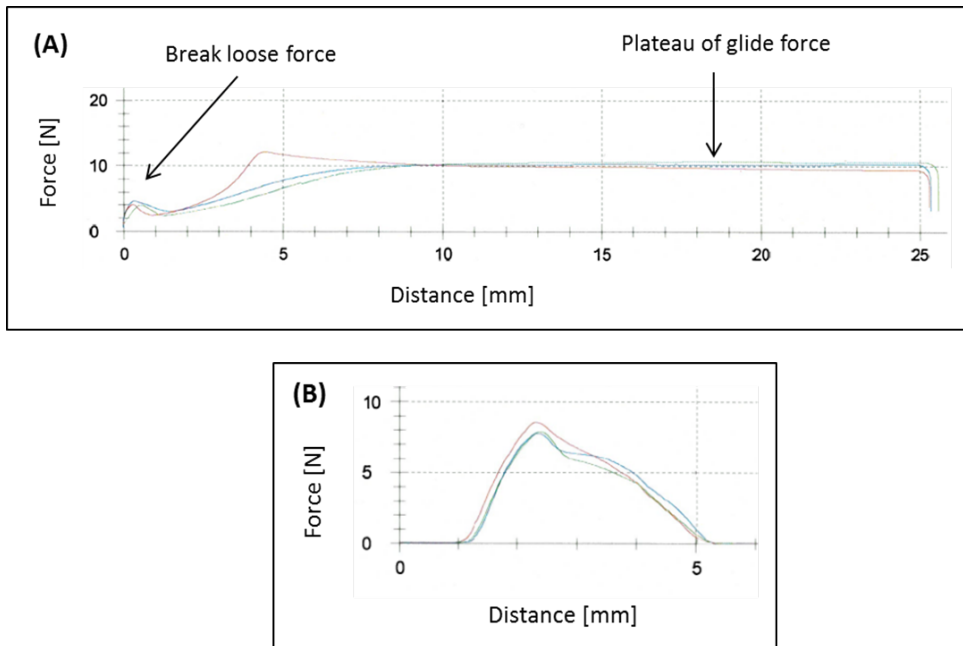
Figure 1.6: (A) Injection force profile into air for CPT 3 PFS as a function of distance with differentiation into break loose and glide force. (B) Force profile of the removal of the needle cover of CPT 1 PFS as a function of distance. Measurements were performed and reported as triplicates.
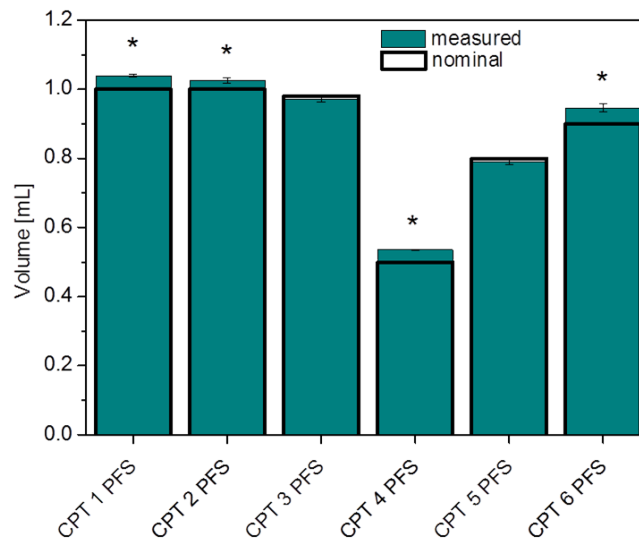
Figure 1.7: Measured and nominal extractable volume for prefilled syringes (PFS). Measurements were performed as triplicates and the average and standard deviation of the mean are reported. * = Statistical significant difference between measured and nominal extractable volume tested by student-t-test (α=0.05; 2 degrees of freedom).

Product	Generic set-up: Glide force ±sd [N] (1 mL/10 s)	Original primary container: Glide force ±sd [N] (0.5 mL/10 s)	Force needed to remove needle cover ±sd [N]
CPT 1 PFS	3.1 ±0.1	11.0 ±6.1	8.1 ±0.4
CPT 2 PFS	27 G: - 25 G: 10.77 ±1.2	39.9 ±1.8	10.8 ±0.5
CPT 3 PFS	4.3 ±0.3	11.0 ±0.9	12.0 ±8.2
CPT 4 PFS	4.1 ±0.2	13.1 ±4.8	5.4 ±1.2
CPT 5 PFS	3.7 ±0.8	3.7 ±0.1	10.3 ±2.2
CPT 6 PFS	7.6 ±1.6	24.0 ±2.0	15.8 ±2.1
CPT 7 L	5.3 ±<0.1	-	-
CPT 8 L	5.2 ±0.4	-	-
CPT 9 L	3.8 ±0.6	-	-
CPT 10 L	21.9 ±0.5	-	-

Table 1.8: Glide force of injection into air from a generic device system and from the original primary container and maximal force needed to remove the needle cover of the prefilled syringes. Measurements were performed as triplicates. The average and standard deviation of the mean (sd) are reported. (PFS = prefilled syringe; L = lyophilisate)

Information on the administration process

Information on correct preparation and handling of the product and device is compiled in the Summary of Product Characteristics (SPC) and the Patient Information leaflets (PIL) to provide guidance for safe and complete administration of the product. Important data are summarized in Table 1.9: Before administration, autoinjectors must be equilibrated to room temperature between 15 and 30 minutes in advance (see Table 1.9). For three out of five prefilled syringes, an equilibration time between 15 and 30 minutes is proposed in the packaging insert. For the remaining two products (CPT 1 PFS, CPT 5 PFS), there is no recommendation. For lyophilisates, a reconstitution time between 5 minutes (CPT 8 L) and >20 minutes (CPT 10 L) is recommended. In Figure 1.8, the measured reconstitution times were compared to the recommended reconstitution times and were found to vary between 1:25 ±0:16 min:s (CPT 9 L) and 15:25 ±3:37 min:s (CPT 10 L). The difference between measured and recommended reconstitution time in general may account for product variability. As an example, the recommended reconstitution time for CPT 9 was 20 minutes. Compared to the measured time of 1:25 ±0:16 min:s, the recommended reconstitution time exceeded the measured one by more than 18 minutes.

After equilibration of the pre-filled syringes or autoinjector, correct handling of the device during the administration process is crucial. This includes preparation of the autoinjector before administration with either unlocking of the safety interlock (CPT 3 and CPT 4), or removal of an extra cap from the activation button to avoid pre-activation (CPT 5).

Table 1.9 summarizes the recommended injection times for the prefilled syringes as recommended in the packaging insert and the waiting time after activation for the autoinjectors: for CPT 5 PFS, the injection

Product	Syringe and needle type/dimension	Head space ±sd [mm]	PFS/AI: Recom. room equilibration time	PFS: Recom. injection time AI: Recom. holding time after activation	PFS: Safety device AI: 1. Safety interlock 2. Needle retraction 3. Needle shield after injection
CPT 1 PFS	BD syringe 1 mL; 27 G 5B 1/2 inch staked-in needle	1.86 ±<0.1	not labeled	until activation of needle shield	PFS: ✔
CPT 2 PFS	BD syringe 1 mL with scaled syringe; 25 G 3B 1/2 inch staked-in needle	5.61 ±0.2	30 min	up to 10 s	PFS: X
CPT 3 PFS and AI	BD syringe 1 mL; 27 G 5B 1/2 inch staked-in needle	4.56 ±0.3	PFS/AI: 15-30 min	PFS: not labeled AI: 10 s or 2nd click	PFS: X AI: 1. and 3. ✔ 2. X
CPT 4 PFS and AI	1 mL syringe; 27 G 5B 1/2 inch staked-in needle	3.70 ±0.1	PFS/AI: 30 min	PFS: until activation of needle shield AI: 2nd click $(3-15s)$	PFS: X AI: 1. – 3. ✔
CPT 5 PFS and AI	BD syringe 1 mL; 27 G 5B 1/2 inch staked-in needle	5.87 ±0.2	PFS: not labeled AI: $15-20$ min	PFS: $2-5$ s AI: 10 s	PFS: X AI: 1. ✔ 2. X 3. ✔
CPT 6 PFS and AI	Ompi syringe 1 mL; 27 G 3B 1/2 inch staked-in needle	3.41 ±0.2	$25-30$ min	(product not yet approved)	PFS: ✔
CPT 7 L	27 G ½ inch needle included	nd	-	-	-
CPT 8 L	25 G ½ inch needle included	nd	-	-	-
CPT 9 L	No recommendation	nd	-	-	-
CPT 10 L	Recommended: 25 G needle	nd	-	-	-

Table 1.9: Device characteristics and information on the administration process including syringe and needle type/dimensions, head space of prefilled syringes (PFS) (N = 3), recommended (recom.) room equilibration time for PFS and autoinjectors (AI), recom. injection time (PFS), recom. holding time after activation (AI) and information on the safety of the device. For triplicates, the average and standard deviation of the mean (sd) are reported. (nd = not determined)
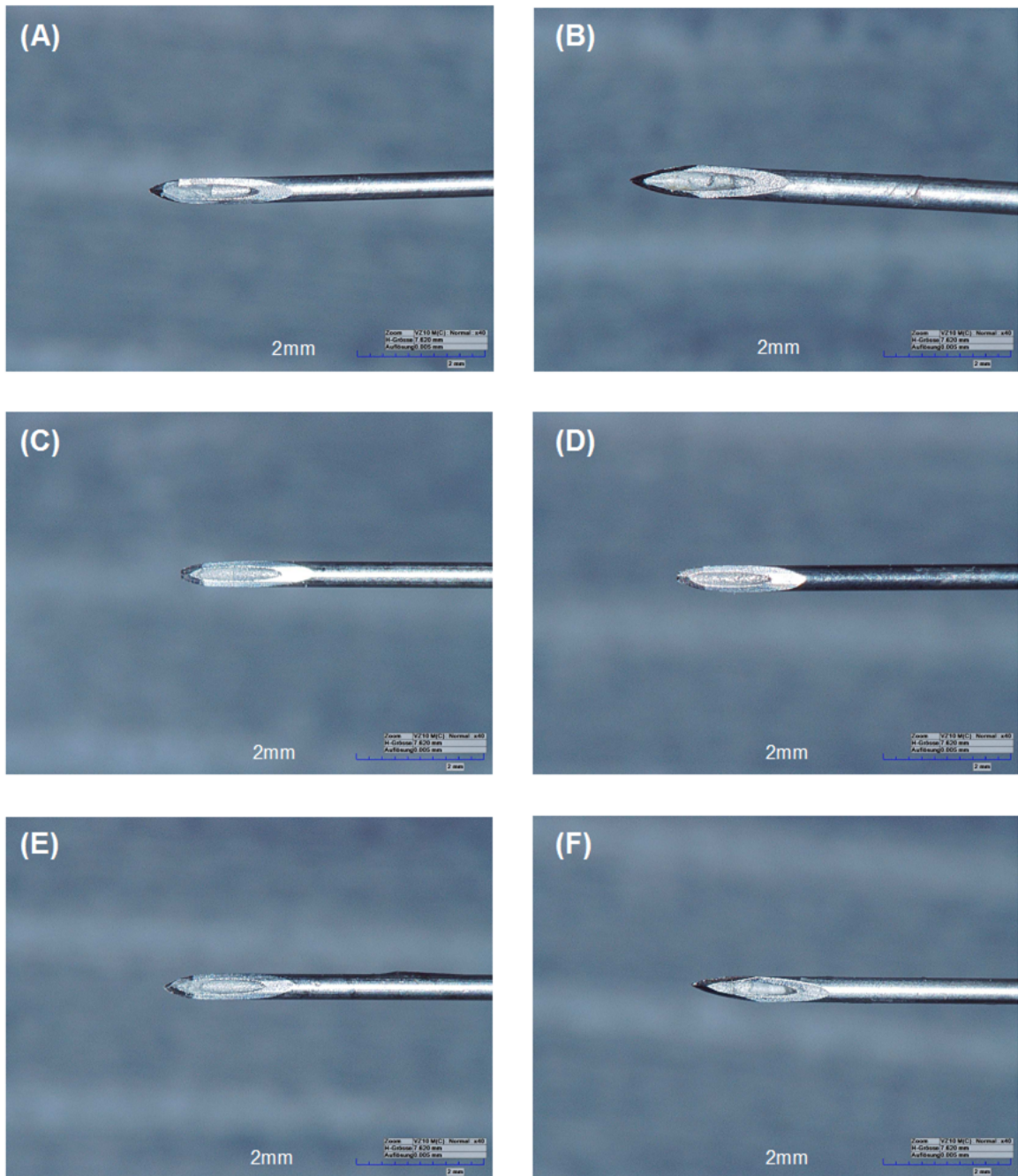
Picture 7: Needle tips of (A) CPT 1 PFS, (B) CPT 2 PFS, (C) CPT 3 PFS, (D) CPT 4 PFS, (E) CPT 5 PFS, and (F) CPT 6 PFS. (PFS = prefilled syringe)
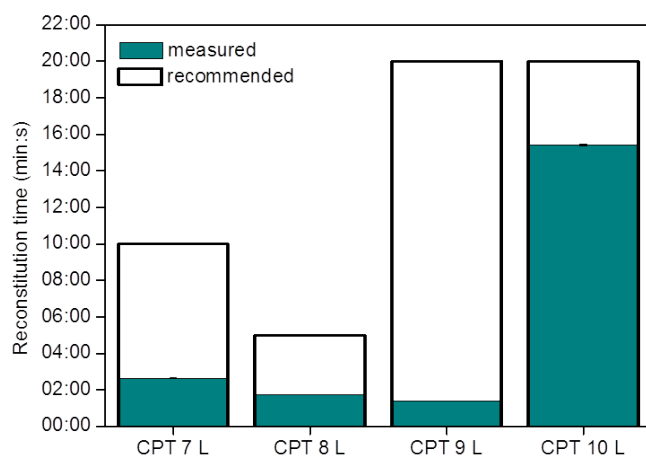
Figure 1.8: Measured and recommended reconstitution time for lyophilisates (L). Measurements were performed as triplicates and average and standard deviation of the mean are reported.
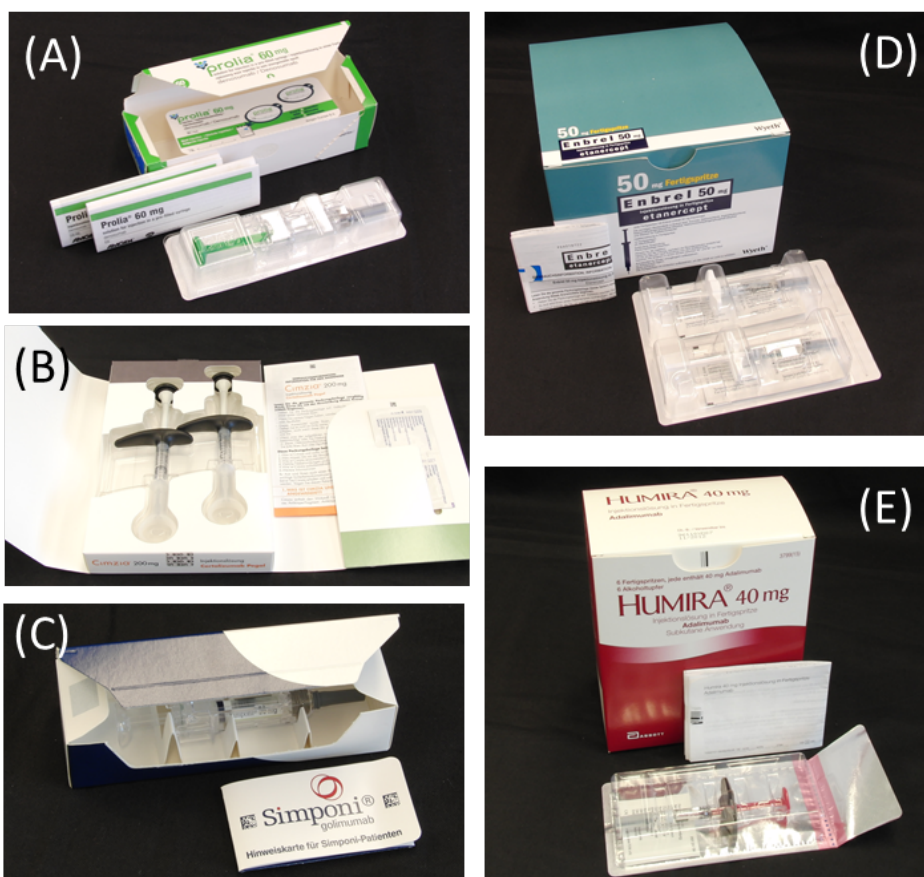
Figure 1.9: Secondary packaging of marketed products obtained as prefilled syringes (PFS). (A) Prolia, (B) Cimzia, (C) Simponi, (D) Enbrel, (E) Humira.

time is recommended as 2 s and for CPT 2 PFS up to 10 s. For CPT 1 PFS and CPT 4 PFS, the injection time is defined until activation of the needle shield, and for CPT 3 PFS it is not recommended at all. For CPT 6 PFS, the data is not included in Table 1.9 as it is subject of ongoing discussion with the health authorities. For the three investigated autoinjectors, the holding time after activation varies between 3 and 15 s.

Two additional features of the autoinjector ensure the correct application of the product. These are an audible signal (click) at the beginning of injection for CPT 3, CPT 4 and CPT 5 and a second click after completed injection (CPT 3 and CPT 4). Additionally, a visual signal indicates the complete administration of the product by a color change seen through the control window for all three autoinjectors.

The injection angle is recommended as 90°C for all autoinjectors and 45°C for the prefilled syringes except of CPT 3 PFS (45–90°C) and CPT 1 PFS (without any recommendation). The injection sites for the sc administered products are the top of the thigh, the lower part of the abdomen, and the outer areas of the upper arms (the latter solely for CPT 5 PFS and CPT 2 PFS). For the prefilled syringes, injection into a skin fold is recommended whereas for the autoinjectors it is not required to inject into a pinched skin fold (excluding CPT 5 PFS). For the lyophilisates, the manufacturers do not provide injection time, angle, or give recommendation to inject into a skin fold. These products are typically administered by a healthcare professional. Three out of five prefilled syringes exhibit a safety device that covers the needle after injection (CPT 1 PFS, CPT 4 PFS, and CPT 6 PFS) for safe handling and disposal of the syringes after administration. This is also a FDA requirement in the US. All of the investigated autoinjectors cover the needle after administration, and CPT 4 AI even retracts the needle after a completed injection (see Table 1.9).

Secondary packaging of prefilled syringes

Figure 1.9 shows the pictures of the secondary packaging for each product. The secondary packaging of the prefilled syringes consisted either of a simple folding box (B,C) or the syringe was additionally enclosed in a blister (A, D, E). It was not tested if water vapor can penetrate the blister. However, blister - which are impermeable for water vapor - might protect the product additionally from environmental changes such as a decrease in humidity or evaporation, and could prevent drying of the product.

1.5   Conclusion

This study provides an overview of commercial highly concentrated biotech products and summarizes requirements defined by the European Pharmacopoeia. In total, ten commercial protein therapeutics were characterized which are currently approved by the EMA.

1.6   Acknowledgment

Special thanks goes to Robert Mueller, for providing his previously collected raw data on the characterization of the lyophilisates CPT 10®, CPT 3®, CPT 9®, and CPT 8®. [38]

1.7 References

1. EUROPEAN.COMMISSION. http://ec.europa.eu/health/documents/community-register/html/. [cited 2011 25. August].

2. Walsh, G., Biopharmaceutical benchmarks 2010. Nat Biotechnol, 2010. 28(9): p. 917-924.

3. Ph.Eur., 2.2.1. Clarity and degree of opalescence of liquids, in European Pharmacopoeia 7th edition 2012 (7.3), European Directorate for the Quality of Medicines and Healthcare of the Council of Europe.

4. Ph.Eur., 2.2.2. Degree of coloration of liquids, in European Pharmacopoeia 7th edition 2012 (7.3), European Directorate for the Quality of Medicines and Healthcare of the Council of Europe.

5. Ph.Eur., 2.2.35. Osmolality, in European Pharmacopoeia 7th edition 2012 (7.3), European Directorate for the Quality of Medicines and Healthcare of the Council of Europe.

6. Ph.Eur., 2.2.1. Clarity and degree of opalescence of liquids, in European Pharmacopoeia 7th edition 2012 (7.3)2012, European Directorate for the Quality of Medicines and Healthcare of the Council of Europe.

7. Ph.Eur., 2.9.19. Particulate Contamination: Sub-visible particles, in European Pharmacopoeia 7th edition 2012 (7.3), European Directorate for the Quality of Medicines and Healthcare of the Council of Europe.

8. Ph.Eur., 2.9.20. Particulate contamination: visible particles, in European Pharmacopoeia 7th edition 2012 (7.3), European Directorate for the Quality of Medicines and Healthcare of the Council of Europe.

9. Ph.Eur., 2.9.17. Test for extractable volume of parenteral preparations, in European Pharmacopoeia 7th edition 2012 (7.3), European Directorate for the Quality of Medicines and Healthcare of the Council of Europe.

10. Ph.Eur., Monograph of Parenteral preparations, in European Pharmacopoeia 7th edition 2012 (7.3), European Directorate for the Quality of Medicines and Healthcare of the Council of Europe.

11. EMEA/CHMP/20857/2009 European Medicines Agency Press office: PRESS RELEASE: European Medicines Agency recommends suspension of the marketing authorisation of Raptiva (efalizumab), London 2009.

12. Ph.Eur., 2.9.20. Particulate contamination: visible particles, in European Pharmacopoeia 7th edition 2012 (7.3), European Directorate for the Quality of Medicines and Healthcare of the Council of Europe.

13. Ph.Eur., 2.9.19. Particulate Contamination: Sub-visible particles, in European Pharmacopoeia 7th edition 2012 (7.3), European Directorate for the Quality of Medicines and Healthcare of the Council of Europe.

14. Ph.Eur., 2.9.17. Test for extractable volume of parenteral preparations, in European Pharmacopoeia 7th edition 2012 (7.3), European Directorate for the Quality of Medicines and Healthcare of the Council of Europe.

15. Ph.Eur., Monograph of Monoclonal antibodies for human use, in European Pharmacopoeia 7th edition 2012 (7.3), European Directorate for the Quality of Medicines and Healthcare of the Council of Europe.

16. Blackwell, H.R., Contrast thresholds of the human eye. J Opt Soc Am, 1946. 36(11): p. 624-43.

17. Mahler, H.C., *et al.*, Protein Aggregation: Pathways, Induction Factors and Analysis. J Pharm Sci, 2009. 98(9): p. 2909-2934.

18. Salinas, B.A., *et al.*, Understanding and Modulating Opalescence and Viscosity in a Monoclonal Antibody Formulation. J Pharm Sci, 2010. 99(1): p. 82-93.

19. Sukumar, M., *et al.*, Opalescent appearance of an IgG1 antibody at high concentrations and its relationship to noncovalent association. Pharm Res, 2004. 21(7): p. 1087-93.

20. Wang, N., *et al.*, Opalescence of an IgG1 Monoclonal Antibody Formulation is Mediated by Ionic Strength and Excipients. Biopharm International, 2009. 22(4): p. 36-47.

21. Buttel, I.C., *et al.*, Taking immunogenicity assessment of therapeutic proteins to the next level. Biologicals, 2011. 39(2): p. 100-109.

22. Fradkin, A.H., J.F. Carpenter, and T.W. Randolph, Immunogenicity of Aggregates of Recombinant Human Growth Hormone in Mouse Models. J Pharm Sci, 2009. 98(9): p. 3247-3264.

23. Hermeling, S., *et al.*, Structure-Immunogenicity Relationships of Therapeutic Proteins. Pharm Res, 2004. 21(6): p. 897-903.

24. Rosenberg, A., Effects of Protein Aggregates: An Immunologic Perspective. AAPS Journal, 2006. 8(3): p. 501-508.

25. Cleland, J.L., M.F. Powell, and S.J. Shire, The Development of Stable Protein Formulations - a Close Look at Protein Aggregation, Deamidation, and Oxidation. Critical Reviews in Therapeutic Drug Carrier Systems, 1993. 10(4): p. 307-377.

26. Voigt, R., Pharmazeutische Technologie: Kapitel 20.5.4. Isohydrische Lösungen. 10th edition, Deutscher Apotheker Verlag, Stuttgartd (2006).

27. Klement, W. and J.O. Arndt, Pain on Iv Injection of Some Anesthetic Agents Is Evoked by the Unphysio-logical Osmolality or Ph of Their Formulations. Brit J Anaesth, 1991. 66(2): p. 189-195.

28. Brazeau, G.A., *et al.*, Current perspectives on pain upon injection of drugs. J Pharm Sci, 1998. 87(6): p. 667-677.

29. Gatlin, L.A. and C.B. Gatlin, Formulation and administration techniques to minimize injection pain and tissue damage associated with parenteral products, in Injectable drug development - Techniques to reduce pain and irritation, P.K.G. PK and G.A. Brazeau, Editors, Interpharm Press: Denver, Colorado (1999) p. 401-421.

30. Bauer, K., Lehrbuch der pharmazeutischen Technologie: Kapitel 9 Parenteralia. 8th edition, Wissenschaftliche Verlagsgesellschaft mbH, Stuttgart (2006).

31. EliTechGroup. Vapro 5600: Vapor Pressure Osmometer, http://www.wescor.com/biomedical/osmometer/vapro5600.html [cited 2011 15. August].

32. Winzor, D.J., Reappraisal of disparities between osmolality estimates by freezing point depression and vapor pressure deficit methods. Biophys Chem, 2004. 107(3): p. 317-323.

33. Winter, C., US Patent: Process for concentration of antibodies and therapeutic products., in US20090214522 A12009: USA.

34. Rathore, N., *et al.*, Characterization of protein rheology and delivery forces for combination products. J Pharm Sci, 2012. 101(12): p. 4472-80.

35. Rathore, N., *et al.*, Variability in syringe components and its impact on functionality of delivery systems. PDA J Pharm Sci Technol, 2011. 65(5): p. 468-80.

36. Sheikhzadeh, A., *et al.*, The effect of a new syringe design on the ability of rheumatoid arthritis patients to inject a biological medication. Appl Ergon, 2012. 43(2): p. 368-75.

37. Jaber, A., *et al.*, A novel needle for subcutaneous injection of interferon beta-1a: effect on pain in volunteers and satisfaction in patients with multiple sclerosis. Bmc Neurology, 2008. 8.

38. Mueller, R., Characterization of a High Concentration Antibody Formulation: Protein Stability and Formulation Properties. Ph.D. Thesis. , 2011, University of Halle-Wittenberg.

1.8   Appendix

	Product	Amorphous Particles	Silicone oil droplets	Air bubbles	Unidentified Particles
(A)					
	CPT 1 PFS	0.1 ±0.1	86.1 ±3.2	10.1 ±2.2	3.7 ±2.2
	CPT 2 PFS	56.9 ±9.3	13.9 ±1.1	24.7 ±11.5	4.6 ±2.8
	CPT 3 PFS	67.4 ±14.0	30.1 ±14.6	2.3 ±1.0	1.6 ±0.3
	CPT 4 PFS	2.0 ±1.8	73.1 ±5.4	18.4 ±3.4	6.7 ±2.8
	CPT 5 PFS	0.2 ±0.2	86.0 ±1.2	13.7 ±1.3	0.1 ±0.1
	CPT 6 PFS	0.9 ±1.0	82.1 ±8.0	10.3 ±3.6	7.5 ±10.4
(B)					
	CPT 1 PFS	0.3 ±0.4	99.7 ±0.5	<0.1 ±<0.1	<0.1 ±<0.1
	CPT 2 PFS	57.1 ±16.0	8.8 ±3.56	34.2 ±17.8	<0.1 ±<0.1
	CPT 3 PFS	79.9 ±14.8	22.4 ±17.8	0.3 ±0.2	<0.1 ±<0.1
	CPT 4 PFS	1.7 ±2.6	96.0 ±2.5	2.2 ±1.1	<0.1 ±<0.1
	CPT 5 PFS	0.1 ±0.2	99.1 ±0.8	0.8 ±0.7	<0.1 ±<0.1
	CPT 6 PFS	0.5 ±0.8	64.1 ±9.9	29.2 ±5.6	7.1 ±12.2

Table 1.10: Characterization of sub-visible particles of the products purchased as prefilled syringes (PFS) measured by digital fluid imaging. Sub-visible particles were classified into four subclasses with either a particle size of (A) ≥ 10 μm or (B) ≥ 25 μm: amorphous particles including protein aggregates, silicone oil droplets, air bubbles and unidentified particles. Quantification of the sub-visible particles/mL of each class was carried out with reference to the total sub-visible particle count/mL in %. Measurements were performed as triplicates. The average and standard deviation of the mean (sd) are reported.

Chapter 2

High-throughput viscosity measurement using capillary electrophoresis instrumentation and its application to protein formulations

Authors:
Andrea Allmendinger

Le-Ha Dieu
Stefan Fischer
Robert Mueller
Hanns-Christian Mahler
Joerg Huwyler

Viscosity characterization of protein formulations is of utmost importance for the development of subcutaneously administered formulations. However, viscosity determinations are time-consuming and require large sample volumes in the range of hundreds of microliters to a few milliliters, depending on the method used. In this article, an automated, high-throughput method is described to determine dynamic viscosity of Newtonian fluids using standard capillary electrophoresis (CE) equipment. CE is an analytical method routinely used for the separation and characterization of proteins. In our set-up, the

capillary is filled with the test sample, and a constant pressure is applied. A small aliquot of riboflavin is subsequently loaded into the capillary and used as a dye to monitor movement of protein samples. Migration time of the riboflavin peak moving through the filled capillary is converted to the viscosity by applying the Hagen-Poiseuille's law. The instrument is operated without using an electrical field. Repeatability, robustness, linearity, and reproducibility were demonstrated for different capillary lots and instruments, as well as for different capillary lengths and diameters. Accuracy was verified by comparing the viscosity data obtained by CE instrumentation with those obtained by plate/cone rheometry. The suitability of the method for protein formulations was demonstrated, and limitations were discussed. Typical viscosities in the range of 5 to 40 mPas were reliably measured with this method. Advantages of the CE instrumentation-based method included short measurement times (1 – 15 min), small sample volumes (few microliters) for a capillary with a diameter of 50 μm and a length of 20.5 cm as well as potential to be suitable for high-throughput measurements.

2.1 Introduction

Viscosity of protein formulations is a key challenge during formulation development of biologics, such as monoclonal antibodies, for subcutaneous use. At high protein concentrations (>50 – 100 mg/mL), antibodies form viscous solutions due to volume exclusion, protein-protein interactions, and macromolecular crowding [1]. The viscosity increases exponentially with increasing protein concentration leading to limitations during manufacture (e.g., filtration) and drug administration/injection [2-4]. Therefore, it is essential to characterize viscosity during formulation and process development. However, only a limited number of rheological methods suitable for viscosity characterization of protein formulations are available. Preferably, viscosity determination should require small amounts of material (in the microliter range) as only limited quantities tend to be available during formulation development. Moreover, viscosity determination should cover a broad viscosity range (preferably between 1 and approximately 100 mPas) [5], and the method should be manageable in an automated, high-throughput mode. Current methods are sample- and time-consuming and allow a throughput of only a few samples per hour.

Capillary viscosimeters have been used for over a century. The best-known and most frequently used capillary viscosimeters are instruments based on the Ostwald-viscosimeter, the Ubbelohde-, and the Canon-Fenske-viscosimeter. These viscometers consist of a glass capillary which is filled with the sample fluid. The sample flows through the capillary driven by gravity, and the migration time for a defined sample volume is measured. The migration time can be converted into the dynamic viscosity of the sample by applying the Hagen-Poiseuille's law. However, large sample volumes in the milliliter range are needed for the commercially available instruments. In the recent decades, various efforts have been made to optimize capillary viscometers for smaller sample consumption [6-12]. However, these methods do not fulfill all requirements for protein preparations. In 1994, Bello *et al.* have described a method to determine the viscosity using CE instrumentation which was taken as a basis for the present study [13]. In this study, accurate results were only obtained for viscosities up to 3 mPas due to non-linearity leading to revision of the basic method principle and further optimization for the present study.

It was the aim of the present study to establish an automated, high-throughput method to determine the dynamic viscosity of Newtonian liquids using standard capillary electrophoresis (CE) equipment. The method was tested for repeatability, robustness, linearity, accuracy, and reproducibility using different capillary lots, instruments, capillary lengths, and diameters. Viscosity data obtained by the CE instrument were compared to viscosity data obtained by plate/cone rheometry. Application of the CE instrumentation-based method was demonstrated for different protein formulations, and the advantages and limitations of the CE instrumentation-based method were explored in comparison to different rheological methods (plate/cone rheometry, capillary viscosimeters, falling ball viscosimeter) used in protein formulation development.

2.2 Materials and Methods

Materials

Aqueous sucrose and glycerol solutions

For calibration of the CE instrument, standard solutions with defined viscosities consisting of 0% to 60%

(m/v) sucrose (Ferro Pfanstiehl, Waukegan, IL, USA) were prepared. The aqueous sucrose solutions covered a viscosity range from 1 to 75 mPas. Viscosity was verified by plate/cone rheometry. For accuracy testing, glycerol/water mixtures were produced by diluting glycerol (99.9%, Acros Organics, Morris Planes, NJ, USA) with water for injection to achieve concentrations between 0% and 80% (m/m) covering a viscosity range of 1 to 65 mPas.

Commercial protein therapeutics

Five commercial protein therapeutics (CPT) were used which were obtained as either prefilled syringes for CPT 1 (IgG, 60 mg/mL), CPT 2 (IgG, 100 mg/mL), CPT 3 (IgG, 50 mg/mL), and CPT 4 (fusion protein, 50 mg/mL), or as a lyophilisate for CPT 5 (IgG, 100 mg/mL). The products were stored at 2 – 8°C and were used before expiry.

Monoclonal antibody formulation

The purified monoclonal antibody mAb1 (IgG$_1$, pI = 8.5; M$_r$ = ~150 kDa; k$_D$ = 5.97 mL/g determined according to Lehermayr *et al.* [14]) was provided by F. Hoffmann-La Roche Ltd (Basel, CH), and was formulated in a 20 mM histidine-acetate buffer (Ajinomoto, Louvain-la-Neuve, Belgium) pH 5.5 at concentrations of 20 to 150 mg/mL.

Methods

Viscosity measurement using a CE instrument

A ProteomeLab PA 800 CE instrument (Beckman Coulter Inc., Fullerton, CA, USA) equipped with a photodiode array detector was used. The temperature for sample storage and the capillary was set to 20°C. Bare fused-silica capillaries eCapTM with inner diameters of 50 μm and 75 μm were obtained from Beckman Coulter Inc. (Brea, CA, USA). The instrument was operated without application of an electrical field. After rinsing steps with water, 0.1 M HCl, and 0.1 M NaOH at 70 psi (equivalent to 4.8 x 10^5 Pa, 5 min), the capillary was filled with the test sample at high pressure (80 psi equivalent to 5.5 x 10^5 Pa) during 5 min. To load the dye consisting of a 0.02% (m/v) riboflavin 5'-phosphate sodium salt hydrate solution (Sigma Aldrich, St. Louis, MO, USA), a pressure of 1 psi (6.9 x 10^3 Pa) was applied for 15 s. Before and after loading, the inlet of the capillary was placed in a vial filled with water to remove remaining dye/sample from the surface of the capillary inlet. After performing an autozero, constant pressure was applied to the system (4 $\pm$0.05 psi equivalent to 2.76 $\pm$0.03 x 10^4 Pa) with the sample vial positioned at the capillary entrance. The dye moved towards the detection window and was detected at 445 nm. Migration time was recorded and related to viscosity. The sample volume for a single measurement was dependent on the capillary properties. A volume of 100 μL in the storage vial with a sample consumption of a few microliters was found to be sufficient for the tested viscosities and set-ups.

Plate/cone rheometry

For comparison, dynamic viscosity was measured on a MCR 301 plate and cone rheometer (Anton Paar AG Switzerland, Zofingen, CH) at 20°C (N = 2). The rheometer was equipped with a measuring cone with an angle of 0.5° and a diameter of 25 mm (Anton Paar AG Switzerland, Zofingen, CH), and a sample volume of 80 μL was used. After equilibration of the sample at a shear rate of 100 s^{-1} for 1 min, the shear rate was increased from 100 s^{-1} to 2 000 s^{-1} over 1 min. Dynamic viscosity was determined as the mean of 6 consecutive measurements at a shear rate of 2 000 s^{-1}.

2.3   Theoretical Basis

Fig. 2.1 shows the instrumental set-up and measuring principle based on a capillary with an inner diameter D and total length L. The distance between the capillary entrance and window for UV detection corresponds to the capillary length l. At time zero (t$_0$), the capillary is completely filled with the sample. A small amount of dye (riboflavin) is injected into the capillary by applying constant pressure by the CE apparatus (t$_1$). The instrument is operated without use of an electrical field. The volume of the dye is considered negligible compared to the sample volume in the capillary. When applying a constant pressure ΔP, the dye migrates through the capillary. During this time period, the fluid is continuously drawn up into the capillary which remains completely filled (t$_2$). At t$_3$, the dye is detected as a peak at the capillary window. The migration time t is converted into dynamic viscosity as follows:

The flow of a fluid through a capillary driven by a constant pressure can be described by the Hagen-Poiseuille's law (Equation 2.1). Equation 2.1 describes the dynamic viscosity η [Pas] as a function of the applied pressure ΔP [Pa], inner capillary diameter D [m], and time t [s] that the sample takes to flow through the capillary with the length l [m].

$$\eta = \frac{\Delta P \cdot D^2}{32 \cdot l^2} \cdot t \tag{2.1}$$

In our set-up, the migration time t was equal to the migration time of the dye, representing the time needed for the sample to flow from the inlet of the capillary to the detection window. This distance is equal to the capillary length l. Equation 2.1 shows that the dynamic viscosity η of the fluid is directly proportional to the migration time t. To ensure consistent flow and applicability of the Hagen-Poiseuille's law, special attention has to be paid to the completely filled capillary during the measurement.

The Hagen-Poiseuille's equation is valid for laminar flow in a tube defined by a Reynolds number Re2300 [15-17]. For all tested set-ups, the Reynolds number was equal to 4.5 or smaller and was calculated for the worst case as follows: Re = $\frac{l D \rho}{\eta t}$ = 4.5 with l = 30 cm, D = 50 μm, density $\rho_{(20°C)}$ = 1 g/mL, $\nu_{(20°C)}$ = 1 mPas, and migration time t = 33 s.

Fig. 2.2 shows the migration time of the dye as a function of dynamic viscosity determined by plate/cone rheometry for different concentrations of sucrose solutions. With increasing viscosity, the migration time increased linearly. Fig. 2.2 compares the measured and calculated migration times based on Equation 2.1.
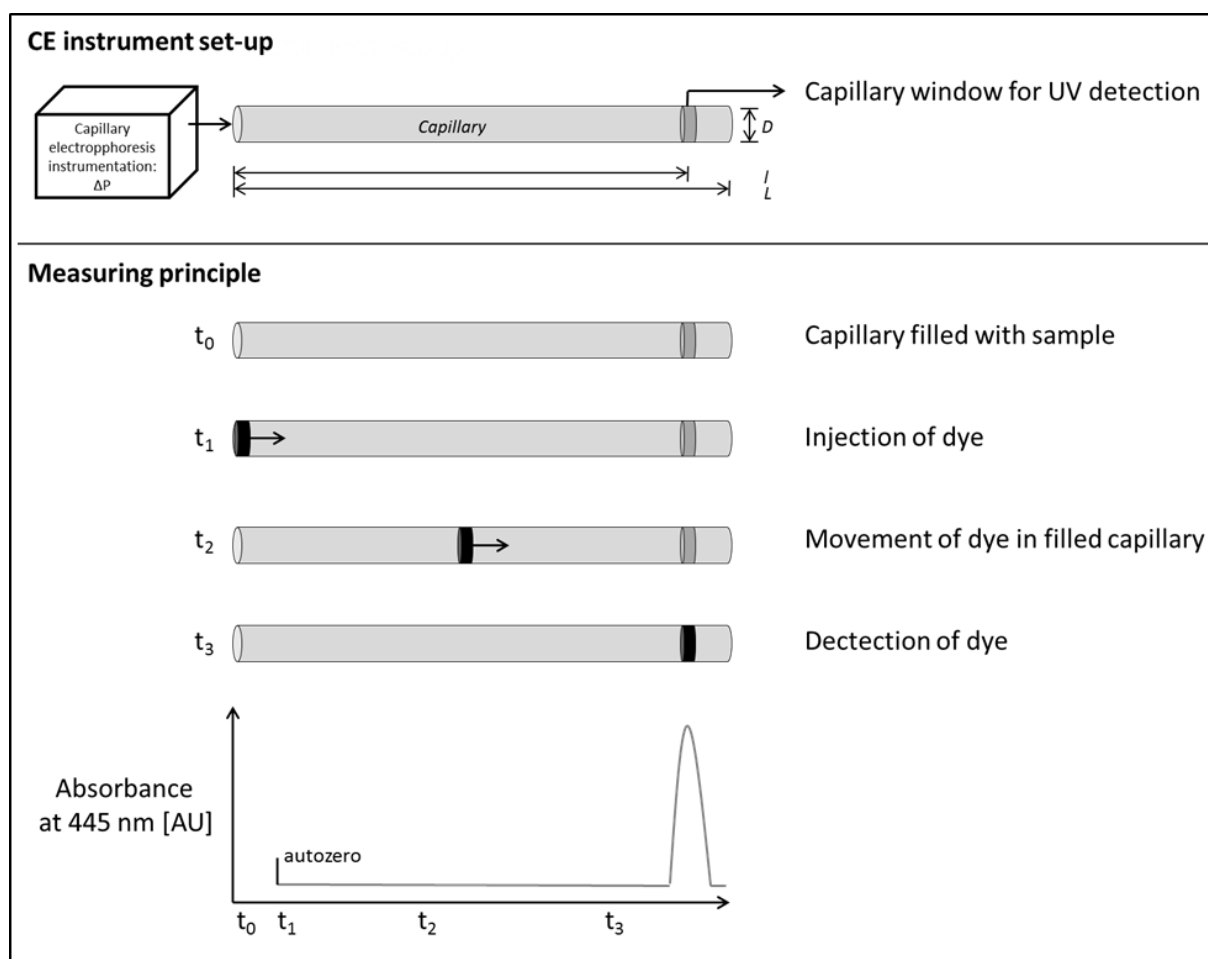
Figure 2.1: Instrumental set-up and measuring principle of viscosity measurement using CE instrumentation. ΔP = applied pressure [Pa], L = total length of capillary [m], l = length of capillary from inlet to detection window [m], D = inner capillary diameter [m], OD = optical density.

A shift to higher values was found for the measured values due to a lag phase at the beginning of the measurement where the pressure is built up. Therefore, calibration of the system is required before start of the measurement.

Fig. 2.3 (A) shows representative examples of riboflavin peaks with corresponding migration times for different glycerol and sucrose solutions with viscosities between 1 and 25 mPas ($D = 50$ μm and $l = 20.5$ cm). The migration time increases with increasing viscosity. The symmetrical peaks are broadening and their intensity decreases with increasing migration time due to Taylor dispersion [18, 19]. This leads to an upper viscosity limit of the method. Exceeding this limit leads to detection of asymmetrical peaks. Representative examples are shown in Fig. 2.3 (B) for viscosities of 41, 63, and 74 mPas ($D = 50$ μm, $l = 20.5$ cm). However, the viscosity limit changes depending on the capillary diameter and capillary length as described below. The sample volume required for one measurement depends on the diameter and length of the capillary. A volume of 100 μL (storage vial) with a sample consumption of a few microliters was found to be sufficient for the tested viscosities and set-ups.
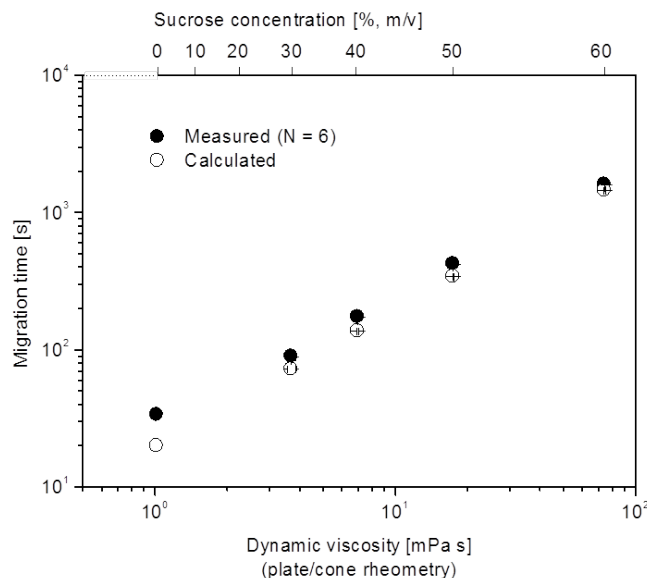
Figure 2.2: Comparison of measured and calculated migration times based on Hagen-Poiseuille's law. Different concentrations of sucrose solutions were analyzed as a function of dynamic viscosity determined by plate/cone rheometry ($2\,000\ \mathrm{s}^{-1}$; 20°C). Mean values and standard deviations are reported.

2.4 Results and Discussion

The present study aimed to establish an automated method for high-throughput measurement of dynamic viscosity using standard CE equipment. CE is routinely used for the separation and characterization of macromolecules, such as monoclonal antibodies for example [20-24]. In 1994, Bello *et al.* have described a method to determine the viscosity using CE instrumentation. They determined the migration time of a boundary between the test liquid and a reference fluid, which was related to the dynamic viscosity of the sample. However, accurate results were only obtained for viscosities up to 3 mPas due to non-linearity [13]. This limitation was overcome in our set-up by the completely filled capillary thus complying with Hagen-Poiseuille's law. A small amount of dye (riboflavin) was injected into the capillary to monitor the movement of protein samples. The CE instrumentation-based method was tested with respect to linearity, robustness, accuracy, reproducibility, and limitations. The results are shown in Fig. 2.4 for different (A) capillaries, (B) instruments, (C) capillary lengths, and (D) capillary inner diameters. After calibration of the equipment set-up with the sucrose solutions (1 – 75 mPas, Fig. 2.4 left column), dynamic viscosity data for different glycerol concentrations (1 – 65 mPas) were compared to viscosity data obtained by plate/cone rheometry (Fig. 2.4, right column). The method was then applied to analyze highly concentrated therapeutic protein formulations.
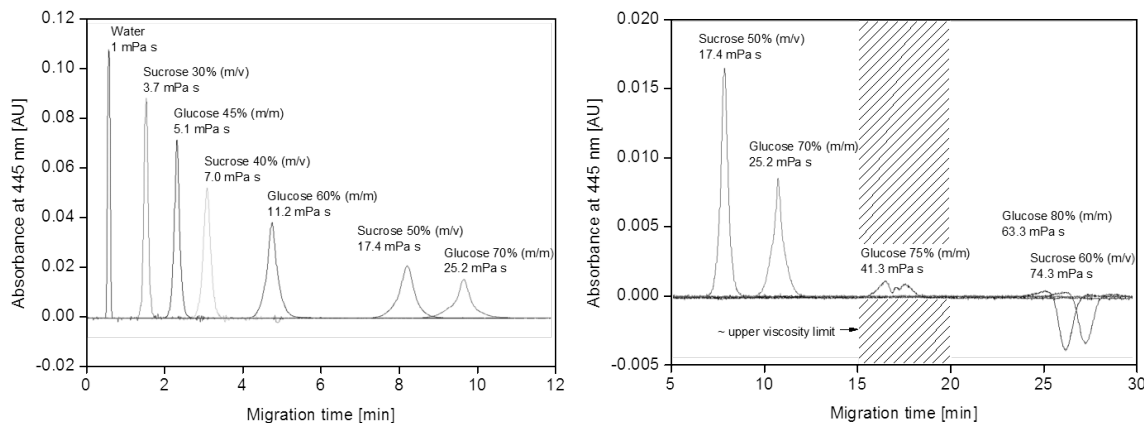
Figure 2.3: Determination of viscosity limits. (A) Representative examples of dye peaks (445 nm) for viscosities between 1 and 25 mPas at 20°C. (B) Representative examples of dye peaks (445 nm) below and above the viscosity limit of approximately 40 mPas at 20°C (hatched area). Capillary: $l = 20.5$ cm, $D = 50$ μm.

Linearity

In all set-ups used, migration time and dynamic viscosity for the different sucrose solutions (0 – 60% (m/v); 1 – 75 mPas) correlated in a linear fashion (Fig. 2.4). The correlation coefficients were between R = 0.9993 and 0.9999. This confirms the direct proportionality of viscosity and migration time in accordance with Hagen-Poiseuille's law. For further details see Supporting Information, Table 2.2, which also includes a summary of corresponding slope, y-intercept, and residual sum of squares.

Repeatability (intra-assay precision) and robustness

Repeatability and robustness were tested by triplicate measurements of different sucrose solutions using three different capillary lots ($D = 50$ μm, $l = 20.5$ cm, Fig. 2.4, A). Maximal relative standard deviations of 0.5%, 0.7%, and 4.3% were found for the three different capillary lots and different sucrose solutions. Details are provided in the Supporting Information, Table 2.2.

Accuracy and viscosity limit

Fig. 2.4 (A, right column) shows the correlation between CE and plate/cone viscosity data for the glycerol solutions and the three different capillary lots. Good agreement between viscosity data obtained from plate/cone rheometry and CE instrumentation was found for viscosities between 5 and 40 mPas. The upper viscosity limit was defined at approximately 40 mPas due to the irregular shape of the riboflavin peak. Accuracy was determined as 97.4% ±3.5%, 99.7% ±3.1%, and 104.4% ±6.9% for the three tested capillaries (for details see Supporting Information, Table 2.2).
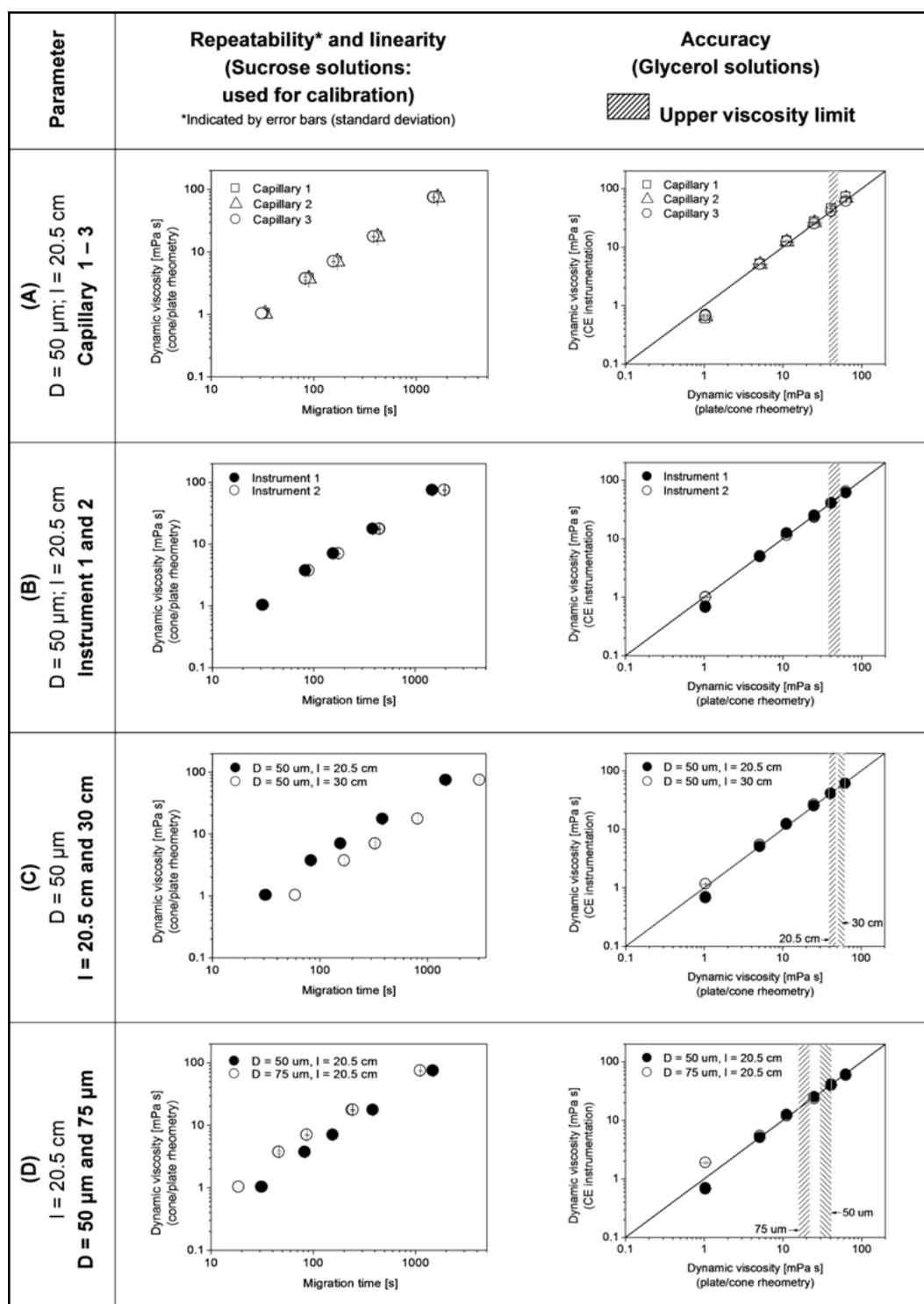
Figure 2.4: Repeatability, linearity, accuracy, and limit of viscosity measurements at 20°C for different (A) capillaries, (B) instruments, (C) capillary lengths, and (D) capillary diameters. Measurements were performed in triplicates (CE) or duplicates (plate/cone), and mean values and standard deviation are reported. (D = inner capillary diameter, l = capillary length from inlet to detection window)

Reproducibility

For reproducibility testing, measurements were performed on two different CE instruments in different laboratories on different days. Sucrose calibration curves were almost identical for the two CE instruments (Fig. 2.4, B, left column). Reproducibility was found as 3.1% maximal relative standard deviation. Further details are summarized in the Supporting Information, Table 2.2, including minimal relative standard deviation and maximal standard deviation. The viscosity range ensuring accurate measurements was 5 to 40 mPas as shown also for the first set-up (Fig. 2.4, A). Accuracies of 97.4% $\pm 3.5\%$ (first instrument) and 97.9% $\pm 3.6\%$ (second instrument) were found when comparing the viscosity data obtained by CE and plate/cone instrumentation.

Optimization: Capillary length

To optimize the method in terms of a shorter measuring time and larger viscosity range, two different capillary lengths (Fig. 2.4, C) and capillary diameters (Fig. 2.4, D) were tested. Fig. 2.4 (C) shows the results for two different capillary lengths, namely 20.5 cm and 30 cm ($D = 50$ μm). The shorter capillary (20.5 cm) was the shortest length feasible and represented the smallest distance between inlet vial and the detection window of the capillary. Comparison of the calibration curves showed that elongation of the capillary led to a shift of the calibration curve to longer migration times, in accordance with Equation 2.1, indicating that the migration time t is directly proportional to the capillary length l. Comparison of viscosity data of the glycerol solutions obtained by plate/cone rheometry and the CE instrument showed good agreement in the range of 5 to 40 mPas (20.5 cm) and 5 – 60 mPas (30 cm), respectively. Although migration time for the 30 cm capillary increased leading to peak broadening and lower intensity, the upper viscosity limit increased to approximately 60 mPas. For the 30 cm capillary, an accuracy of 96.1% $\pm 3.4\%$ was found.

Optimization: Capillary diameter

Fig. 2.4 (D) shows the comparison of two different capillary diameters, i.e., 50 μm and 75 μm ($l = 20.5$ cm). The calibration curve for the 75 μm capillary shifted to shorter migration times. This is again explained by the Hagen-Poiseuille's equation (Equation 2.1) as the capillary diameter D is inversely proportional to the migration time t. Comparison of viscosity data of the glycerol solutions obtained by plate/cone rheometry and the CE instrumentation-based method revealed good agreement in the viscosity range of 5 to 40 mPas for the 50 μm capillary. However, the upper viscosity limit decreased to approximately 15 mPas when using the 75 μm capillary. An accuracy of 99.6% $\pm 6.8\%$ was found for the 75 μm capillary. We conclude that a short capillary with a larger inner diameter should be chosen for optimization/reduction of measuring time. However, expansion of the viscosity range requires longer capillaries with a small inner diameter. Therefore, a capillary with a diameter of 50 μm and a length of 20.5 cm represents a good compromise of short measuring time (1 – 15 min) and a viscosity range relevant for protein formulations.

Application of the CE instrumentation-based method to protein formulations

Application of the CE instrumentation-based method to protein formulations The method to measure viscosity using a CE instrument ($D = 50$ μm, $l = 20.5$ cm) was applied to protein formulations. Riboflavin, which has an absorption maximum at 445 nm, was chosen as a dye. At this wavelength, the absorption of protein formulations was tested and is considered negligible. Therefore, the protein formulations do not interfere with the detection of the dye during UV absorption measurement which shows the specificity of the method.

Commercial protein therapeutics

Table 2.1 compares the viscosity data obtained by plate/cone rheometry with those obtained by the CE instrumentation for the CPT 1 to 5 (20°C). Viscosities were within the range of 5 to 40 mPas. Good agreement was found between the two methods. Maximum deviation between the viscosity data obtained by the two methods was found for CPT 5 (3.5 mPas) with a deviation of 0.7 mPas.

Product concentration [mg/mL]	Protein	Dynamic viscosity (CE) [mPas]	Dynamic viscosity (plate/cone) [mPas]
CPT 1	60	2.1 ±0.1	2.0
CPT 2	100	3.2 ±0.1	3.0
CPT 3	50	1.6 ±0.1	1.6
CPT 4	50	3.9 ±0.1	3.7
CPT 5	100	4.2 ±0.1	3.5

Table 2.1: Viscosity of commercial protein therapeutics measured using a CE instrument and by plate/cone viscosimeter (20°C). Measurements were performed in triplicates (CE) or duplicates (plate/cone). Mean values and standard deviations are reported. (CPT = commercial protein therapeutic)

Concentration series of a monoclonal antibody formulation

Viscosity of a monoclonal antibody formulation (mAb1) was determined by the CE instrumentation-based method and plate/cone rheometry at different protein concentrations. Fig. 2.5 (A) shows representative peaks of the dye riboflavin obtained by the CE instrument with the corresponding migration times for the different protein concentrations. With increasing protein concentration and viscosity, migration time increased as expected; the peaks were broadening, and the intensity decreased. As an example, a migration time of 7.8 min was measured for the highest protein concentration of 151 mg/mL with a viscosity of 13.1 mPas. Fig. 2.5 (B) shows the correlation between the viscosity data obtained by the CE instrumentation-based method and plate/cone rheometry. Generally, the viscosity of the different protein concentrations agreed well although a small systematic deviation was found for this example for higher viscosities and higher migration times for the data obtained by the CE instrument. One explanation might be an increase/change in capillary wall-protein interaction. We speculate that this increase might
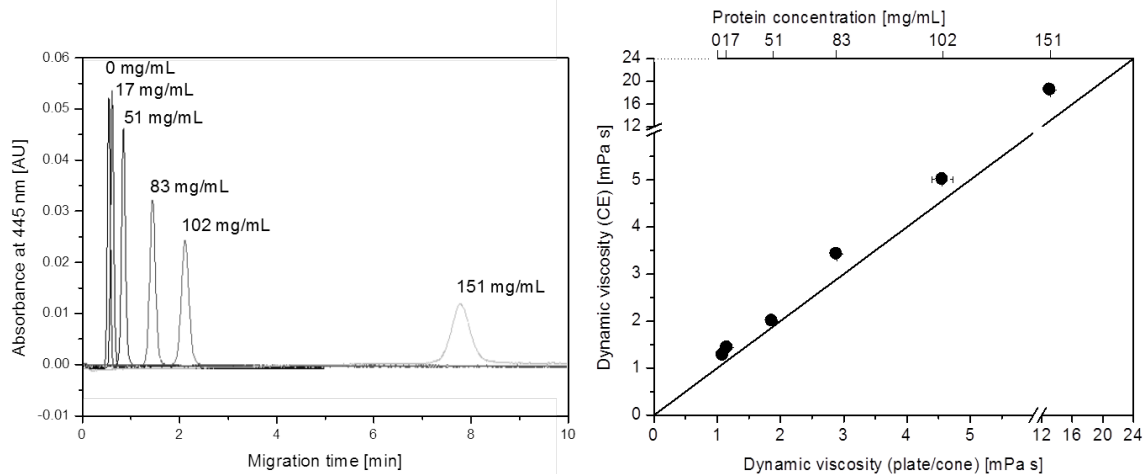
Figure 2.5: (A) Representative examples of riboflavin peaks during viscosity measurement (CE) for different concentrations of mAb1 at 20°C. Riboflavin was used as a dye. (B) Correlation of dynamic viscosity determined by plate/cone rheometry (N = 2) and CE instrumentation (N = 3) as a function of protein concentration of mAb1. Mean values and standard deviations are reported. The solid line represents the line of identity.

have resulted from a change in protein-protein interaction (PPI) with increasing protein concentration. As reported in the literature, attractive PPIs may become predominant with increasing protein concentration for some antibodies [25-27]. Even a change from repulsive forces at low protein concentration to the predominant attractive forces at high protein concentration was reported [27]. The interaction parameter k_D between two molecules can be determined by dynamic light scattering (DLS) experiments, as was previously described by our group [14]. This was found to be positive (5.97 mL/g) for mAb1, indicating repulsive interaction at low protein concentration. Therefore, the change from repulsive interaction at low protein concentration to predominating attractive forces at higher protein concentration might be responsible for the altered interaction between capillary wall and protein sample. As the deviation was systematic, it can be overcome by calibration with the drug product or studies requiring only relative viscosity determination. Another possibility is the use of differently coated capillaries, which is the subject of ongoing research.

Viscosity characterization of protein formulations

Viscosity characterization is essential during protein formulation and process development. Methods involving low material consumption (in the microliter range) and a high throughput at a viscosity range between approximately 1 and 100 mPas are desirable. Compared to other rheological methods used in protein formulation development, such as capillary viscosimeters (e.g., Micro-Ubbelohde-Viscosimeter/ViscoClock, Schott instruments [2 – 4 mL]; Texture Analyzer milliliters] [28, 29]), falling ball viscosimeters (e.g., AMVn Microviscosimeter, Anton Paar [150 – 300 μL]), or standard plate/cone rheometer (e.g., MCR301, Anton Paar [80 μL]), the established CE instrumentation-based method

requires a small sample volume in the storage vial (100 μL) and a sample consumption of only a few microliters. The volume of 100 μL is a limitation of the instrument used and may be optimized by vial design or optimization of the inlet position. The CE instrumentation is a closed system which is temperature-controlled. The latter is a critical prerequisite for viscosity measurements. Most importantly, a unique feature of the CE instrumentation is that no time-consuming cleaning is needed due to automation of the method and cleaning process. This constitutes an advantage over other viscosimeters (including also e.g. the micro-viscosimeter m-Vroc RheoSense [10]). As a result, the CE instrumentation allows for measurements in an automated manner with a throughput of approximately 30 samples per load defined by the capacity of the sample tray of the instrument used.

A method that provides a significantly higher throughput is based on DLS. This method measures the diffusion coefficient of polystyrene beads added to the sample solution. The diffusion coefficient is related to the dynamic viscosity according to the Stokes-Einstein equation [29]. The system involves a disposable 384-well plate (e.g., DynaoPro Plate Reader, Wyatt, 45 μL) and also requires no cleaning. A drawback of the DLS method is that it requires the addition of the polystyrene beads leading to dilution of the sample by 10% thus inducing a change of sample composition. This limits the method to the non-exponential viscosity range at low protein concentrations or to studies requiring relative rather than absolute determination of viscosity. Additionally, prior exclusion of the risk of interaction/aggregation of protein with the polystyrene beads is mandatory.

A limitation of the CE instrumentation-based method may be the potential for clogging of the capillary with particles. However, since filtration of protein samples (using sterilizing-grade filters) is routinely performed during sample preparation, particles >0.2 μm are typically excluded. Furthermore, potential interaction of the sample with the capillary wall at high protein concentration might require coated capillaries. An alternative approach is the calibration of the capillary with the specific product itself or the measurement of relative viscosity values.

Our method reliably determined the viscosity of Newtonian solutions between 5 and 40 mPas. Variation in capillary length and capillary diameter led to different minimal and maximal viscosities. The subject of ongoing research is the variation of the applied pressure which leads to measurements at different/adjustable shear rates. Therefore, the method would also be applicable to non-Newtonian liquids showing shear-rate-dependent behavior. This is of considerably importance as we have recently reported that protein formulations can show shear-thinning behavior especially at high protein concentrations [28]. A complete list of methods to determine viscosity in protein formulations, including the established CE instrumentation-based method, is provided in the Supporting Information, Table 2.3. The table details the measuring principle, application, required volume, advantages, and limitations from an experimental point of view, highlighting that each method has its advantages and limitations. Therefore, the viscosity method most suited to the formulation in question has to be carefully chosen.

2.5 Conclusions

There is an increasing need for therapeutic protein formulations, which can be administered by the patient him-/herself using subcutaneous injections. Injection volumes by this route are currently considered to be limited to 1.5 mL. This necessitates the use of highly concentrated protein formulations (>50 mg/ml), which show an elevated viscosity with increasing protein concentration. Viscosity needs to be monitored since this parameter has an impact on e.g. syringeability and consequently patient convenience and

compliance. The automated method presented in the present work allows for a high-throughput analysis of protein formulations using small sample volumes. This will facilitate the development of parenteral formulations and the cost-effective quality monitoring of biopharmaceuticals.

2.6 Acknowledgments

2.7 References

1. R.J. Harris, S.J. Shire, C. Winter, Commercial manufacturing scale formulation and analytical characterization of therapeutic recombinant antibodies, Drug. Develop. Res. 61 (2004) 137-154.

2. S.J. Shire, Formulation and manufacturability of biologics, Curr. Opin. Biotech. 20 (2009) 708-714.

3. S.J. Shire, Z. Shahrokh, J. Liu, Challenges in the development of high protein concentration formulations, J. Pharm. Sci. 93 (2004) 1390-1402.

4. S.L. Shire, J., Friess, W., Matheus, S., Mahler, H.C. , Considerations for high concentration antibody formulations; in: Hershenson, S., Jameel, F. (ed) Formulation and Process Development Strategies for Manufacturing of a Biopharmaceutical., John Wiley Sons, 2010.

5. J. Jezek, M. Rides, B. Derham, J. Moore, E. Cerasoli, R. Simler, B. Perez-Ramirez, Viscosity of concentrated therapeutic protein compositions, Adv. Drug Deliv. Rev. 63 (2011) 1107-1117.

6. H. Mach, T. Arvinte, Addressing new analytical challenges in protein formulation development, Eur. J. Pharm. Biopharm. 78 (2011) 196-207.

7. Z. Han, X. Tang, B. Zheng, A PDMS viscometer for microliter Newtonian fluid, J. Micromech. Microeng. 17 (2007) 1828-1834.

8. N. Srivastava, R.D. Davenport, M.A. Burns, Nanoliter viscometer for analyzing blood plasma and other liquid samples, Anal. Chem. 77 (2005) 383-392.

9. A. Grupi, A.P. Minton, Capillary viscometer for fully automated measurement of the concentration and shear dependence of the viscosity of macromolecular solutions, Anal. Chem. 84 (2012) 10732-10736.

10. C.J. Pipe, T.S. Majmudar, G.H. McKinley, High shear rate viscometry, Rheol. Acta. 47 (2008) 621-642.

11. J. Lee, A. Tripathi, Intrinsic viscosity of polymers and biopolymers measured by microchip, Anal. Chem. 77 (2005) 7137-7147.

12. Y. Francois, K. Zhang, A. Varenne, P. Gareil, New integrated measurement protocol using capillary electrophoresis instrumentation for the determination of viscosity, conductivity and absorbance of ionic liquid-molecular solvent mixtures, Anal. Chim. Acta. 562 (2006) 164-170.

13. M.S. Bello, R. Rezzonico, P.G. Righetti, Capillary Electrophoresis Instrumentation as a Bench-Top Viscometer, J. Chromatogr. A. 659 (1994) 199-204.

14. C. Lehermayr, H.C. Mahler, K. Mader, S. Fischer, Assessment of net charge and protein-protein interactions of different monoclonal antibodies, J. Pharm. Sci. (2011).

15. O. Reynolds, An Experimental Investigation of the Circumstances Which Determine Whether the Motion of Water Shall Be Direct or Sinuous, and of the Law of Resistance in Parallel Channels., Philos. Transactions. 174 (1883) 935-982.

16. O. Reynolds, On the dynamical theory of incompressible viscous fluids and the determination of the criterion, Philos. Transactions. (1895).

17. T.G. Mezger, Das Rheologie Handbuch, 3rd ed., Vincentz Network, Hannover, 2010.

18. A.J.S. Chapman, D.M. Goodall, A novel approach to measurement of hydrodynamic radius for a standard protein using UV area imaging detection, Chromatography Today. 1 (2008).

19. A. Lewandrowska, A. Majcher, A. Ochab-Marcinek, M. Tabaka, R. Holyst, Taylor Dispersion Analysis in Coiled Capillaries at High Flow Rates, Anal. Chem. 85 (2013) 4051-4056.

20. C. Wacker, C.N. Berger, P. Girard, R. Meier, Glycosylation profiles of therapeutic antibody pharmaceuticals, Eur. J. Pharm. Biopharm. 79 (2011) 503-507.

21. C. Cianciulli, T. Hahne, H. Watzig, Capillary gel electrophoresis for precise protein quantitation, Electrophoresis. 33 (2012) 3276-3280.

22. J. Zhang, S. Burman, S. Gunturi, J.P. Foley, Method development and validation of capillary sodium dodecyl sulfate gel electrophoresis for the characterization of a monoclonal antibody, J. Pharm. Biomed. Anal. 53 (2010) 1236-1243.

23. N. Stackhouse, A.K. Miller, H.S. Gadgil, A high-throughput UPLC method for the characterization of chemical modifications in monoclonal antibody molecules, J. Pharm. Sci. 100 (2011) 5115-5125.

24. S.S. Zhao, D.D. Chen, Applications of capillary electrophoresis in characterizing recombinant protein therapeutics, Electrophoresis. 35 (2014) 96-108.

25. S. Yadav, T.M. Laue, D.S. Kalonia, S.N. Singh, S.J. Shire, The influence of charge distribution on self-association and viscosity behavior of monoclonal antibody solutions, Mol. Pharm. 9 (2012) 791-802.

26. A. Saluja, D.S. Kalonia, Nature and consequences of protein-protein interactions in high protein concentration solutions, Int. J. Pharm. 358 (2008) 1-15.

27. S. Yadav, S.J. Shire, D.S. Kalonia, Viscosity behavior of high-concentration monoclonal antibody solutions: correlation with interaction parameter and electroviscous effects, J. Pharm. Sci. 101 (2012) 998-1011.

28. A. Allmendinger, J. Huwyler, H.C. Mahler, E. Schwarb, D. Zarraga, R. Mueller, Rheological characterization and injection forces of concentrated protein formulations: An alternative predictive model for non-Newtonian solutions, Eu J Pharm Biopharm, 87 (2014) 318-328.

29. F. He, G.W. Becker, J.R. Litowski, L.O. Narhi, D.N. Brems, V.I. Razinkov, High-throughput dynamic light scattering method for measuring viscosity of concentrated protein solutions, Anal. Biochem. 399 (2010) 141-143.

2.8 Supporting Information

(see next page)

Parameter	Linearity (R, slope, y-intercept, RSS) Repeatability and Reproducibility (MIN/MAX RSD) (Sucrose solutions)	Accuracy (Glycerol solutions)
(A) **Capillary 1 − 3** D = 50 μm l = 20.5 cm ϑ = 20°C	Capillary 1: ·R = 0.9998 ·Slope = 0.04 mPa ·y-intercept = -0.25 mPas ·RSS = 0.05 mPas^2 ·MIN/MAX RSD = 0.3%0.7% Capillary 2: ·R = 0.9993 ·Slope = 0.04 mPa ·y-intercept = -0.23 mPas ·RSS = 0.06 mPas^2 ·MIN/MAX RSD = 0.1%4.3% Capillary 3: ·R = 0.9998 ·Slope = 0.05 mPa ·y-intercept = -0.28 mPas ·RSS = 0.05 mPas^2 ·MIN/MAX RSD = 0.1%0.5%	Capillary 1: ·Accuracy = 97.4% ±3.5% Capillary 2: ·Accuracy = 99.7% ±3.1% Capillary 3: ·Accuracy = 104.4% ±6.9%
(B) **Instrument 1 and 2** D = 50 μm l = 20.5 cm ϑ = 20°C	Instrument 1: ·R = 0.9998 ·Slope = 0.04 mPa ·y-intercept = -0.25 mPas ·RSS = 0.05 mPas^2 Instrument 2: ·R = 0.9999 ·Slope = 0.04 mPa ·y-intercept = -0.01 mPas ·RSS = 0.09 mPas^2 Reproducibility: ·MIN/MAX RSD = 0.1%3.1%	Instrument 1: ·Accuracy = 97.4% ±3.5% Instrument 2: ·Accuracy = 97.9% ±3.6%
(C) **l = 20.5 and 30 cm** D = 50 μm ϑ = 20°C	20.5 cm ·R = 0.9998 ·Slope = 0.04 mPa ·y-intercept = -0.25 mPas ·RSS = 0.05 mPas^2 30 cm ·R = 0.9998 ·Slope = 0.02 mPa ·y-intercept = -0.10 mPas ·RSS = 0.05 mPas^2	20.5 cm ·Accuracy = 97.4% ±3.5% 30 cm ·Accuracy = 96.1% ±3.4%
(D) **D = 50 and 75 μm** l = 20.5 cm ϑ = 20°C	50 μm ·R = 0.9998 ·Slope = 0.04 mPa ·y-intercept = -0.25 mPas ·RSS = 0.05 mPas^2 75 μm ·R = 0.9994 ·Slope = 0.07 mPa ·y-intercept = 0.55 mPas ·RSS = 0.19 mPas^2	50 μm ·Accuracy = 97.4% ±3.5% 75 μm ·Accuracy = 99.6% ±6.8%

Table 2.2: Supplementary data to Table 2. Linearity is represented by the correlation coefficient R, slope, y-intercept, and residual sum of squares (RRS). Repeatability and reproducibility are represented by the minimal (MIN) and maximal (MAX) relative standard deviations (RSD). Accuracy of viscosity measurements is shown for different (A) capillaries, (B) instruments, (C) capillary lengths, and (D) capillary diameters. Abbreviations: D = inner capillary diameter, l = capillary length from inlet to detection window, = temperature. Measurements were performed as triplicates and means and standard deviations are reported. RSD values are indicated for either the characterization of individual capillaries (repeatability) or the comparison of instruments (reproducibility).

Method	Measuring principle	Application and required volume	Advantage	Disadvantage / Limitation
Rotational viscosimeter 1. Plate/cone 2. (Plate/plate 3. Concentric cylinder)	A measurement device is rotating in the sample fluid. The measured torque at a defined rotation speed is related to the dynamic viscosity. [S- 1]	Shear-rate dependent viscosity for Newtonian and Non-Newtonian fluids $(0.7 - 10^9 \, \text{mPa s*})$ 80 µL* (*for a plate/cone device as described in the Materials and Methods section)	• Constant shear rate/stress over conical gap (homogeneous flow profile) compared to plate/plate device (correction needed) [S- 2, 3] • Shear stress-dependent viscosity • Shear rate profile with only one measurement • Low sample volumes in the µL-range* compared to cylinder device → few mL	• Surface related effects for shear rates $<100 \, \text{s}^{-1}$ possible[S- 4] • Easy, but time-consuming cleaning (own experience)
Dynamic light scattering	The Diffusion coefficient of a small amount of polystyrene beads added to the sample fluid is measured and is related to the dynamic viscosity of the sample. (Stokes-Einstein equation) [S- 5]	Large screening of Newtonian fluids (zero shear rate) 45 µL (¥384 well-plate)	• High-throughput method • Low sample volume¥ • No cleaning • Viscosity at zero shear rate	• Dilution of 10% with polystyrene beads, therefore • limitation to non-exponential viscosity range (own experience) • Interaction of polystyrene beads with proteins has to be excluded • No information on shear rate/stress
Falling ball viscosimeter	A ball is falling through a sample fluid which is filled in a glass tube with a defined inclination. The falling time for a defined distance is measured and is proportional to the dynamic viscosity (Stokes' equation). [S- 1]	Newtonian fluids $(0.3 - 2'500 \, \text{mPa s}^\ddagger)$ $150 - 300$ µL (‡e.g. AMVn automated Microviscometer, Anton Paar)	• Low sample volume‡ • Simple operation • No evaporation (closed system)	• No information on shear rate/stress • No defined flow profile: inhomogeneous/non-laminar [S- 1] • Knowledge of density for dynamic viscosity • Difficult, time-consuming cleaning • Different capillaries for different viscosity ranges

Table 2.3: Overview of commercially available methods for the determination of dynamic viscosity during protein formulation development. The measuring principle, application, required volume, advantages, and limitations are summarized.

Method	Measuring principle	Application and required volume	Advantage	Disadvantage / Limitation
Capillary viscosimeters (basic principle: Hagen-Poiseuille's law [S- 6, 7, 8])				
Glass capillary viscosimeter (according to Ostwald, Ubbelohde, or Cannon-Fenske)	A vertical installed glass capillary is filled with a sample fluid which flows through the capillary by gravity. The time for a defined sample volume is measured and proportional to dynamic viscosity. [S- 1, 9, 10, 11, 12, 13]	Newtonian fluids (0.35–10'000 mPa s $\rho_{20°C} = 1\ mg/mL$: maximal viscosity range obtained with different capillaries) $2 - 4$ mL[‡] ([‡]e.g. Micro-Ubbelohde-Viscometer/ViscoClock, Schott instruments)	-	• Large sample volume[‡] • No information on shear rate/stress • Knowledge of density for dynamic viscosity • Difficult, time-consuming cleaning (own experience) • Different capillaries for different viscosity ranges
m-Vroc™ micro-viscosimeter (RheoSense, Inc.)	A sample flows through a rectangular slit at a defined volumetric flow and a sensor array measures the pressure at separate locations. The slope of the pressure drop is used to calculate the dynamic viscosity dependent on the shear stress. [S- 4, 14]	Shear-rate dependent viscosity for Newtonian and Non-Newtonian fluids dependent on the apparent shear rate (0.2 – 10 kPas: maximal viscosity range obtained with different measuring cell/syringe combinations) $\mu L - mL$ ([¤]dependent on sample viscosity, shear rate, and set-up)	• Shear stress-dependent viscosity • Measurement at high shear rates possible (up to $3 \times 10^5\ s^{-1}$ dependent on sample viscosity/set-up) • Closed system: No drying effects • No surface-related effects	• Sensitive for particle contamination • Difficult, time-consuming cleaning (own experience) • Maximum shear rate and required volume is dependent on measuring cell/syringe combination, and sample viscosity[¤] • Different measuring cell/syringe combination required for different viscosity ranges • No shear rate profile with one measurement
Texture analyzer	A syringe is filled with the sample under consideration and a needle (=capillary) is attached. A constant speed is applied to the system by the texture analyzer and the restoring glide force is measured and related to dynamic viscosity. [S- 15, 16, 17, 18]	Shear-rate dependent viscosity for Newtonian and Non-Newtonian fluids (viscosity range dependent on needle, syringe diameter, and test speed) mL ([ȷ]dependent on sample viscosity, shear rate, and measuring set-up)	• Shear stress-dependent viscosity • High-shear viscosity ($10^5 - 10^6\ s^{-1}$) • Easy change of syringe and needle dimensions to obtain different viscosity/shear rate ranges • Disposable set-up • Closed system • Simulated injection	• Large sample volume[ȷ] • Maximum shear rate and required volume is dependent on syringe/needle set-up, test speed, and sample viscosity[ȷ] • Different measuring set-ups required for different viscosity/shear rate ranges • No shear rate profile with one measurement

Method	Measuring principle	Application and required volume	Advantage	Disadvantage / Limitation
Texture analyzer			• Simulated injection into air at the same time • Comparability for Newtonian and non-Newtonian fluids to plate/cone viscosity data dependent on the shear rate was shown by Allmendinger et al.	
Capillary electrophoresis instrumentation	A capillary is filled with a sample fluid. The migration time of a small dye peak moving through the capillary under defined pressure is measured which is proportional to the dynamic viscosity.	Large screening of Newtonian fluids (2 - 40 mPa s) Load volume: 100 µL$^{\pm}$ Material consumption: few µL ($^{\pm}$for a CE instrument as described in the Materials and Methods section)	• High-throughput method • Low sample volume$^{\pm}$ • Automated cleaning • Closed system	• Calibration required • No shear rate-dependent measurement up to date • Sensitive to clogging of capillary • Potential interaction of protein and capillary at high protein concentrations

References (Supporting information)

S-1 T.G. Mezger, Das Rheologie Handbuch, 3rd ed., Vincentz Network, Hannover, 2010.

S-2 C.W. Macosko, Rheology: principles, measurements, and applications, 1st ed., Wiley-VCH, New York, 1994.

S-3 J. Jezek, M. Rides, B. Derham, J. Moore, E. Cerasoli, R. Simler, B. Perez-Ramirez, Viscosity of concentrated therapeutic protein compositions, Adv. Drug Deliv. Rev. 63 (2011) 1107-1117.

S-4 C.J. Pipe, T.S. Majmudar, G.H. McKinley, High shear rate viscometry, Rheol. Acta. 47 (2008) 621-642.

S-5 F. He, G.W. Becker, J.R. Litowski, L.O. Narhi, D.N. Brems, V.I. Razinkov, High-throughput dynamic light scattering method for measuring viscosity of concentrated protein solutions, Anal. Biochem. 399 (2010) 141-143.

S-6 G.H.L. Hagen, Über die Bewegung des Wassers in engen zylindrischen Röhren., Poggendorf's Annalen der Physik und Chemie. 46 (1939 (reprinted 1933, see Schiller)) 423-442.

S-7 J.L.M. Poiseuille, Recherches experimentales sur le mouvement des liquides dans les tubes de tres petits diametres, C.R. Acad. Sci. 11 (1840) 1041-1048.

S-8 L. Schiller, Drei Klassiker der Strömungslehre: Hagen, Poiseuille, Hagenbach, Akademische Verlagsgesellschaft, Leipzig, ed. 1933.

S-9 W.s. Ostwald, Lehrbuch der allgemeinen Chemie, Steinkopff, Leipzig, 1891.

S-10 W.s. Ostwald, Grundriss der allgemeinen Chemie Engelmann, Leipzig, 1899.

S-11 L. Ubbelohde, Das einfachste und genaueste Viskosimeter und andere Geräte mit dem hängenden Niveau, J. Öl und Kohle. 12 (1936).

S-12 L. Ubbelohde, Zur Viskosimetrie, Hirzel, Stuttgart, 1965.

S-13 M.R. Cannon, R.E. Manning, J.D. Bell, The kinetic energy correction and a new viscometer, Anal. Chem. 32 (1960) 355-358.

S-14 C.J. Pipe, G.H. McKinley, Microfluidic rheometry, Mech. Res. Commun. 36 (2009) 110-120.

S-15 N. Rathore, P. Pranay, J. Bernacki, B. Eu, W. Ji, E. Walls, Characterization of protein rheology and delivery forces for combination products, J. Pharm. Sci. 101 (2012) 4472-4480.

S-16 N. Rathore, P. Pranay, B. Eu, W. Ji, E. Walls, Variability in syringe components and its impact on functionality of delivery systems, PDA J. Pharm. Sci. Technol. 65 (2011) 468-480.

S-17 A. Allahham, P. Stewart, J. Marriott, D.E. Mainwaring, Flow and injection characteristics of pharmaceutical parenteral formulations using a micro-capillary rheometer, Int. J. Pharm. 270 (2004) 139-148.

S-18 A. Allmendinger, S. Fischer, J. Huwyler, H.C. Mahler, E. Schwarb, I.E. Zarraga, R. Mueller, Rheological characterization and injection forces of concentrated protein formulations: An alternative predictive model for non-Newtonian solutions, Eu J Pharm Biopharm, 87 (2014) 318-328.

Chapter 3

Rheological characterization and injection forces of concentrated protein formulations

– an alternative predictive model for non-Newtonian solutions

Authors:
Andrea ALLMENDINGER

Stefan FISCHER
Joerg HUWYLER
Hanns-Christian MAHLER
Erward SCHWARB
Isidro E. ZARRAGA
Robert MUELLER

Development of injection devices for subcutaneous drug administration requires a detailed understanding of user capability and forces occurring during the drug administration process. Injection forces of concentrated protein therapeutics are influenced by syringe properties (e.g., needle diameter) and injection speed, and are driven by solution properties such as rheology. In the present study, it is

demonstrated that concentrated protein therapeutics may show significantly reduced injection forces because of shear-thinning (non-Newtonian) behavior. A mathematical model was thus established to predict/correlate injection forces of Newtonian and non-Newtonian solutions with viscosity data from plate/cone rheometry. The model was verified experimentally by glide-force measurements of reference and surrogate solutions. Application of the suggested model was demonstrated for injection force measurements of concentrated protein solutions to determine viscosity data at high shear rates $(3 \times 10^4 - 1.6 \times 10^5 \text{ s}^{-1})$. By combining these data with viscosity data obtained by different viscosity methods (plate/cone and capillary rheometry), a viscosity-shear rate profile of the protein solution between 10^2 and $1.6 \times 10^5 \text{ s}^{-1}$ was obtained, which was mathematically described by the Carreau model. Characterization of rheological properties allows to accurately predict injection forces for different syringe-needle combinations as well as injection rates, thus supporting the development of injection devices for combination products.

3.1 Introduction

For subcutaneous drug administration, concentrated protein therapeutics are typically required to achieve clinical doses in the magnitude of mg per kg bodyweight in a small volume (<1.5 mL) [1-3]. In contrast to dried dosage forms, liquid formulations can easily be provided in pre-filled syringes or injection devices and thus can offer convenience for the patient or healthcare provider. Advantages of these systems in comparison with vials are the ease of administration, the potential for self-administration, and the fewer handling steps by the patient or healthcare provider before administration [4, 5]. However, the development of high-concentration protein formulations is accompanied by technical challenges such as concentration-dependent protein degradation (e.g., aggregation or precipitation) and increased solution viscosity [6-9]. The latter might lead to challenges during manufacturing (e.g., ultrafiltration/diafiltration, sterile filtration, filling) and drug administration. [1-3]. More precisely, increased viscosity leads to higher injection forces potentially affecting the suitability of pre-filled syringes for self-administration and the energy required for injection – and thus design for autoinjectors. The first limitation is of particular concern for patients with a functional impairment and dexterity limitation, such as patients suffering from rheumatoid arthritis [10]. To ensure complete and safe administration of the product, it is therefore important to characterize, control, and possibly minimize injection forces for pre-filled syringe products. Moreover, the design of such devices must take the specific limitations of the targeted patient population into account.

The estimation of injection forces based on rheological data was recently described. Burckbuchler *et al.* have studied the injection behavior of a concentrated human polyclonal immunoglobulin solution by applying the Hagen-Poiseuille's law to calculate injection forces [11]. They used viscosity data from a plate/cone viscosimeter assuming Newtonian behavior of the immunoglobulin solutions. Overcashier *et al.* have added the contribution of the friction between stopper and syringe barrel to the hydrodynamic force model [5]. The frictional forces are dependent on contact area between stopper and syringe barrel, thickness and viscosity of the lubricant layer (silicone oil), and injection speed [12].

A previously published study reported that concentrated protein solutions can show shear-thinning behavior leading to reduced viscosity with increasing shear rate [13]. In order to correctly predict injection forces from viscosity data of concentrated protein solutions, a new model is needed which considers both Newtonian and Non-Newtonian flow behavior. Rathore *et al.* extended the existing model to predict injection forces for shear-thinning behavior [12, 13]. The authors used viscosity data at the shear rate occuring at the needle wall, which is described by the Weissenberg-Rabinowitsch-Mooney equation for non-Newtonian solutions [14-16].

The aim of the present project was to study the viscosity and injection behavior of highly concentrated protein solutions in comparison with Newtonian liquids (glycerol/water solutions). To describe the experimental data, an alternative mathematical model to predict injection forces of non-Newtonian liquids was developed. This model allows to use/correlate viscosity data from plate/cone rheometry. The model was verified by experimental data using plate/cone viscosity data of Carbopol gels as a model substance for non-Newtonian behavior and glycerol/water mixtures as a surrogate solution for Newtonian behavior.

In the following, the model was further discussed and compared to the approach based on the Weissenberg-Rabinowitsch-Mooney equation using the shear rate at the needle wall. Application of

the established model was demonstrated for the measured injection forces of a concentrated protein formulation of a monoclonal antibody mAb1 to obtain viscosity data at high shear rates (3×10^4 – 1.6×10^5 s^{-1}). These viscosity data were combined with rheological data obtained by plate/cone and capillary rheometry resulting in a rheological profile of the protein solutions between 10^2 and 1.6×10^5 s^{-1}.

3.2 Materials and Methods

Materials

Monoclonal antibodies

The purified monoclonal antibodies mAb1 (IgG$_1$, pI 8.4; estimated M$_w$ 145.5 k$_D$) and mAb2 (IgG$_1$, pI 9.4; estimated M$_w$ 148 k$_D$) were provided by F. Hoffmann-La Roche Ltd (Basel, Switzerland). mAb1 was formulated in a 5 mM L-histidine/L-histidine-HCl buffer (Ajinomoto, Louvain-la-Neuve, Belgium) pH 6.0 with 0.06% polysorbate 20 (Sigma-Aldrich Chemie GmbH, Steinheim, Germany) at protein concentrations of 120, 170, 210, and 225 mg/mL, respectively.

Commercial protein therapeutics

The commercial protein therapeutics (CPT) CPT 1 (IgG$_2$, 60 mg/mL), CPT 2 (IgG$_1$, 100 mg/mL), CPT 3 (fusion protein, 50 mg/mL), CPT 4 (IgG$_1$, 180 mg/mL), CPT 5 (IgG$_1$, 50 mg/mL), and CPT 10 (pegylated Fab fragment, 200 mg/mL) were purchased as pre-filled syringes. The commercial products CPT 6 (IgG$_1$, 100 mg/mL), CPT 7 (fusion protein, 50 mg/mL), CPT 8 (IgG$_1$, 100 mg/mL), and CPT 9 (IgG$_1$, 125 mg/mL) were purchased as lyophilisates. All therapeutics, except CPT 8, are currently approved on the EU market. The commercial proteins contained different pharmaceutical excipients which are listed as follows:

- Sodium acetate/phosphate/citrate/histidine/TRIS buffer

- Polysorbate 20 or 80

- Sorbitol, mannitol, glycine, sucrose

- Arginine-HCl, NaCl

- Methionine

The products were stored at $2 - 8\,^\circ$C and were used before the expiry date.

Carbopol gels

Carbopol 981 NF (BF Goodrich, Dsseldorf, Germany) gels were manufactured in a melamine-coated mortar with pistil by dissolution of the powder in water to achieve concentrations of 0.2% to 0.8% (w/w). The gel-forming process was initiated by addition of 1 N sodium hydroxide solution (Merck,

Darmstadt, Germany) until a pH of 7.0 ± 0.1 was reached. The gel was centrifuged at 2 000 rpm for 2 min to remove potential air bubbles.

Glycerol/water solutions

Glycerol/water solutions were produced by dilution of glycerol 99.5% (Acros Organics, Morris Planes, NJ) with water for injection to concentrations between 45% and 80% (w/w).

Syringes and needles

For measuring the injection force of the commercial protein products, the samples were drawn up into a 1 Plastipak^{TM} syringe (BD, Madrid, Spain) and a Microlance^{TM} 3 27 G 3/4" needle (BD, Drogheda, Ireland) or a Sterican$^{®}$ 25 G 1" needle (B. Braun, Melsungen, Germany) was attached. For all other injection force measurements, 1 mL Hypak SCF^{TM} Luer CCT pre-fillable glass syringes (BD, Le pont-de-ClaixCedex, France) were used in combination with Sterican$^{®}$ 27 G 1" needles (B. Braun, Melsungen, Germany). Filling of the glass syringes and stopper setting were done manually, ensuring that there was no air space between the stopper and contents of the syringe.

	Frictional force [N]	Syringe inner radius [mm]
1 mL Hypak SCF^{TM} Luer CCT pre-fillable glass syringe	1.62 (0.5 mL/10s) 3.60 (1 mL/10s) 6.73 (2 mL/10s)	4.3
1 mL Plastipak^{TM} syringe	1.26 (1 mL/10s)	3.2

	Needle inner diameter [μm]	Needle length s [mm]
Microlance^{TM}3 27 G 3/4" needle	237	20.9
Sterican$^{®}$ 27 G 1" needle	217	27.1
Sterican$^{®}$ 25 G 1" needle	276	27.1

Table 3.1: Needle and syringe dimensions.

Materials

Injection force measurements

Fig. 3.1 shows the experimental set-up of the injection force measurements. All force measurements were performed on a material testing instrument with a 500 N force sensor (Zwick GmbH Co.KG, Ulm, Germany). The samples were equilibrated to controlled room temperature for at least 1 h before
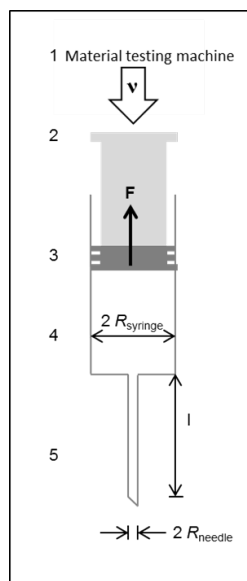
Figure 3.1: Schematic description of experimental set-up of injection force measurements. A constant speed ν was applied by the material testing instrument (1) which measured the counteracting force (F). (2) plunger, (3) stopper, (4) syringe ($R_{syringe}$ = inner radius of syringe), (5) needle (R_{needle} = inner radius of needle, l = length of needle).

starting the measurement. The syringes were emptied by pushing down the plunger at a constant speed corresponding to a volumetric flow of 0.05 mL, 0.1 mL, and 0.2 mL/s (protein formulations and glycerol/water solutions) or 0.004 mL and 0.008 mL/s (Carbopol gels and glycerol/water solutions). The counteracting force was measured as a function of distance and the maximal force of the plateau as representative for glide force at the end of injection was read off from the force-travel distance graph and defined as glide force as shown in Figure 3.9 in the supporting information. The temperature was 25 ±0.5°C.

Table 3.1 summarizes the syringe and needle dimensions used for the calculations. Syringe inner diameter and needle length were measured with a digimatic caliper CD-15CXR (Mitutoyo America Corporation, Chicago, IL). The inner needle diameter and the frictional forces between stopper and syringe barrel were determined for each syringe-needle set-up and injection speed as follows: Representative syringe samples were either left empty or filled with either 45% or 60% (w/w) glycerol/water solution. At the desired volumetric flow, the maximal force of the plateau was read off from the force-travel distance graph representative for glide force at the end of injection (N = 3). The linear regression of the glide force as a function of viscosity gives the needle diameter from the slope and the frictional force as the intercept using the Hagen-Poiseuille's law [5]. The frictional force represents the sliding friction as well as the contribution from the compression of the plunger which is in equilibrium in the gliding force plateau. The instrumental set-up does not account for static friction which is relevant at the beginning of injection and has to be overcome by the break loose force.

Viscosity measurements

Plate/cone rheometry

Dynamic viscosity was measured on a MCR 301 plate and cone rheometer (Anton Paar AG Switzerland, Zofingen, Switzerland) between shear rates of 10^2 and maximal 4 x 10^4 s^{-1} at a fixed temperature between 5 and 25°C. The rheometer was equipped with a measuring cone with an angle of 0.5° and a diameter of 25 mm (Anton Paar AG Switzerland, Zofingen, Switzerland) using 80 μL of sample.

Micro-capillary viscosimeter

Viscosity at an apparent shear rate between $\sim 10^3$ to 10^5 s^{-1} was measured on a micro-capillary rheometer m-VROC™ 3.0 (RheoSense Inc., San Ramon, CA) at 25°C. The viscosimeter was equipped with a RD05-100-116 flow cell with 50 μm cell depth. The samples were filled into a 10 mL Hamilton syringe (not containing any air bubbles) which was mounted on the viscosimeter. Depending on the viscosity of the sample and the shear rate, a few microliters up to a few milliliters of sample were required for one measurement at a defined shear rate.

3.3 Results and Discussion

Injection forces of concentrated protein therapeutics

In a first study, the injection forces of different commercial protein solutions (CPT 1 – CPT 10) were measured and correlated with viscosity data. A standardized set-up was chosen consisting of a 1 mL plastic syringe with an attached 27 G 3/4" needle. For the product CPT 10, a 25 G 1" needle instead of a 27 G 3/4" needle was used as the glide force exceeded the technical limit of the instrumental set-up (>>50 N) at the chosen test speed. An injection rate of 1 mL/10s was chosen as this is an injection rate which is appropriate for the end-user [10] and commonly used for testing. Fig. 3.2 shows the relationship between glide force and dynamic viscosity (2 x 10^3 s^{-1}) of the concentrated protein solutions. Glide forces of the products were compared to glide forces calculated based on the modified Hagen-Poiseuille's equation [5] which served as a control for Newtonian flow behavior. All products (except CPT 9 and CPT 10) showed good agreement with the calculated values based on the Newtonian model. Consequently, all tested products exhibited apparent Newtonian behavior except for CPT 9 and 10, which showed a significant reduction in glide force in our set-up.

In a second set of experiments, injection force of the mAb1 formulation was determined for protein concentrations between 120 mg/mL and 225 mg/mL. Fig. 3.3 (B) shows the glide force of mAb1 as a function of dynamic viscosity (2 x 10^3 s^{-1}) and protein concentration for three different injection rates (0.5 mL/10s, 1 mL/10s, and 2 mL/10s). When comparing the measured glide forces to glide forces calculated according to the Newtonian model [5], the concentrated mAb1 solutions showed a progressively higher deviation from the Newtonian model with increasing protein concentration and injection rate.

Data on protein integrity and particle load (visible, sub-visible) before and after injection are given for a worst case scenario (injection rate 2 mL/10s) for mAb1 225 mg/mL in the supporting information (Figure 3.11). The data show no difference before and after injection force experiments indicating that the protein integrity of mAb1 is not affected by shear stress during injection.

In addition, injection forces of different concentrations of glycerol/water solutions were analyzed for the
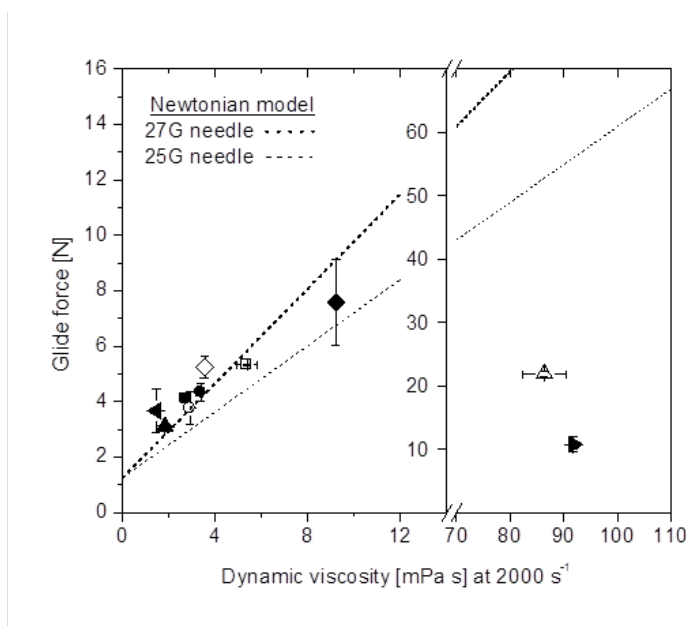
Figure 3.2: Glide force of commercial protein therapeutics determined at a volumetric flow of 1 mL/10s (25°C) as a function of dynamic viscosity (2×10^3 s^{-1}, 25°C). CPT 1 (x), CPT 2 (x), CPT 3 (x), CPT 4 (x), CPT 5 (x), CPT 6 (x), CPT 7 (x), CPT 8 (x), CPT 9 (x), CPT 10 (x). Mean values and standard deviation are reported (N = 3). The dashed lines represent glide forces calculated based on the Hagen-Poiseuille's model [5]. These served as a control for Newtonian flow behavior.

same viscosity range as that obtained for the mAb1 formulations. The glycerol/water solutions, used as control samples for Newtonian behavior (Fig. 3.3, A), fitted well with the Newtonian model. Therefore, it can be excluded that the observed deviation of the mAb1 formulations from the Newtonian model is caused by sample heating during viscous flow through the needle.

In summary, mAb1, CPT 9, and CPT 10 showed lower injection forces than expected from the linear viscosity-glide force correlation (Fig. 3.2 and Fig. 3.3, B). We speculate that this observation could be shear-thinning behavior occurring at high shear rates. Therefore, we studied the viscosity profile as a function of shear rate of the different protein solutions. Fig. 3.4 (A) shows the viscosity profile of mAb1 (225 mg/mL). Fig. 3.4 (B) and Fig. 3.4 (C) show the viscosity profiles of the commercial products CPT 4 and CPT 10 which showed apparent Newtonian and non-Newtonian behavior during glide-force measurements, respectively. As expected, constant viscosity regardless of the shear rate was found for CPT 4 at all temperatures tested (5 – 25°C), indicating Newtonian behavior of the CPT 4 formulation at these shear rates. In contrast, rheological profiles of mAb1 and CPT 10 showed shear-rate dependent viscosity revealing shear-thinning behavior with increasing shear rate and decreasing temperature.

Simulated injections using a 27 G needle (needle diameter 0.21 mm) with injection rates between 0.5 mL and 2.0 mL/10s produce needle shear rates between ∼3.3 x 10^4 and 1.3 x 10^5 s^{-1} (calculation of shear rate based on Eq. 3.6 for a Newtonian formulation with a power law index of n = 1). This exceeds the shear rates applied during standard plate/cone rheometry measurements by more than one magnitude. Thus, a capillary rheometer was additionally used to obtain viscosity data at an apparent shear rate between 10^4 and 10^5 – 10^6 s^{-1} depending on sample viscosity. Fig. 3.4 (D) shows the viscosity
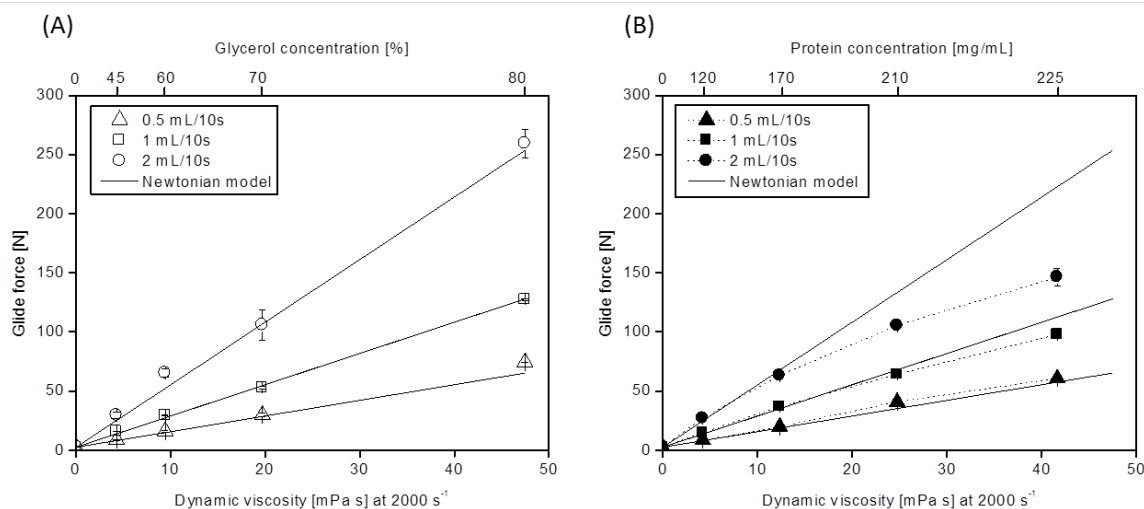
Figure 3.3: Glide forces as a function of viscosity determined at 2×10^3 s^{-1} (25°C) compared to glide forces calculated based on the Hagen-Poiseuille's equation (solid lines). The glide forces were measured at a volumetric flow of 0.5 mL/10s (triangle), 1 mL/10s (square), and 2 mL/10s (circle). Mean values and standard deviation are reported (N = 3). (A) Different concentrations of glycerol/water solutions which serve as a control for Newtonian flow behavior. (B) Different concentrations of mAb1. The dotted lines are presented to guide the eye.

profile of mAb1 as a function of the apparent shear rate at 25°C obtained by the capillary rheometer for different protein concentrations (120 – 225 mg/mL). Shear-rate dependent viscosity was found with shear-thinning behavior at increasing shear rate and increasing protein concentration. These findings are consistent with the glide-force measurements where a deviation from Newtonian behavior was observed with increasing injection rate (shear rate), as well as with increasing protein concentration.

Due to the direct evidence of shear-thinning behavior during rheological characterization studies by plate/cone and capillary rheometry measurements, we conclude that concentrated protein therapeutics can show reduced injection forces compared to Newtonian fluids due to shear-thinning behavior. Therefore, the correct prediction of glide forces from rheological characterization data requires a sophisticated mathematical model which considers the non-Newtonian behavior of the solution.
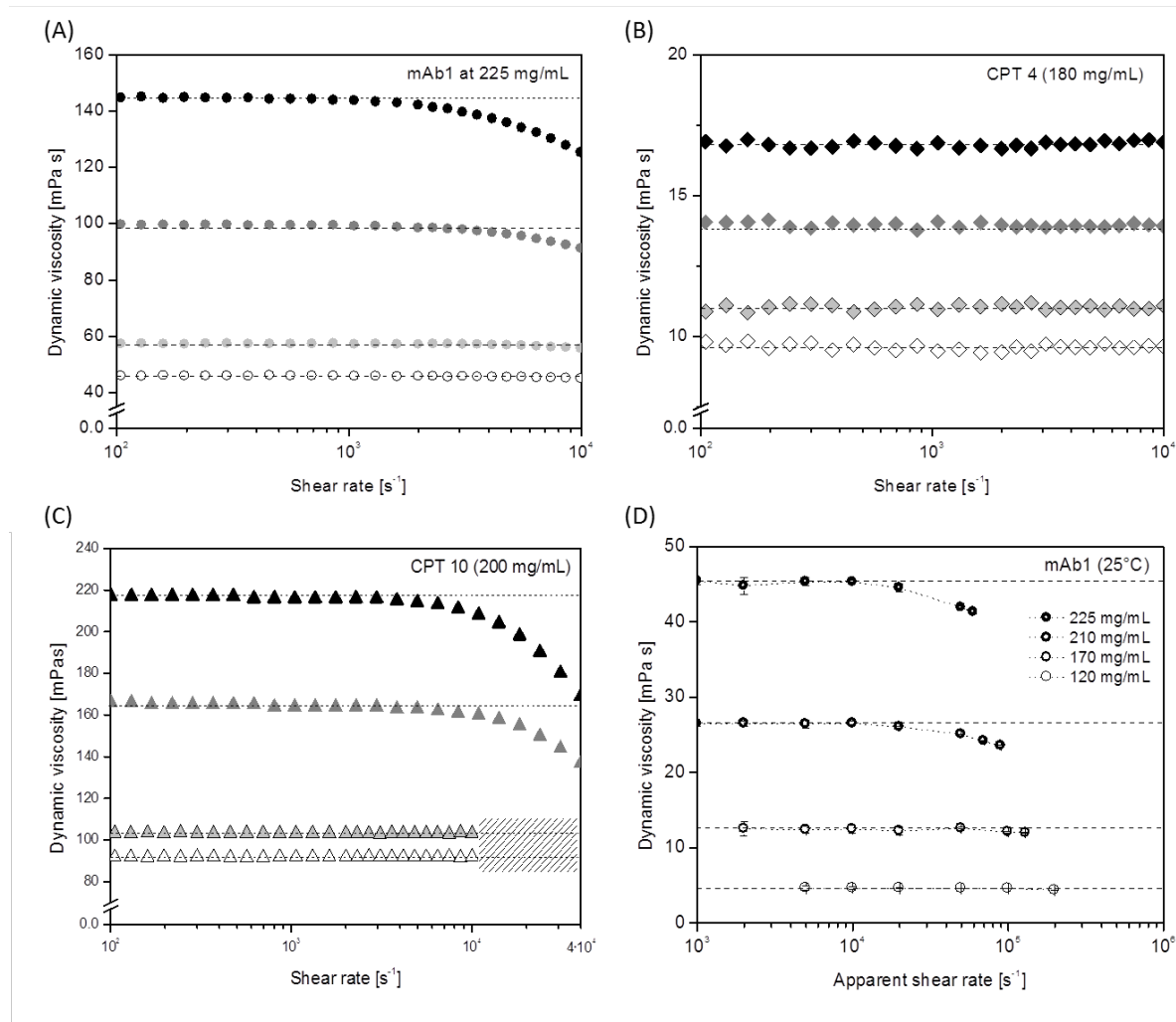
Figure 3.4: Dynamic viscosity as a function of shear rate measured on a plate/cone rheometer at 5°C (black), 10°C (dark grey), 20°C (light grey), and 25°C (white): (A) mAb1 at 225 mg/mL, (B) CPT 4, and (C) CPT 10. For mAb1, the dynamic viscosity was additionally measured on a micro-capillary viscosimeter at 25°C and is presented for 120, 170, 210, and 225 mg/mL as a function of shear rate (D). The dashed and dotted lines are presented to guide the eye. The hatched region indicates that the sample would be ejected from the measuring gap.

Mathematical model to predict the glide force of non-Newtonian liquids from plate/cone viscosity data

In the following section, a mathematical model was developed based on hydrodynamic equations [5, 11, 24-26] in order to correlate glide forces with viscosity data obtained by plate/cone rheometry. Injection of a liquid through a needle results in a counteracting force which is described by the Hagen-Poiseuille's law (Eq. 3.1) [5, 11]. Entry losses and the conical symmetry of the syringe are considered to be negligible (see Fig. 3.1).

$$F = \frac{8\frac{\partial V}{\partial t} \cdot l \cdot R_{syringe}^2}{R_{needle}^4} \cdot \eta + F_{friction;f\left(\frac{\partial V}{\partial t}\right)} \tag{3.1}$$

Eq. 3.1 describes the glide force F [N] as a function of dynamic viscosity η [Pas], volumetric flow rate $\delta V/\delta t$ [m^3/s], length of needle l [m], inner syringe radius $R_{syringe}$ [m], and inner needle radius R_{needle} [m]. Besides hydrodynamic forces, frictional forces between stopper and syringe barrel are considered ($F_{friction}$ [N]) [5] and were determined as described in the Materials and Methods section. Eq. 3.1 is valid for laminar flow in a tube which is defined by a Reynolds number Re $<<$ 2 300 [17-23]. For all tested set-ups, the Reynolds number was equal or smaller than 1 312 and was calculated for the worst case as follows:

$$Re = \frac{2\frac{\partial V}{\partial t}\rho}{\pi R_{needle}\eta} = 1312 \tag{3.2}$$

with $\frac{\partial V}{\partial t} = \frac{2\,\mathrm{ml}}{10\,\mathrm{s}}$, density $\rho_{25°C} = 1$ g/mL, $R_{needle(27G1'')} = 0.109$ mm, and $\eta_{25°C} = 0.89\,mPa\,s$..
The Hagen-Poiseuille's law requires a defined viscosity for the correct prediction of the glide force. However, the viscosity of a non-Newtonian solution is dependent on the shear rate.
The most commonly used equation to describe the viscosity-shear rate relationship of non-Newtonian fluids is the Ostwald-de Waele equation (Eq. 3.2) [24, 25].

$$\eta = K \cdot \dot{\gamma}^{n-1} \tag{3.3}$$

The viscosity is described as a product of the flow consistency index K [Pas^n], and the shear rate $\dot{\gamma}$ [s^{-1}] to the power of n (power law index; dimensionless). Double log transformation of Eq. 3.2 results in a linear viscosity-shear rate profile of the sample. From this profile, K and n were obtained as intercept (log K) and slope (n-1), which is shown in Fig. 3.6 further below. n <1 represents shear thinning behavior, n $=1$ Newtonian behavior, and n >1 shear thickening behavior.
Based on the knowledge of the power law index n, the shear rate profile of non-Newtonian fluids in a needle is derived in the following.
The velocity ν of a non-Newtonian fluid flowing through the needle can be expressed in terms of the average velocity $\nu_{average}$ applied to the system during injection and the variable distance r between the center of the needle (r = 0) and the needle wall (r = R_{needle}) [26]:

$$\nu = \nu_{average} \cdot \left[\frac{3n+1}{n+1} \right] \left[1 - \left[\frac{r}{R_{needle}} \right]^{\frac{n+1}{n}} \right] \qquad (3.4)$$

Differentiation of Eq. 3.3 gives the shear rate $\dot\gamma$ dependent on the power law index n:

$$\dot\gamma = -\frac{d\nu}{dr} = \nu_{average} \cdot \left[\frac{3n+1}{n+1} \right] R_{needle}^{\frac{-(n+1)}{n}} \cdot r^{\frac{1}{n}} \qquad (3.5)$$

The velocity and shear rate profile according to Eq. 3.3 and 3.4 are shown in Fig. 3.5 (A) and (B), respectively. Here, $n = 1$ represents a Newtonian fluid, and $n = 0.4$ and $n = 0.8$ represent two examples of non-Newtonian liquids. For Newtonian fluids, the velocity profile is a parabola where the maximum velocity is 2ν at the center of the tube ($r = 0$) and zero velocity at the tube wall ($r = R_{needle} = 1$). Maximum velocity of a non-Newtonian solution at the same volumetric flow is thereby smaller than that of a Newtonian solution (see Fig. 3.5, A). The maximum shear rate occurs at the wall of the tube, and zero shear rate occurs at the center of the pipe as presented in Fig. 3.5 (B) for a 27 G needle and a volumetric flow of 1 mL/10s. However, the shear rate is not only a function of the distance r between the center and needle wall, but it is also dependent on the rheological properties of the solution. The shear rate of a Newtonian solution increases linearly from the center of the needle ($\dot\gamma = 0$) to the needle wall. In contrast, the shear rate of a non-Newtonian solution is initially smaller than the shear rate of a Newtonian solution, but subsequently exceeds the Newtonian shear rate as the needle wall is approached (Fig. 3.5, B).

Because the viscosity of a non-Newtonian solution is shear-rate dependent, it changes continuously over the needle cross-section in response to the varying shear rate and is therefore a function of the distance r between the center and the needle wall. As the Hagen-Poiseuille's law (Eq. 3.1) requires a defined viscosity to predict the glide force during injection, we defined an average shear rate (here termed effective shear rate) from the shear rate profile in the needle. The appropriate viscosity at the effective shear rate was then obtained from the viscosity-shear rate profile of the sample.

The effective shear rate $\overline\gamma$ is derived by integration of Eq. 3.5 over the tube cross-section divided by the circular area of the needle. The average velocity is expressed as a fraction of volumetric flow and needle cross section $\nu_{average} = \dfrac{\partial V/\partial t}{\pi R_{needle}^2}$:

$$\overline\gamma = \frac{1}{\pi R_{needle}^2} \int_0^R 2\pi r \cdot \dot\gamma(r)\, dr = \frac{2 \frac{\partial V}{\partial t}}{\pi R_{needle}^3} \frac{3n+1}{2n+1} \qquad (3.6)$$

To eventually predict the glide force based on the viscosity-shear rate profile, Eq. 3.6 is inserted into Eq. 3.2 to calculate the viscosity at the effective shear rate. This viscosity is then used in the Hagen-Poiseuille equation (Eq. 3.1) to predict the glide force. As a result, combination of Eq. 3.1, 3.2, and 3.5 gives:
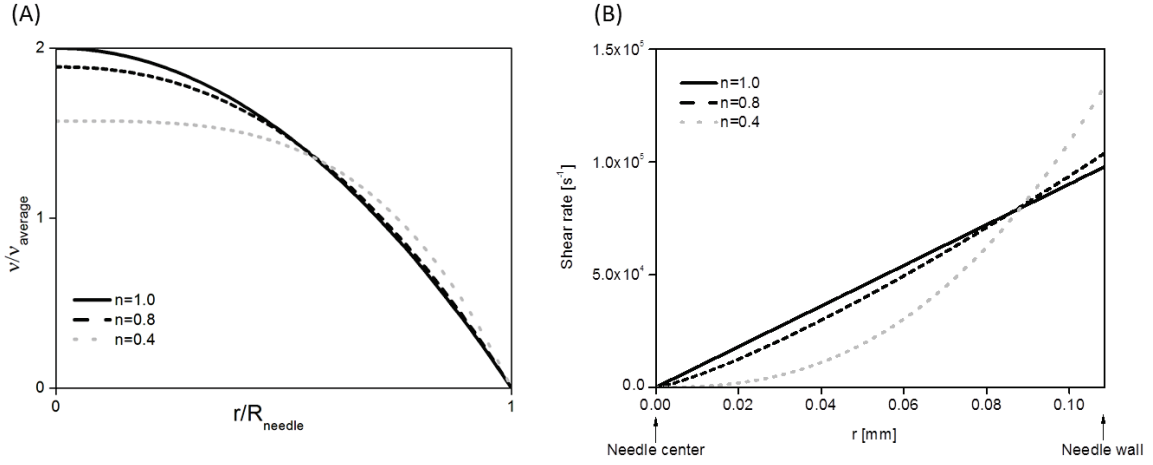
Figure 3.5: Velocity and shear rate profiles for a Newtonian (n = 1) and for two non-Newtonian fluids (n = 0.4, n = 0.8). (A) Normalized velocity profile based on Eq. 3.3 (ν = velocity, $\nu_{average}$ = average velocity, r = distance between needle center ($r = 0$) and needle wall ($r = R_{needle}$)). (B) Shear rate profile in a 27 G needle ($R_{needle} = 0.109$ mm) for an injection rate of 1 mL/10s as a function of r based on Eq. 3.5.

$$F = 2^{n+2}\pi^{1-n} \cdot l \cdot R_{syringe}^2 \cdot K \cdot \left(\frac{\partial V}{\partial t}\right)^n \cdot R_{needle}^{-(3n+1)} \cdot \left(\frac{3n+1}{2n+1}\right)^{n-1} + F_{friction;f\left(\frac{\partial V}{\partial t}\right)} \qquad (3.7)$$

Eq. 3.7 describes the glide force of a non-Newtonian fluid based on the viscosity-shear rate profile from plate/cone rheometry dependent on the syringe/needle dimensions, volumetric flow, and rheological properties of the solution.

Dynamic viscosity is highly dependent on temperature. This relation is predictable and can be described and quantified by the Arrhenius equation. Application to monoclonal antibodies was recently reported by Zarraga *et al.* [40]. Control experiments of the present study confirm these findings and are shown in the supporting information for mAb1 at protein concentration of 120, 170, 210, and 225 mg/mL (Figure 3.10).

In the current set-up, temperature dependence was not considered as injection force experiments as well as viscosity measurements were performed at 25°C. An increase in temperature during injection however was excluded by control measurements (glycerol water solutions) as these measurements showed a linear increase in injection forces with increasing injection rate and viscosity following the Hagen-Poiseuille's law. This will be discussed further below in context to Figure 3.3 (A, Injection forces of concentrated protein therapeutics).
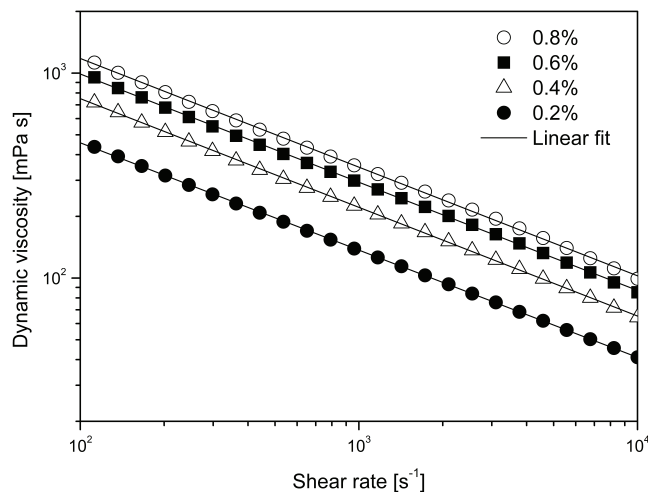
Figure 3.6: Dynamic viscosity of Carbopol 981 gels as a function of shear rate at 25°C: 0.2% (filled circle), 0.4% (triangle), 0.6% (square), 0.8% (open circle). The linear fit was used to determine the consistency index K and the power law index n from the intercept ans the slope $(n-1)$, respectively.

Model verification using Carbopol gels as a surrogate for non-Newtonian liquids

The suitability of Eq. 3.7 to predict the glide force of non-Newtonian liquids was experimentally verified using Carbopol® 981 NF gels. Carbopol was chosen as it is highly water soluble, and concentrations can be achieved exhibiting shear thinning behavior at a shear rate below 10^4 s^{-1}. This is the typical shear-rate range of plate/cone viscosity measurements. Furthermore, such concentrations have a viscosity in the range of concentrated protein products (1 – 100 mPas) at 10^4 s^{-1}.

Fig. 3.6 shows the dynamic viscosity of the Carbopol gels at concentrations of 0.2%, 0.4%, 0.6%, and 0.8% (w/w) as a function of the shear rate measured by plate/cone rheometry. The Carbopol preparations showed shear-thinning behavior with a viscosity between 437 mPas (0.2% w/w) and 1 126 mPas (0.8% w/w) at a shear rate of 10^2 s^{-1} and 41 mPas (0.2% w/w) and 99 mPas (0.8% w/w) at 10^4 s^{-1}. From these viscosity-shear rate profiles (double-logarithmized diagram), the consistency index K and the power law index n were determined from the linear fit as intercept (K) and slope (n-1), respectively (see Eq. 3.2). Table 3.2 summarizes the values of K and n for the different Carbopol concentrations. The consistency index increased with the Carbopol concentration from 5.4 (0.2% w/w) to 15.3 ^{n} (0.8% w/w). The power law index n remained constant with increasing Carbopol concentration (n = 0.46) as indicated by the parallel viscosity profiles (Fig. 3.6).

To summarize, Eq. 3.2 (Ostwald-de Waele law) is suitable to fit the viscosity-shear rate profile of the Carbopol gels. This allows to determine the consistency index K and the power law index n of the solutions needed to predict the glide forces.

In a next step, the glide forces of the Carbopol samples were compared to predicted values using several approaches (Fig. 3.7, B – Fig. 3.7, D). Glide forces were determined at two injection rates (0.04 and 0.08 mL/10s). The injection rates corresponded to shear rates in the range of those obtained during

c_{Carbopol} (w/w)	K [Pas^n]	n [dimensionless]	R^2 (Fig. 3.6)
0.2%	5.4	0.46	1.0
0.4%	9.5	0.46	0.999
0.6%	12.5	0.46	0.999
0.8%	15.4	0.46	0.999

Table 3.2: Rheological parameters of Carbopol gels (25°C). ($c_{Carbopol}$= Carbopol concentration; $K =$ consistency index; $n =$ power law index)

plate/cone viscosity measurements ($10^2 - 10^4$ s^{-1}). Two injection rates were chosen representing a shear rate range where the slope of the viscosity profile changes only minor (few mPas) with an increase in shear rate (0.008 mL/s), and an injection speed (0.004 mL/s) where viscosity is changing over few 100 mPas as shown in Figure 6 (continuous log-log plot).

Different concentrations of glycerol/water solutions served as a control for Newtonian flow behavior and warming effects. Fig. 3.7 (A) compares the measured and the predicted glide forces of the glycerol/water solutions by applying Eq. 3.1 (Hagen-Poiseuille's law). The good agreement (minimum to maximum deviation = <0.1 to 2.5 N) confirms the suitability of the Hagen-Poiseuille's equation to predict glide forces for Newtonian fluids. Furthermore, warming of the solutions was excluded at these shear rates as the samples did not show any deviation from Newtonian behavior.

Fig. 3.7 (B) and (C) show the application of the Hagen-Poiseuille's law (Eq. 3.1) to non-Newtonian fluids. As pointed out, Eq. 3.1 requires a defined viscosity for the prediction of the glide force. In a first attempt, viscosity of the Carbopol samples was read off the viscosity-shear rate profile (Fig. 3.6) at a shear rate of 10^2 and 10^3 s^{-1} and was used for the prediction of the glide force by Eq. 3.1 . Fig. 3.7 (B) shows that the measured glide forces were overestimated by the model with increasing deviation at higher glide forces and lower shear rate.

In Fig. 3.7 (C), the viscosity corresponding to the shear rate at the needle wall $\dot{\gamma}_{wall}$ was used for the prediction of the glide force by Eq. 3.1 ($\dot{\gamma}_{wall} = 645$ and 1.29 x 10^3 s^{-1} for 0.04 mL/10s and 0.08 mL/10s, respectively). The shear rate at the wall is described by the Weissenberg-Rabinowitsch-Mooney equation (Eq. 3.8) [14-16] and was recently used for description of injection forces/viscosity data [13] as discussed in detail further below. This corresponds to Eq. 3.5 solved for the boundary condition $r = R_{needle}$:

$$\dot{\gamma}_{wall} = \frac{\frac{\partial V}{\partial t}}{\pi R_{needle}^3} \frac{(3n+1)}{n} \tag{3.8}$$

Fig. 3.7 (C) shows that the measured glide forces for the different Carbopol concentrations were underestimated by this model. The deviation increased with increasing glide force. This indicates that the selected shear rates (10^2 and 10^3 s^{-1} in Fig. 3.7, B, and wall in Fig. 3.7, C) did not correspond to the correct shear rate for prediction of glide forces based on viscosity data obtained by plate/cone
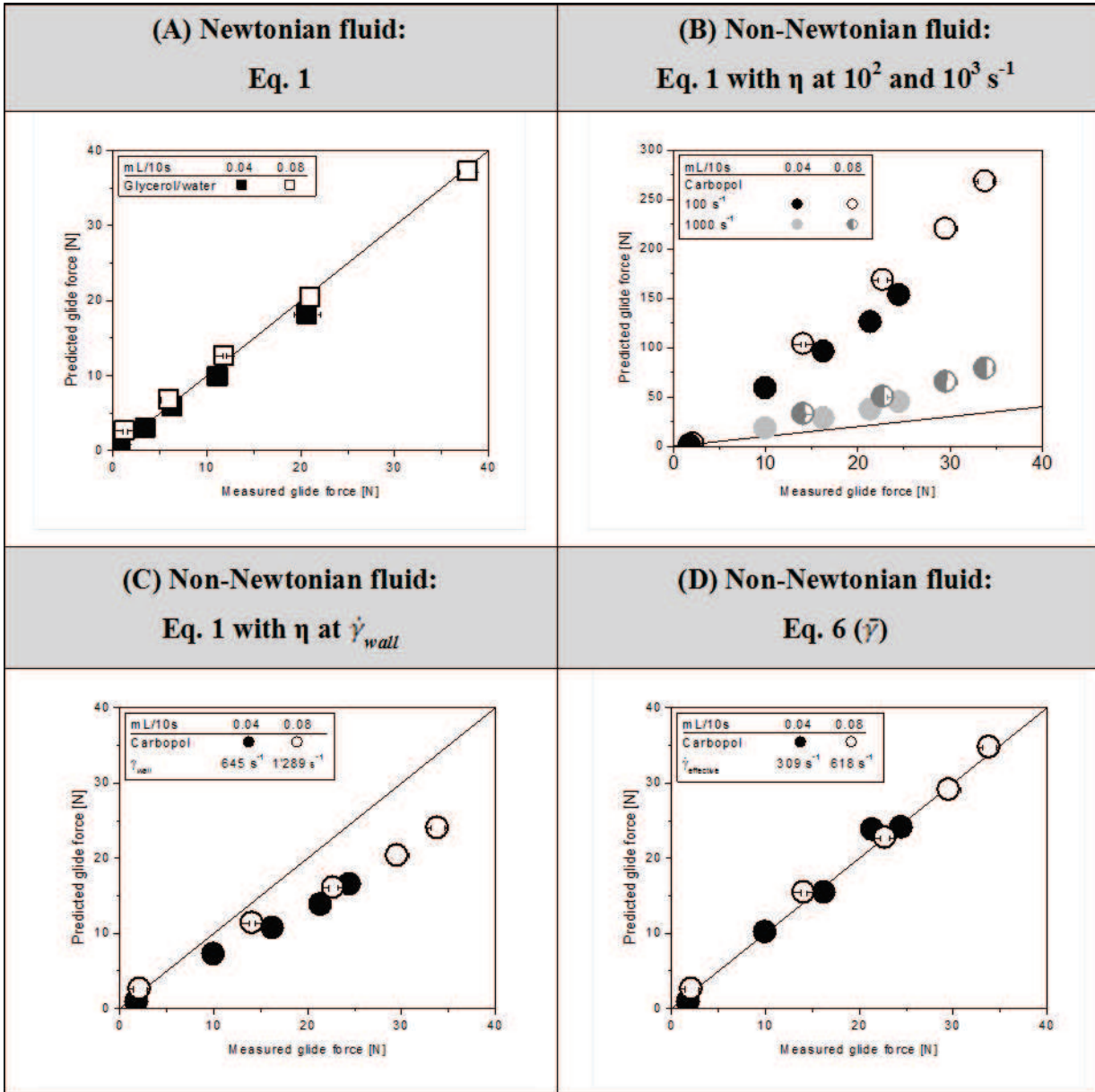
Figure 3.7: Correlation between measured and predicted glide forces at two injection rates (0.04 and 0.08 mL/10s). (A) Different concentrations of glycerol/water solutions (Newtonian fluid) correlated with glide force calculated according to Hagen-Poiseuille's law (Eq. 3.1). (B) (D) Glide forces of Carbopol gels (non-Newtonian fluids) correlated with glide forces calculated according to (B) Eq. 3.1 using the measured viscosity at a shear rate of 102 and 10^3 s^{-1}, (C) Eq. 3.1 using the measured viscosity at the shear rate at the wall $\dot{\gamma}_{wall}$ (Eq. 3.8), and (D) Eq. 3.7 which was based on the effective shear rate $\overline{\gamma}$ (Eq. 3.6). The mean values and standard deviation are reported (N = 3).

rheometry.

In the previous section, the glide force of a non-Newtonian solution was described (Eq. 3.7) by definition of the effective shear rate (Eq. 3.6). Thereby, the effective shear rate is smaller than the shear rate at the wall by the factor of $[1 + (2n)^{-1}]$. Fig. 3.7 (D) shows the application of Eq. 3.7 and compares the measured and predicted glide forces of the Carbopol samples. The correlation plot indicates good agreement between our model and the measured values of the glide force (range: 1.5 N - 35 N) with a deviation ranging from 0.1 N to 2.4 N.

The advantage of our proposed model is that the derivation of the effective shear rate allows to predict glide forces based on viscosity obtained by plate/cone rheometry. The shear rate during plate/cone viscosity measurements remains constant across the gap of the conical measuring device [22]. Our data confirmed that this shear rate corresponded to the effective shear rate during injection through a needle, defined as an average shear rate over the needle cross section.

Another approach to predict glide forces involves the use of viscosity data obtained by a capillary rheometer. This approach is less complex because the principle of operation is the same as for the injection force measurements. A liquid flows through a tube in line with gravity or applied pressure, and the shear rate in the tube is a function of distance between the center of the tube and the tube wall. Therefore, the only prerequisite to predict glide forces based on viscosity data obtained by capillary rheometry is to use the equivalent shear rates. This can be the shear rate at the wall (described by the Weissenberg-Rabinowitsch-Mooney Equation), the apparent shear rate which is the shear rate at the wall for a Newtonian solution, or the effective shear rate. The latter is another advantage of the suggested model as viscosity data from different viscosity methods, such as plate/cone and capillary rheometry, can be used to predict the glide force of a solution.

An advantage of capillary viscosimeters over typical plate/cone instrumentations is the possibility of measuring at higher shear rates (>4 x 10^4 s^{-1}). However, a limitation is the large sample volumes required (in the milliliter range depending on sample viscosity) while measuring at only one specific shear rate per experiment. An advantage of plate/cone rheometry is that it is an established method which is widely used for characterization of protein viscosity [6, 11, 27, 28]. Moreover, viscosity measurements require only small sample volumes ($\sim$80 μL) and a large range of shear rates (1 s^{-1} up to maximal 4 x 10^4 s^{-1}) can be measured in a single experiment.

In summary, the suggested model to predict glide forces of non-Newtonian solutions was experimentally verified by Carbopol gels. Definition of the effective shear rate allows to predict glide forces and correlate them to viscosity data obtained by plate/cone rheometry.

Rheological characterization of concentrated protein therapeutics using the model

Generation of viscosity-shear rate profiles from force measurements was recently reported by Rathore *et al.* The authors used force measurements which were performed on a mechanical testing system (Instron 5564) by applying the Weissenberg-Rabinowitsch-Mooney equation (Eq. 3.8) [13]. Viscosity was presented as a function of the apparent shear rate which is the shear rate at the wall for Newtonian solutions.

The advantage of using force measurements is to obtain viscosity data at high shear rates ($10^5 - 10^6$ s^{-1}). However, application of our model (Eq. 3.7) offers the possibility to obtain viscosity data from glide

force measurements/capillary viscosimeters which can be combined with viscosity data from plate/cone rheometry to produce a single shear-rate profile. This approach allows to generate a broad viscosity profile over several shear rate decades.

The approach of calculating viscosity data from glide force measurements was applied to the mAb1 solutions. Viscosity of the mAb1 samples was determined from the glide force measurements (Fig. 3.3, B) by applying Eq. 3.1. To define the corresponding effective shear rate of the mAb1 solutions, the power law index n of the different mAb1 concentrations was determined based on the following equation:

$$\log \eta = (n - 1) \cdot \log C + (n - 1) \cdot \log \left(\frac{\partial V}{\partial t} \right) \tag{3.9}$$

$$\text{with } C = \frac{2K^{1-n} \ (3n + 1)}{\pi R_{needle}^3 \ (2n + 1)}$$

Eq. 3.9 is obtained by insertion of Eq. 3.6 into Eq. 3.3, followed by taking the logarithm. Fig. 3.8 (A) shows the application of Eq. 3.9 to the experimental data of mAb1 and displays the viscosity ($\log \eta$) as a function of injection rate ($\log \delta V/\delta t$). The power law indices were determined from the slope (n^{-1}) of the linear viscosity profiles ($R^2 = 0.972 - 0.999$). For the mAb1 solutions, the power law index decreased with increasing protein concentrations indicating an increase in shear thinning properties. For the lowest protein concentration (120 mg/mL) tested, a power law index of 0.84 was found and n = 0.57 for the 225 mg/mL solution. Table 3.3 summarizes the power law indices and correlation coefficients for all concentrations.

After determination of the power law indices, the effective shear rate was calculated by Eq. 3.6. This allows the generation of the viscosity-shear rate profile for the mAb1 formulations shown in Fig. 3.8 (B). The dynamic viscosity is presented as a function of the effective shear rate with viscosity data from the plate/cone rheometer (shear-rate range: $<1 \ \mathrm{s}^{-1}$ – $10^4 \ \mathrm{s}^{-1}$), the capillary viscosimeter (shear-rate range dependent on flow cell and viscosity: e.g. $\sim 2 \ \mathrm{x} \ 10^3$ – $1.5 \ \mathrm{x} \ 10^5 \ \mathrm{s}^{-1}$ for a 10 mPas sample), and the glide force measurements (shear-rate range: variable due to injection rate and syringe-needle set-up; presented: $3 \ \mathrm{x} \ 10^4$ – $1.6 \ \mathrm{x} \ 10^5 \ \mathrm{s}^{-1}$). The viscosity of the mAb1 solutions increased with increasing protein concentration. The different protein solutions showed a Newtonian plateau at low shear rates which is known from polymer chemistry as the zero shear-rate plateau [22, 27]. Between $8 \ \mathrm{x} \ 10^3$ and $1.6 \ \mathrm{x} \ 10^5 \ \mathrm{s}^{-1}$, the mAb1 solutions showed shear-thinning behavior depending on the protein concentration. This is known as the power law region of a sample. The 225 mg/mL solution, for example, shows a viscosity of 46 mPas at the low shear-rate plateau followed by a decrease in viscosity to 21.5 mPas at $\sim 1.6 \ \mathrm{x} \ 10^5 \ \mathrm{s}^{-1}$. With lower protein concentrations, the beginning of the power law region is shifted to higher shear rates. Additionally, the shear-thinning properties are diminishing with almost no shear-thinning behavior at 120 mg/mL.

The rheological profile of the mAb1 solutions resembles the rheological behavior of various polymers such as polyacrylamide or xanthan gum solutions, for example [28-32]. This is characterized by a Newtonian plateau with the zero shear rate viscosity η_0 followed by the power law region and converging to a secondary plateau (infinite shear rate viscosity η_∞) [33], which was not yet reached for the mAb1 solutions at the measured shear rates. This three-step behavior can be described mathematically by the Carreau-model (Eq. 3.10).
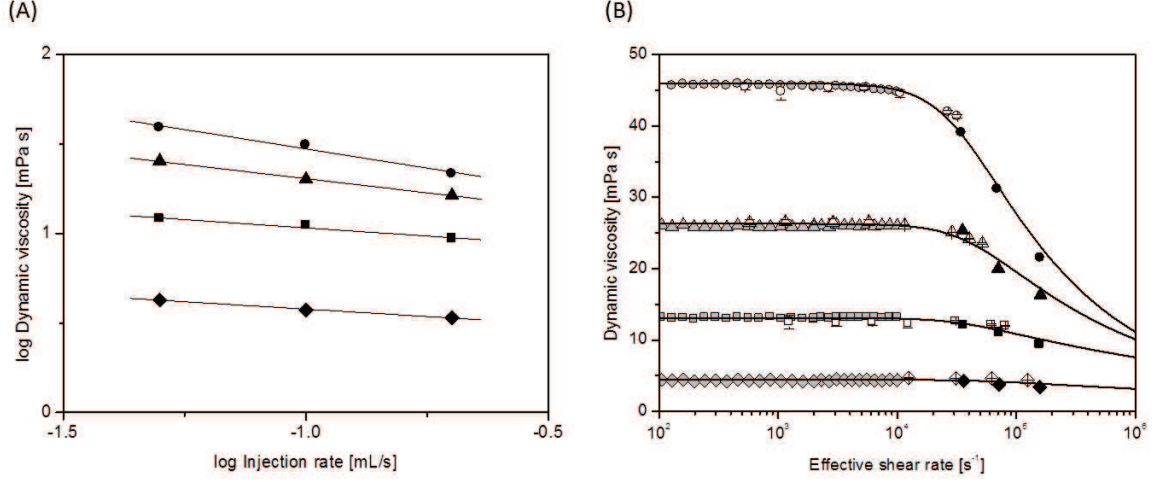
Figure 3.8: mAb1 at 120 mg/mL (diamond), 170 mg/mL (square), 210 mg/mL (triangle), and 225 mg/mL (circle). (A) Dynamic viscosity (log η) obtained by force measurements as a function of injection rate (log $\partial V/\partial t$). The power law indices n were determined from the slope (n^{-1}) of the linear fit (solid line) based on Eq. 3.9 and are summarized with the corresponding correlation coefficients in Table 3. (B) Viscosity profile of different concentrations of mAb1 as a function of the effective shear rate (25°C). The viscosity was measured using a plate/cone rheometer (grey, filled symbols), the capillary viscosimeter mVROC (empty symbols), and glide force experiments (black symbols). The viscosity profile was modeled by the Carreau model (solid line) based on Eq. 3.10 and the corresponding fitting parameters are summarized in Table 3.3.

$$\eta = \eta_\infty + (\eta_0 - \eta_\infty) \cdot \left(1 + \Gamma^2 \dot{\gamma}^2\right)^{\frac{n-1}{2}} \tag{3.10}$$

The shear thinning region is defined by a modified power law term in Eq. 3.10 containing the factor $\left(1 + \Gamma^2 \dot{\gamma}^2\right)^{\frac{n-1}{2}}$ similar to Eq. 3.3 (Ostwald-de Waele equation) which was used to generate the model. However, the difference is that the Ostwald-de Waele equation breaks down in the region of the first Newtonian plateau [33]. In contrast, the Carreau model includes the Newtonian plateau (η_0) and extends the power law by the factor +1 giving the sigmoidal shape to the shear thinning region. Γ [s] is a time constant reflecting the critical shear rate $\dot{\gamma}_{crit} = \Gamma^{-1}$ marking the end of the zero shear-rate plateau and the onset of the shear thinning region [33, 34].

Fitting of Eq. 3.10 to the viscosity-shear rate profiles of the different concentrations of mAb1 using the software Origin 7.5 (OriginLab Corporation, MA) is shown in Fig. 3.8 (B). Here, η_0 was defined as the viscosity at 2 x 10^3 s^{-1}, n was already determined as described above, and η_∞ was set to the minimal viscosity possible (1 mPas) corresponding to the viscosity of water. $\dot{\gamma}_{crit} = \Gamma^{-1}$ was set as a variable parameter. Table 3.3 lists the values for the different protein concentrations. The quality of the fittings is indicated by the correlation coefficients which were 0.939 and 0.984 for the protein concentrations of 210 mg/mL and 225 mg/mL, respectively. The coefficients imply that the Carreau model allows to describe the rheological behavior of the mAb1 solutions at high protein concentrations. For the lower protein concentrations however, only a poor fit was obtained (R^2 = 0.219 and 0.817 for 120 mg/mL

$c_{protein}$ [mg/m]	η [mPas]	n [dimensionless]	Γ^{-1} [10^3 s]	R^2 (Fig. 3.8, A)	R^2 (Fig. 3.8, B)
120	4.4	0.84	33 ±10	0.996	0.219
170	13.1	0.82	57 ±67	0.972	0.817
210	26.3	0.68	41 ±5	0.999	0.939
225	46.0	0.57	31 ±2	0.981	0.984

Table 3.3: Rheological parameters of mAb1 (25°C). ($c_{protein}$ = protein concentration; η = dynamic viscosity at 2 x 10^3 s^{-1}; n = power law index; Γ = time constant)

and 170 mg/mL, respectively). The assumption for application of the Carreau model is that the data points for determination of the power law index n by Eq. 3.9 are in the exponentially decreasing power law region. At lower protein concentration however, the power law region shifts to higher shear rates limiting the shear-thinning region to a few data points for the tested shear-rate range (Fig. 3.8, B). Additionally, for the 120 mg/mL for example, viscosity data obtained by the glide-force measurements were in the shear-rate region close to the Newtonian plateau where the Ostwald-de Waele equation breaks down. Therefore, the shear-thinning behavior cannot be accurately described by the Carreau model at the tested shear-rate range for the protein concentrations of 120 mg/mL (i.e., at lower protein concentrations).

The Carreau model describes the rheological profile of a solution acting at high shear rates like a Newtonian fluid with a viscosity of η_∞ and like a Newtonian fluid with a viscosity of η_0 at low shear rates connected by a shear-thinning region. The origin of shear-thinning behavior characterized by a power law index 1 can be manifold. In the literature, dissociation of aggregates or polymeric entanglements, deformation or degradation, and alignmentorientation of three-dimensional structures to the flow field are described for polymers [22]. For the Carbopol gels, it is suggested that the shear-thinning properties originate from deformation of the three-dimensional network of the polymer [35]. Moreover, the power law index was found to be constant with increasing Carbopol concentrations (Table 3.2). This indicates that the shear-thinning properties are independent of polymer concentration suggesting a consistent microstructure (e.g. similar physical entanglement) with increasing polymer concentrations.

For the mAb1 solutions in contrast, the power law index was found to decrease with increasing protein concentrations. This indicates an increase in shear-thinning properties with increasing protein concentration implying an increase in the microstructural arrangements. The formation of these microstructural arrangements/oligomeric networks/clusters was recently proposed for a monoclonal antibody solution at high(er) protein concentrations [6, 9, 36-41]. The strength of the microstructure formed can increase rapidly with concentration [40]. The disruption or deformation of these self-associating mAb networks clusters (e.g. held together by weak non-covalent attractive forces) might be a possible explanation for the shear-thinning behavior of concentrated mAb solutions. We use the phrase 'self-associating mAb clusters' in accordance with e.g. Zarraga *et al.* [40], Yadav *et al.* [36]. These mAb self-associations responsible for increasing the viscosity are reversible, and unlikely to be physical entanglements or long range elasticity such as observed in polymer systems (e.g. the mAb solutions have low G'/G", data not

shown). Instead, the mAb clusters are likely to be governed by colloidal interactions with electrostatic and hydrophobic attractive wells that are rendered anisotropic by the mAb shape and heterogeneous surface charge distribution [37-41]. The timescales for association and dissociation depend on the intricate balance of colloidal, Brownian, and shear forces. Experiments of increasing and decreasing shear rates show that the viscosity response to changes in shear rate occur in the order of seconds, implying a relatively fast relaxation time (under negligible instrument inertia and comparing with Newtonian viscosity controls). The substantial reduction in viscosity at shear rates of around 1×10^3 s^{-1} or higher also points to a very fast relaxation time. This suggests that the mAb clusters are unable to form to full extent due to the competing fast timescale associated with shearing motion.

Referring to the rheological profile, this implies that at low shear rates, the self-associating networks are not influenced by the shear stress showing a Newtonian plateau. With increasing shear rate, dissociation and/or alignment of the clusters may occur which manifests in the shear-thinning region and eventually in the second Newtonian plateau with an optimally oriented microstructure or deformation of the clusters. This has been observed through the anisotropic normal stresses measured in a related study [40]. A detailed understanding of the relationship between shear-thinning behavior of a mAb formulation indicated by the power law index and the occurrence of mAb clustering with increasing protein concentration is subject of ongoing research.

3.4 Conclusion

Determination of injection forces of several highly concentrated protein formulations revealed a significant reduction in injection forces compared to Newtonian fluids due to shear-thinning behavior. In order to correctly predict injection forces from rheological data, different mathematical models considering Newtonian and non-Newtonian flow behavior were compared and the assumptions, advantages, and limitations were discussed.

The suggested model was used to determine viscosity data at high shear rates (3×10^4 to 1.6×10^5 s^{-1}) from injection force measurements of concentrated protein solutions. These data could be directly combined to viscosity data from rotational plate/cone and capillary rheometry. The rheological profile with a shear rate between 10^2 and 1.6×10^5 s^{-1} was described mathematically by the Carreau model. Knowledge of the rheological characterization data allows to accurately predict injection forces for different syringe-needle combinations as well as a large range of injection rates. The added value is that by use of this model viscosity data from different measuring systems can be combined meaning that we can now characterize viscosity at a much higher shear rate than what can be measured with commercial available instruments up to date. This is highly relevant for the design of devices for combination products (e.g. autoinjectors or injection pumps) to assess the limits and robustness during evaluation, planning and design phases of development. Moreover, consideration of shear-thinning behavior may extend the viscosity/concentration limit due to consequent reduction of injection forces while maintaining the overall user requirements.

3.5 Acknowledgments

3.6 References

1. S.J. Shire, Formulation and manufacturability of biologics, Curr. Opin. Biotech., 20 (2009) 708-714.

2. S.J. Shire, Z. Shahrokh, J. Liu, Challenges in the development of high protein concentration formulations, J. Pharm. Sci., 93 (2004) 1390-1402.

3. N.W. Warne, Development of high concentration protein biopharmaceuticals: the use of platform approaches in formulation development, Eur. J. Pharm. Biopharm., 78 (2011) 208-212.

4. M. Adler, Challenges in the Development of Pre-filled Syringes for Biologics from a Formulation Scientists Point of View, Am. Pharm. Rev., 15 (2012).

5. D.E. Overcashier, E.K. Chan, C.C. Hsu, Technical considerations in the development of prefilled syringes for protein products, Am. Pharm. Rev., 9 (2004) 77-83.

6. S. Kanai, J. Liu, T.W. Patapoff, S.J. Shire, Reversible self-association of a concentrated monoclonal antibody solution mediated by Fab-Fab interaction that impacts solution viscosity, J. Pharm. Sci., 97 (2008) 4219-4227.

7. S. Yadav, J. Liu, S.J. Shire, D.S. Kalonia, Specific interactions in high concentration antibody solutions resulting in high viscosity, J. Pharm. Sci., 99 (2010) 1152-1168.

8. A. Saluja, D.S. Kalonia, Nature and consequences of protein-protein interactions in high protein concentration solutions, Int. J. Pharm., 358 (2008) 1-15.

9. J. Liu, M.D. Nguyen, J.D. Andya, S.J. Shire, Reversible self-association increases the viscosity of a concentrated monoclonal antibody in aqueous solution, J. Pharm. Sci., 94 (2005) 1928-1940.

10. A. Sheikhzadeh, J. Yoon, D. Formosa, B. Domanska, D. Morgan, M. Schiff, The effect of a new syringe design on the ability of rheumatoid arthritis patients to inject a biological medication, Appl. Ergon., 43 (2012) 368-375.

11. V. Burckbuchler, G. Mekhloufi, A.P. Giteau, J.L. Grossiord, S. Huille, F. Agnely, Rheological and syringeability properties of highly concentrated human polyclonal immunoglobulin solutions, Eur. J. Pharm. Biopharm., 76 (2010) 351-356.

12. N. Rathore, P. Pranay, B. Eu, W. Ji, E. Walls, Variability in syringe components and its impact on functionality of delivery systems, PDA J. Pharm. Sci. Tech., 65 (2011) 468-480.

13. N. Rathore, P. Pranay, J. Bernacki, B. Eu, W. Ji, E. Walls, Characterization of protein rheology and delivery forces for combination products, J. Pharm. Sci., 101 (2012) 4472-4480.

14. K. Weissenberg, Über die Viskosität und Elastizität von Solen, Z. Phys. Chem., (1929).

15. B. Rabinowitsch, Über die Viskosität und Elastizität von Solen, Z. Phys. Chem., 145 (1929).

16. R. Eisenschitz, Rabinowitsch B., Weissenberg, K., Mitteilung der deutschen Materialprüfungsanstalten, Sonderheft 8 (1929) 91.

17. G.H.L. Hagen, Über die Bewegung des Wassers in engen zylindrischen Röhren., Poggendorf's Annalen der Physik und Chemie, 46 (1939 (reprinted 1933, see Schiller)) 423-442.

18. J.L.M. Poiseuille, Recherches experimentales sur le mouvement des liquides dans les tubes de tres petits diametres, C.R. Acad. Sci., 11 (1840) 1041-1048.

19. L. Schiller, Drei Klassiker der Strömungslehre: Hagen, Poiseuille, Hagenbach, Akad. Verlagsgesellschaft, Leipzig, ed. 1933.

20. O. Reynolds, An Experimental Investigation of the Circumstances Which Determine Whether the Motion of Water Shall Be Direct or Sinuous, and of the Law of Resistance in Parallel Channels., Philos. Transactions., 174 (1883) 935-982.

21. O. Reynolds, On the dynamical theory of incompressible viscous fluids and the determination of the criterion, Philos. Transactions., (1895).

22. T.G. Mezger, Das Rheologie Handbuch, third ed., Vincentz Network, Hannover, 2010.

23. C.W. Macosko, Rheology: principles, measurements, and applications, first ed., Wiley-VCH, New York, 1994.

24. F.W. Ostwald Über die Geschwindigkeits-Funktion der Viskosität in dispersen Systemen., Kolloid Z., 36 (1925).

25. A. De Waele, Viscometry and plastometry, Oil and Color Chem. Assoc. J., (1923).

26. R.T. Toledo, Fundamental of Food Process Engeneering, third ed., Springer Science and Business Media, New York, 2007.

27. S.M. Loveday, L.K. Creamer, H. Singh, M.A. Rao, Phase and rheological behavior of high-concentration colloidal hard-sphere and protein dispersions, J. Food. Sci., 72 (2007) R101-107.

28. A.S. Cavadas, F.T. Pinho, J.B.L.M. Campos, Laminar non-Newtonian impinging jet flow confined by sloping plane walls, J. Non-Newton. Fluid., 169 (2012) 1-14.

29. C.A. Hieber, H.H. Chiang, Shear-Rate-Dependence Modeling of Polymer Melt Viscosity, Polym. Eng. Sci., 32 (1992) 931-938.

30. I. Wagstaff, C.E. Chaffey, Shear Thinning and Thickening Rheology - 1. Concentrated Acrylic Dispersions, J. Colloid. Interf. Sci., 59 (1977) 53-62.

31. Y. Xia, P.T. Callaghan, Study of Shear Thinning in High Polymer-Solution Using Dynamic NMR Microscopy, Macromolecules, 24 (1991) 4777-4786.

32. M.M. Cross, Relation between Viscoelasticity and Shear-Thinning Behavior in Liquids, Rheol. Acta., 18 (1979) 609-614.

33. N. Phan-Thien, Understanding viscoelasticity: Basics in Rheology, first ed., Springer Verlag, Heidelberg, 2002.

34. R. Byron Bird, P.J. Carreau, A nonlinear viscoelastic model for polymer solutions and melts, Chem. Eng. Sci., 23 (1968) 427-434.

35. M.T. Hernandez, J. Pellicer, J. Delegido, M. Dolz, Rheological characterization of easy-to-disperse (ETD) Carbopol hydrogels, J. Disper. Sci. Technol., 19 (1998) 31-42.

36. S. Yadav, T.M. Laue, D.S. Kalonia, S.N. Singh, S.J. Shire, The influence of charge distribution on self-association and viscosity behavior of monoclonal antibody solutions, Mol. Pharm., 9 (2012) 791-802.

37. A. Chaudhri, I.E. Zarraga, T.J. Kamerzell, J.P. Brandt, T.W. Patapoff, S.J. Shire, G.A. Voth, Coarse-Grained Modeling of the Self-Association of Therapeutic Monoclonal Antibodies, J. Phys. Chem. B, 116 (2012) 8045-8057.

38. A. Chaudhri, I.E. Zarraga, S. Yadav, T.W. Patapoff, S.J. Shire, G.A. Voth, The role of amino acid sequence in the self-association of therapeutic monoclonal antibodies: insights from coarse-grained modeling, J. Phys. Chem. B, 117 (2013) 1269-1279.

39. W.G. Lilyestrom, S. Yadav, S.J. Shire, T.M. Scherer, Monoclonal Antibody Self-Association, Cluster Formation, and Rheology at High Concentrations, J. Phys. Chem. B, 117 (2013) 6373-6384.

40. I.E. Zarraga, R. Taing, J. Zarzar, J. Luoma, J. Hsiung, A. Patel, F. Lim, High Shear Rheology and Anisotropy in Concentrated Solutions of Monoclonal Antibodies, J. Pharm. Sci., 102 (2013) 2538-49.

41. E.J. Yearley, I.E. Zarraga, S.J. Shire, T.M. Scherer , Y. Gokarn, N.J. Wagner, Y. Liu, Small-angle neutron scattering characterization of monoclonal antibody conformations and interactions at high concentrations. Biophys. J.,105(2013), 720-31.

42. S. Kiese, A. Papppenberger, W. Friess, H.C. Mahler, Shaken, not stirred: mechanical stress testing of an IgG1 antibody. J. Pharm. Sci., 97 (2008), 4347-66.

43. D.K. Sharma, D. King, P.Oma, C. Merchant, Micro-Flow Imaging: Flow Microscopy Applied to Sub-visible Particulate Analysis in Protein Formulations. AAPS J., Volume 12(2010), 455-464.

44. R. Strehl, V. Rombach-Riegraf, M. Diez, K. Egodage, M. Bluemel, M. Jeschke, A.V. Koulov, Discrimination between silicone oil droplets and protein aggregates in biopharmaceuticals: a novel multiparametric image filter for sub-visible particles in microflow imaging analysis, Pharm. Res., 29(2012), 594-602.

3.7 Supporting information

The supporting information contains one Table 3.4 and three Figures 3.9, 3.10, and 3.11.

1. Figure 3.9 shows a detailed approach of data analysis of injection force measurements.

2. Figure 3.10 shows the temperature dependence of different protein concentrations of mAb1 described by the Arrhenius equation.

3. Table 3.4 and Figure 3.11 display data on protein integrity before and after injection for mAb1 at a worst case injection rate (2 mL/10s).
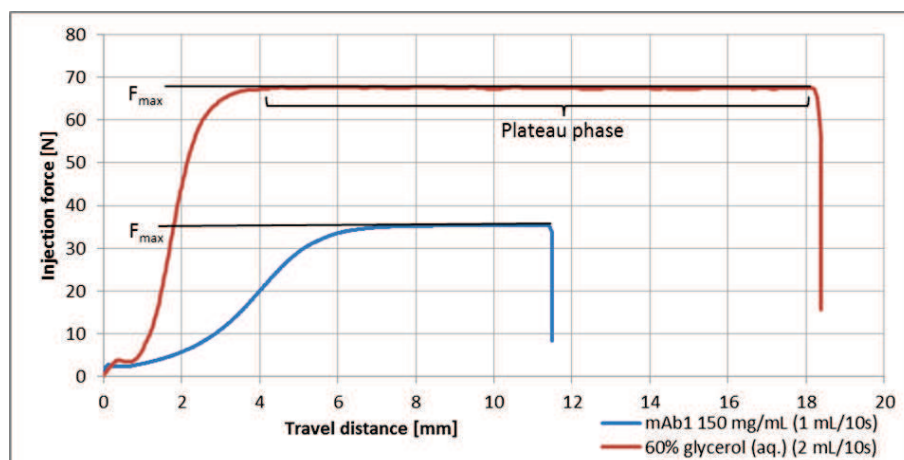
Figure 3.9: Representative injection force profiles and data analysis of injection force experiments. For determination of the glide force, the plateau of the force profile was analyzed and the maximum of this plateau was taken as representative for glide force at the end of injection. Examples are shown for a 60% aqueous glycerol solution (2 mL/10s) and for a 150 mg/mL mAb1 formulation (1 mL/10s).
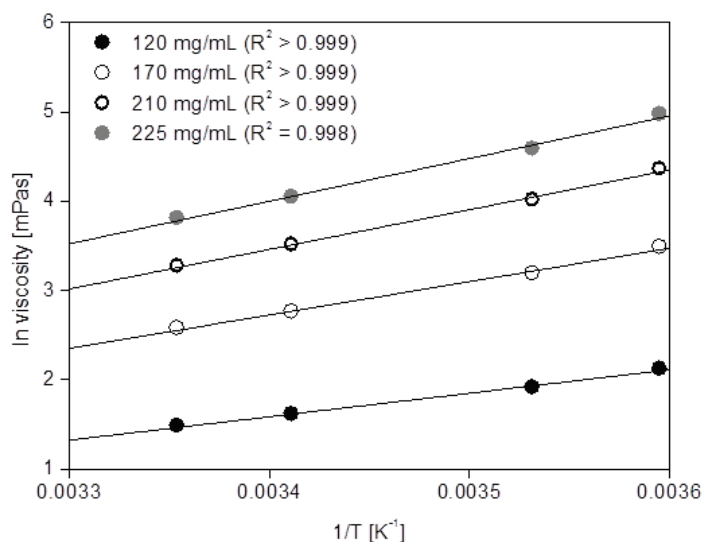
Figure 3.10: Arrhenius plot for mAb1 at 120, 170, 210, and 225 mg/mL. Dynamic viscosity was measured as triplicates and the average is reported. (T = absolute temperature)

Data analysis of injection force profiles

For data analysis of injection force profiles, the maximal force of the plateau was read off from the force-travel distance graph as representative for glide force at the end of injection as shown in Figure 3.9.
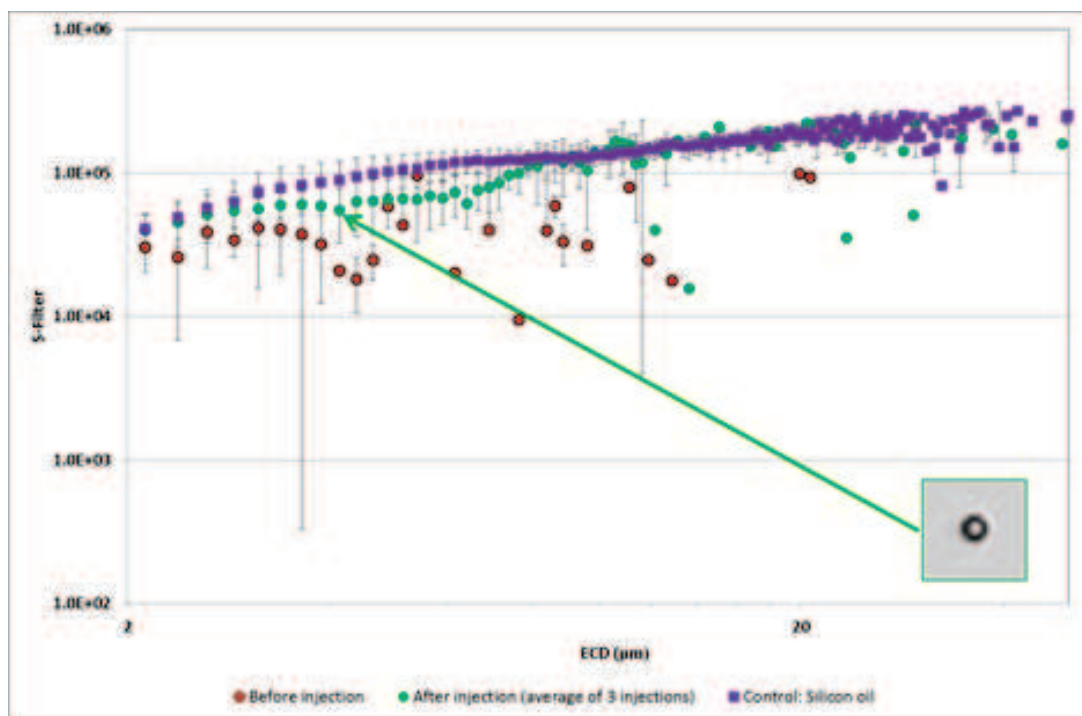
Figure 3.11: Sub-visible particle characterization by micro-flow imaging of mAb1 before and after injection. Silicon oil droplets were identified as described by Koulov *et al.* [44],based on reference measurements of pure silicon oil. Measurements were performed for a worst case scenario (injection rate 2 mL/10s) as triplicates.

Temperature dependence of viscosity

The temperature dependence of viscosity can be described by the Arrhenius equation/plot [40]. Figure 3.10 shows that the Arrhenius equation is applicable to the mAb1 formulations indicated by a linear profile with $R^2 = 0.995 - 0.997$.

Protein integrity of mAb1 (225 mg/mL) before and after injection

Data on protein integrity measured by HP-SEC [42] and particle load (visible particles as described by Kiese *et al.* [42] and sub-visible particles measured by light obscuration [42] and by micro-flow imaging [43]) before and after injection were determined for a worst case scenario (injection rate 2 mL/10s) for mAb1 at 225 mg/mL. The data are summarized in Table 3.4 and Figure 3.11. The measurements were performed as triplicates and average and standard deviation are reported.

The data show no difference before and after injection force experiments for the visible particle and the protein aggregate measurements. For the sub-visible particles, particle load increased after injection as measured by light obscuration. However, micro-flow imaging measurements showed by differentiation of the reported sub-visible particles between silicon oil droplets and others as reported previously [44], that this increase is due to silicon oil droplets coming from the syringe wall during exertion of the syringe.

		Before injection	After injection
Visible particles		Free of particles	Free of particles
Sub-visible particles (Light obscuration) [cumulative counts per mL]	$\geq$2 μm	34	1402 $\pm$696
	$\geq$5 μm	11	682 $\pm$303
	$\geq$10 μm	4	359 $\pm$168
	$\geq$25 μm	1	11 $\pm$2
	$\geq$50 μm	0	1 $\pm$1
SEC	Monomer	97.7	97.7 $\pm$0.0
	High molecular weight species	1.3	1.3 $\pm$0.0
	Low molecular weight species	1.0	1.0 $\pm$0.0

Table 3.4: Visible particles, sub-visible particle counts measured by light obscuration and characterization by micro-flow imaging, monomer content, and high and low molecular weight species (HP-SEC) before and after injection. Measurements were performed for a worst case scenario (injection rate 2 mL/10s) for mAb1 at 225 mg/mL as triplicates. Average and standard deviation are reported.Needle and syringe dimensions.

Chapter 4

Measuring tissue backpressure – *in vivo* injection forces during subcutaneous injection

Authors:
Andrea Allmendinger

Robert Mueller
Edward Schwarb
Mark Chipperfield
Joerg Huwyler
Hanns-Christian Mahler
Stefan Fischer

Purpose:

Injection forces of parenterals are well understood and were intensively characterized in the past *in vitro*. However, limited information is available about the *in vivo* situation and how *in vitro* testing is actually representative of *in vivo* situations. Thus, the scope of the present study was to investigate the contribution of the backpressure of the subcutaneous (sc) tissue layer to injection forces during *in vivo* injection.

Methods:

Göttingen minipigs were chosen based on the sc tissue of these animals best resembling humans compared to other animal models. 10 Göttingen minipigs received injections of isotonic dextran solutions (1 – 100 mPas) into the *plica inguinalis* using different injection rates and volumes (0.025 – 0.2 mL/s and 2.5 vs. 4.5 mL). The force related to sc backpressure was determined by use of an instrumental set-up built for this purpose and defined as the difference in injection force between *in vitro* and *in vivo* measurement

corrected by a temperature factor.

<u>Results:</u>

The contribution of the sc backpressure to injection forces was found to increase linearly with viscosity and injection rate in the range of 0.6 – 1.0 N (1 mPas) and 1.8 – 4.7 N (20 mPas) for an injection rate of 0.025 mL/s and 0.2 mL/s, and 6.7 N for 100 mPas at 0.025 mL/s. Variability increased with viscosity and injection rate resulting in a minimum and maximum contribution of backpressure of 2.0 to 12.9 N for 20 mPas at the highest injection speed tested. No difference was found between the tested injection volumes of 2.5 and 4.5 mL for the conditions tested. Macroscopic evaluation of the injection sites showed well-localized injection sites in the sc tissue layer. In this study, the contribution of the sc backpressure to injection forces was differentiated from the contribution of the injection device as well as from a local temperature effect leading to warming of the (equilibrated) sample in the needle and therefore smaller injection forces than expected.

<u>Conclusions:</u>

The quantitative amount of sc tissue backpressure is significant and ranged in average from 0.6 to 4.7 N (1 – 20 mPas, 0.025 – 0.2 mL/s) with a maximum value of 12.9 N (20 mPas, 0.2 mL/s). Besides the contribution of the tissue, local warming of the sample in the needle during injection has to be considered when estimating injection forces representative for the *in vivo* situation.

4.1   Introduction

Subcutaneous (sc) drug administration of parenterals is a convenient way for easier drug application compared to the intravenous (iv) route of injection [1-7]. This offers the possibility of home-treatment by the patient him-/herself or treating healthcare professional, especially if combination products like pre-filled syringes, autoinjectors or injection pumps are used [8-10]. The development of these combination products requires a comprehensive assessment and understanding of parameters contributing to injection forces. These include (1) device components, (2) drug solution properties, and (3) human factors, such as the capability of the end-user to apply the product. In particular, device components contribute to the hydrodynamic component of injection forces, which can be described by the Hagen-Poiseuille's law. These are the syringe diameter, the needle inner diameter, and the needle length. Dynamic viscosity of the solution (2) is itself dependent on temperature (described by Arrhenius equation), formulation, and concentration of the active substance [9, 11-14]. Besides hydrodynamic forces, frictional forces between stopper and plunger have to be considered as well. These are usually influenced by siliconization of the syringe barrel and plunger dimensions among others [11, 15].

An anthropometric strength study showed that the force that a user can exert onto a syringe plunger is determined by multiple (human) factors including the strength of the individual, the upper limb, and hand posture required for injection (health status) [16]. It should also be considered that the personal preference and training of the individual may influence their actual behavior [16]. In reality, users are able to moderate the injection force (when using pre-filled syringes) by adjusting their injection speed and may choose a slower injection resulting in a lower injection force to fit their capability or preference. Human factor studies usually do not target actual sc administration but usage of injection pads. Thus, deriving injection force data from these studies lack a potential impact of sc backpressure. The same applies for *in vitro* testing of injection forces as well as syringe functionality testing (break loose and glide force) which is usually performed into air, thus, ignoring the *in vivo* situation and potential impact of sc backpressure.

Predictive *in silico* models were described in literature to estimate injection forces of parenterals [9, 11, 13]. However, only limited data is available dealing with the contribution of the tissue during injection. Cilurzo *et al.* have recently performed an experiment where they injected a 19 mPas and a 101 mPas solution into the abdominal skin (sc) from an Eurasian female who underwent cosmetic surgery. They found an increase in injection force by a factor of 1.1 compared to injection into air due to tissue resistance. This experiment was performed *ex vivo* at a constant injection speed of 1 mm/s, which was equivalent to approximately 0.03 mL/s [17]. Vosseler and co-workers have measured the in-line pressure during intradermal injection into pig ears using microneedles (*ex vivo*). They found significant backpressure of the intradermal tissue when tested for a viscosity of 1 and 55 mPas at (slow) injection rates of 0.1 and 0.5 mL/h. The authors reported that the backpressure is a non-linear function of flow rate [18]. In different studies, the intestinal fluid pressure in the forelimb of Yorkshire pigs (3.9 $\pm$1.4 mmHg) [19], in human foot skin (5.9 $\pm$2.9 mmHg) [20], and in human sc tissue of the lower limb (2.5 $\pm$3.0 mmHg) [21] was measured giving a hint towards a contribution of the tissue pressure to injection forces. However, up to date there is no *in vivo* study available which characterizes the contribution of the sc backpressure to injection forces.

The aim of the present study is to investigate the contribution of the backpressure of the sc tissue layer

to injection forces during injection into the *plica inguinalis* of Göttingen minipigs. Göttingen minipigs are considered as a relevant animal model to study sc tissue as the structure of their hypodermis resembles that in humans more than any other investigated animal (e.g. rodent, monkey) [2, 22-24]. Different concentrations of isotonic dextran solutions corresponding to viscosities of 1, 10, 20, and 100 mPas were administered at injection rates of 0.025, 0.1, and 0.2 mL/s and two injection volumes (2.5 and 4.5 mL) were tested. The contribution of the sc backpressure to injection forces was defined and determined by comparing subsequent *in vitro* and *in vivo* measurements of injection force profiles corrected by a temperature factor by use of an instrumental set-up built for this purpose. After termination, the injection sites were dissected and inspected macroscopically as well as histologically.

4.2 Materials and Methods

Materials

Dextran solutions

Isotonic dextran solutions were prepared in concentrations of 0%, 14.9%, 20.8%, and 34.8% by dissolution of dextran 40 (BioChemica, Darmstadt, DE) in water for injection and by addition of sodium chloride (Merck, Darmstadt, DE). The pH was determined as 5.5 $\pm$0.4. The dextran concentrations corresponded to viscosities of 1, 10, 20, and 100 mPas at room temperature characterized by plate/cone rheometry as described previously [11]. For the tested injection rates, the dextran solutions showed Newtonian flow behavior.

Disposable injection equipment

Disposable 5 mL plastic syringes (BD, Franklin Lakes, NJ) from a single lot with luer-lock tip were connected by male or female luer fittings (1/16, Nylon) to a one-way stopcock with luer connection obtained from Cole-Parmer (Vernon Hills, IL) and non-expanding PTFE tubing with an inner diameter of 1.6 mm and a length of 100 cm (Scat Europe, Mörfelden, DE). The tubing was connected to a Microlance^{TM} 3 26 G 3/8 needle (BD, Drogeda, IRL) as shown in Figure 4.1 (A).

Methods

Injection force measurements and data analysis

The instrumental set-up for the injection force measurements is shown in Figure 4.1 (A). A PHD 2000 Infusion syringe pump from Harvard Apparatus (Holliston, MA) was used in combination with a RSB5 Subminiature load cell (force sensor) with an accuracy of $\pm$0.5% of the full calibrated scale (0 – 100 N). The load cell was connected to a DI-100U interface obtained from Loadstar Sensors (Fremont, CA). Injection force measurements were performed at constant injection rates of 0.025, 0.1, and 0.2 mL/s applied by the syringe pump. An injection rate of 0.1 mL/s was chosen which is considered as appropriate for the end-user and commonly used and accepted for functionality testing [11, 16]. 0.2 mL/s was chosen as a maximum test rate, whereas 0.025 mL/s represents a slow injection rate as e.g. used

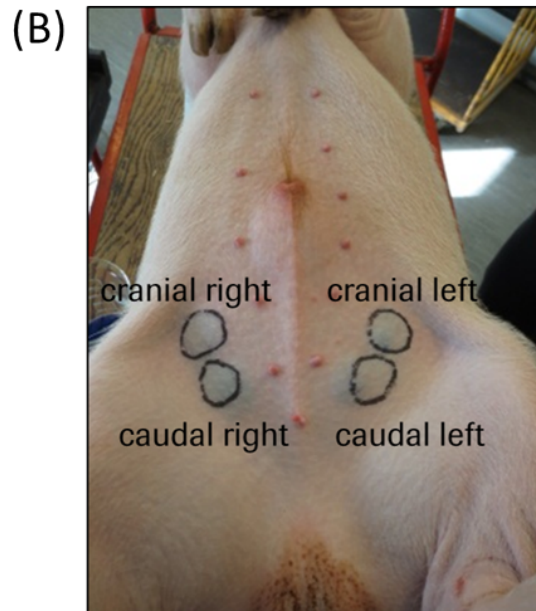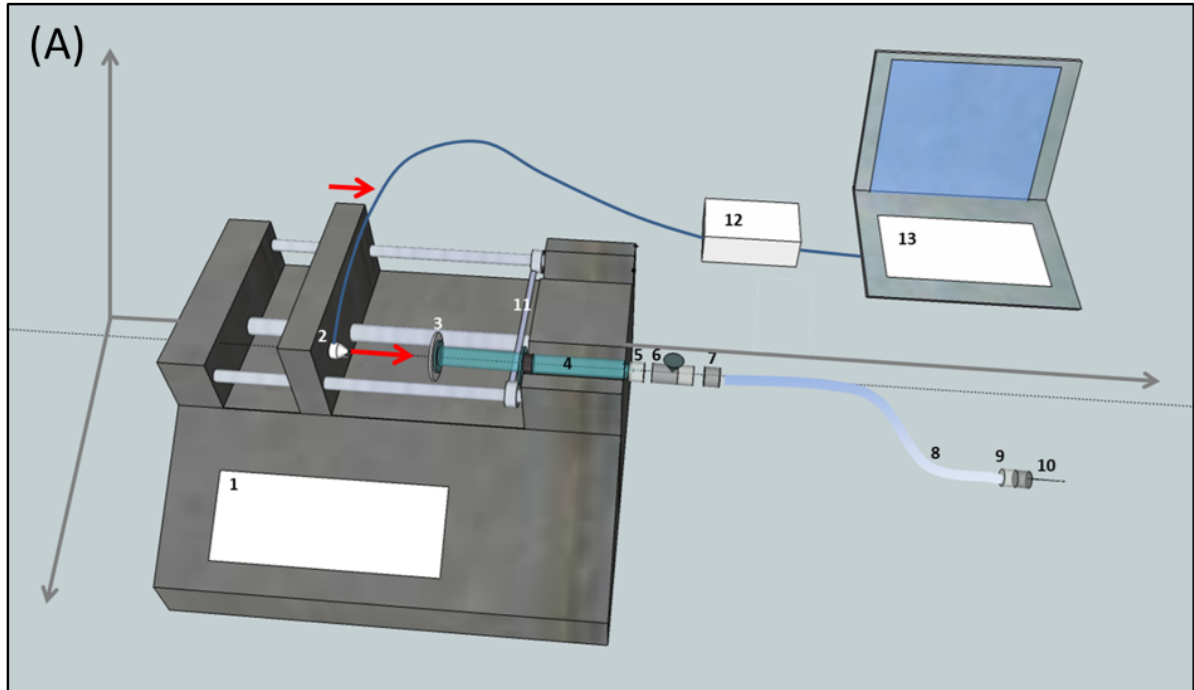**Figure 4.1:** Instrumental set-up for the injection force experiments (A), and injection sites for sc injection into the *plica inguinalis* of the minipig (B). (1) Syringe pump, (2) load cell (force sensor), (3) sticking metal platelet, (4)/(5) syringe with luer-lock tip, (6) one-way cock, (7)/(9) luer lock connections, (8) PTFE tubing, (10) needle, (11) fixation, (12)/(13) computer and interface.

by injection devices for high-volume sc dosing [8]. The force exerted to the plunger of the syringe was recorded by the load cell each 0.1 s using the software Single-channel LV-1000 LoadVUE Pro (Loadstar Sensors, Fremont, CA). The injection equipment and the test solutions were equilibrated to controlled room temperature overnight. Before each experiment, the injection equipment was rinsed with the sample under consideration. Directly before the *in vivo* measurements, control measurements into air (*in vitro*) were performed to exclude differences in injection forces caused by differences in temperature as well as differences in injection equipment. The temperature was monitored and found as 20°C ±1.5 (MIN 17.6°C and MAX 23.6°C).

Data analysis of the injection force profiles was performed by calculating the average value of the injection force plateau which was reached for all profiles between 0.25 – 2.5 mL for an injection rate of 0.025 mL/s, between 0.5 – 1 mL for 0.1 mL/s, and between 1 – 2 mL for 0.2 mL/s. Representative profiles are shown in Figure 4.2 for *in vitro* as well as for *in vivo* measurements for different injection rates, viscosities, and injection volumes tested. Arrows indicate the range used for data analysis to determine the average value of the plateau of the force profile.

Control for local temperature effect at the injection site

To account for the effect of body temperature on solution temperature in the needle and thus viscosity, control measurements were performed (*in vitro*, N = 3) by injection of dextran solutions into water which was tempered to 39°C - equal to the body temperature of minipigs [25]. Only the needle was inserted into the water to simulate *in vivo* injection. The instrumental set-up is shown in the Supporting information Figure 4.7. A representative example of the injection force profile is shown in Figure 4.2 (B). The measurements were performed dependent on viscosity and injection rate, and were compared to subsequent injections into air at room temperature. Based on the difference, the decrease in injection force per degree Celsius caused by warming of the sample in the needle was calculated using the Arrhenius equation [26]. This correction factor per degree Celsius was then applied to each individual *in vivo* measurement. (No difference was measured between injections into air and injections into water at the same temperature.)

For final data analysis, the correction factor was substracted from the difference between injection forces determined by subsequent *in vitro* and *in vivo* measurement. To give an order of magnitude, correction factors are presented in Table 4.1 of the Supporting information dependent on viscosity and injection rate for a temperature increase from 20 – 39°C (minipig) and additionally from 20 – 37°C (humans).

***In vivo* testing set-up**

Ten Göttingen minipigs (male) with a body weight between 21.5 – 27.3 kg received four sc injections per dosing occasion into the *plica inguinalis* as shown in Figure 4.1 (B). There were three dosing occasions per pig during the study with a recovery period of at least 48 h before the next four injections. Prior to dosing, the minipigs were anaesthetized using Zoletil® dosed as 0.1 ml/kg. Before each injection, the injection sites were inspected for absence of infections. Upon puncture, it was verified visually that the needle was in the sc tissue layer indicated by loose movement of the needle in the tissue. The injection angle was in parallel with the body surface to avoid penetration of the sc tissue layer. During and/or after each injection, the injection site was inspected for successful injection into the sc tissue layer by

(temporarily observed) blister formation.

The dextran concentrations were administered with different injection rates and volumes and performed ten times for each condition. The injections were randomized for minipig, injection site, viscosity, and injection rate. The study was approved and conducted in accordance with local legislation for animal welfare (Pipeline Biotech A/S license number 2011/561-2006, schedule C2 and extension).

Macroscopic evaluation after dissection of the injection sites and histology

At termination after the third dosing, macroscopic evaluation of the dissected injection sites was conducted to ensure successful injection into the sc tissue layer. To facilitate the recognition of the injection sites, 1 drop of ink (blue stamp ink, Carfa, Richterswil, CH) was added to 20 mL of sample (which was determined to not affect viscosity). The length, width, and height of the injection sites (as shown in Figure 4.5, B and C) was measured and recorded by the same person.

For histological characterization of the injection sites, the dissected tissue was transferred and fixed in 10% neutral buffered formalin, and embedded in paraffin. Slices of 4 μm were prepared, stained with standard hematoxylin-eosin, and investigated under the light microscope.

4.3   Results

In vivo characterization of sc backpressure

The contribution of the backpressure of the sc tissue layer to injection forces was investigated in Göttingen minipigs dependent on solution viscosity (1 – 20 mPas) and injection rate (0.025 – 0.2 mL/s). Figure 4.3 (A) shows the force related to backpressure as a function of viscosity for the different injection rates for an injection volume of 2.5 mL. It is presented as mean values from 10 randomized measurements with standard deviation as well as minimum and maximum values. Overall, the force related to sc tissue backpressure was measured between 0.1 to 12.9 N. In detail, it was found in the range of 0.6 – 1.0 N for 1 mPas, 0.7 – 2.4 N for 10 mPas, and 1.8 – 4.7 N for 20 mPas for an injection rate of 0.025 to 0.2 mL/s (mean values). Variability of mean values increased with higher viscosity and injection rate as indicated by error bars in Figure 4.3. Maximum contribution of tissue backpressure to injection forces of 1.7 N, 6.4 N, and 12.9 N were found for the samples with 1, 10, and 20 mPas for the highest injection rate, respectively. The highest dextran concentration with a viscosity of 100 mPas was found to show an additional force related to backpressure of 6.7 N (mean value) with a maximum value of 7.2 N measured at an injection rate of 0.025 mL/s.

Figure 4.3 (A) shows that a linear increase of the contribution of sc backpressure to injection forces was found with increasing viscosity for all three injection rates. This is emphasized in Figure 4.3 (A) for the lowest injection speed of 0.025 mL/s indicating a linear increase ($R^2 = 0.99$) of sc backpressure related contribution to injection forces between 1 mPas up to the highest viscosity tested, which was 100 mPas. A linear increase was also found dependent on injection rate for the tested solution viscosities (correlation not shown separately).

In a follow-up experiment, the injection volume was increased to 4.5 mL and the sc backpressure was tested for a viscosity of 10 mPas at an injection rate of 0.1 mL/s, in order to study potential impact of
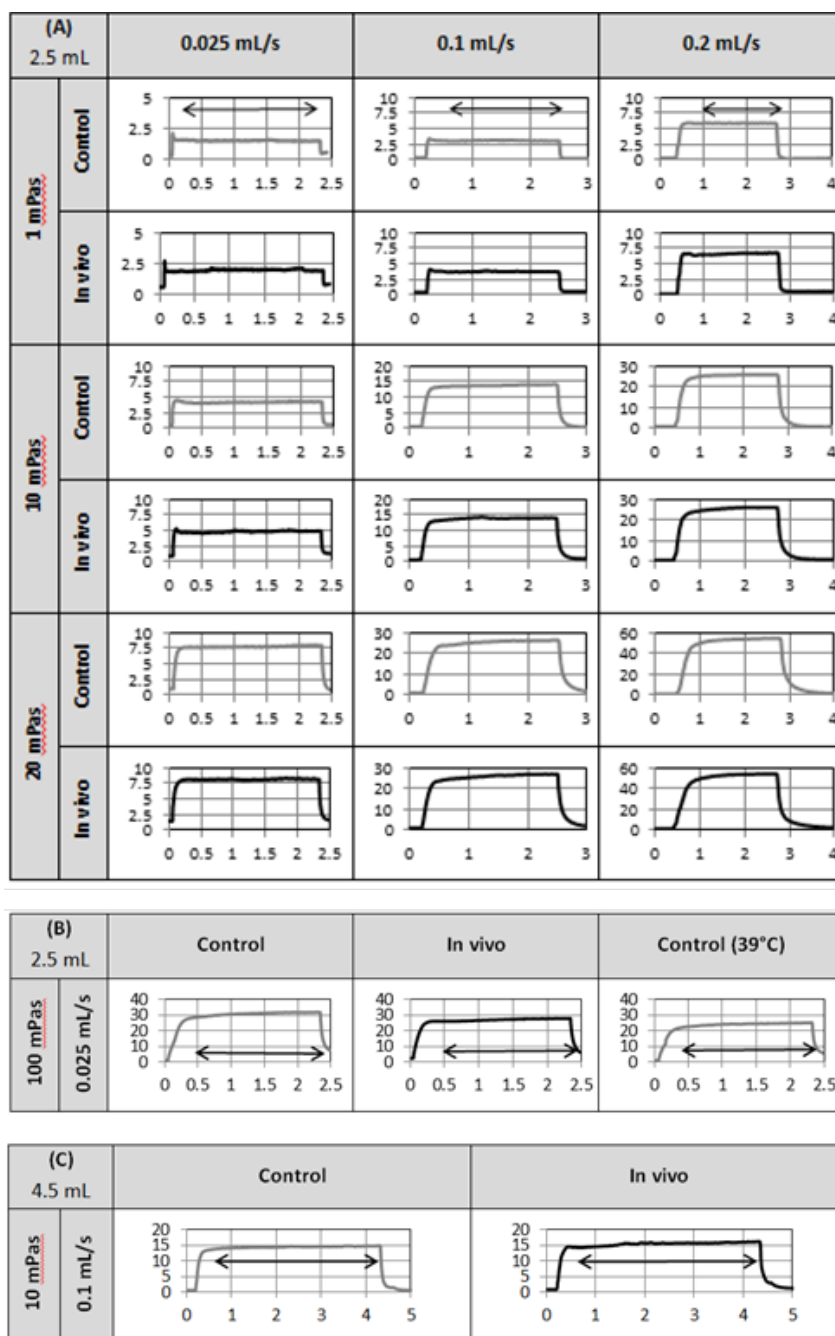
Figure 4.2: Representative examples of injection force profiles for *in vitro* (control) and *in vivo* measurements. The injection force is presented as a function of injection volume for all profiles shown. (A) Different viscosities (1 –20 mPas) and injection rates (0.025 – 0.2 mL/s) for an injection volume of 2.5 mL. (B) Viscosity of 100 mPas at 0.025 mL/s (2.5 mL) including injection force profile from temperature control measurement (39°C). (C) Injection volume of 4.5 mL for a viscosity of 10 mPas at 0.1 mL/s. The arrows indicate the range used for data analysis to determine the average value of the plateau of the profile which was 0.25 – 2.5 mL for an injection rate of 0.025 mL/s, 0.5 – 1 mL for 0.1 mL/s, and between 1 – 2 mL for 0.2 mL/s.

injection volume on sc tissue backpressure. Figure 4.3 (B) shows the corresponding mean values from 10 injections as well as minimum and maximum values with comparison of the 2.5 and 4.5 mL. No difference in the contribution of injection forces of sc backpressure was found between the two injection volumes, however variability as indicated by error bars of the mean value decreased for the larger injection volume indicating a stabilization of the measured injection force signal.

For all tested conditions, the injection force profile reached a plateau as shown in Figure 4.2 for the different viscosities and injection rates, including the higher injection volume of 4.5 mL (Figure 4.2, C). This indicates that - up to the maximal tested injection volume - the visually observed blister formation for some injection sites of the tissue due to the injected volume itself has a negligible influence on injection force or is in the magnitude of the measurement error.

It has to be highlighted that the contribution of the sc backpressure was quantified in this study and differentiated from the contribution of the injection device as well as separated from a local temperature effect. This temperature effect was quantified as a temperature correction factor as outlined in the Methods section. To our knowledge, this is the first study to report a local temperature effect at the injection site leading to warming of the (equilibrated) sample during sc injection in the needle and smaller injection forces than expected. This will be discussed in detail later in this article.

Injections were performed ten times for each condition and were randomized for minipig, injection site, viscosity, and injection rate. Figure 4.4 displays the box plots of the contribution of sc backpressure to injection forces (average values) dependent on minipig (named as 1 to 10, Figure 4.4, A), injection site (Figure 4.4, B), and observed blister formation after injection (Figure 4.4, C) showing no differences in sc backpressure related injection force between these parameters. Most interestingly, Figure 4.4 (C) does not show a difference in the contribution of backpressure to injection forces between injections where blister formation after injection was observed and those where it was not observed. This confirms the previous findings, that the sc backpressure does not increase with increasing injection volume (2.5 vs. 4.5 mL) and that the visually observed blister formation due to the injected volume itself during injection has a negligible contribution or is within the variation of injection force measurements for the conditions tested. Thereby, the number of injection sites showing blister formation after injection was found to decrease with increasing bodyweight of the minipig as shown in the Supporting information in Figure 4.8.

Verification of injection into the sc tissue layer

As the *plica inguinalis* has only a thickness of a few mm, a short needle (3/8") was chosen to facilitate injection into the sc tissue layer. It was verified for all injections that they were indeed occurring into the sc space by: (1) visual inspection before *in vivo* injection indicated by loose movement of the needle inserted into the tissue. (2) During injection, where differentiation between sc and intradermal (id) injection is possible as id injection manifests in characteristic blister formation of the skin. Besides the visual inspection of the injection sites, sc injection was verified on the last study day for the full set of injections, including all different conditions for injection, by dissection of the injection sites followed by (3) macroscopic evaluation and (4) histology.
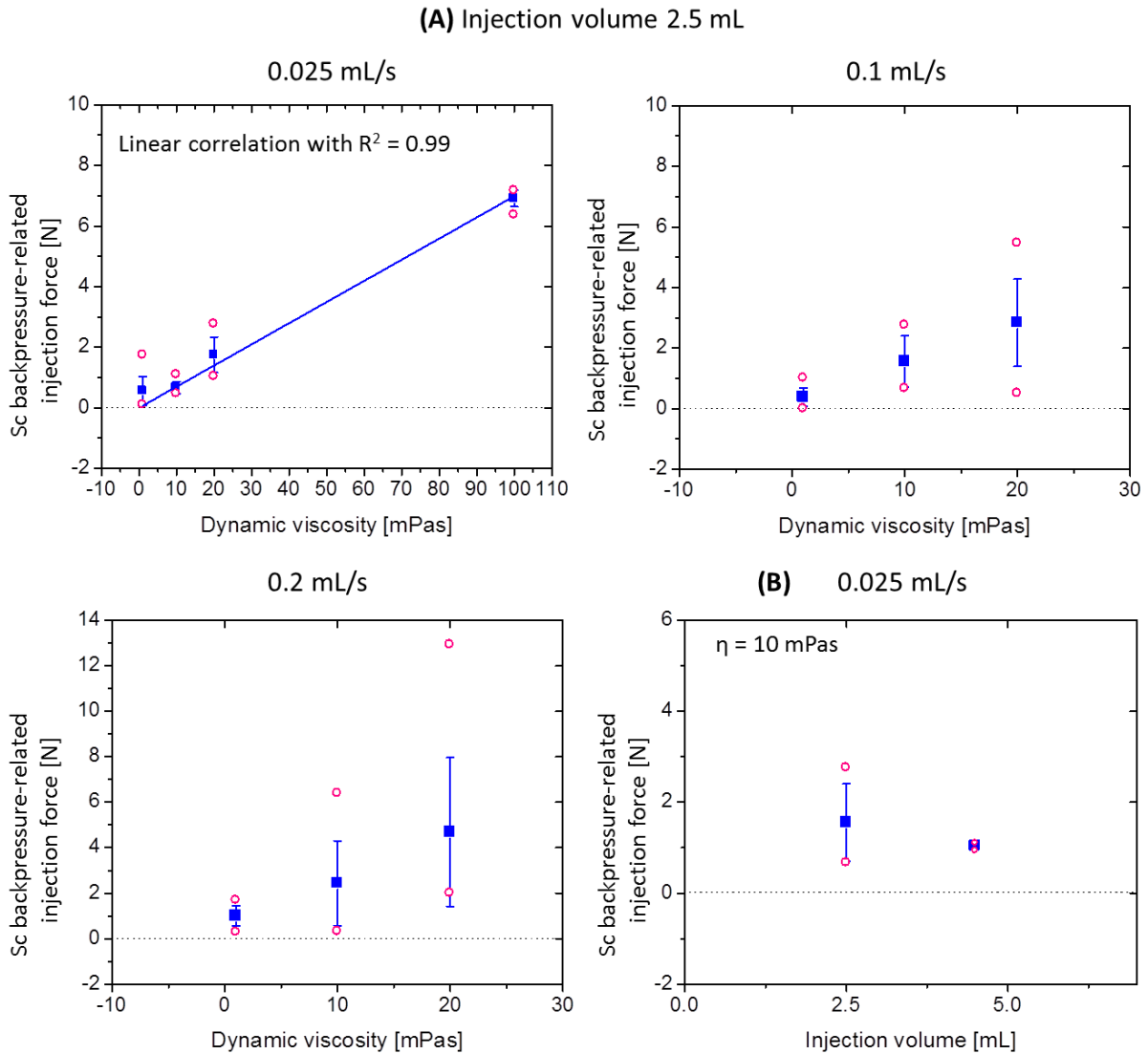
Figure 4.3: Contribution of sc backpressure to injection forces dependent on injection rate (0.025, 0.1, and 0.2 mL/s), viscosity (1 – 100 mPas) of dextran solutions, and injection volume (2.5 mL, A, or 4.5 mL, B). The contribution of backpressure to injection forces was analyzed as value of the injection force plateau. Measurements were performed as N = 10 randomized by minipig, injection site, injection rate, and viscosity and were reported as mean value with standard deviation (squares), minimum and maximum value (circle).
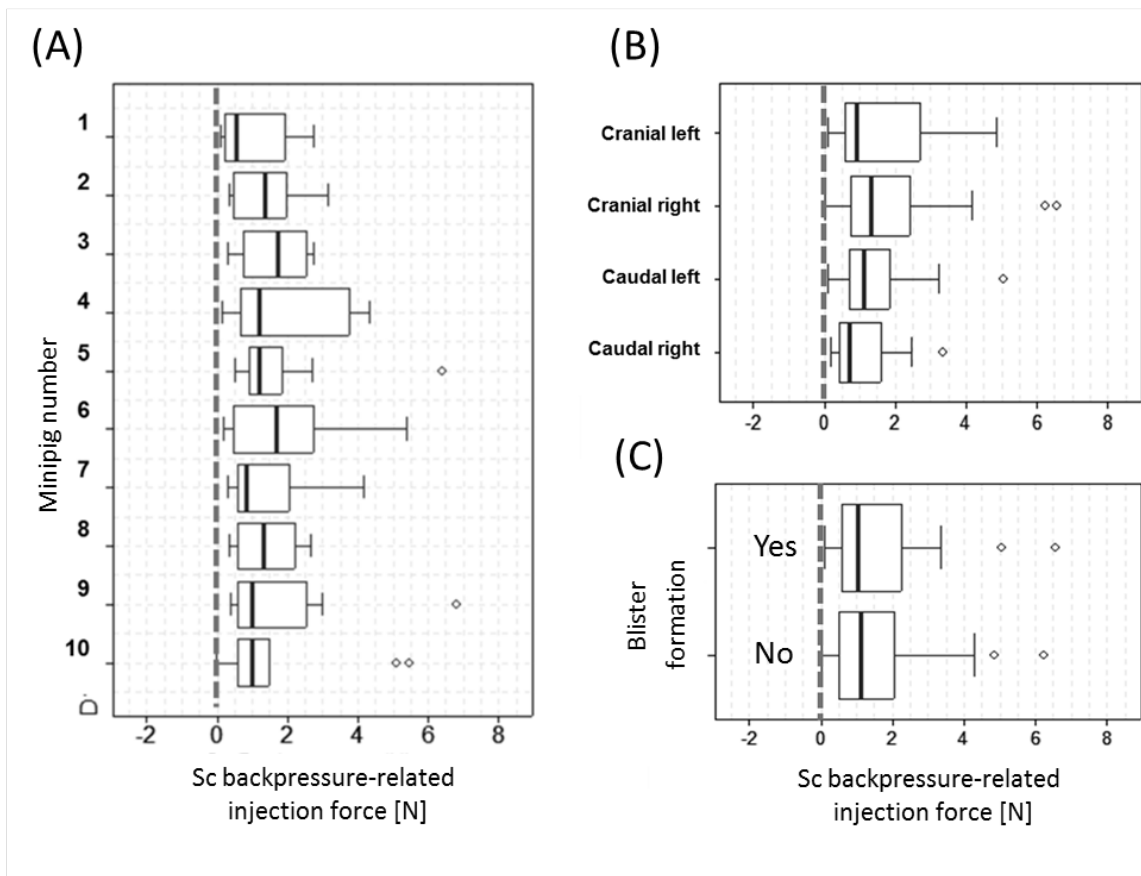
Figure 4.4: Box plots of the contribution of sc backpressure to injection forces (mean value) dependent on (A) minipig (1 to 10), (B) injection site, and (C) blister formation after injection. The box plot represents mean, upper and lower quartile (box), minimum and maximum values (whiskers) as well as outlier defined by >1.5 times of the interquartile range (circle).
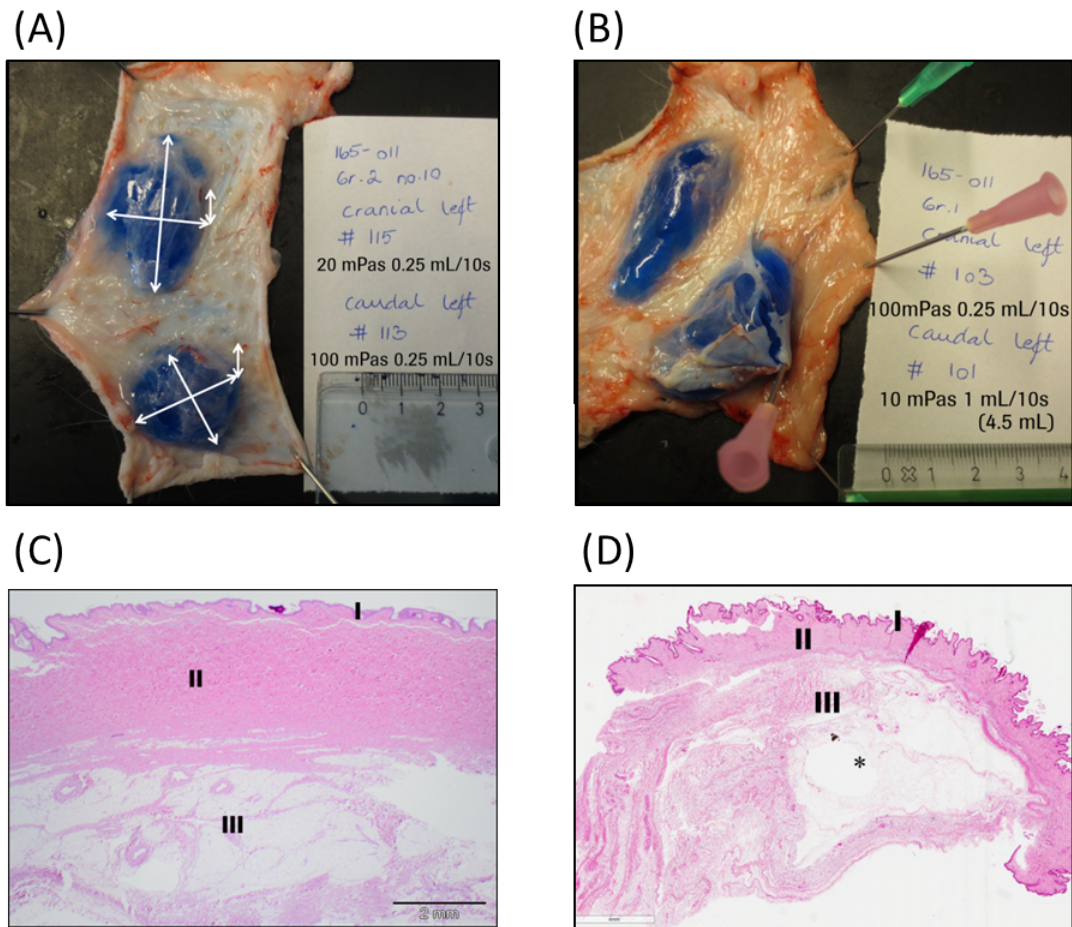
Figure 4.5: (A, B) Representative pictures of dissected injection sites (*plica inguinalis*) after injection of a colored dextran solution (20 and 100 mPas/0.025 mL/s/2.5 mL and 10 mPas/ 0.1 mL/s/4.5 mL). The white arrows (A) indicate how the measurement of the dimensions of the injection sites was performed. (C, D) Representative histological sections before (C) and after (D) injection of an isotonic dextran solution with a viscosity of 10 mPas at an injection rate of 1 mL/10s. I: epidermis, II: dermis with adnexe e.g. hairs and sebeceous glands, III: subcutis, (*) subcutaneous edema due to injection.

Macroscopic evaluation after dissection of the injection site

On the last study day, a dye was added to the dextran solutions prior to injection and each injection site was dissected and inspected. Each injection was recovered as defined, well-localized injection site in the sc tissue layer for all conditions tested. Representative pictures of the injection sites are shown in Figure 4.5 (A, B). The width, height, and length of the sites were measured by the same person (indicated by arrows in Figure 4.5, A).

Figure 4.6 shows the dimensions sorted according to viscosity and injection speed as well as injection volume. For an injection volume of 2.5 mL, dimensions of 1.7 – 4.2 cm, 2.7 – 5.6 cm, and 0.3 – 1.9 cm were found for width, length, and height, respectively. With higher injection volume (4.5 mL), the

dimensions increased to 2.0 – 3.3 cm, 2.7 – 9.0 cm, and 0.4 – 1.3 cm (width, length, and height). The calculated distribution volume in the sc tissue based on these dimensions assuming oval spreading was found as 3.7 and 7.2 mL for an injection volume of 2.5 and 4.5 mL. This corresponds to an increase in distribution volume in the sc space by 50% compared to the initial injected volume. Overall, the macroscopic evaluation of the injection sites at termination showed that all injections were located in the subcutaneous tissue layer.

Histology

Figure 4.5 shows histological slices of the skin of the injection site (*plica inguinalis*) before (C) and after (D) injection of a dextran solution with a viscosity of 10 mPas injected at an injection rate of 0.1 mL/s. The histology shows the epidermis, dermis with adnexa like hairs and sebaceous glands, and subcutis. Figure 4.5 (D) clearly shows a subcutaneous edema due to the dextran injection when compared to Figure 4.5 (A). In general, there were no differences found in histology between the four injection sites.
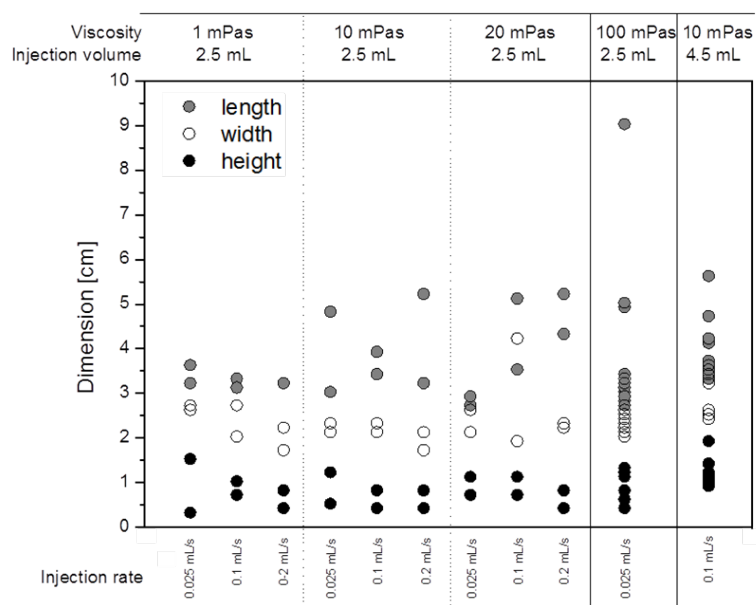
4.4   Discussion

Göttingen minipigs as *in vivo* model for sc tissue

The minipig is currently considered as the most appropriate translational animal model to study the pharmacokinetics of biotherapeutics after sc injection e.g. for studies of monoclonal antibody therapeutics [2, 27, 28]. Most importantly, the structure of the hypodermis of the pigs was reported to

resemble that in humans more than any other animal (e.g. rodent, monkey) [2, 22-24]. The skin of the pig is, like in humans, connected to the deep *fascia* via a fibrous network which defines the spreading behavior of a sample. A relevant difference between humans and e.g. rodents, monkeys, and pigs is the presence of the *panniculus carnosus* for the latter three animal species [3, 22, 24, 29]. However, the *panniculus carnosus* is missing in some parts of the pig, like in the groin, and therefore ressembling human tissue structure [22]. Thus, the *plica inguinalis* was chosen as injection site in minipigs for this study. Only the height of the subcutaneous tissue layer differs between the human skin (approximately 11 mm) [30] and the *plica inguinalis* of the minipig (few mm). Therefore, a short needle with a length of 3/8 was chosen to control and ensure injection of the solutions in the sc tissue space in our study. Adsorption of the dextran was not investigated and not in scope of our study as only the injection process was considered. The injections were randomized for each minipig animal, injection rate, viscosity, and injection site.

In summary, mean values of the contribution of tissue backpressure to injection forces were determined in the range of 0.6 to 4.7 N for injection rates between 0.025 and 0.2 mL/s and viscosities between 1 and 20 mPas. A minimum value of 0.1 N and a maximum value of 12.9 N were measured. The injection force related to sc tissue backpressure was found to be linear dependent on injection rate as well as on viscosity. Injection force profiles reached a plateau for all conditions as outlinedtested. No increase in the contribution of sc backpressure was observed for an increase in injection volume from 2.5 to 4.5 mL. Moreover, the occurrence of blisters in the sc tissue during/after injection due to the injected volume per se was found to be independent on the force related to sc backpressure. These findings together indicate that the contribution of blister formation during/after injection to injection forces is smaller or in the magnitude of the variation of the force measurement for the conditions tested. Based on these data, we may assume that the dextran solution might rapidly diffuse to the connective tissue. However, the macroscopic evaluation of the injection sites on the last study day has shown well-localized compartments for all conditions tested.

Influence of body temperature on injection forces

As outlined previously, the data analysis of the contribution of sc backpressure to injection forces was performed by subtraction of the *in vivo* from the *in vitro* measurement which were determined subsequently, corrected by an individual temperature factor. The *in vitro* and the *in vivo* experiment were performed subsequently under same temperature conditions using the same injection equipment. The injection equipment was rinsed before start of the experiment with the sample to be injected which was equilibrated to room temperature over several hours in the facility.

An interesting observation was made when injecting the 100 mPas dextran solution. The data suggested that the measured injection forces of the control measurements were significantly higher than the injection forces of the *in vivo* experiment. However, as the *in vitro* experiment was performed prior the *in vivo* experiment under same temperature conditions using the same injection equipment, the data suggested another parameter to additionally influence injection forces under *in vivo* conditions. As the sample was equilibrated to room temperature for several hours and most importantly the tubing/injection equipment was not in contact with the body surface of the minipig at any time (except of the needle tip), the hypothesis was that a local, fast decrease in viscosity in the needle tip may consequently lead to the reduction in injection forces. This local decrease might be a result of the fast warming of the sample in the needle during the injection process due to the body temperature of the minipig (39°C). To proof this,

a simple control measurement was performed. The dextran samples were injected into tempered water of 39°C, equal to the body temperature of minipigs [25], with only the needle inserted into the water bath. Prior to this experiment as a control, the same injections were performed into air for comparison under the same conditions (sample, temperature, equipment). The experiments confirmed that injection forces were significantly decreased if the needle tip – although only few millimeters in length – faces warmer environmental conditions than room temperature during injection than compared to injections into air (at room temperature). This additional negative contribution to injection forces was found and quantified to be dependent on viscosity and injection rate indicating a hydrodynamic process. In detail, the contribution of the body temperature of the minipig to injection forces was separated for each individual experiment from the contribution of the sc backpressure and the hydrodymanic component as follows: the decrease in injection force per degree Celcius was obtained from the experimental data of the control measurements (waterbath vs. air) using the Arrhenius equation dependent on injection rate and viscosity. Based on these factors, the decrease in injection force was calculated (Arrhenius equation) for each individual experiment based on the temperature difference between control measurement (39°C) and the actual monitored temperature during the *in vitro/in vivo* experiment. Examples for a temperature difference of 20 – 39°C and 20 – 37°C are given in Table 4.1 in the Supporting Information. In summary, we concluded, that the observed temperature effect manifests as a localized temperature effect at the injection site. This leads to warming of the (equilibrated) sample in the needle during injection, thus smaller viscosity and smaller injection forces than expected. As the temperature factor was found to be dependent on viscosity and injection rate, this indicates a hydrodynamic process and strengthens our conclusion that the temperature at the animal body/at the injection site leads to adjustment of the fluid temperature in the needle during sc injection.

Implications of sc backpressure and local warming in context of user capability

As outlined in the introduction, injection forces of highly concentrated protein products are influenced by device dimensions like needle inner diameter, product properties like viscosity – itself dependent on temperature and concentration of active substance, and by the injection rate which is defined by the capability of the end-user. Also frictional forces between plunger and syringe barrel contribute to injection forces. These parameters are well understood and were investigated in detail in the past. Current literature models use these factors to predict injection forces, however limited to the *in vitro* situation neglecting actual *in vivo* conditions [11]. Dependent on the indication, patients might be limited in their strength like e.g. for rheumatoid arthritis patients, stating a challenge to expel a syringe. Therefore, the limits for maximal required injection force have to be carefully evaluated before design of an injection device. A highly concentrated protein therapeutic with a viscosity of 100 mPas has been previously studied [16]. This protein therapeutic was tested for injectability by Sheikhzadeh and co-workers in an anthropometric study. The authors reported that rheumatoid arthritis patients were capable to exert a force of approximately 17 N (95% percentile) and 48 N (mean) in average onto the syringe plunger [16]. Setting this into relation to our findings assuming a constant, slow injection speed of 0.025 mL/s, the injection force of this product would be higher by approximately 7 N due to the contribution of the sc backpressure compared to *in vitro* injection forces which are in general tested against air. The local temperature effect for a body temperature of 37°C leading to warming of the sample in the needle would decrease injection forces by approximately 4 N assuming similar viscosity-temperature dependence of

the therapeutic as dextran. This would result in an overall higher injection force by 3 N compared to the estimated or measured injection force in the *in vitro* situation. Testing of injection force *ex vivo* still remains questionable of being representative of *in vivo* injection forces. Moreover, it may lead to unexpected modifications/distortions and may therefore not be representative for the *in vivo* situation. The data indicate that consideration of the actual *in vivo* sc backpressure is essential when assessing injection forces. Moreover, compensation of the increase in injection forces by the tissue backpressure due to the local temperature effect, as observed for the minipig, should be considered.

Based on the above findings, the current *in silico* model to predict injection forces [11] can be extended to:

$$F_{total} = F(Q, \eta)_{hydrodynamic} + F(Q)_{friction} + F(Q, \eta)_{tissue\,backpressure} - F(Q, \eta)_{body\,temperature}$$

(F = force, Q = volumetric flow, η = dynamic viscosity)

Sc injection volume

The present study showed that injection volumes up to 4.5 mL into the sc tissue space were forming localized, well-defined injection sites, without any observed leakage. This is of high importance as the sc tissue layer of the *plica inguinalis* of the minipig is even thinner than the one of humans. The localized injection sites were found for all conditions tested independent on viscosity and injection rate. Compared to literature, the current sc injectable volume is considered to be limited to 1 to 1.5 mL for human use [31]. Frost *et al.* described the volume for sc injection to be generally limited to less than 2 mL due to compliance of the tissue space to injected fluids [32]. This is driven by the fibrous bands in the *panniculus adiposus* that reach into the deep *fascia* for humans and other furless animals [22, 33, 34] which might lead to pain and tissue distortion upon sc injection. Current marketed products for sc administration are to date limited to 1 to 1.5 mL volume of administration [1].

Recent approaches have shown that higher injection volumes are feasible for sc injection by co-injection with recombinant human hyaluronidase, an enzyme that temporarily and reversibly degrades hyaluronan which is a major component of the extracellular matrix of the skin besides collagen. This facilitates the penetration and diffusion of the co-administered drug [34-37]. Shpilberg and colleagues showed that administration of up to 15 mL of a co-formulation of hyaluronidase and a monoclonal antibody into healthy volunteers (phase Ib study) was feasible [7, 38].

The present study showed that injection of up to 4.5 mL was feasible from the point of view that the sc tissue was capable to keep the solution at a defined injection site as outlined above. Moreover, another study suggested local tolerance in beagles with good tolerability up to an injection volume of 5 mL into the sc tissue space [39].

4.5 Conclusions

The development of injection devices for combination products (e.g. autoinjectors or pre-filled syringes) requires a detailed understanding of injection forces dependent on device dimensions like needle diameter, and formulation properties like viscosity. Current literature provides experimentally verified *in silico* models for prediction of injection forces into air. To our knowledge, this is the first study which provides

quantitative data on the backpressure of the sc tissue contributing to injection forces measured during *in vivo* injection. In summary, mean values were determined in the range of 0.6 to 4.7 N for injection rates between 0.025 and 0.2 mL/s and viscosities between 1 and 20 mPas. A minimum value of 0.1 N and a maximum value of 12.9 N were measured. These data demonstrate that the sc tissue backpressure during injection can be significant. All force profiles reached a plateau during injection, even for the higher injection volume of 4.5 mL forming well-localized compartments in the sc tissue layer. Moreover, we reported that a local temperature effect led to warming of the (equilibrated) drug solution in the needle due to the body temperature of the minipig . This led to smaller measured injection forces than expected relieving the increase in injection forces due to sc backpressure – to some parts. As the structure of the sc tissue layer was shown to be comparable between the *plica inguinalis* of minipigs and humans, the current data set presents – to our knowledge – the first appropriate quantitative data on injection forces during sc administration considering *in vivo* conditions representative for humans.

The present study separates the contribution of the tissue backpressure from the contribution of the injection device as well as from the local temperature effect which was quantified dependent on viscosity and injection rate. Based on these findings, the current *in silico* model to predict injection forces [11] can be extended to:

$$F_{total} = F(Q, \eta)_{hydrodynamic} + F(Q)_{friction} + F(Q, \eta)_{tissue\,backpressure} \text{ - } F(Q, \eta)_{body\,temperature}$$

(F = force, Q = volumetric flow, η = dynamic viscosity)

To conclude, this knowledge is of key importance to further develop and define limits and setup for testing of device robustness during the evaluation, planning, and design phase of the development of injection devices.

4.6 Acknowledgments

4.7   References

1. S.J. Shire, Z. Shahrokh, J. Liu, Challenges in the development of high protein concentration formulations, J. Pharm. Sci., 93 (2004) 1390-1402.

2. W.F. Richter, S.G. Bhansali, M.E. Morris, Mechanistic determinants of biotherapeutics absorption following SC administration, AAPS J., 14 (2012) 559-570.

3. T.A. McDonald, M.L. Zepeda, M.J. Tomlinson, W.H. Bee, I.A. Ivens, Subcutaneous administration of biotherapeutics: current experience in animal models, Curr. Opin. Mol. Ther., 12 (2010) 461-470.

4. R.J. Harris, S.J. Shire, C. Winter, Commercial manufacturing scale formulation and analytical characterization of therapeutic recombinant antibodies, Drug Develop. Res., 61 (2004) 137-154.

5. S. Kanai, J. Liu, T.W. Patapoff, S.J. Shire, Reversible self-association of a concentrated monoclonal antibody solution mediated by Fab-Fab interaction that impacts solution viscosity, J. Pharm. Sci., 97 (2008) 4219-4227.

6. X. Pivot, J. Gligorov, V. Muller, P. Barrett-Lee, S. Verma, A. Knoop, G. Curigliano, V. Semiglazov, G. Lopez-Vivanco, V. Jenkins, N. Scotto, S. Osborne, L. Fallowfield, Preference for subcutaneous or intravenous administration of trastuzumab in patients with HER2-positive early breast cancer (PrefHer): an open-label randomised study, Lancet Oncol., 14 (2013) 962-970.

7. C. Wynne, V. Harvey, C. Schwabe, D. Waaka, C. McIntyre, B. Bittner, Comparison of Subcutaneous and Intravenous Administration of Trastuzumab: A Phase I/Ib Trial in Healthy Male Volunteers and Patients With HER2-Positive Breast Cancer, J. Clin. Pharmacol., 53 (2013) 192-201.

8. C.J. Wynne, R.B. Ellis-Pegler, D.S. Waaka, C. Schwabe, M. Lehle, D. Heinzmann, R. Mangat, C. Li, A.E. Dick, N.A. Cranshaw, B.L. Lum, Comparative pharmacokinetics of subcutaneous trastuzumab administered via handheld syringe or proprietary single-use injection device in healthy males, Cancer Chemother. Pharmacol., 72 (2013) 1079-1087.

9. N. Rathore, P. Pranay, J. Bernacki, B. Eu, W. Ji, E. Walls, Characterization of protein rheology and delivery forces for combination products, J. Pharm. Sci., 101 (2012) 4472-4480.

10. C. Berteau, F. Schwarzenbach, Y. Donazzolo, M. Latreille, J. Berube, H. Abry, J. Cotten, C. Feger, P.E. Laurent, Evaluation of performance, safety, subject acceptance, and compliance of a disposable autoinjector for subcutaneous injections in healthy volunteers, Patient Prefer. Adherence, 4 (2010) 379-388.

11. A. Allmendinger, S. Fischer, J. Huwyler, H.C. Mahler, E. Schwarb, I.E. Zarraga, and R. Mueller, Rheological characterization and injection forces of concentrated protein formulations: An alternative predictive model for non-Newtonian solutions, Eur. J. Pharm. Biopharm. 87 (2014) 318-328.

12. M. Adler, Challenges in the Development of Pre-filled Syringes for Biologics from a Formulation Scientists Point of View, Am. Pharm. Rev., 15 (2012).

13. V. Burckbuchler, G. Mekhloufi, A.P. Giteau, J.L. Grossiord, S. Huille, F. Agnely, Rheological and syringeability properties of highly concentrated human polyclonal immunoglobulin solutions, Eur. J. Pharm. Biopharm., 76 (2010) 351-356.

14. W. Rungseevijitprapa, R. Bodmeier, Injectability of biodegradable in situ forming microparticle systems (ISM), Eur. J. Pharm. Sci., 36 (2009) 524-531.

15. N. Rathore, P. Pranay, B. Eu, W. Ji, E. Walls, Variability in syringe components and its impact on functionality of delivery systems, PDA J. Pharm. Sci. Technol., 65 (2011) 468-480.

16. A. Sheikhzadeh, J. Yoon, D. Formosa, B. Domanska, D. Morgan, M. Schiff, The effect of a new syringe design on the ability of rheumatoid arthritis patients to inject a biological medication, Appl. Ergon., 43 (2012) 368-375.

17. F. Cilurzo, F. Selmin, P. Minghetti, M. Adami, E. Bertoni, S. Lauria, L. Montanari, Injectability evaluation: an open issue, AAPS Pharm. Sci. Tech., 12 (2011) 604-609.

18. M. Vosseler, M. Jugl, R. Zengerle, A smart interface for reliable intradermal injection and infusion of high and low viscosity solutions, Pharm. Res.-DORD, 28 (2011) 647-661.

19. N.P. Reddy, V. Palmieri, G.V. Cochran, Subcutaneous interstitial fluid pressure during external loading, Am. J. Physiol., 240 (1981) R327-329.

20. M.J. Husmann, M. Barton, B.R. Amann-Vesti, U.K. Franzeck, Postural effects on interstitial fluid pressure in humans, J.Vasc. Res., 43 (2006) 321-326.

21. W.L. Olszewski, P. Jain, G. Ambujam, M. Zaleska, M. Cakala, T. Gradalski, Tissue fluid pressure and flow during pneumatic compression in lymphedema of lower limbs, Lymphat. Res. Biol., 9 (2011) 77-83.

22. E.H. Rose, L.M. Vistnes, and G.A. Ksander, The panniculus carnosus in the domestic pig, Plast. Reconstr. Surg., 59 (1977) 94-97.

23. G. Bode, P. Clausing, F. Gervais, J. Loegsted, J. Luft, V. Nogues, and J. Sims, The utility of the minipig as an animal model in regulatory toxicology, J. Pharmacol. Toxicol. Methods, 62 (2010) 196-220.

24. J.T. Mortensen, P. Brinck, and J. Lichtenberg, The minipig in dermal toxicology. A literature review, Scand. J. Lab. Anim. Sci., 5 (1998) 77-83.

25. Gesellschaft für Versuchstierkunde: Auschuss fr Ernährung der Versuchstiere - Minipig, http://www.gv-solas.de (07. April 2014), 1999.

26. K. Monkos, Viscosity analysis of the temperature dependence of the solution conformation of ovalbumin, Biophys. Chem., 85 (2000) 7-16.

27. Y. Zheng, D.B. Tesar, *et al.*, and W.F. Richter, Minipig as a potential translatable model for monoclonal antibody pharmacokinetics after intravenous and subcutaneous administration, Mabs, 4 (2012) 243-255.

28. N.C. Ganderup, W. Harvey, J.T. Mortensen, W. Harrouk, The minipig as nonrodent species in toxicology– where are we now?, Int. J. Toxicol., 31 (2012) 507-528.

29. A. Henning, D. Neumann, K.H. Kostka, C.M. Lehr, U.F. Schaefer, Influence of human skin specimens consisting of different skin layers on the result of in vitro permeation experiments, Skin. Pharmacol. Phys., 21 (2008) 81-88.

30. F. Mirrashed, J.C. Sharp, V. Krause, J. Morgan, B. Tomanek, Pilot study of dermal and subcutaneous fat structures by MRI in individuals who differ in gender, BMI, and cellulite grading, Skin. Res. Technol., 10 (2004) 161-168.

31. Gatlin, L.A., Gatlin, C.B., Formulation and administration techniques to minimize injection pain and tissue damage associated with parenteral products., in: P.K. Gapta, G.A. Brazeau (Eds.) Injectable drug development: techniques to reduce pain and irritation, Interpharm Press, Denver, 1999, pp. 401-425.

32. G.I. Frost, Recombinant human hyaluronidase (rHuPH20): an enabling platform for subcutaneous drug and fluid administration, Expert Opin. Drug Deliv., 4 (2007) 427-440.

33. R.M.H. McMinn, Lasts Anatomy: Regional and applied, 9th ed., Churchill Livingstone, London (1994).

34. L.H. Bookbinder, A. Hofer, M.F. Haller, M.L. Zepeda, A. Keller, J.E. Lim, T.S. Edgington, H.M. Shepard, J.S. Patton, G.I. Frost, A recombinant human enzyme for enhanced interstitial transport of therapeutics, J. Control. Release, 114 (2006) 230-241.

35. S. Hamizi, G. Freyer, N. Bakrin, E. Henin, A. Mohtaram, O. Le Saux, C. Falandry, Subcutaneous trastuzumab: development of a new formulation for treatment of HER2-positive early breast cancer, Onco. Targets Ther., 6 (2013) 89-94.

36. B. Bittner, W.F. Richter, F. Hourcade-Potelleret, C. McIntyre, F. Herting, M.L. Zepeda, J. Schmidt, Development of a subcutaneous formulation for trastuzumab - nonclinical and clinical bridging approach to the approved intravenous dosing regimen, Arzneimittelforschung, 62 (2012) 401-409.

37. R.D. Pirrello, C.T. Chen, S.H. Thomas, Initial experiences with subcutaneous recombinant human hyaluronidase, J. Palliat. Med., 10 (2007) 861-864.

38. O. Shpilberg, C. Jackisch, Subcutaneous administration of rituximab (MabThera) and trastuzumab (Herceptin) using hyaluronidase, Br. J. Cancer, 109 (2013) 1556-1561.

39. K. Jochims, J. Kemkowski, T. Nolte, T. Bartels, A. Heusener, Local tolerance testing of parenteral drugs: how to put into practice, Regul. Toxicol. Pharm., 38 (2003) 166-182.

4.8   Supporting Information

Temperature correction factor [N] for 20-39°C / 20-37°C	0.025 mL/s	0.1 mL/s	0.2 mL/s
1 mPas	0.0 /0.0	-0.2 /-0.1	0.0 /0.0
10 mPas	0.3 /0.2	1.0 /0.7	1.4 /0.9
20 mPas	1.4 /0.9	2.8 /1.9	4.2 /2.8
100 mPas	6.2 /4.2		

Table 4.1: Temperature correction factor for sc backpressure related injection force to account for local temperature effect in the needle/at the injection site of the minipig. The correction factor is presented in this table as an example for a temperature increase from 20 – 39°C (minipig) and additionally from 20 – 37°C (humans) between *in vivo* and control measurement (injection into tempered water bath) dependent on viscosity and injection rate. As outlined in the Methods section, the temperature correction factor was calculated individually for each *in vivo* injection according to the Arrhenius equation based on temperature monitoring.
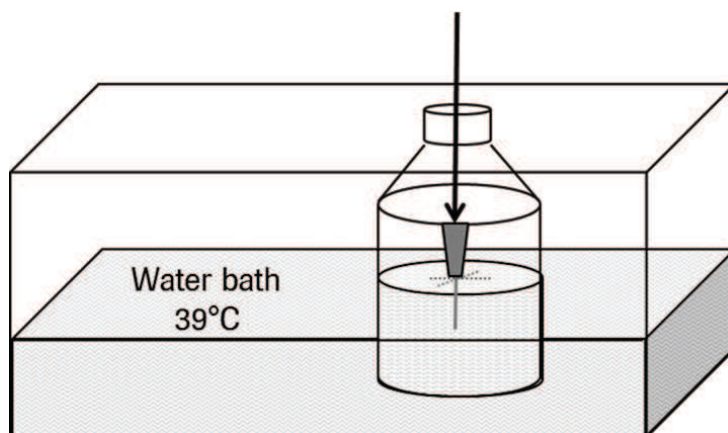
Figure 4.7: Instrumental set-up of control measurements (*in vitro*, 39°C) for correction of local temperature effect at the body surface of the minipig/at the injection site. Injections were performed with only the needle inserted into the water bath to simulate *in vivo* conditions. The water was tempered to 39°C which is the body temperature of minipigs.
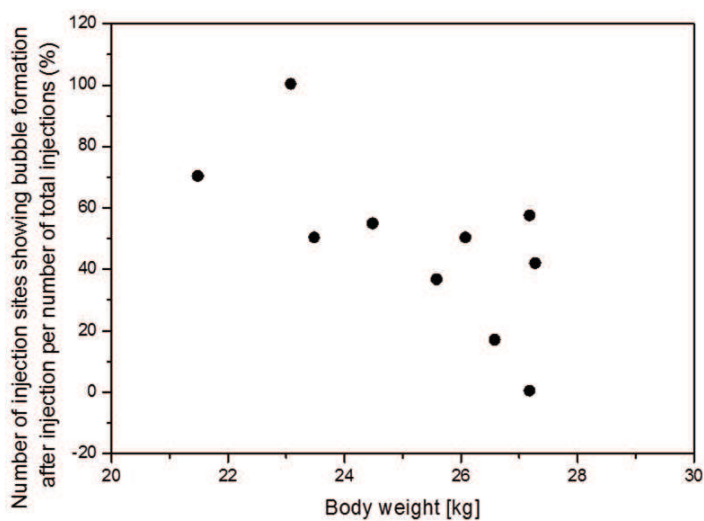
Figure 4.8: Number of injection sites showing blister formation after injection per number of total injections as a function of body weight of the minipigs.

Chapter 5

Sterile filtration of highly concentrated protein formulations

– impact of formulation, viscosity, protein concentration, and filter material

Authors:
Andrea Allmendinger

Stefan Fischer
Joerg Huwyler
Hanns-Christian Mahler
Robert Mueller

During filtration within the aseptic drug product manufacturing process of biologics, differences in filtration behavior of highly concentrated protein formulations can be observed dependent on the formulation composition. Filtration time can be influenced by filtration pressure, filter material with a distinct filter area, filter resistance, which is defined by surface properties and pore size distribution, by viscosity, and by physical properties of the solution (e.g. hydro-/lipophilicity).

The present study investigates the filtration forces of monoclonal antibody formulations in a small-scale setup using PVDF (polyvinylidene difluoride) or PES (polyethersulfone) filters. Different factors like formulation composition (buffer system, excipients, presence and absence of surfactant) and protein

concentration, which are linked to viscosity, as well as different filtration rates were evaluated.

Shear rates during the filtration process, which are defined by pore size distribution interdependent with filtration pressure (in the magnitude of 0.4 – 1.0 bar), were shown to lead to non-Newtonian behavior of the protein formulations with increasing protein concentration and filtration rate. Therefore, smaller absolute filtration forces than expected were found for highly concentrated protein formulations dependent on the formulation composition when compared to Newtonian control solutions of the same low-shear viscosity. Different buffer valences of the formulations (histidine vs. citrate buffer) showed significant impact on the non-Newtonian behavior, whereas excipients like arginine-HCl or sucrose did not impact the extent of shear thinning for the monoclonal antibody tested.

The addition of polysorbate was shown to have a significant influence on filter resistance dependent on filter material. An increase in filter resistance was found for the PES but not for the PVDF filter in comparison to surfactant-free solutions.

The current study highlights the influence of formulation composition on the filtration process and emphasizes the relevance to assess possible limitations during manufacture caused by elevated viscosity of highly concentrated protein formulations.

5.1   Introduction

Highly concentrated protein formulations which are administered by subcutaneous injection are desirable
for chronic indications which require a frequent dosing regimen. They may also offer the possibility for
either self-administration by the patient or home-treatment by a healthcare professional. [1-3] Especially
the rheological behavior of these concentrated solutions have a major impact on processing during
product manufacture (e.g. aseptic filling and filtration [4-6]) and parenteral administration of the
product. [7-9] For filtration of parenteral products, hydrophilic PVDF (polyvinylidene difluoride) and
PES (polyethersulfone) filters are routinely used during the fill-finish process. [6, 10, 11] Besides filter
area, filtration pressure, pore size, and surface properties of the filter material, the filtration process can
be influenced by different parameters including solution viscosity and formulation. [6, 11, 12]

To protect the protein from interfacial stress occurring during manufacture (e.g. filtration, freeze/thawing)
and storage (e.g. glass as primary packaging, shaking stress), protein formulations often require the
addition of stabilizers like surfactants. [13-21] Currently, most commonly used surfactants of marketed
protein therapeutics are polysorbate 20 or 80. [10, 11, 22, 23] These nonionic surfactants bind with a
higher affinity to interfaces than proteins, such as to the air-liquid or ice-liquid interfaces, thus preventing
interfacial protein adsorption and protein aggregation. [20, 24] However, it was recently reported, that
polysorbate 80 significantly adsorbs to PES sterilizing-grade filters. [11] Furthermore, Zhou *et al.* have
recently shown that polysorbate 20 also adsorbs to filter material (PES and PVDF) suggesting a
non-specific hydrophobic binding mechanism. [10] They furthermore reported that PES filters adsorb
polysorbate 20 to a much greater extent than the PVDF membranes. Both articles therefore suggested
pre-conditioning of the filters for saturation of the binding sites with formulation buffer or protein
formulation, or the evaluation of more suitable and compatible filter membranes.

Little information is available about the influence of the formulation composition (e.g. surfactants,
isotonizers, viscosity reducers, buffer systems) on filtration behavior especially for highly concentrated
protein solutions. In own observations, differences in filtration behavior of highly concentrated protein
formulations were found during aseptic filtration within the fill-finish process of monoclonal antibody
solutions dependent on the composition of the formulation (data not shown).

Therefore, the present study aimed to investigate filtration forces of different monoclonal antibody
formulations during filtration in a standardized lab-scale set-up. Different filter materials, i.e. hydrophilic
PVDF and PES filters, were tested with a nominal pore size of 0.2 μm. Filtration behavior of two
different monoclonal antibody formulations (mAb 1 and mAb2) was tested in particular in dependence
on protein concentration and viscosity. The influence of filtration rate on filtration forces as well
as of formulation composition (buffer systems, excipients) at high protein concentration was further
investigated. Differences in filtration forces between the two tested filter materials were linked to filter
resistance and pore size distribution. Additionally, solution with or without polysorbate were investigated
with regard to filter resistance.

5.2 Materials and Methods

Materials

Monoclonal antibody formulations

The purified monoclonal antibodies mAb1 (IgG$_1$, pI 8.4; estimated M$_w$ 146) and mAb2 (IgG$_1$,pI 9.4; estimated M$_r$ 148 kD) were provided by F. Hoffmann-La Roche Ltd (Basel, Switzerland). mAb1 was formulated in an arginine succinate buffer (Ajinomoto, Louvain-la-Neuve, Belgium; Merck, Darmstadt, Germany) at pH 6.5 with addition of methionine (Ajinomoto, Louvain-la-Neuve, Belgium) and 0.06% (m/v) polysorbate 20 (Croda, Edison, NJ, USA) at a protein concentration between 20 and 180 mg/mL. For investigation of different formulation properties, mAb1 was additionally formulated at a protein concentration of 20 and 150 mg/mL at pH 6.5 in either a 20 mM histidine-HCl buffer (Ajinomoto, Louvain-la-Neuve, Belgium) or a 20 mM sodium citrate buffer (Jungbunzlauer, Basel, Switzerland) with addition of 0.06% (m/v) polysorbate 20 and either (A) no excipient, (B) 150 mM arginine-HCl (Ajinomoto, Louvain-la-Neuve, Belgium), or (C) 200 mM sucrose (Ferro Pfanstiehl, IL, USA).

mAb2 was formulated at protein concentrations between 20 and 180 mg/mL in a histidine-HCl buffer (pH 6.0) with addition of arginine-HCl (Ajinomoto, Louvain-la-Neuve, Belgium) and 0.02% (m/v) polysorbate 80 (Croda, Edison, NJ, USA). Surfactant concentrations are above the critical micelle concentration (CMC) for all tested solutions, which are 0.006% and 0.001% (m/v) for PS 20 and 80, respectively. [24]

Surrogate solutions

Glycerol solutions were used as surrogate for viscous solutions. Aqueous glycerol solutions were prepared by dilution of 99.5% (m/v) glycerol (Acros Organics, Morris Planes, NJ) with either water for injection, 20 mM histidine-HCl, or 20 mM sodium citrate buffer in concentrations between 0 – 60% (m/v, pH 6.0 and 6.5) with addition of 0.06% (m/v) polysorbate 20.

Aqueous 0.001 M potassium chloride solution (Metrohm, Zofingen, Switzerland) was prepared at a pH of 6.5 with and without addition of 0.06% (m/v) polysorbate 20. The pH was adjusted by addition of 0.1 N sodium hydroxide solution (Merck, Darmstadt, Germany).

Syringe filters with a hydrophilic PVDF (polyvinylidene difluoride) or a PES (polyethersulfone) filter membrane from the same supplier were used for the filtration experiments in combination with 5 mL plastic syringes with luer-lok^{TM} tip (BD, Franklin Lakes, NJ, USA). The syringe filters had a nominal pore size diameter of 0.2 μm and a filter area of 3.9 cm^2.

Methods

Small-scale filtration

Filtration experiments were performed using a standardized small-scale set-up on a TA.HDplus Texture analyzer (Stable Micro Systems, Surrey, UK). A plastic syringe was filled with the sample under consideration and all air bubbles were removed. A syringe filter was mounted on the syringe and placed

on the texture analyzer with the syringe pointing to the bottom. A constant speed was applied to the plunger and the restoring force was measured during filtration of the sample. Filtration forces can be easily converted to filtration pressure by knowledge of filtration area. The experiments were performed as triplicates at room temperature (23 ±1°C). Before each filtration, the filter was tested for filter integrity and washed/equilibrated with water and placebo subsequently to saturate the surfactant binding sites as suggested by Mahler *et al.* and Zhou *et al.* [10, 11] Data analysis was performed using the Exponent Stable Micro Systems software (Stable Micro Systems, Surrey, UK). The filtration force was determined as average value from the plateau of the force-travel distance graph. A representative example for data analysis is shown in Figure 5.7 of the supporting information.

Characterization of samples

Viscosity measurement
Dynamic viscosity was measured by plate/cone rheometry at 20°C as duplicates at a shear rate of 2 x 10^3 s^{-1} as recently described by Allmendinger *et al.* [25]

Light obscuration
Sub-visible particles were counted by light obscuration as described by Kiese*et al.* using a low-volume method. [21]

Zeta potential measurement
Zeta potential of the protein samples was determined as duplicates by laser Doppler electrophoresis as outlined in Lehermayr *et al.* [26]

Dynamic light scattering
The protein-protein interaction parameter A_2 was determined for the protein samples by DLS (dynamic light scattering) as described by Lehermayr *et al.* [27] The measuring time was adjusted to 5 s and 20 consecutive measurements were performed per dilution (N = 3). This method measures A_2 at low protein concentrations (1 – 10 mg/mL) as there are currently only limited methods available to measure PPIs at high concentrations. [27, 28] However, A_2 is considered to be a good qualitative predictive factor for PPIs in highly concentrated protein formulations as previously reported by Yadav *et al.* [29]

Size exclusion chromatography
Monomer, high molecular and low molecular weight species were analyzed for the protein samples by size exclusion chromatography (SEC) according to Kiese *et al.* [21] The monomer content was found >98% for all samples.

Characterization of syringe filter

Filter resistance
Filter resistance β [m^{-1}] was determined by filtration force experiments (N = 3). The filtration process can be described by the modified Darcy equation [12] if cake formation is neglected:

$$\Delta P = \frac{\Delta F + F_{friction}}{A} = \frac{Q}{A} \cdot \eta \cdot \beta + \frac{\Delta F_{friction}}{A} \tag{5.1}$$

$$
\begin{array}{lll}
\Delta P & [\text{Pa}] & = \text{pressure drop} \\
F & [\text{N}] & = \text{filtration force} \\
A & [\text{m}^2] & = \text{filter cross-sectional area } (3.9 \times 10^{-4} \text{ m}^2) \\
Q & [\text{m}^3/\text{s}] & = \text{volumetric flow} = \partial V/\partial t \\
V & [\text{m}^3] & = \text{filtration volume} \\
t & [\text{s}] & = \text{filtration time} \\
\eta & [\text{Pas}] & = \text{dynamic viscosity} \\
\beta & [\text{m}^{-1}] & = \text{filter resistance}
\end{array}
$$

Therefore, the filter resistance β [m^{-1}] was determined from the slope of the filtration force F as a function of (a) dynamic viscosity η or (b) filtration rate Q/A [m/s]. Method (a) was applied to the different aqueous glycerol concentrations in histidine or sodium citrate buffer, respectively. Method (b) was used for determination of the filter resistance for the 0.001 M potassium chloride solution with and without addition of 0.06% (m/v) polysorbate 20 ($\eta = 1$ mPas) at 1.85, 9.25, and 18.5 x 10^3 L/m^{2}h.

Mercury porosimetry
Pore size distribution of the two different syringe filters was analyzed by mercury porosimetry as outlined in Stirnimann *et al.* [30] using four filters within one measurement.

Scanning electron microscopy
Scanning electron microscopy (SEM) pictures of the syringe filter were taken at 3.4 x 10^3 and 6.7 x 10^3 times magnification using a FEI/Philips XL30 FEG apparatus (Philips, Netherlands). Sample preparation was performed as described by Stirnimann *et al.* [30]

5.3 Results

Protein concentration

Sterile filtration of two monoclonal antibody formulations mAb1 and mAb2 was investigated using PES and hydrophilic PVDF filters with a nominal pore size of 0.2 μm. Filtration forces were measured on a small-scale set-up at a filtration rate of 1.85 x 10^3 L/m^{2}h for increasing protein concentration of 20, 50, 80, 150, and 180 mg/mL. Figure 5.1 shows the filtration force of mAb1 (A, B) and mAb2 (C, D) for the PES and PVDF filter respectively as a function of dynamic viscosity (2 x 10^3 s^{-1}). mAb1 and mAb2 both showed increasing filtration force with increasing viscosity. In general, absolute filtration forces through the PVDF filter (Figure 5.1 B, D) were lower than those of the PES filter (Figure 5.1 A, C) for the formulation tested (containing polysorbate (PS) 20 or 80). Figure 5.1 also compares the filtration forces of the protein solutions with control measurements of aqueous glycerol solutions of

different concentrations (0 – 60%, m/v), also containing PS (20). The reason for the addition of PS to the control solution and differences on filtration forces between PS 20 (mAb1 formulation) and PS 80 (mAb2 formulation) including surfactant concentration will be outlined later in this text. Linear correlation of absolute filtration force and viscosity was found for the control measurements using glycerol solutions ($R^2_{PVDF} = 0.995$ and $R^2_{PES} = 0.979$) indicating Newtonian flow behavior of the control solutions and exclusion of warming of the sample during the small-scale filtration process. However, clear deviation from Newtonian model was found for both mAbs through the PES filter and minor deviation for the PVDF filter with increasing viscosity (protein concentration) when compared to the control.

Filter material

Both filters assessed have a nominal pore size of 0.2 μm. The FDA defines the sterilizing grade filters on the basis of its ability to sustain a bacterial challenge of 1 x 10^7 CFU of *Brevundimonas diminuta* per cm^2 of filter surface, grown and challenged under specific, standardized parameters. Therefore, sterilizing filters – although nominally labeled as 0.2 μm – can have different actual pore sizes/pore size distributions and still be able to retain the bacterial challenge. [31]

Filter materials were characterized by electron scanning microscopy (SEM). Figure 5.2 shows the pictures of the PES and PVDF filter in two different magnifications revealing structural differences in pore shape and pore size distribution. The pictures show larger pore sizes for the PVDF filter as compared to the PES filter.

The pore size distribution was further investigated using mercury porosimetry. Figure 5.3 shows the pore volume as a function of pore size of the PES filter and the PVDF filter. The PVDF filter consists of two filter layers which showed the comparable pore size distribution. The PES filter showed a narrow pore size distribution with a maximum of 8.31 mL/g at 0.43 μm whereas the PVDF filter showed a wide pore size distribution with maximum values of 1.2 mL/g. This reflects the results from the SEM measurements and indicates that the PES filter consists of a large number of small pores (modus of 0.43 μm) compared to the PVDF filter with a smaller amount of more heterogeneous pores.

Besides pore size distribution which was found to differ between the two filters, filter materials were characterized by their surface properties (e.g. electrostatic and hydrophilic properties) influencing filtration forces interdependent with physical properties of the solution under consideration (hydro-/lipophilicity). These (surface) properties can be quantified as the filter resistance β at a defined pH which is the proportional factor between volumetric flow per cross-sectional area, viscosity, and filtration pressure as outlined in the Materials and Methods section. The filter resistance was found to be 20.7 m^{-1} and 8.8 m^{-1} for the PES and PVDF filter, respectively, determined for the control solutions (aqueous glycerol solution with 0.06% PS 20).

Surfactant: polysorbate 20 and 80

In a side experiment, a 0.001 M potassium chloride solution with and without addition of 0.06% (m/v) PS 20 was filtered through the PES and PVDF filter. Filter resistance was found to increase from 7.0 m^{-1} to 20.8 m^{-1} for the PES filter revealing a significant influence of the surfactant on filtration forces. The filter resistance of the PVDF filter did not change by addition of PS 20 and was found as 10.4 m^{-1}. Figure 5.7 of the supporting information also shows that there was no difference in filtration
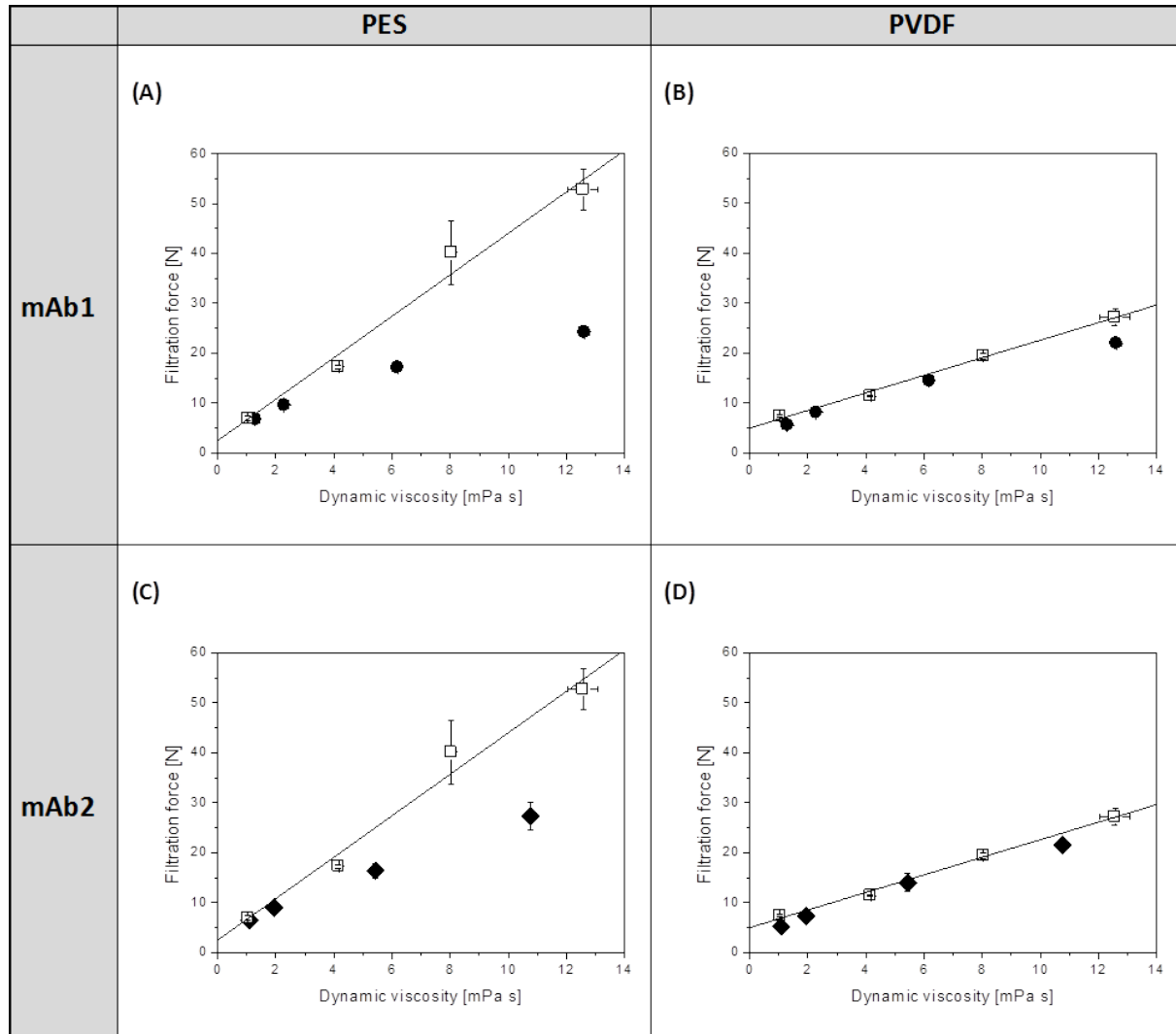
Figure 5.1: Filtration forces of different concentrations of mAb1 (circle), mAb2 (diamond), and aqueous glycerol solutions (square) at a filtration rate of 1.85 x 10^3 L/m^{2}h (N = 3) as a function of dynamic viscosity (20°C, 2 x 10^3 s^{-1}) for two different filters (PES, PVDF). Mean values and standard deviation are reported. The solid lines show the linear fit to the glycerol solutions with R^2 = 0.995 (PVDF) and 0.979 (PES).
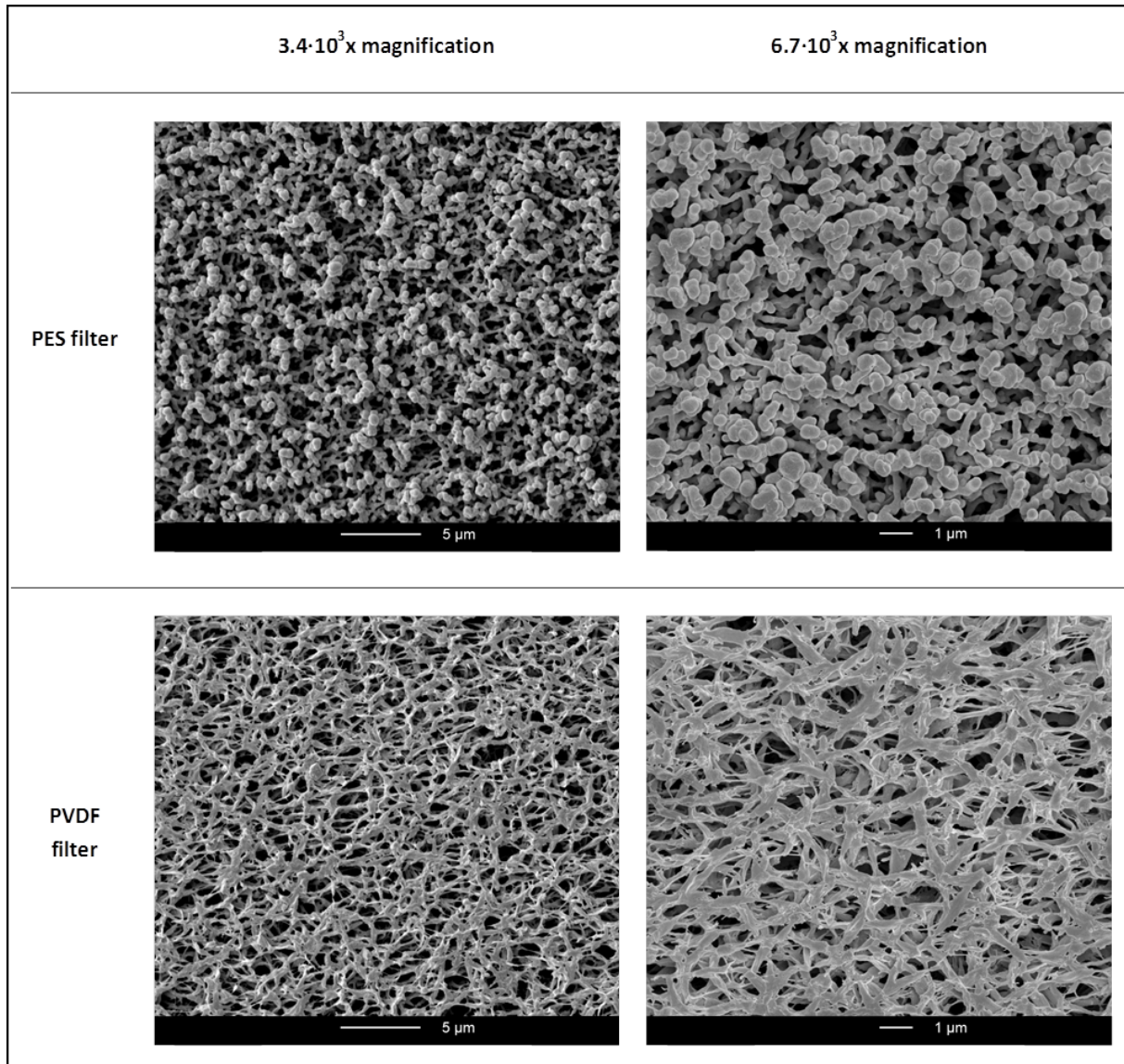
Figure 5.2: Scanning electron microscopy pictures of PES and PVDF filters at different magnifications.
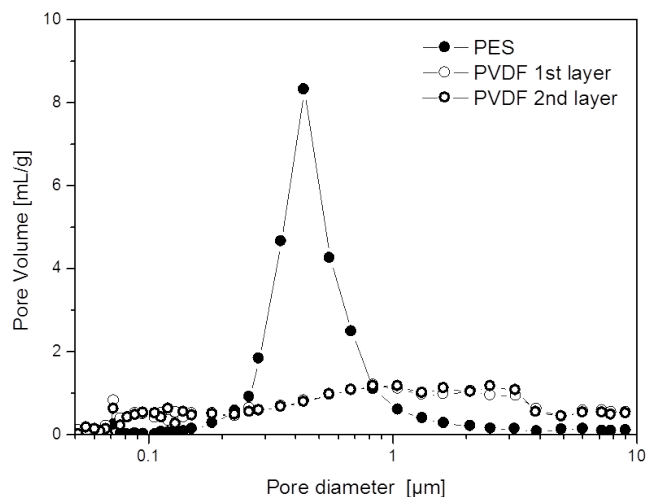
Figure 5.3: Representative example of pore size distribution measured by mercury porosimetry for PES and PVDF filter. The pore volume is shown as a function of pore diameter. The PVDF filter consisted of two filter layers which were measured independently.

forces found for the potassium chloride solution between addition of PS 20 versus PS 80 in amounts above the CMC for both filters. Due to its impact on filter resistance, PS 20 was added to the control solutions, in order to guarantee comparable filter resistance during filtration of the control solutions as well as for the protein solutions. The findings highlight that the filter resistance is defined by the (surface) properties of the filter material interdependent with the hydrophilicity - and consequentially - by the surface-active properties of the solution to be filtered.

Filtration rate

To further investigate the deviation of filtration forces of monoclonal antibody formulations from linear flow behavior of the control solutions with increasing viscosity, filtration forces of mAb2 at the highest protein concentration (180 mg/mL) were assessed. Figure 5.4 shows the filtration force normalized by dynamic viscosity (measured at low shear rate of 2×10^3 s^{-1} showing Newtonian behavior) for mAb2 through a PES filter in comparison to the control solution (60% (m/v) glycerol solution with PS) as a function of filtration rate. In comparison to the control solution, mAb2 showed an increasing deviation from Newtonian flow behavior indicating significant influence of filtration rate on the parameter which led to reduced filtration forces.
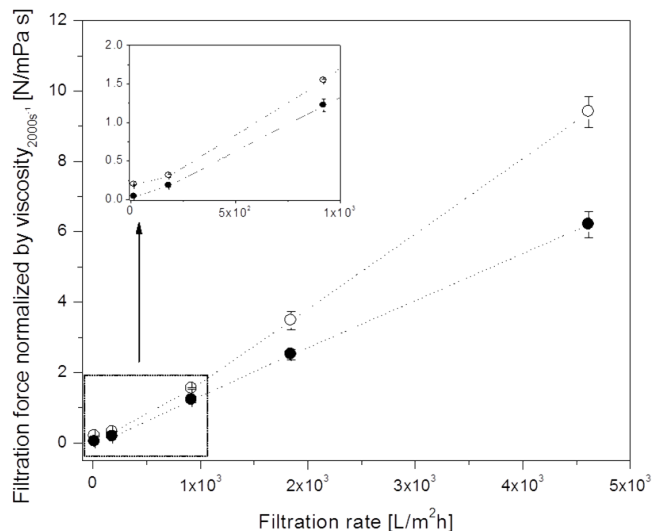
Figure 5.4: Filtration forces for mAb2 at 180 mg/mL (filled circle) and 60% (m/v) aqueous glycerol
solution (open circle, control) normalized by viscosity ($20°C$, 2×10^3 s^{-1}) for the PES filter as a function
of filtration rate. Mean values and standard deviation are reported. The dotted lines were drawn to guide
the eye.

Excipients

To investigate the influence of different excipients in solution, mAb1 was formulated in either a 20 mM
histidine hydrochloride or a 20 mM sodium citrate buffer at a protein concentration of 20 and 150 mg/mL
with further addition of the following excipients: (1) no further addition of excipients, (2) addition of
150 mM arginine-HCl, or (3) addition of 200 mM sucrose. These were selected in order to evaluate different
ionic strength (e.g., arginine-HCL), viscosities (i.e., viscosity increase in sucrose-containing formulation
and decrease in arginine-HCl containing solutions), and to compare formulations with different buffer
valences. All formulations contained PS 20. Figure 5.5 shows the filtration forces measured at a filtration
rate of 1.85×10^3 L/m^2h for the different formulations at 20 mg/mL (A) and 150 mg/mL (B) as white
(PES) and hatched (PVDF) bars (left y-axis) and the corresponding dynamic viscosity as black dots
(right y-axis). Clear differences between the PES and the PVDF were found for both protein concentra-
tions: in general, lower filtration forces were found for the PVDF filter as already shown in the previous
experiments. For the 20 mg/mL, Figure 5.5 (A) shows that there are no significant differences in filtration
forces between the mAb1 formulations. This was consistent with the dynamic viscosity which also showed
no difference between the formulations. For the 150 mg/mL formulations, differences in filtration forces
were found between the solutions with different excipients, consistent with the extent of viscosity if a
single buffer system is considered. Significant differences of filtration forces were found between the two
buffer systems – especially as viscosities were approximately similar between the corresponding formula-
tions or did not differ in the same direction as filtration forces.
 Table 5.1 lists the zeta potential of the mAb1 formulations measured at 150 mg/mL and the interaction
parameter A_2 which was measured between $1 - 10$ mg/mL. The zeta potential representing the elec-
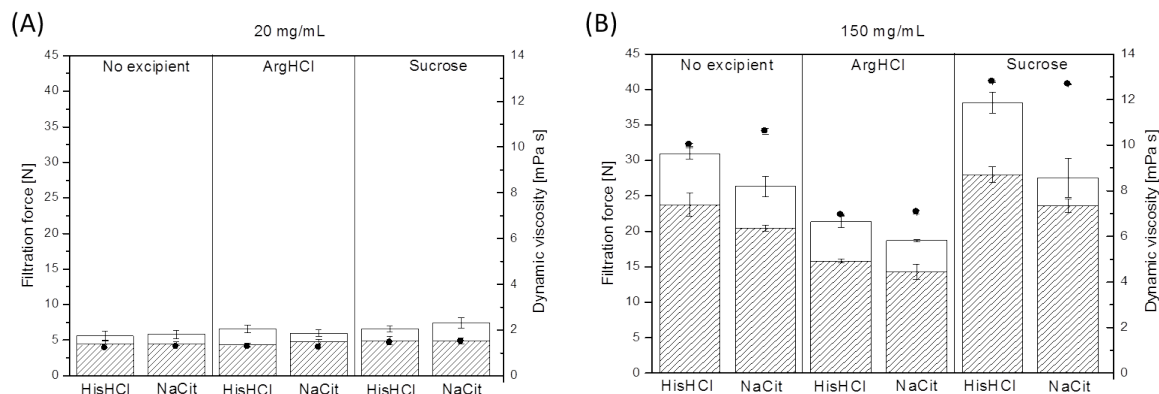
Figure 5.5: Filtration forces of different formulations of mAb1 at (A) low protein concentration (20 mg/mL) and (B) high protein concentration (150 mg/mL), (left y-axis). The white bars correspond to filtration forces through the PES filter and the hatched bars to the PVDF filter. Corresponding viscosity data to the formulations (2 x 10^3 s^{-1}, 20°C) are shown as filled symbols (circles), (right y-axis). Mean values and standard deviation are reported.

trokinetic potential of the formulation was found positive for the formulations consisting of histidine-HCl buffer with no addition of excipients or addition of sucrose, and around zero for the other formulations due to the increase in ionic strength. The parameter A_2, which characterizes protein-protein interactions (PPI) between two molecules, was also found positive for the formulations consisting of histidine-HCl buffer with no addition of excipients or addition of sucrose indicating repulsive PPIs. For the other formulations with a higher ionic strength, A_2 was found smaller by the factor of 10 indicating a reduction in repulsive and increase in attractive PPIs, respectively, due to ion shielding. After normalization of the filtration forces by low-shear viscosity which are also reported in Table 5.1, no correlation was found between filtration forces and the investigated parameters. Additionally, sub-visible particle counts were determined before filtration to assess possible particle burden of the solution. However, particle counts between 0 – 14 ($\geq 10\,\mu$m) and 0 – 9 ($\geq 25\,\mu$m) cumulative counts/mL were found, which were far below compendial requirements with ≤ 600 and $\leq 6\,000$ counts/mL for particles ≥ 10 and $\geq 25\,\mu$m, respectively. Detailed counts are provided in Table 5.2 in the supporting information.

Figure 5.6 shows the filtration forces of the different mAb1 formulations as presented in Figure 5.5 as a function of dynamic viscosity in comparison to a Newtonian control which showed linear correlation with $R^2_{PES} = 0.993$ and $R^2_{PVDF} = 0.997$ in citrate buffer and $R^2_{PES} = 0.968$ and $R^2_{PVDF} = 0.994$ in histidine buffer. The control solutions consisted of different concentrations of glycerol (0 – 60%, m/v) in either a histidine-HCl or sodium citrate buffer with addition of polysorbate 20. The filter resistance was found consistent with the previous controls (aqueous) of 20.8 and 20.6 m^{-1} (PES) and 9.8 and 10.1 m^{-1} (PVDF) for the histidine and citrate buffer system, respectively, indicating that the surface properties were mainly defined by the interaction of filter membrane with the added polysorbate in aqueous solution and not by the buffer system. Figure 5.6 shows filtration forces through the PES (A) and PVDF (B) filter, generally with smaller filtration forces for the PVDF compared to the PES filter, as already found for the previous experiments (Figure 5.1). For both filters, filtration forces of mAb1 showed systematic deviation

Formulation		F/η [N/mPas] (PES)	F/η [N/mPas] (PVDF)	ζ [mV]	A$_2$ [mol mL/g^2]
20 mM HisHCl	No excipient	3.09 ±0.08	2.37 ±0.17	3.6	10.1 ±0.1
	150 mM ArgHCl	3.08 ±0.13	2.28 ±0.03	0.1	1.0 ±0.1
	200 mM Sucrose	2.98 ±0.12	2.19 ±0.09	2.8	9.7 ±0.1
20 mM NaCit	No excipient	2.48 ±0.14	1.93 ±0.04	0.0	0.8 ±0.1
	150 mM ArgHCl	2.64 ±0.02	2.19 ±0.21	0.9	1.4 ±0.1
	200 mM Sucrose	2.17 ±0.22	1.86 ±0.08	0.3	-0.7 ±0.1

Table 5.1: Filtration force F for PES and PVDF filter normalized by dynamic viscosity $\eta_{20°C, 2x10^3 \ s^{-1}}$ (Newtonian behavior, N = 2), zeta potential ζ (N = 2), and interaction parameter A$_2$ (N = 3) for different formulations of mAb1. Mean values and standard deviation are reported.
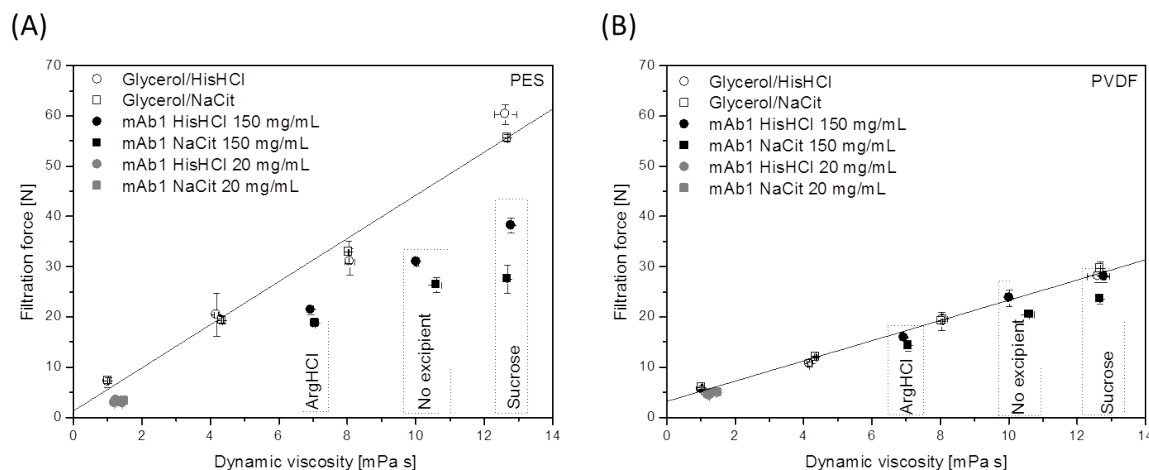
Figure 5.6: Filtration forces of mAb1 at 20 mg/mL (grey symbols) and 150 mg/mL (black symbols) in HisHCl (circle) or NaCit buffer (square) with different excipients, and glycerol solutions (Newtonian control, empty symbols) through a PES (A) and a PVDF filter (B). Filtration forces are presented as mean values with standard deviation (N = 3) as a function of dynamic viscosity (2 x 10^3 s^{-1}, 20°C) and were measured at a filtration rate of 1.85 x 10^3 L/m^{2}h.

from the Newtonian control with increasing viscosity/protein concentration. However, this deviation was smaller for the PVDF filter than for the PES filter. These findings were also consistent with the results of Figure 5.1. Interesting to note, that the deviation of the different mAb1 formulations was found to be systematic (increasing with higher viscosity) when a single buffer system was considered, and thus independent on the tested excipients. Figure 5.6 (A) also showed that the deviation increased for the citrate buffer compared to the histidine formulations.

5.4 Discussion

Bioburden-reduction and sterile filtration are unit operations performed during aseptic drug product manufacturing for parenteral pharmaceutical products, such as monoclonal antibodies. The filtration pressure needed is determined besides solution contaminants by filter area, filtration rate/volumetric flow, solution viscosity, and filter resistance. The latter is defined by pore size distribution and surface properties of the filter material. The present study shows that besides these parameters, particular properties of protein solutions, depending on protein concentration can have an additional, significant influence on the filtration process.

Non-Newtonian behavior

Filtration of two monoclonal antibody formulations mAb1 and mAb2 revealed systematic deviation from Newtonian control solutions with increasing viscosity and protein concentration depending on filter material (PES and PVDF filter, Figure 5.1). The control solutions followed the linear hydrodynamic model which is described by the Hagen-Poiseuilles law. [32-34] Further analysis of mAb2 at the highest protein concentration (180 mg/mL) showed that this deviation after normalization of filtration forces to viscosity (measured at low shear rates showing Newtonian behavior) increased with filtration rate (Figure 5.4). An increase in filtration force is consistent with an increase in shear rate (= first derivative of velocity). Having excluded warming effects by the Newtonian control, we therefore conclude that the deviation from linear filtration forces - which is shear rate dependent - is most likely due to shear thinning (non-Newtonian) behavior.

The higher extent of shear thinning observed for mAb1 and mAb2 for the PES filter (compared to the PVDF filter) was consistent with our findings from the filter characterization experiments: The PES filter showed a narrow pore size distribution at small pore sizes (maximum pore volume at 0.43 μm) compared to the PVDF filter with a broader pore size distribution with no clear maximum (Figure 5.3). The shear rate $\dot{\gamma}$ [s^{-1}] is defined by the following equation dependent on volumetric flow $\partial V/\partial t$ [m^3/s], [7]:

$$\dot{\gamma} = \frac{16/\partial t}{3\pi D^3} \tag{5.2}$$

As the shear rate is inverse proportional to the third power of pore diameter D [m], the shear rate for the PES filter is supposed to be much higher than the shear rate for the PVDF filter. This supports the observation that stronger shear thinning behavior was found for mAb1 and mAb2 when using the PES filter compared to the PVDF filter. However, exact calculation of the shear rate during filtration is challenging and needs further investigation as the shear rate is defined by the smallest pore size interdependent with the number of pores of the respective size as well as the distribution within the filter. A smaller pore size distribution also influences absolute filtration forces. This is reflected in our data with higher filtration forces for the tested PES filter than for the tested PVDF filter and quantified by the higher filter resistance.

In a related study, we have already shown shear thinning behavior for mAb1 at high protein concentrations. [7] We found an increase in non-Newtonian behavior at high shear rates ($10^5 - 10^6$ s^{-1}) with increasingly high protein concentration. This is consistent with the increase in deviation from the Newtonian control solutions with increasing viscosity and protein concentration in the first experiment (Figure

5.1). In literature, it is proposed that the reason for shear thinning behavior might be a deformation of self-associating mAb networks/clusters to the flow field. These (reversible) clusters are likely to form at higher protein concentrations and are held together by weak non-covalent, attractive interactions being electrostatic and hydrophobic in nature. These clusters seem to be also responsible for increasing viscosity. [35-41] In the related study, we showed that mAb1 was not sensitive to shear stress, which was representative for shear stress during injection, as no influence on protein integrity (protein aggregation) and particle formation (visible and sub-visible) was observed by shear thinning behavior for this mAb. Furthermore, Kiese *et al.* reported that the addition of polysorbate reduces aggregation of a monoclonal antibody induced by shear stress by protecting the protein from interaction with hydrophobic surfaces. [21] Liu *et al.* have recently shown that the influence of filtration pressure on product quality might not be the limiting parameter during filtration. They suggested that the shear stress exposure found during usual manufacturing processes of an IgG_1 formulation (100 mg/mL) was not considered important for final product quality. More important causes of aggregation were suggested to be the presence of air-bubbles, adsorption to solid surfaces, or contamination by particulates. [42] However, sensitivity to shear stress representative for the filtration process needs to be investigated on a case-by case basis in particular for higher protein concentrations and formulations showing pronounced shear-thinning behavior dependent on product and process characteristics.

Setting our small-scale filtration set-up (3.9 cm^2) into relation to large scale production where e.g. 10 inch filter capsules are used (0.69 m^2), the filtration of a sample with a dynamic viscosity of 5 mPas or 10 mPas corresponds to a filtration pressure of 0.58 bar and 1.13 (PES) or 0.34 bar and 0.60 bar (hydrophilic PVDF) at the chosen filtration rate of 1.85 x 10^3 L/m^{2}h (equivalent to 2 mL in 10 s for the tested set-up). Filtration forces in the magnitude of 15 – 40 N as shown in Figure 5.1, Figure 5.5, and Figure 5.6, where shear thinning behavior of the different mAb formulations was shown, correspond to a filtration pressure in the range of 0.4 – 1.0 bar which is consistent with routinely used filtration pressures during production of biotech products.

Change of filter resistance by addition of polysorbate

Zhou *et al.* have previously reported that PS 20 adsorbs to PES as well as PVDF aseptic filter membranes although to the latter to a much less extent. They proposed a hydrophobic-based, non-specific binding to the filter membrane and found that protein concentration did not have an influence on the amount of adsorbed surfactant. [10] Mahler *et al.* have reported significant adsorption of PS 80 to PES filters. [11] Both authors therefore suggest to carefully select filter material for processing and/or – if quality systems allow – pre-conditioning of the filter (independent on flow rate) as also performed within this study. This ensures appropriate PS concentration in the final product and mitigates the possible impact of PS adsorption.

By the investigation of filter resistance, our data strengthen the reported findings that polysorbates significantly adsorb to the PES filter membranes. The filter resistance of the PES filter significantly increased upon addition of PS (filtration of a simple salt solution) whereas the filter resistance of the PVDF filter did not change. Moreover, a slower increase of filtration force during pre-conditioning with the salt solution was found for both filters (filtration profile) as when compared to the increase in filtration force after pre-conditioning on a comparable time-scale. The increase was slower for the PES filter (data/filtration profile not shown). This also suggests a higher adsorption of PS to the PES filter

than to the PVDF filter. However, this needs to be further characterized. In summary, the presence or absence of surfactant in combination with intrinsic surface properties of the filter and its pore size distribution can have a major influence on filter resistance and thus, filtration forces.

Formulation properties

The impact of different excipients on filtration forces was investigated for mAb1 at low (20 mg/mL) and high (150 mg/mL) protein concentrations. The formulation composition differed in their ionic strength (type of buffer, addition of arginine-HCL), viscosity (increased by addition of sucrose, decreased by addition of arginine-HCl), and buffer valence (histidine-HCl and citrate buffer). At low protein concentration (20 mg/mL), the tested formulations did not show significant differences in filtration forces, consistent with no differences in viscosity. Lower filtration forces were generally found using the PVDF filter than compared to the PES filter – for both protein concentrations containing PS, which was consistent with the previous experiments. However, at high protein formulations (150 mg/mL), differences in filtration forces between the solutions with different excipients were found. The forces normalized by viscosity (as measured at low shear rates indicating Newtonian behavior) could neither be correlated to zeta potential measurements (150 mg/mL) as a measure for the electrochemical potential of the formulations, neither to the particle burden in solution prior filtration (cumulative sub-visible particle counts), nor to the interaction parameter A_2 as a measure for protein-protein interactions.

In detail, although the formulations which contained either histidine or citrate buffer showed identical viscosity if the same excipient was added, the formulations with the citrate buffer showed significantly lower filtration forces than compared to the histidine formulations (for both filter materials). If a single buffer system is considered, the differences between the formulations were found to change in line with viscosity. Additionally, if the filtration forces of those formulations are considered as a function of viscosity (Figure 5.6), a systematic deviation from control samples was found with the latter showing linear relation of filtration forces and viscosity as expected from Newtonian flow behavior. These findings are consistent with the data shown in Figure 5.1: Deviation from linear increase in filtration forces with increasing viscosity with the difference that in Figure 5.1 the increase in viscosity was due to increasing protein concentration (and not due to the addition of different excipients). Moreover, the behavior with respect to the different filter material was consistent with in general higher filtration forces and also higher deviation of the linear relation for the PES filter. The PES filter showed a smaller pore size distribution and therefore potentially higher shear rates during the filtration process leading to more pronounced shear thinning behavior with increasing viscosity. The data shown in Figure 5.6 thus support the conclusion, that shear thinning behavior significantly influences filtration forces, and should be considered as an important factor during sterile filtration of highly concentrated protein formulations.

We have shown in a related study that mAb1 – in a different formulation – exhibits viscosity behavior following the Carreau model with a Newtonian plateau at low shear rates, a shear thinning region converging to a secondary Newtonian plateau at higher shear rates. To date, the relation between the level of viscosity, the beginning and shear rate range of the shear thinning region, as well as the relation to formulation properties (excipients) remained unclear. [7] However, the current findings suggest that the buffer ions/valence seems to have a possible influence on shear thinning behavior of mAb1 independent on the excipients tested. These excipients may only trigger the extent of viscosity of the first Newtonian plateau (an increase in viscosity by addition of sucrose and a decrease in viscosity by addition

of arginine-HCl). Open question remains if shear rates during filtration are likely to be in the range of
the shear thinning region or even in the secondary Newtonian plateau, which is subject to further research.

5.5 Conclusion

The rheological behavior of highly concentrated protein solutions have a major impact on hydrodynamic
processes for example during parenteral drug administration, as investigated in a related study [7], as
well as during manufacture of the product like during filtration within the drug product manufacturing
process. With the present study, the impact by various factors on filtration forces were evaluated. Besides
the commonly known parameters as filter area, filtration rate/volumetric flow, solution viscosity, and
filter resistance (defined by pore size distribution and surface properties), the following parameters were
identified to significantly influence filtration forces: (a) the presence/absence of surfactant (polysorbate)
was observed to have a major influence on filter resistance dependent on filter material. It was shown
that the addition of polysorbate 20 significantly increased the filter resistance of the PES filter, whereas
it remained relatively unchanged for the PVDF filter. (b) the interaction of (1) pore size distribution,
which was found significantly different for the tested filter materials, and (2) filtration pressure, which
trigger the shear rate, were found to lead to non-Newtonian, shear thinning behavior, which increased
with higher protein concentration and filtration rate. The study showed that non-Newtonian behavior
led to differences in filtration dependent on formulation composition. Differences in buffer valences
of the formulation showed a major impact on the non-Newtonian behavior with a higher extent of
shear thinning for the citrate buffer compared to the histidine buffer independent on the addition of
excipients like arginine-HCl or sucrose. The latter were found to not contribute to the extent of shear
thinning behavior. These findings emphasize the importance of considering formulation composition on
hydrodynamic processes like filtration and highlights the relevance to assess possible limitations during
manufacture caused by elevated viscosity of highly concentrated protein formulations.

5.6 Acknowledgments

5.7 References

1. S.J. Shire, Formulation and manufacturability of biologics, Curr Opin Biotech, 20 (2009) 708-714.

2. S.J. Shire, Z. Shahrokh, J. Liu, Challenges in the development of high protein concentration formulations,
   J of Pharm Sci, 93 (2004) 1390-1402.

3. N.W. Warne, Development of high concentration protein biopharmaceuticals: the use of platform ap-
   proaches in formulation development, Eu J Pharm Biopharm, 78 (2011) 208-212.

4. S.Y. Patro, E. Freund, B.S. Chang, Protein formulation and fill-finish operations, Biotechnol Annu Rev, 8 (2002) 55-84.

5. N. Rathore, N. Bhasin, P. Kolhe, R. Law, A. Abdul-Fattah, L. Li, W.C. Ji, K. Murphy, BIOT 305-Bench scale cleaning characterization of drug products in a fill-finish facility, Abstr Pap Am Chem S, 234 (2007).

6. J.A. Ge, A. Thummala, M.V.S. Wadhwa, Applications of Statistical Regression and Modeling in Fill-Finish Process Development of Structurally Related Proteins, J Pharm Sci, 100 (2011) 464-481.

7. A. Allmendinger, S. Fischer, J. Huwyler, H.-C. Mahler, E. Schwarb, I.E. Zarraga, R. Mueller, Rheological characterization and injection forces of concentrated protein formulations: An alternative predictive model for non-Newtonian solutions, Eu J Pharm Biopharm, 87 (2014) 318-328.

8. V. Burckbuchler, G. Mekhloufi, A.P. Giteau, J.L. Grossiord, S. Huille, F. Agnely, Rheological and syringeability properties of highly concentrated human polyclonal immunoglobulin solutions, Eu J Pharm Biopharm, 76 (2010) 351-356.

9. M. Adler, Challenges in the Development of Pre-filled Syringes for Biologics from a Formulation Scientists Point of View, Am Pharm Rev, 15 (2012).

10. J.X. Zhou, J.S. Qiu, G. Jiang, C. Zhou, N. Bingham, H. Yeung, B. Dransart, M.V. Wadhwa, T. Tressel, Non-specific binding and saturation of Polysorbate-20 with aseptic filter membranes for drug substance and drug product during mAb production, J Membrane Sci, 325 (2008) 735-741.

11. H.C. Mahler, F. Huber, R.S. Kishore, J. Reindl, P. Ruckert, R. Muller, Adsorption behavior of a surfactant and a monoclonal antibody to sterilizing-grade filters, J Pharm Sci, 99 (2010) 2620-2627.

12. S. Ripperger, W. Goesele, C. Alt, T. Loewe, Filtration, 1. Fundamentals, in: Ullmann's Encyclopedia of Industrial Chemistry, Wiley-VCH Verlag GmbH und Co., Weinheim (2002) 1-38.

13. B.S. Chang, B.S. Kendrick, J.F. Carpenter, Surface-induced denaturation of proteins during freezing and its inhibition by surfactants, J Pharm Sci, 85 (1996) 1325-1330.

14. M. Katakam, L.N. Bell, A.K. Banga, Effect of surfactants on the physical stability of recombinant human growth hormone, J Pharm Sci, 84 (1995) 713-716.

15. H.-C. Mahler, R. Muller, W. Friess, A. Delille, S. Matheus, Induction and analysis of aggregates in a liquid IgG1-antibody formulation, Eu J Pharm Biopharm, 59 (2005) 407-417.

16. N.B. Bam, J.L. Cleland, J. Yang, M.C. Manning, J.F. Carpenter, R.F. Kelley, T.W. Randolph, Tween protects recombinant human growth hormone against agitation-induced damage via hydrophobic interactions, J Pharm Sci, 87 (1998) 1554-1559.

17. D.K. Chou, R. Krishnamurthy, T.W. Randolph, J.F. Carpenter, M.C. Manning, Effects of Tween 20 and Tween 80 on the stability of Albutropin during agitation, J Pharm Sci, 94 (2005) 1368-1381.

18. B.A. Kerwin, Polysorbates 20 and 80 used in the formulation of protein biotherapeutics: Structure and degradation pathways, J Pharm Sci, 97 (2008) 2924-2935.

19. B.A. Kerwin, M.C. Heller, S.H. Levin, T.W. Randolph, Effects of Tween 80 and sucrose on acute short-term stability and long-term storage at -20 degrees C of a recombinant hemoglobin, J Pharm Sci, 87 (1998) 1062-1068.

20. T.W. Randolph, L.S. Jones, Surfactant-protein interactions, Pharm Biotechnol, 13 (2002) 159-175.

21. S. Kiese, A. Papppenberger, W. Friess, H.C. Mahler, Shaken, not stirred: mechanical stress testing of an IgG1 antibody, J Pharm Sci, 97 (2008) 4347-4366.

22. S. Nema, R.J. Brendel, Excipients and their role in approved injectable products: current usage and future directions, PDA J Pharm Sci Technol, 65 (2011) 287-332.

23. S. Nema, R.J. Washkuhn, R.J. Brendel, Excipients and their use in injectable products, PDA J Pharm Sci Technol, 51 (1997) 166-171.

24. E. Dickinson, Proteins at interfaces and in emulsions - Stability, rheology and interactions, J Chem Soc Faraday T, 94 (1998) 1657-1669.

25. A. Allmendinger, S. Fischer, J. Huwyler, H.C. Mahler, R. Mueller, High-throughput viscosity measurement using capillary electrophoresis instrumentation Anal Chem, (2013).

26. C. Lehermayr, K. Mr, H.C. Mahler, S. Fischer, Second viral coefficient (A_2) and valence of none different therapeutic monoclonal antibodies, in: PharmSci Fair, Nice, France, 2009.

27. C. Lehermayr, H.C. Mahler, K. Mader, S. Fischer, Assessment of net charge and protein-protein interactions of different monoclonal antibodies, J Pharm Sci, 100 (2011) 2551-2562.

28. A. Saluja, A.V. Badkar, D.L. Zeng, S. Nema, D.S. Kalonia, Ultrasonic Storage Modulus as a Novel Parameter for Analyzing Protein-Protein Interactions in High Protein Concentration Solutions: Correlation with Static and Dynamic Light Scattering Measurements, Biophys J, 92 (2007) 234-244.

29. S. Yadav, S.J. Shire, D.S. Kalonia, Viscosity behavior of high-concentration monoclonal antibody solutions: correlation with interaction parameter and electroviscous effects, J Pharm Sci, 101 (2012) 998-1011.

30. T. Stirnimann, N. Di Maiuta, D.E. Gerard, R. Alles, J. Huwyler, M. Puchkov, Functionalized Calcium Carbonate as a Novel Pharmaceutical Excipient for the Preparation of Orally Dispersible Tablets, Pharm Res-Dordr, 30 (2013) 1915-1925.

31. T.J. Meltzer, MW, The sterilizing filter and its pore size rating, American Pharmaceutical Review, 10 (2003) 44-52.

32. L. Schiller, Drei Klassiker der Strömungslehre: Hagen, Poiseuille, Hagenbach, Akademische Verlagsgesellschaft, Leipzig (1933).

33. G.H.L. Hagen, Über die Bewegung des Wassers in engen zylindrischen Röhren., Poggendorfs Annalen der Physik und Chemie, 46 (1939) 423442.

34. J.L.M. Poiseuille, Recherches experimentales sur le mouvement des liquides dans les tubes de tres petits diametres, CR Acad Sci, 11 (1840) 10411048.

35. S. Kanai, J. Liu, T.W. Patapoff, S.J. Shire, Reversible self-association of a concentrated monoclonal antibody solution mediated by Fab-Fab interaction that impacts solution viscosity, J Pharm Sci, 97 (2008) 4219-4227.

36. J. Liu, M.D. Nguyen, J.D. Andya, S.J. Shire, Reversible self-association increases the viscosity of a concentrated monoclonal antibody in aqueous solution, J Pharm Sci, 94 (2005) 1928-1940.

37. S. Yadav, T.M. Laue, D.S. Kalonia, S.N. Singh, S.J. Shire, The influence of charge distribution on self-association and viscosity behavior of monoclonal antibody solutions, Mol Pharm, 9 (2012) 791-802.

38. A. Chaudhri, I.E. Zarraga, T.J. Kamerzell, J.P. Brandt, T.W. Patapoff, S.J. Shire, G.A. Voth, Coarse-Grained Modeling of the Self-Association of Therapeutic Monoclonal Antibodies, J Phys Chem B, (2012).

39. A. Chaudhri, I.E. Zarraga, S. Yadav, T.W. Patapoff, S.J. Shire, G.A. Voth, The role of amino acid sequence in the self-association of therapeutic monoclonal antibodies: insights from coarse-grained modeling, Journal of Physical Chemistry B, 117 (2013) 1269-1279.

40. W.G. Lilyestrom, S. Yadav, S.J. Shire, T.M. Scherer, Monoclonal Antibody Self-Association, Cluster Formation, and Rheology at High Concentrations, J Phys Chem B, 117 (2013) 6373-6384.

41. E.J. Yearley, I.E. Zarraga, S.J. Shire, T.M. Scherer, Y. Gokarn, N.J. Wagner, Y. Liu, Small-angle neutron scattering characterization of monoclonal antibody conformations and interactions at high concentrations, Biophys J, 105 (2013) 720-731.

42. L. Liu, W. Qi, D.K. Schwartz, T.W. Randolph, J.F. Carpenter, The effects of excipients on protein aggregation during agitation: an interfacial shear rheology study, J Pharm Sci, 102 (2013) 2460-2470.

5.8   Supporting information

Buffer	Excipient	$\geq$10 μm [cumulative counts/mL]	$\geq$25 μm [cumulative counts/mL]
20 mM HisHCl	No excipient	10	1
0.06% PS 20	150 mM ArgHCl	1	1
	200 mM Sucrose	0	0
20 mM NaCit	No excipient	3	3
0.06% PS 20	150 mM ArgHCl	10	9
	200 mM Sucrose	14	0

Table 5.2: Sub-visible particle count as cumulative count per mL $\geq$10 and $\geq$25 μm for the different formulations of mAb1 at 150 mg/mL. Measurements were performed as duplicates and mean values are reported.
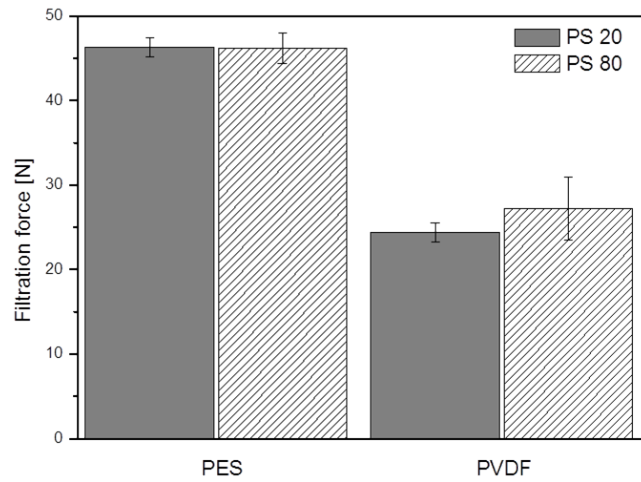
Figure 5.7: Representative example of a filtration profile of a 60% (m/v) glycerol solution (20 mM
HisHCl buffer, 0.06% (m/v) PS 20) through a PES (open circle) and a PVDF (filled circle) filter at a
filtration rate of 1.85 x 10^3 L/m^{2}h. Filters were pre-conditioned with the respective solution before the
experiment.
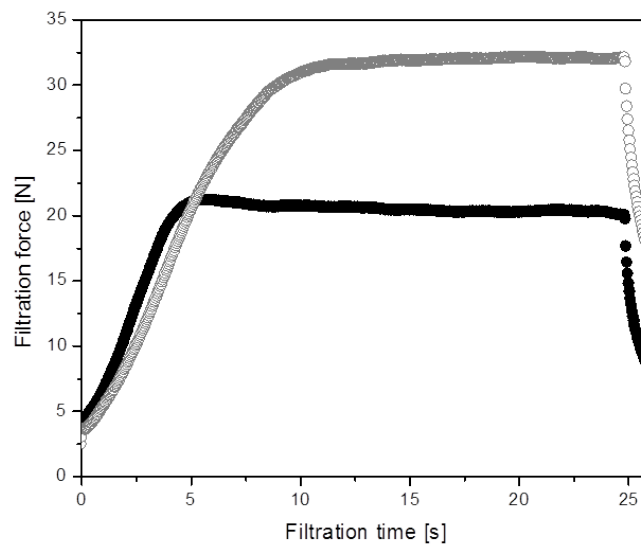
Figure 5.8: Comparison of filtration forces of a 0.001 M potassium chloride solution with 0.06% (m/v)
polysorbate 20 or 80 through PES and PVDF filter at a filtration rate of 1.85 x 10^3 L/m^{2}h.

Discussion

Highly concentrated protein therapeutics can offer a convenient way for subcutaneous drug administration by the patient him-/herself or a healthcare professional. During the manufacturing process, concentration of the protein leads to a decrease in volume available to the protein which may favor self-association/aggregation and increases viscosity. Severe limitations are thus given by the rheological behavior during pharmaceutical formulation, processing, and drug administration. The elevated viscosity at high protein concentrations leads to an increase in pressure required to manufacture or administer the protein solution.

The focus of this work was to investigate the rheological behavior of protein solutions at high protein concentrations. The main objective was to obtain a profound understanding of the drug administration as well as of the filtration process and to elucidate the role of viscosity with regard to potential limitations. In summary, the present work provides an overview of commercial highly concentrated protein formulations as well as of methods used for viscosity characterization including a new high-throughput method using CE equipment. Based on these studies, the role of viscosity of highly concentrated protein formulations was investigated in two critical aspects which were: i) the impact of viscosity on filtration within the fill-finish process and ii) the rheological behavior during drug administration of concentrated protein solutions.

Commercial highly concentrated protein solutions

Chapter 1 provides a technical overview of commercial highly concentrated biotherapeutics. The products which are intended to be administered using the sc or im route of injection were characterized for formulation properties including pH, osmolality, physical stability like the extent of soluble aggregates, as well as requirements defined by the European Pharmacopoeia, such as visible and sub-visible particles. Thus, this study may be used as reference for formulation development of highly concentrated protein therapeutics. The study revealed significant differences between the products especially for viscosity which was determined by plate/cone rheometry and found in the range of 2 mPas to 102 mPas (20°C) for protein concentrations between 50 and 200 mg/mL. A viscosity of 100 mPas was thus chosen as a benchmark for highest viscosity in the following studies, like for the study described in Chapter 4, which characterized the contribution of sc backpressure to injection forces.

The current benchmark for maximum protein concentration as well as of viscosity was a liquid formulation at 200 mg/mL with a dynamic viscosity of 102 mPas measured at 20°C. Interestingly, this commercial product is indicated for rheumatoid arthritis, with patients who are limited in their dexterity/flexibility. This was likewise addressed by the design of the pre-filled syringe of the product using an extended finger flunge and a special ring-shaped RNS to facilitate removal. Most importantly, this product also had the largest inner needle diameter of 25 G compared to other commercial products using a 27 G needle for the injection device. Increasing the needle inner diameter facilitates injection and reduces injection forces significantly, which was investigated in the following chapters in detail.

The viscosity of each commercial product investigated was reflected in the corresponding injection forces which were tested both in respective marketed injection device and a generic device. The latter served

to normalize the data. The viscosity data was correlated to injection forces applying currently described models based on the Hagen-Poiseuilles' law, dependent on viscosity, injection rate/volumetric flow, and frictional forces as follows:

$$F_{total} = F(Q, \eta)_{hydrodynamic/Hagen-Poiseuille} + F(Q)_{friction}$$

(F = force, Q = volumetric flow, η = dynamic viscosity)

Deviations from linear correlation were found for some of the commercial products leading to deeper investigation of injection forces of protein solutions at high protein concentrations (Chapter 3). Moreover, injection forces were calculated and experimentally verified by simulated injection into air, and thus neglecting the *in vivo* situation. The present data were used as a basis for further investigation of the correlation between viscosity and injection forces representative for the *in vivo* situation as outlined in Chapter 4.

High-throughput method for viscosity measurement

Viscosity characterization of protein formulations is challenging requiring methods involving low material consumption (in the microliter range) and a high throughput at a viscosity range between approximately 1 and 100 mPas. Commercially available methods are time-consuming and require large sample volumes in the range of hundreds of microliters to a few milliliters. Therefore, an automated, high-throughput method to measure dynamic viscosity of Newtonian solutions using standard capillary electrophoresis equipment was developed. Chapter 2 describes the development of this method as well as the application to protein therapeutics by comparison to our routinely used method for viscosity determination during protein formulation development which is plate/cone rheometry. Typical viscosities in the range of 5 to 40 mPas were accurately measured with measurement times between 1 and 15 minutes, small sample volumes (few microliters) by use of a capillary with a diameter of 50 μm and a length of 20.5 cm.

Compared to other rheological methods used in protein formulation development, such as capillary viscosimeters [2 – 4 mL], falling ball viscosimeters [150 – 300 μL], or standard plate/cone rheometer [80 μL], the established CE instrumentation-based method requires a small sample volume in the storage vial of 100 μL and a sample consumption of only a few microliters. The volume of 100 μL is a limitation of the instrument used and may be optimized by vial design or optimization of the inlet position. Most importantly, a unique feature of the CE instrumentation is that no time-consuming cleaning is needed due to automation of the method and cleaning process. This constitutes an advantage over the above mentioned viscosimeters, which require at least about 10 minutes per measurement. As a result, the CE instrumentation allows for measurements in an automated manner with a throughput of approximately 30 samples per load defined by the capacity of the sample tray of the instrument used.

A limitation of the CE instrumentation-based method may be the potential for clogging of the capillary with particles. However, since filtration of protein samples (using sterilizing-grade filters) is routinely performed during sample preparation, particles >0.2 μm are typically excluded. Furthermore, potential interaction of the sample with the capillary wall at high protein concentration might require coated capillaries. An alternative approach is the calibration of the capillary with the specific product itself or

the measurement of relative viscosity values.

Our method reliably determined the viscosity of Newtonian solutions between 5 and 40 mPas. Variation in capillary length and capillary diameter led to different minimal and maximal viscosities. The subject of ongoing research is the variation of the applied pressure which leads to measurements at different/adjustable shear rates. Therefore, the method would also be applicable to non-Newtonian liquids showing shear-rate-dependent behavior. This is of considerably importance as we have recently reported that protein formulations can show shear-thinning behavior especially at high protein concentrations (Chapter 3). CE is an analytical method routinely used for the separation and characterization of proteins. Therefore, this instrument is usually available in most protein formulation development laboratories and can be used straight forward for viscosity determination.

Injection forces (*in vitro/in silico*)

Based on the preliminary study on characterization of commercial products (Chapter 1), which showed smaller injection forces than estimated from currently described models, injectability of highly concentrated protein formulations was further investigated in Chapter 3 and 4. In Chapter 3, injection forces of a monoclonal antibody (mAb, IgG_1) at maximum protein concentration considered feasible (250 mg/mL) as well as of the different commercial products were characterized dependent on various parameters like injection rate, and linked to rheological behavior. Based on the law of Hagen-Poiseuille, injection forces were found to be linearly dependent on viscosity. However, deviation from linear flow behavior was found for some of the products compared to the Newtonian control. Based on these findings, a mathematical *in silico* model was established to predict injection forces from viscosity data applicable for Newtonian and non-Newtonian fluids. It was experimentally verified (*in vitro*) by use of surrogate samples (Carbopol gels). Subsequent viscosity characterization of our model antibody mAb1 at high shear rates ($10^{5-6}\,\mathrm{s}^{-1}$) as well as of some commercial products revealed non-Newtonian, shear thinning behavior which was increasing with higher shear rates as well as protein concentration and viscosity. The rheological profile of mAb1 at high protein concentrations was thereby described by the Carreau model indicating a first Newtonian plateau ($10^4\,\mathrm{s}^{-1}$), a shear thinning region, and potentially converging to a secondary Newtonian plateau at $>10^6\,\mathrm{s}^{-1}$. The detailed characteristics of the secondary plateau depending on type of antibody, protein concentration, and formulation composition need to be further investigated. The findings of this study emphasize that shear thinning behavior leads to smaller injection forces than expected from linear flow behavior. This is of outmost importance as the limits (e.g. used for device robustness and device design) currently predicted based on Newtonian behavior would significantly overestimate injection forces. The presence of non-Newtonian flow behavior at high shear rates may offer the possibility to exceed these limits and to consider even higher protein concentrations and viscosities.

However, the crucial factor for the definition of injection force limits likely remains the patient population or health care professionals and their capability to administer the product. Anthropometric strength studies showed that the force that a user can exert onto a syringe plunger is determined by multiple factors including the health status and the strength of the individual, and the upper limb and hand posture required for injection.[1] These human factors also include the personal preference and training of the individual. In reality, users moderate the injection force by adjusting their injection speed and may choose a slower injection resulting in a lower injection force to fit their capability or preference.

Injection forces (*in vivo*)

A mathematical model for prediction of injection forces was described in Chapter 3. It is based on the Hagen-Poiseuille's law and representative for simulated injections into air. This model depends on a hydrodynamic part which is influenced by dimensions of the device components (e.g. needle inner diameter), injection rate, and formulation properties like viscosity. Besides hydrodynamic forces, frictional forces between stopper and plunger are considered which are among others driven by siliconization of the syringe barrel and dimensions of the stopper. However, for a comprehensive picture of parameters contributing to injection forces, they should be tested in an *in vivo* situation and parameters like hydrodynamic contribution, tissue backpressure, and other factors should be separately assessed.

Chapter 4 investigated injection forces during sc administration in Göttingen minipigs (*in vivo*) dependent on viscosity, injection rate, and injection volume providing quantitative data on the backpressure of the sc tissue. The quantitative amount of the contribution of sc tissue backpressure to injection forces is significant and ranged in average from 0.6 to 4.7 N (1 – 20 mPas, 0.025 – 0.2 mL/s) with a maximum value of 12.9 N (20 mPas, 0.2 mL/s).

The minipig is currently considered as the most appropriate translational animal model to study the pharmacokinetics of biotherapeutics after sc injection e.g. for studies of monoclonal antibody therapeutics [2, 3, 4]. Most importantly, the structure of the hypodermis of the pigs was reported to resemble that in humans more than any other animal (e.g. rodent, monkey) [2, 5-7]. The skin of the pig is, like in humans, connected to the deep *fascia* via a fibrous network which defines the spreading behavior of a sample. A relevant difference between humans and e.g. rodents, monkeys, and pigs is the presence of the *panniculus carnosus* for the latter three animal species [3, 5, 7, 8]. However, the *panniculus carnosus* is missing in some parts of the pig, like in the groin, and therefore ressembling human tissue structure [5]. Thus, the *plica inguinalis* was chosen as injection site in minipigs for this study. Only the height of the subcutaneous tissue layer differs between the human skin (approximately 11 mm) [9] and the *plica inguinalis* of the minipig (few mm). Therefore, a short needle with a length of 3/8" used for injection in parallel to the body surface, was chosen to control and ensure injection of the solutions in the sc tissue space in our study. The two differences between injection into the skin of minipigs versus injection into human tissue are on the one hand the difference in the height of the sc tissue layer and of the injection angle on the other hand. This might lead to the question whether and how the obtained results may be translated to humans. This question cannot be fully answered at this point of time as this study is the first one to provide quantitative data on the contribution of the tissue backpressure to sc injection forces in an *in vivo* situation. However, the structure of the skin is considered comparable between humans and the inguinal region of the minipig, as previously outlined. Therefore, similar spreading/distribution of the injected sample in the sc tissue layer is expected. Up to date, current literature only provides a study which was conducted by Cilurzo *et al.* dealing with the contribution of the tissue to injection forces during sc injection. They have recently performed an *ex vivo* experiment where they injected a 19 mPas and a 101 mPas solution into the abdominal skin (sc) from an Eurasian female who underwent cosmetic surgery. They found an increase in injection force by a factor of 1.1 compared to injection into air due to tissue resistance. Although only measured at a constant injection speed of 1 mm/s (approximately 0.03 mL/s), this study also suggested a significant contribution of the tissue to injection forces [10]. However, testing of injection forces *ex vivo* is not yet fully understood. It may lead to unexpected modifications/distortions. Therefore, further investigation is needed to show if and how *ex vivo* testing may be representative for the *in vivo* situation.

Besides the contribution of the tissue, the study showed that local warming of the (equilibrated) sample in the needle during injection has to be considered when estimating injection forces representative for the *in vivo* situation. This local temperature effect led to reduced viscosity of the sample in the needle and therefore smaller injection forces than initially expected. The temperature effect was experimentally quantified dependent on viscosity and injection rate and is applicable to any desired body temperature (e.g. also to humans). The control experiments in a tempered water bath confirmed that injection forces were significantly decreased if the needle tip – although only few millimeters in length – faces warmer environmental conditions than room temperature during injection than compared to injections into air (at room temperature). This additional negative contribution to injection forces was found and quantified to be linear dependent on viscosity and injection rate indicating a hydrodynamic process.

The positive contribution of the sc backpressure and the negative contribution of the local temperature effect were described to compensate each other to some extent. This is of utmost importance with respect to potential limitations given by the user capability of the patient. Dependent on the indication, patients might be limited in their strength like e.g. for rheumatoid arthritis patients, stating a challenge to expel a syringe. Therefore, the limits for maximal required injection force have to be carefully evaluated before design of an injection device. A highly concentrated protein therapeutic with a viscosity of 100 mPas has been previously studied [1]. This protein therapeutic was tested for injectability by Sheikhzadeh and co-workers in an anthropometric study. The authors reported that rheumatoid arthritis patients were capable to exert a force of approximately 17 N (95% percentile) and 48 N (mean) in average onto the syringe plunger [1]. Setting this into relation to our findings assuming a constant, slow injection speed of 0.025 mL/s, the injection force of this product would be higher by approximately 7 N due to the contribution of the sc backpressure compared to *in vitro* injection forces, which are in general tested against air. The local temperature effect for a body temperature of 37°C (human) leading to warming of the sample in the needle would decrease injection forces by approximately 4 N assuming similar viscosity-temperature dependence of the therapeutic as dextran. This would result in an overall higher injection force by 3 N compared to the estimated or measured injection force in the *in vitro* situation.

The data indicate that consideration of the actual *in vivo* sc backpressure is essential when assessing injection forces. Moreover, compensation of the increase in injection forces due to tissue backpressure by the local temperature effect, as observed for the minipig and reported to our knowledge for the first time, needs to be evaluated and confirmed in humans. In summary, the *in vivo* study provides a detailed insight into injection forces and led to the following extension of the *in silico* model to predict injection forces [11]

$$F_{total} = F(Q, \eta)_{hydrodynamic} + F(Q)_{friction} + F(Q, \eta)_{tissue\,backpressure} - F(Q, \eta)_{body\,temperature}$$

(F = force, Q = volumetric flow, η = dynamic viscosity)

The final limiting parameter for the injection process is given by the user capability of the patient population. However, the needle inner diameter was shown to have major influence on injection forces as outlined in detail in Chapter 3. The inner diameter of the needle is related to injection forces by the power of four compared to other parameters, like viscosity, injection rate, and sc tissue backpressure being directly proportional.

This study is of key importance during the development of injection devices like e.g. for combination products (e.g. autoinjectors or pre-filled syringes). Furthermore, the reported findings of this study suggest additional studies to be performed to fully understand the *in vivo* situation. With regards to

the observation of the local temperature effect, e.g. the development of tempered injection pads might be considered. These pads could be used for device testing or patient training.

Within this study, we found that the force profiles for all tested conditions reached a plateau and no difference in backpressure was found when two injection volumes (2.5 and 4.5 mL) were compared. Therefore, also even higher injection volumes might be tested to investigate if there is a limit in volume when the force profile starts to leave the plateau and start to further increase during injection due to the backpressure/lifting of the skin. This would also trigger reconsideration of maximum feasible injection volume as discussed in Chapter 4.

The potential of the instrumental set-up which was built for this study might be still huge. Especially the use of the injection equipment (including some modifications) to measure injection forces in human beings like e.g. during clinical studies would be beneficial. These studies might provide detailed information on actual injection forces and potentially confirm the findings of our *in vivo* study. Moreover, the measured injection force data might be directly linked to other human factors as well as providing information on related pain.

Last but not least, the instrumental set-up might be also used in upcoming *in vivo* studies to simulate injection by an autoinjector by application of an artificial pressure on the injection site mimicking the depression of the needle shield and activation of the autoinjector.

Filtration of highly concentrated protein formulations

Besides drug administration, the increase in viscosity with higher protein concentration may cause limitations during process development like during manufacture. Filtration was identified as the most critical process step related to viscosity during the manufacturing process. Therefore, filtration of different mAb formulations was investigated in detail in a lab-scale set-up as the second hydrodynamic process to complete this work. Chapter 5 provides a detailed look into filtration of highly concentrated protein formulations and summarized key factors having an impact on filtration forces. Filtration forces were determined dependent on filter material, protein concentration, and viscosity, and differences were linked to filter resistance, pore size distribution, and formulation composition. Most important, the study showed that dependent on the pore size distribution of the filter (which defines the shear rate dependent on the filtration pressure), the model antibodies mAb1 and mAb2 showed shear thinning behavior increasing with increasing filtration rate and protein concentration, thus confirming the findings from the injection force experiments. However, subject of ongoing research is the exact calculation of the shear rate during filtration due to distribution of the pressure over the pores of the cross-sectional area of the filter.

The study showed that the non-Newtonian behavior of mAb1 and therefore differences in filtration forces were influenced by the formulation composition. Especially differences in buffer valences of the formulation showed a major impact on the non-Newtonian behavior. This effect was independent on the addition of further excipients which were found to define the viscosity of the first Newtonian plateau (at low shear rates), however did not contribute to the extent of shear thinning behavior. These findings emphasize the importance of formulation composition on hydrodynamic processes like filtration.

Limitations for the filtration process may be discussed controversially. The study showed that the filtration pressure, which also triggered the rheological behavior at high protein concentrations dependent on filtration rate, is mainly defined by the pore size distribution of the filter material besides the other

investigated parameters like viscosity. Moreover, literature data reported that the influence of filtration pressure on product quality might not be the limiting parameter during filtration. For the formulations previously tested (up to a protein concentration of $100\,\mathrm{mg/mL}$ at $250\,000\,\mathrm{s^{-1}}$), the shear stress exposure during manufacture was not considered important for final product quality. More important causes of aggregation were suggested to be the presence of air-bubbles, adsorption to solid surfaces, or contamination by particulates. [12] However, future studies have to show the impact of shear-thinning behavior triggered by the applied pressure on product quality dependent on protein, formulation compositions, and especially protein concentration. This has to be evaluated on a case-by-case basis dependent on product and process characteristics.

Molecular consideration for shear-thinning behavior

The presented studies within this work have demonstrated that highly concentrated protein formulations may exhibit non-ideal flow behavior under high shear like e.g. during drug administration through a 27/25 G needle (Chapter 3) or during filtration (Chapter 5). The molecular mechanism for this shear thinning behavior is not yet fully understood and subject of ongoing research. One hypothesis is that monoclonal antibodies may form so-called self-associating clusters at high protein concentrations, as outlined. [13-18] Experiments showed that these mAb clusters are likely to be governed by anisotropic, colloidal interactions with hydrophobic attractive wells and heterogeneously distributed surface charges. [15] These clusters may be responsible for the increase in viscosity at higher protein concentrations as reported by Lilyestrom *et al.* [14] Similar findings are reported in literature for polymers like carbopols forming three-dimensional networks at high volume fractions. [19] These entanglements were shown to be responsible for an increase in viscosity. Furthermore, non-Newtonian rheological behavior was observed of these polymers at high shear rates potentially caused by alignment of these entanglements to the flow field. [19, 20] Therefore, shear thinning behavior of our mAbs may be caused by cluster aligning to the flow field if shear stress is applied, although Zarraga and colleagues have recently reported that the mAb self-associations are likely to be reversible and unlikely to be physical entanglements or long range elasticity, such as observed in polymer systems. Ongoing studies have to show if different formulations of mAb1, which were in some parts characterized during the injection experiments of Chapter 3, exhibit heterogeneous, self-associating structures dependent on protein concentration and how this relates to viscosity. Studies are ongoing using e.g. small-angel neutron scattering experiments which is one of the few methods capable to investigate protein-protein interactions and molecular structures at high protein concentrations as outlined in the 'Introduction'. Besides cluster formation, these data will also help to understand and to identify differences in attractive and repulsive PPIs of mAb1 dependent on formulations composition and the relation to viscosity data.

References (Discussion)

1. A. Sheikhzadeh, J. Yoon, D. Formosa, B. Domanska, D. Morgan, M. Schiff, The effect of a new syringe design on the ability of rheumatoid arthritis patients to inject a biological medication, Appl Ergon, 43 (2012) 368-375.

2. W.F. Richter, S.G. Bhansali, M.E. Morris, Mechanistic determinants of biotherapeutics absorption following SC administration, AAPS J., 14 (2012) 559-570.

3. Y. Zheng, D.B. Tesar, *et al.*, and W.F. Richter, Minipig as a potential translatable model for monoclonal antibody pharmacokinetics after intravenous and subcutaneous administration, Mabs, 4 (2012) 243-255.

4. N.C. Ganderup, W. Harvey, J.T. Mortensen, W. Harrouk, The minipig as nonrodent species in toxicology– where are we now?, Int. J. Toxicol., 31 (2012) 507-528.

5. E.H. Rose, L.M. Vistnes, and G.A. Ksander, The panniculus carnosus in the domestic pig, Plast. Reconstr. Surg., 59 (1977) 94-97.

6. G. Bode, P. Clausing, F. Gervais, J. Loegsted, J. Luft, V. Nogues, and J. Sims, The utility of the minipig as an animal model in regulatory toxicology, J. Pharmacol. Toxicol. Methods, 62 (2010) 196-220.

7. J.T. Mortensen, P. Brinck, and J. Lichtenberg, The minipig in dermal toxicology. A literature review, Scand. J. Lab. Anim. Sci., 5 (1998) 77-83.

8. A. Henning, D. Neumann, K.H. Kostka, C.M. Lehr, U.F. Schaefer, Influence of human skin specimens consisting of different skin layers on the result of in vitro permeation experiments, Skin. Pharmacol. Phys., 21 (2008) 81-88.

9. F. Mirrashed, J.C. Sharp, V. Krause, J. Morgan, B. Tomanek, Pilot study of dermal and subcutaneous fat structures by MRI in individuals who differ in gender, BMI, and cellulite grading, Skin. Res. Technol., 10 (2004) 161-168.

10. A. Allmendinger, S. Fischer, J. Huwyler, H.C. Mahler, E. Schwarb, I.E. Zarraga, and R. Mueller, Rheological characterization and injection forces of concentrated protein formulations: An alternative predictive model for non-Newtonian solutions, Eur. J. Pharm. Biopharm. 87 (2014) 318-328.

11. F. Cilurzo, F. Selmin, P. Minghetti, M. Adami, E. Bertoni, S. Lauria, L. Montanari, Injectability evaluation: an open issue, AAPS Pharm. Sci. Tech., 12 (2011) 604-609.

12. L. Liu, W. Qi, D.K. Schwartz, T.W. Randolph, J.F. Carpenter, The effects of excipients on protein aggregation during agitation: an interfacial shear rheology study, J. Pharm. Sci., 102 (2013) 2460-70

13. J. Liu, M.D. Nguyen, J.D. Andya, S.J. Shire, Reversible self-association increases the viscosity of a concentrated monoclonal antibody in aqueous solution, J Pharm Sci, 94 (2005) 1928-1940.

14. W.G. Lilyestrom, S. Yadav, S.J. Shire, T.M. Scherer, Monoclonal Antibody Self-Association, Cluster Formation, and Rheology at High Concentrations, J Phys Chem B, 117 (2013) 6373-6384.

15. S. Yadav, T.M. Laue, D.S. Kalonia, S.N. Singh, S.J. Shire, The influence of charge distribution on self-association and viscosity behavior of monoclonal antibody solutions, Mol Pharm, 9 (2012) 791-802.

16. A. Chaudhri, I.E. Zarraga, T.J. Kamerzell, J.P. Brandt, T.W. Patapoff, S.J. Shire, G.A. Voth, Coarse-Grained Modeling of the Self-Association of Therapeutic Monoclonal Antibodies, J Phys Chem B, (2012).

17. A. Chaudhri, I.E. Zarraga, S. Yadav, T.W. Patapoff, S.J. Shire, G.A. Voth, The role of amino acid sequence in the self-association of therapeutic monoclonal antibodies: insights from coarse-grained modeling, J Phys Chem B, 117 (2013) 1269-1279.

18. T.M. Scherer, J. Liu, S.J. Shire, A.P. Minton, Intermolecular interactions of IgG_1 monoclonal antibodies at high concentrations characterized by light scattering, J Phys Chem B, 114 (2010) 12948-12957.

19. M.T. Hernandez, J. Pellicer, J. Delegido, M. Dolz, Rheological characterization of easy-to-disperse (ETD) Carbopol hydrogels, J Disper Sci Technol, 19 (1998) 31-42.

20. A.Y. Bai Xu, Mitchell A. Winnik, Kayvan Sadeghy-Dalivand, David F. James, Richard Jenkins, David Bassett, Viscoelastic Properties in Water of Comb Associative Polymers Based On Poly(ethylene oxide), Langmuir, 13 (1997) 6903-6911.

Conclusions

The demand for highly concentrated protein concentrations for sc administration is still increasing due to patient convenience offering the possibility for home treatment. The development of concentrated formulations exceeding 50 – 100 mg/mL includes several challenges like solution viscosity. Viscosity of concentrated protein solutions is governed by multiple factors including but not limited to formulation composition, temperature, and formulation pH, and increases in an exponential fashion with higher protein concentration. The increase in viscosity leads to an increase in pressure needed to manufacture the product and to an increase of the force which is required by the patient or healthcare professional to administer the product. Thereby, high shear rates exceeding 10^5 s^{-1} may occur during processing, especially during filtration, and injection dependent on the flow rate, which significantly influence the rheological behavior of the protein solution.

The present work investigated the rheological behavior of protein solutions at high protein concentrations. The detailed investigation of two hydrodynamic processes considered critical with regard to increased viscosity, which were filtration and drug administration by injection, showed that the potential limitation defined by the proportional increase in pressure based on Newtonian flow behavior was overestimated due to the presence of shear-thinning behavior, which was shown for highly concentrated protein formulations.

In the first study, the current work has provided a detailed overview on highly concentrated marketed product characteristics including formulation properties like viscosity, physico-chemical properties, as well as injection device properties. This study showed that the benchmark for maximum protein concentration and viscosity was a commercial protein therapeutic with a protein concentration of 200 mg/mL and a viscosity of 102 mPas (20°C) being administered using an injection device/pre-filled syringe with a 25 G needle.

In the second study, a high-throughput method was established providing an automated, time-saving, and low-volume method for measuring dynamic viscosity of protein solutions. This method was discussed in context of advantages and limitations of different methods for viscosity determination used during pharmaceutical development of protein formulations.

Based on these two initial studies, the present work has investigated and characterized in detail the subcutaneous drug administration process of highly concentrated protein formulations and provided quantitative *in vitro* and *in vivo* data (Göttingen minipigs) of injection forces. An *in silico* model to predict injection forces was established depending on syringe and needle dimensions, solution viscosity, and injection rate and extended for shear thinning behavior (non-Newtonian flow behavior). The needle inner diameter was shown to have major influence on injection forces. It is related to injection forces by the power of four compared to other parameters, like viscosity, and injection rate being directly proportional. The study demonstrated that lower effective injection forces were obtained for highly concentrated protein solutions due to shear-thinning behavior than expected from current literature models.

To address the *in vivo* situation, the contribution of the subcutaneous tissue backpressure was quantified and specifically the additional influence of the body temperature on injection forces was reported. Both were found to be significant and linear dependent on viscosity and injection rate. The quantitative amount of the contribution of sc tissue backpressure to injection forces ranged in average from 0.6 to 4.7 N (1 – 20 mPas, 0.025 – 0.2 mL/s) with a maximum value of 12.9 N (20 mPas, 0.2 mL/s). However, the

positive contribution of the sc backpressure and the negative contribution of the local temperature effect were described to compensate each other to some extent dependent on viscosity and injection rate, as outlined.

Correct prediction of injection forces is of utmost importance, especially when intended for use by patients who are limited in their dexterity/flexibility. These are e.g. rheumatoid arthritis patients. Although the needle inner diameter was shown to have the major influence on injection forces as outlined, the final limiting parameter for the injection process is still given by the user capability of the patient population.

Overall, an extended model to predict injection forces representative for the *in vivo* situation was developed, which addresses the injection force as a function of viscosity, volumetric flow/injection rate, needle/device dimensions, shear-thinning behavior, sc backpressure, and body temperature. This knowledge is of key importance for the development of injection devices for combination products (e.g. autoinjectors or pre-filled syringes), which requires a detailed understanding of injection forces dependent on device dimensions like needle diameter and formulation properties like viscosity. This knowledge may be used for the definition of limits as well as for testing of device robustness and design during the evaluation, planning, and design phase of the development of injection devices.

Besides drug administration, filtration was investigated as the second critical hydrodynamic process for highly concentrated protein formulations, dependent on formulation composition and filter material. Similar to the drug administration process by injection, shear thinning behavior was found for some of the products during the filtration process depending on viscosity and protein concentration, formulation composition, and shear rate. The data demonstrate that the potential limitation defined by the proportional increase in pressure based on Newtonian flow behavior was overestimated for highly concentrated protein formulations. The stability behavior of mAb formulations was tested in previous studies at shear rates up to $250\,000\,\mathrm{s}^{-1}$ and protein concentrations of up to $100\,\mathrm{mg/mL}$. The study showed that high shear was not critical for final product quality. More important causes of aggregation were suggested to be the presence of air-bubbles, adsorption to solid surfaces, or contamination by particulates. However, the stability of a formulation showing pronounced shear-thinning behavior at high shear rates, which will most likely only be the case for higher protein concentrations than previously tested, needs further experiments.

The present work provided a deeper insight into the filtration and injection processes of highly concentrated mAb formulations. Still, open questions arose during the different studies. These questions need further investigation as outlined in the 'Discussion's' section in detail and will be summarized in the following. This includes at a first place the investigation of the molecular mechanism of shear thinning behavior based on the hypothesis of alignment of mAb clusters to the applied flow field. Information on the structure on a molecular level and on interaction potentials between two molecules can be obtained by using small-angle neutron scattering. Characterization of shear-thinning, non-Newtonian behavior may be obtained by extension and further optimization of the established viscosity method using CE instrumentation for higher shear rates. Although the stability behavior of mAb formulations under high shear was tested in previous studies showing to be not critical for final product quality, the stability of a formulation showing pronounced shear-thinning behavior at high shear rates, which will most likely only be the case for higher protein concentrations than previously tested (up to $100\,\mathrm{mg/mL}$), needs further investigation.

Confirmational studies in humans would be valuable to verify if our *in vivo* data from minipigs are

representative with regard to sc backpressure and influence of body temperature on injection forces. However, ethical concerns might be given. Moreover, investigation of *ex vivo* testing would be beneficial to obtain an understanding if and how *ex vivo* and *in vivo* testing (minipig) relate to each other depending on tissue material used. This would provide a potential rational on substitution of *in vivo* experiments by *ex vivo* testing.

The present studies targeting *in vivo* injection forces used injection volumes up to 4.5 mL showing no difference in injection forces compared to smaller injection volumes tested (2.5 mL). Therefore, higher injection volumes >4.5 mL will have to be evaluated for sc drug administration to investigate the impact on sc backpressure and especially if there is a threshold in injection volume, which leads to a rapid increase in injection forces from the initial injection force plateau. Last but not least, the influence of the contribution of devices to injection forces requires further experiments. As an example, testing of the impact of an artificial pressure on the skin before injection, which is needed for activation of most autoinjectors prior to injection to remove the needle shield, would be valuable.

Reference Summary

1. Adler, M., Challenges in the Development of Pre-filled Syringes for Biologics from a Formulation Scientists Point of View, Am Pharm Rev, (01. February, 2012).

2. Allahham, A., Stewart, P., Marriott, J., Mainwaring, D.E., Flow and injection characteristics of pharmaceutical parenteral formulations using a micro-capillary rheometer, Int J Pharm, 270 (2004) 139-148.

3. Allmendinger, A., Dieu, L.-H., Fischer, S., Mueller, R., Mahler, H.-C., Huwyler, J., High-throughput viscosity measurement using capillary electrophoresis instrumentation and its application to protein formulations, J Pharm Biomed Anal, 99 (2014) 51-58.

4. Allmendinger, A., Fischer, S., Huwyler, J., Mahler, H.-C., Schwarb, E., Zarraga, I.E., Mueller, R., Rheological characterization and injection forces of concentrated protein formulations: An alternative predictive model for non-Newtonian solutions, Eu J Pharm Biopharm, 87 (2014) 318-328.

5. Bai Xu, A.Y., Mitchell A. Winnik, Kayvan Sadeghy-Dalivand, David F. James, Richard Jenkins, David Bassett, Viscoelastic Properties in Water of Comb Associative Polymers Based On Poly(ethylene oxide), Langmuir, 13 (1997) 6903-6911.

6. Bam, N.B., Cleland, J.L., Yang, J., Manning, M.C., Carpenter, J.F., Kelley, R.F., Randolph, T.W., Tween protects recombinant human growth hormone against agitation-induced damage via hydrophobic interactions, J Pharm Sci, 87 (1998) 1554-1559.

7. Bauer, K., Kapitel 9 Parenteralia, in: Lehrbuch der pharmazeutischen Technologie, Wissenschaftliche Verlagsgesellschaft mbH, Stuttgart (2006).

8. Bello, M.S., Rezzonico, R., Righetti, P.G., Capillary Electrophoresis Instrumentation as a Bench-Top Viscometer, J Chromatogr A, 659 (1994) 199-204.

9. Berteau, C., Schwarzenbach, F., Donazzolo, Y., Latreille, M., Berube, J., Abry, H., Cotten, J., Feger, C., Laurent, P.E., Evaluation of performance, safety, subject acceptance, and compliance of a disposable autoinjector for subcutaneous injections in healthy volunteers, Patient Prefer Adherence, 4 (2010) 379-388.

10. Bittner, B., Richter, W.F., Hourcade-Potelleret, F., McIntyre, C., Herting, F., Zepeda, M.L., Schmidt, J., Development of a subcutaneous formulation for trastuzumab - nonclinical and clinical bridging approach to the approved intravenous dosing regimen, Arzneimittelforschung, 62 (2012) 401-409.

11. Blackwell, H.R., Contrast thresholds of the human eye, J Opt Soc Am, 36 (1946) 624-643.

12. Bode, G., Clausing, P., Gervais, F., Loegsted, J., Luft, J., Nogues, V., Sims, J., The utility of the minipig as an animal model in regulatory toxicology, J Pharmacol Toxicol Methods, 62 (2010) 196-220.

13. Bookbinder, L.H., Hofer, A., Haller, M.F., Zepeda, M.L., Keller, A., Lim, J.E., Edgington, T.S., Shepard, H.M., Patton, J.S., Frost, G.I., A recombinant human enzyme for enhanced interstitial transport of therapeutics, J Control Release, 114 (2006) 230-241.

14. Brazeau, G.A., Cooper, B., Svetic, K.A., Smith, C.L., Gupta, P., Current perspectives on pain upon injection of drugs, J Pharm Sci, 87 (1998) 667-677.

15. Burckbuchler, V., Mekhloufi, G., Giteau, A.P., Grossiord, J.L., Huille, S., Agnely, F., Rheological and syringeability properties of highly concentrated human polyclonal immunoglobulin solutions, Eu J Pharm Biopharm, 76 (2010) 351-356.

16. Buttel, I.C., Chamberlain, P., Chowers, Y., Ehmann, F., Greinacher, A., Jefferis, R., Kramer, D., Kropshofer, H., Lloyd, P., Lubiniecki, A., Krause, R., Mire-Sluis, A., Platts-Mills, T., Ragheb, J.A., Reipert, B.M., Schellekens, H., Seitz, R., Stas, P., Subramanyam, M., Thorpe, R., Trouvin, J.H., Weise, M., Windisch, J., Schneider, C.K., Taking immunogenicity assessment of therapeutic proteins to the next level, Biologicals, 39 (2011) 100-109.

17. Byron Bird, R., Carreau, P.J., A nonlinear viscoelastic model for polymer solutions and melts, Chem Eng Sci, 23 (1968) 427-434.

18. Cannon, M.R., Manning, R.E., Bell, J.D., The kinetic energy correction and a new viscometer, Anal Chem, 32 (1960) 355358.

19. Cavadas, A.S., Pinho, F.T., Campos, J.B.L.M., Laminar non-Newtonian impinging jet flow confined by sloping plane walls, J Non-Newton Fluid, 169 (2012) 1-14.

20. Chang, B.S., Kendrick, B.S., Carpenter, J.F., Surface-induced denaturation of proteins during freezing and its inhibition by surfactants, J Pharm Sci, 85 (1996) 1325-1330.

21. Chapman, A.J.S., Goodall, D.M., A novel approach to measurement of hydrodynamic radius for a standard protein using UV area imaging detection, Chromatography Today, (21. October, 2009).

22. Chari, R., Jerath, K., Badkar, A.V., Kalonia, D.S., Long- and Short-Range Electrostatic Interactions Affect the Rheology of Highly Concentrated Antibody Solutions, Pharm Res, 26 (2009) 2607-2618.

23. Chaudhri, A., Zarraga, I.E., Kamerzell, T.J., Brandt, J.P., Patapoff, T.W., Shire, S.J., Voth, G.A., Coarse-Grained Modeling of the Self-Association of Therapeutic Monoclonal Antibodies, J Phys Chem B, 116 (2012) 8045-8057.

24. Chaudhri, A., Zarraga, I.E., Yadav, S., Patapoff, T.W., Shire, S.J., Voth, G.A., The role of amino acid sequence in the self-association of therapeutic monoclonal antibodies: insights from coarse-grained modeling, J Phys Chem B, 117 (2013) 1269-1279.

25. Chou, D.K., Krishnamurthy, R., Randolph, T.W., Carpenter, J.F., Manning, M.C., Effects of Tween 20 and Tween 80 on the stability of Albutropin during agitation, J Pharm Sci, 94 (2005) 1368-1381.

26. Cianciulli, C., Hahne, T., Watzig, H., Capillary gel electrophoresis for precise protein quantitation, Electrophoresis, 33 (2012) 3276-3280.

27. Cilurzo, F., Selmin, F., Minghetti, P., Adami, M., Bertoni, E., Lauria, S., Montanari, L., Injectability evaluation: an open issue, AAPS Pharm Sci Tech, 12 (2011) 604-609.

28. Cleland, J.L., Powell, M.F., Shire, S.J., The Development of Stable Protein Formulations - a Close Look at Protein Aggregation, Deamidation, and Oxidation, Crit Rev Ther Drug, 10 (1993) 307-377.

29. Cross, M.M., Relation between Viscoelasticity and Shear-Thinning Behavior in Liquids, Rheol Acta, 18 (1979) 609-614.

30. Curtis, R.A., Prausnitz, J.M., Blanch, H.W., Protein-protein and protein-salt interactions in aqueous protein solutions containing concentrated electrolytes, Biotechnol Bioeng, 57 (1998) 11-21.

31. De Waele, A., Viscometry and plastometry, Oil and Color Chem Assoc J, (1923).

32. Demoruelle, K., Guo, B., Kao, S., McDonald, H.M., Nikic, D.B., Holman, S.C., Wilson, W.W., Correlation between the osmotic second virial coefficient and solubility for equine serum albumin and ovalbumin, Acta Crystallogr D Biol Crystallogr, 58 (2002) 1544-1548.

33. Dickinson, E., Proteins at interfaces and in emulsions - Stability, rheology and interactions, J Chem Soc Faraday T, 94 (1998) 1657-1669.

34. Du, W., Klibanov, A.M., Hydrophobic salts markedly diminish viscosity of concentrated protein solutions, Biotechnol Bioeng, 108 (2011) 632-636.

35. Eisenschitz, R., Rabinowitsch B., Weissenberg, K., Mitteilung der deutschen Materialprüfungsanstalten, Sonderheft 8 (1929) 91.

36. EliTechGroup, Vapro 5600: Vapor Pressure Osmometer, http://www.wescor.com/biomedical/osmometer/vapro5600.html (15. August, 2011).

37. EMA/CHMP/20857/2009, European Medicines Agency Press office: PRESS RELEASE: European Medicines Agency recommends suspension of the marketing authorisation of Raptiva (efalizumab) (19. February, 2009).

38. European Commission, http://ec.europa.eu/health/documents/community-register/html/, European Commission, (25. August, 2011).

39. Fradkin, A.H., Carpenter, J.F., Randolph, T.W., Immunogenicity of Aggregates of Recombinant Human Growth Hormone in Mouse Models, J Pharm Sci, 98 (2009) 3247-3264.

40. Francois, Y., Zhang, K., Varenne, A., Gareil, P., New integrated measurement protocol using capillary electrophoresis instrumentation for the determination of viscosity, conductivity and absorbance of ionic liquid-molecular solvent mixtures, Anal Chim Acta, 562 (2006) 164-170.

41. Frost, G.I., Recombinant human hyaluronidase (rHuPH20): an enabling platform for subcutaneous drug and fluid administration, Expert Opin Drug Deliv, 4 (2007) 427-440.

42. Ganderup, N.C., Harvey, W., Mortensen, J.T., Harrouk, W., The minipig as nonrodent species in toxicology-where are we now?, Int J Toxicol, 31 (2012) 507-528.

43. Gatlin, L.A., Gatlin, C.B., Formulation and administration techniques to minimize injection pain and tissue damage associated with parenteral products, in: P.K. Gapta, G.A. Brazeau (Eds.) Injectable drug development - Techniques to reduce pain and irritation, Interpharm Press, Denver, Colorado (1999) 401-421.

44. Ge, J.A., Thummala, A., Wadhwa, M.V.S., Applications of Statistical Regression and Modeling in Fill-Finish Process Development of Structurally Related Proteins, J Pharm Sci, 100 (2011) 464-481.

45. Gesellschaft für Versuchstierkunde: Auschuss fr Ernährung der Versuchstiere - Minipig, http://www.gv-solas.de (07. April 2014), 1999.

46. Granolleras, C., Leskopf, W., Shaldon, S., Fourcade, J., Experience of Pain after Subcutaneous Administration of Different Preparations of Recombinant-Human-Erythropoietin - a Randomized, Double-Blind Crossover Study, Clin Nephrol, 36 (1991) 294-298.

47. Grupi, A., Minton, A.P., Capillary viscometer for fully automated measurement of the concentration and shear dependence of the viscosity of macromolecular solutions, Anal Chem, 84 (2012) 10732-10736.

48. Guo, Z., Chen, A., Nassar, R.A., Helk, B., Mueller, C., Tang, Y., Gupta, K., Klibanov, A.M., Structure-Activity Relationship for Hydrophobic Salts as Viscosity-Lowering Excipients for Concentrated Solutions of Monoclonal Antibodies, Pharm Res, 29 (2012) 3102-3109.

49. Hagen, G.H.L., Über die Bewegung des Wassers in engen zylindrischen Röhren., Poggendorfs Annalen der Physik und Chemie, 46 (1939) 423442.

50. Hamizi, S., Freyer, G., Bakrin, N., Henin, E., Mohtaram, A., Le Saux, O., Falandry, C., Subcutaneous trastuzumab: development of a new formulation for treatment of HER2-positive early breast cancer, Onco Targets Ther, 6 (2013) 89-94.

51. Han, Z., Tang, X., Zheng, B., A PDMS viscometer for microliter Newtonian fluid, J Micromech Microeng, 17 (2007) 1828-1834.

52. Harding, S.E., Rowe, A.J., Insight into protein-protein interactions from analytical ultracentrifugation, Biochem Soc T, 38 (2010) 901-907.

53. Harris, R.J., Shire, S.J., Winter, C., Commercial manufacturing scale formulation and analytical characterization of therapeutic recombinant antibodies, Drug Develop Res, 61 (2004) 137-154.

54. He, F., Becker, G.W., Litowski, J.R., Narhi, L.O., Brems, D.N., Razinkov, V.I., High-throughput dynamic light scattering method for measuring viscosity of concentrated protein solutions, Anal Biochem, 399 (2010) 141-143.

55. Henning, A., Neumann, D., Kostka, K.H., Lehr, C.M., Schaefer, U.F., Influence of human skin specimens consisting of different skin layers on the result of in vitro permeation experiments, Skin Pharmacol Phys, 21 (2008) 81-88.

56. Hermeling, S., Crommelin, D., Schellekens, H., Jiskoot, W., Structure-Immunogenicity Relationships of Therapeutic Proteins, Pharm Res, 21 (2004) 897-903.

57. Hernandez, M.T., Pellicer, J., Delegido, J., Dolz, M., Rheological characterization of easy-to-disperse (ETD) Carbopol hydrogels, J Disper Sci Technol, 19 (1998) 31-42.

58. Hieber, C.A., Chiang, H.H., Shear-Rate-Dependence Modeling of Polymer Melt Viscosity, Polym Eng Sci, 32 (1992) 931-938.

59. Hill, T.L., Theory of Solutions., J Am Chem Soc, 79 (1957) 4885-4890.

60. Hiller, A., Fast Growth Foreseen for Protein Therapeutics, BioMarket Trends, 29 (2009) 153-155.

61. Husmann, M.J., Barton, M., Amann-Vesti, B.R., Franzeck, U.K., Postural effects on interstitial fluid pressure in humans, J Vasc Res, 43 (2006) 321-326.

62. Jaber, A., Bozzato, G.B., Vedrine, L., Prais, W.A., Berube, J., Laurent, P.E., A novel needle for subcutaneous injection of interferon beta-1a: effect on pain in volunteers and satisfaction in patients with multiple sclerosis, Bmc Neurol, 8 (2008).

63. Jezek, J., Rides, M., Derham, B., Moore, J., Cerasoli, E., Simler, R., Perez-Ramirez, B., Viscosity of concentrated therapeutic protein compositions, Adv Drug Deliv Rev, 63 (2011) 1107-1117.

64. Jochims, K., Kemkowski, J., Nolte, T., Bartels, T., Heusener, A., Local tolerance testing of parenteral drugs: how to put into practice, Regul Toxicol Pharm, 38 (2003) 166-182.

65. Kanai, S., Liu, J., Patapoff, T.W., Shire, S.J., Reversible self-association of a concentrated monoclonal antibody solution mediated by Fab-Fab interaction that impacts solution viscosity, J Pharm Sci, 97 (2008) 4219-4227.

66. Katakam, M., Bell, L.N., Banga, A.K., Effect of surfactants on the physical stability of recombinant human growth hormone, J Pharm Sci, 84 (1995) 713-716.

67. Kerwin, B.A., Polysorbates 20 and 80 used in the formulation of protein biotherapeutics: Structure and degradation pathways, J Pharm Sci, 97 (2008) 2924-2935.

68. Kerwin, B.A., Heller, M.C., Levin, S.H., Randolph, T.W., Effects of Tween 80 and sucrose on acute short-term stability and long-term storage at -20 degrees C of a recombinant hemoglobin, J Pharm Sci, 87 (1998) 1062-1068.

69. Kiese, S., Papppenberger, A., Friess, W., Mahler, H.-C., Shaken, not stirred: mechanical stress testing of an IgG1 antibody, J Pharm Sci, 97 (2008) 4347-4366.

70. Kivitz, A., Segurado, O.G., HUMIRA pen: a novel autoinjection device for subcutaneous injection of the fully human monoclonal antibody adalimumab, Expert Rev Med Devices, 4 (2007) 109-116.

71. Klement, W., Arndt, J.O., Pain on Iv Injection of Some Anesthetic Agents Is Evoked by the Unphysiological Osmolality or Ph of Their Formulations, Brit J Anaesth, 66 (1991) 189-195.

72. Laue, T., Proximity energies: a framework for understanding concentrated solutions, J Mol Recognit, 25 (2012) 165-173.

73. Lee, J., Tripathi, A., Intrinsic viscosity of polymers and biopolymers measured by microchip, Anal Chem, 77 (2005) 7137-7147.

74. Lehermayr, C., Mahler, H.-C., Mader, K., Fischer, S., Assessment of net charge and protein-protein interactions of different monoclonal antibodies, J Pharm Sci, 100 (2011) 2551-2562.

75. Lewandrowska, A., Majcher, A., Ochab-Marcinek, A., Tabaka, M., Holyst, R., Taylor Dispersion Analysis in Coiled Capillaries at High Flow Rates, Anal Chem, 85 (2013) 4051-4056.

76. Lilyestrom, W.G., Yadav, S., Shire, S.J., Scherer, T.M., Monoclonal Antibody Self-Association, Cluster Formation, and Rheology at High Concentrations, J Phys Chem B, 117 (2013) 6373-6384.

77. Liu, J., Nguyen, M.D., Andya, J.D., Shire, S.J., Reversible self-association increases the viscosity of a concentrated monoclonal antibody in aqueous solution, J Pharm Sci, 94 (2005) 1928-1940.

78. Liu, J., Shire, S.J., Patent: Reduced-viscosity concentrated protein formulations, WO 2002030463 A2 (2002).

79. Liu, L., Qi, W., Schwartz, D.K., Randolph, T.W., Carpenter, J.F., The effects of excipients on protein aggregation during agitation: an interfacial shear rheology study, J Pharm Sci, 102 (2013) 2460-70

80. Liu, Y., Fratini, E., Baglioni, P., Chen, W.R., Chen, S.H., Effective long-range attraction between protein molecules in solutions studied by small angle neutron scattering, Phys Rev Lett, 95 (2005) 118102.

81. Loveday, S.M., Creamer, L.K., Singh, H., Rao, M.A., Phase and rheological behavior of high-concentration colloidal hard-sphere and protein dispersions, J Food Sci, 72 (2007) R101-107.

82. Mach, H., Arvinte, T., Addressing new analytical challenges in protein formulation development, Eu J Pharm Biopharm, 78 (2011) 196-207.

83. Macosko, C.W., Rheology: principles, measurements, and applications, 1st ed., Wiley-VCH, New York (1994).

84. Mahler, H.-C., Muller, R., Friess, W., Delille, A., Matheus, S., Induction and analysis of aggregates in a liquid IgG$_1$-antibody formulation, Eu J Pharm Biopharm, 59 (2005) 407-417.

85. Mahler, H.-C., Friess, W., Grauschopf, U., Kiese, S., Protein Aggregation: Pathways, Induction Factors and Analysis, J Pharm Sci, 98 (2009) 2909-2934.

86. Mahler, H.-C., Huber, F., Kishore, R.S., Reindl, J., Ruckert, P., Muller, R., Adsorption behavior of a surfactant and a monoclonal antibody to sterilizing-grade filters, J Pharm Sci, 99 (2010) 2620-2627.

87. Malescio, G., Intermolecular potentials-past, present, future, Nat Mater, 2 (2003) 501-503.

88. Manning, M.C., Chou, D.K., Murphy, B.M., Payne, R.W., Katayama, D.S., Stability of protein pharmaceuticals: an update, Pharm Res, 27 (2010) 544-575.

89. McDonald, T.A., Zepeda, M.L., Tomlinson, M.J., Bee, W.H., Ivens, I.A., Subcutaneous administration of biotherapeutics: current experience in animal models, Curr Opin Mol Ther, 12 (2010) 461-470.

90. McMillan Jr., W.G.M., Joseph E. , The Statistical Thermodynamics of Multicomponent Systems J Chem Phys, 13 (1945) 276-305.

91. McMinn, R.M.H., Lasts Anatomy: Regional and applied, 9th ed., Churchill Livingstone, London (1994).

92. Mehl, J.W., Oncley, J.L., Simha, R., Viscosity and the Shape of Protein Molecules, Science, 92 (1940) 132-133.

93. Meltzer, T.J., The sterilizing filter and its pore size rating, American Pharm Rev, 10 (2003) 44-52.

94. Mezger, T.G., Das Rheologie Handbuch, 3rd ed., Vincentz Network, Hannover (2010).

95. Minton, A.P., Influence of excluded volume upon macromolecular structure and associations in 'crowded' media, Curr Opin Biotechnol, 8 (1997) 65-69.

96. Minton, A.P., Macromolecular crowding, Curr Biol, 16 (2006) R269-271.

97. Mirrashed, F., Sharp, J.C., Krause, V., Morgan, J., Tomanek, B., Pilot study of dermal and subcutaneous fat structures by MRI in individuals who differ in gender, BMI, and cellulite grading, Skin Res Technol, 10 (2004) 161-168.

98. Monkos, K., Concentration and temperature dependence of viscosity in lysozyme aqueous solutions, Biochim Biophys Acta, 1339 (1997) 304-310.

99. Monkos, K., On the hydrodynamics and temperature dependence of the solution conformation of human serum albumin from viscometry approach, Bba-Proteins Proteom, 1700 (2004) 27-34.

100. Monkos, K., Viscosity analysis of the temperature dependence of the solution conformation of ovalbumin, Biophys Chem, 85 (2000) 7-16.

101. Monkos, K., Viscosity of bovine serum albumin aqueous solutions as a function of temperature and concentration, Int J Biol Macromol, 18 (1996) 61-68.

102. Monkos, K., Turczynski, B., A comparative study on viscosity of human, bovine and pig IgG immunoglobulins in aqueous solutions, Int J Biol Macromol, 26 (1999) 155-159.

103. Moon, Y.U., Anderson, C.O., Blanch, H.W., Prausnitz, J.M., Osmotic pressures and second virial coefficients for aqueous saline solutions of lysozyme, Fluid Phase Equilibr, 168 (2000) 229-239.

104. Mooney, M., The viscosity of a concentrated suspension of spherical particles, J Colloid Sci, 6 (1951) 162-170.

105. Mortensen, J.T., Brinck, P., Lichtenberg, J., The minipig in dermal toxicology. A literature review., Scand J Lab Anim Sci, 25 (1998) 77-83.

106. Mueller, R., Characterization of a High Concentration Antibody Formulation: Protein Stability and Formulation Properties., Academic Ph.D. Thesis, University of Halle-Wittenberg (2011).

107. Narayanan, J., Liu, X.Y., Protein interactions in undersaturated and supersaturated solutions: A study using light and x-ray scattering, Biophys J, 84 (2003) 523-532.

108. Nema, S., Brendel, R.J., Excipients and their role in approved injectable products: current usage and future directions, PDA J Pharm Sci Technol, 65 (2011) 287-332.

109. Nema, S., Washkuhn, R.J., Brendel, R.J., Excipients and their use in injectable products, PDA J Pharm Sci Technol, 51 (1997) 166-171.

110. Nony, P., Girard, P., Chabaud, S., Hessel, L., Thebault, C., Boissel, J.P., Impact of osmolality on burning sensations during and immediately after intramuscular injection of 0.5 ml of vaccine suspensions in healthy adults, Vaccine, 19 (2001) 3645-3651.

111. Olszewski, W.L., Jain, P., Ambujam, G., Zaleska, M., Cakala, M., Gradalski, T., Tissue fluid pressure and flow during pneumatic compression in lymphedema of lower limbs, Lymphat Res Biol, 9 (2011) 77-83.

112. Ostwald, F.W., Über die Geschwindigkeits-Funktion der Viskosität in dispersen Systemen., Kolloid Z, 36 (1925).

113. Ostwald, W.s., Grundriss der allgemeinen Chemie Engelmann, Leipzig (1899).

114. Ostwald, W.s., Lehrbuch der allgemeinen Chemie, Steinkopff, Leipzig (1891).

115. Overcashier, D.E., Chan, E.K., Hsu, C.C., Technical considerations in the development of prefilled syringes for protein products, Am Pharm Rev, 9 (2004) 77-83.

116. Patel, A.R., Kerwin, B.A., Kanapuram, S.R., Viscoelastic Characterization of High Concentration Antibody Formulations Using Quartz Crystal Microbalance with Dissipation Monitoring, J Pharm Sci, 98 (2009) 3108-3116.

117. Patro, S.Y., Freund, E., Chang, B.S., Protein formulation and fill-finish operations, Biotechnol Annu Rev, 8 (2002) 55-84.

118. Patro, S.Y., Przybycien, T.M., Self-interaction chromatography: A tool for the study of protein-protein interactions in bioprocessing environments, Biotechnol Bioeng, 52 (1996) 193-203.

119. Ph.Eur., 2.2.1. Clarity and degree of opalescence of liquids, in: European Pharmacopoeia 7th edition 2012 (7.3), European Directorate for the Quality of Medicines Healthcare of the Council of Europe, (2012).

120. Ph.Eur., 2.2.2. Degree of coloration of liquids, in: European Pharmacopoeia 7th edition 2012 (7.3), European Directorate for the Quality of Medicines Healthcare of the Council of Europe, (2012).

121. Ph.Eur., 2.2.35. Osmolality, in: European Pharmacopoeia 7th edition 2012 (7.3), European Directorate for the Quality of Medicines Healthcare of the Council of Europe, (2012).

122. Ph.Eur., 2.9.17. Test for extractable volume of parenteral preparations, in: European Pharmacopoeia 7th edition 2012 (7.3), European Directorate for the Quality of Medicines Healthcare of the Council of Europe, (2012).

123. Ph.Eur., 2.9.19. Particulate Contamination: Sub-visible particles, in: European Pharmacopoeia 7th edition 2012 (7.3), European Directorate for the Quality of Medicines Healthcare of the Council of Europe, (2012).

124. Ph.Eur., 2.9.20. Particulate contamination: Visible particles, in: European Pharmacopoeia 7th edition 2012 (7.3), European Directorate for the Quality of Medicine (EDQM), (2012).

125. Ph.Eur., Monograph of Monoclonal antibodies for human use, in: European Pharmacopoeia 7th edition 2012 (7.3), European Directorate for the Quality of Medicines Healthcare of the Council of Europe, (2012).

126. Ph.Eur., Monograph of Parenteral preparations, in: European Pharmacopoeia 7th edition 2012 (7.3), European Directorate for the Quality of Medicines Healthcare of the Council of Europe, (2012).

127. Phan-Thien, N., Understanding viscoelasticity: Basics in Rheology, 1st ed., Springer Verlag Berlin Heidelberg, Heidelberg (2002).

128. Pipe, C.J., Majmudar, T.S., McKinley, G.H., High shear rate viscometry, Rheol Acta, 47 (2008) 621-642.

129. Pipe, C.J., McKinley, G.H., Microfluidic rheometry, Mech Res Commun, 36 (2009) 110-120.

130. Pirrello, R.D., Chen, C.T., Thomas, S.H., Initial experiences with subcutaneous recombinant human hyaluronidase, J Palliat Med, 10 (2007) 861-864.

131. Pivot, X., Gligorov, J., Muller, V., Barrett-Lee, P., Verma, S., Knoop, A., Curigliano, G., Semiglazov, V., Lopez-Vivanco, G., Jenkins, V., Scotto, N., Osborne, S., Fallowfield, L., Preference for subcutaneous or intravenous administration of trastuzumab in patients with HER2-positive early breast cancer (PrefHer): an open-label randomised study, Lancet Oncol, 14 (2013) 962-970.

132. Poiseuille, J.L.M., Recherches experimentales sur le mouvement des liquides dans les tubes de tres petits diametres, CR Acad Sci, 11 (1840) 10411048.

133. Rabinowitsch, B., Über die Viskosität und Elastizität von Solen, Z Phys Chem, 145 (1929) 1-26.

134. Randolph, T.W., Jones, L.S., Surfactant-protein interactions, Pharm Biotechnol, 13 (2002) 159-175.

135. Rathore, N., Bhasin, N., Kolhe, P., Law, R., Abdul-Fattah, A., Li, L., Ji, W.C., Murphy, K., Bench scale cleaning characterization of drug products in a fill-finish facility, Poster presentation at 234th ACS National Meeting, Boston (2007) BIOT 305.

136. Rathore, N., Pranay, P., Bernacki, J., Eu, B., Ji, W., Walls, E., Characterization of protein rheology and delivery forces for combination products, J Pharm Sci, 101 (2012) 4472-4480.

137. Rathore, N., Pranay, P., Eu, B., Ji, W., Walls, E., Variability in syringe components and its impact on functionality of delivery systems, PDA J Pharm Sci Technol, 65 (2011) 468-480.

138. Reddy, N.P., Palmieri, V., Cochran, G.V., Subcutaneous interstitial fluid pressure during external loading, Am J Physiol, 240 (1981) R327-329.

139. Research and Markets, Biopharmaceuticals - A Global Market Overview, published July 2013 (11. September 2014).

140. Research, BCC, Biologic Therapeutic Drugs: Technologies and Global Markets (2012-2017), in: Biotechnology, BCC Research, 2013.

141. Reynolds, O., An Experimental Investigation of the Circumstances Which Determine Whether the Motion of Water Shall Be Direct or Sinuous, and of the Law of Resistance in Parallel Channels., Philos Transactions, 174 (1883) 935-982.

142. Reynolds, O., On the dynamical theory of incompressible viscous fluids and the determination of the criterion, Philos Transactions, (1895).

143. Richter, W.F., Bhansali, S.G., Morris, M.E., Mechanistic determinants of biotherapeutics absorption following SC administration, AAPS Journal, 14 (2012) 559-570.

144. Ripperger, S., Goesele, W., Alt, C., Loewe, T., Filtration, 1. Fundamentals, in: Ullmann's Encyclopedia of Industrial Chemistry, Wiley-VCH Verlag GmbH Co., Weinheim (2002) 1 - 38.

145. Rose, E.H., Vistnes, L.M., Ksander, G.A., The panniculus carnosus in the domestic pig, Plast Reconstr Surg, 59 (1977) 94-97.

146. Rosenberg, A., Effects of Protein Aggregates: An Immunologic Perspective, AAPS Journal, 8 (2006) 501-508.

147. Rosen, M.J., Goldsmith, H.A., Chemical Analysis, Vol. 12, in: Systematic Analysis of Surface-Active Agents, John Wiley and Sons Inc, 2nd edition (1983).

148. Rungseevijitprapa, W., Bodmeier, R., Injectability of biodegradable in situ forming microparticle systems (ISM), J Pharm Sci, 36 (2009) 524-531.

149. Ruppert, S., Sandler, S.I., Lenhoff, A.M., Correlation between the osmotic second virial coefficient and the solubility of proteins, Biotechnol Prog, 17 (2001) 182-187.

150. Saito, S., Hasegawa, J., Kobayashi, N., Kishi, N., Uchiyama, S., Fukui, K., Behavior of Monoclonal Antibodies: Relation Between the Second Virial Coefficient (B-2) at Low Concentrations and Aggregation Propensity and Viscosity at High Concentrations, Pharm Res, 29 (2012) 397-410.

151. Salinas, B.A., Sathish, H.A., Bishop, S.M., Harn, N., Carpenter, J.F., Randolph, T.W., Understanding and Modulating Opalescence and Viscosity in a Monoclonal Antibody Formulation, J Pharm Sci, 99 (2010) 82-93.

152. Saluja, A., Badkar, A.V., Zeng, D.L., Nema, S., Kalonia, D.S., Application of high-frequency rheology measurements for analyzing protein-protein interactions in high protein concentration solutions using a model monoclonal antibody (IgG2), J Pharm Sci, 95 (2006) 1967-1983.

153. Saluja, A., Badkar, A.V., Zeng, D.L., Nema, S., Kalonia, D.S., Ultrasonic Storage Modulus as a Novel Parameter for Analyzing Protein-Protein Interactions in High Protein Concentration Solutions: Correlation with Static and Dynamic Light Scattering Measurements, Biophys J, 92 (2007) 234-244.

154. Saluja, A., Kalonia, D.S., Application of ultrasonic shear rheometer to characterize rheological properties of high protein concentration solutions at microliter volume, J Pharm Sci, 94 (2005) 1161-1168.

155. Saluja, A., Kalonia, D.S., Nature and consequences of protein-protein interactions in high protein concentration solutions, Int J Pharm, 358 (2008) 1-15.

156. Scherer, T.M., Liu, J., Shire, S.J., Minton, A.P., Intermolecular interactions of IgG1 monoclonal antibodies at high concentrations characterized by light scattering, J Phys Chem B, 114 (2010) 12948-12957.

157. Schiller, L., Drei Klassiker der Strömungslehre: Hagen, Poiseuille, Hagenbach, Akademische Verlagsgesellschaft, Leipzig (1933).

158. Scolnik, P.A., mAbs: a business perspective, MAbs, 1 (2009) 179-184.

159. Sharma, D.K., King, D., Oma, P., Merchant, C., Micro-Flow Imaging: Flow Microscopy Applied to Sub-visible Particulate Analysis in Protein Formulations, AAPS J, 12 (2010) 455-464.

160. Sheikhzadeh, A., Yoon, J., Formosa, D., Domanska, B., Morgan, D., Schiff, M., The effect of a new syringe design on the ability of rheumatoid arthritis patients to inject a biological medication, Appl Ergon, 43 (2012) 368-375.

161. Shire, S.J., Formulation and manufacturability of biologics, Curr Opin Biotech, 20 (2009) 708-714.

162. Shire, S.J., Shahrokh, Z., Liu, J., Challenges in the development of high protein concentration formulations, J Pharm Sci, 93 (2004) 1390-1402.

163. Shire, S.L., J., Friess, W., Matheus, S., Mahler, H.-C. , Considerations for high concentration antibody formulations, in: S. Hershenson, Jameel, F. (Ed.) Formulation and Process Development Strategies for Manufacturing of a Biopharmaceutical, John Wiley Sons, Hoboken, NJ (2010).

164. Shpilberg, O., Jackisch, C., Subcutaneous administration of rituximab (MabThera) and trastuzumab (Herceptin) using hyaluronidase, Br J Cancer, 109 (2013) 1556-1561.

165. Srivastava, N., Davenport, R.D., Burns, M.A., Nanoliter viscometer for analyzing blood plasma and other liquid samples, Anal Chem, 77 (2005) 383-392.

166. Stackhouse, N., Miller, A.K., Gadgil, H.S., A high-throughput UPLC method for the characterization of chemical modifications in monoclonal antibody molecules, J Pharm Sci, 100 (2011) 5115-5125.

167. Stirnimann, T., Di Maiuta, N., Gerard, D.E., Alles, R., Huwyler, J., Puchkov, M., Functionalized Calcium Carbonate as a Novel Pharmaceutical Excipient for the Preparation of Orally Dispersible Tablets, Pharm Res, 30 (2013) 1915-1925.

168. Strehl, R., Rombach-Riegraf, V., Diez, M., Egodage, K., Bluemel, M., Jeschke, M., Koulov, A.V., Discrimination Between Silicone Oil Droplets and Protein Aggregates in Biopharmaceuticals: A Novel Multiparametric Image Filter for Sub-visible Particles in Microflow Imaging Analysis, Pharm Res, 29 (2012) 594-602.

169. Sukumar, M., Doyle, B.L., Combs, J.L., Pekar, A.H., Opalescent appearance of an IgG1 antibody at high concentrations and its relationship to noncovalent association, Pharm Res, 21 (2004) 1087-1093.

170. Tessier, P.M., Lenhoff, A.M., Sandler, S.I., Rapid measurement of protein osmotic second virial coefficients by self-interaction chromatography, Biophys J, 82 (2002) 1620-1631.

171. Toledo, R.T., Chapter 6 Flow of fluids in: D.R. Heldman (Ed.) Fundamental of Food Process Engeneering, Food Science Text series, Springer ScienceBusiness Media, New York (2007) 582 p.

172. Ubbelohde, L., Das einfachste und genaueste Viskosimeter und andere Geräte mit dem hängenden Niveau, J Öl und Kohle, 12 (1936).

173. Ubbelohde, L., Zur Viskosimetrie, Hirzel, Stuttgart (1965).

174. Velev, O.D., Kaler, E.W., Lenhoff, A.M., Protein interactions in solution characterized by light and neutron scattering: comparison of lysozyme and chymotrypsinogen, Biophys J, 75 (1998) 2682-2697.

175. Veys, N., Dhondt, A., Lameire, N., Pain at the injection site of subcutaneously administered erythropoietin: phosphate-buffered epoetin alpha compared to citrate-buffered epoetin alpha and epoetin beta, Clin Nephrol, 49 (1998) 41-44.

176. Vilker, V.L., Colton, C.K., Smith, K.A., The Osmotic-Pressure of Concentrated Protein Solutions - Effect of Concentration and Ph in Saline Solutions of Bovine Serum-Albumin, J Colloid Interf Sci, 79 (1981) 548-566.

177. Vlachy, V., Prausnitz, J.M., Donnan Equilibrium - Hypernetted-Chain Study of One-Component and Multicomponent Models for Aqueous Polyelectrolyte Solutions, J Phys Chem, 96 (1992) 6465-6469.

178. Voigt, R., Kapitel 20.5.4. Isohydrische Lösungen, in: Pharmazeutische Technologie, Deutscher Apotheker Verlag, Stuttgart (2006).

179. Vosseler, M., Jugl, M., Zengerle, R., A smart interface for reliable intradermal injection and infusion of high and low viscosity solutions, Pharm Res, 28 (2011) 647-661.

180. Wacker, C., Berger, C.N., Girard, P., Meier, R., Glycosylation profiles of therapeutic antibody pharmaceuticals, Eu J Pharm Biopharm, 79 (2011) 503-507.

181. Wagstaff, I., Chaffey, C.E., Shear Thinning and Thickening Rheology - 1. Concentrated Acrylic Dispersions, J Colloid Interf Sci, 59 (1977) 53-62.

182. Walsh, G., Biopharmaceutical benchmarks 2010, Nat Biotechnol, 28 (2010) 917-924.

183. Walsh, G., Pharmaceutical biotechnology products approved within the European Union, Eu J Pharm Biopharm, 55 (2003) 3-10.

184. Wang, N., Hu, B., Ionescu, R., Mach, H., Sweeney, J., Hamm, C., Kirchmeier, M.J., Meyer, B.K., Opalescence of an IgG1 Monoclonal Antibody Formulation is Mediated by Ionic Strength and Excipients, Biopharm Int, 22 (2009) 36-47.

185. Warne, N.W., Development of high concentration protein biopharmaceuticals: the use of platform approaches in formulation development, Eu J Pharm Biopharm, 78 (2011) 208-212.

186. Weissenberg (cited by B. Rabinowitsch), K., Über die Viskosität und Elastizität von Solen, Z Phys Chem, (1929).

187. Winter, C., US Patent: Process for concentration of antibodies and therapeutic products., US20090214522 A1 (2009).

188. Winzor, D.J., Reappraisal of disparities between osmolality estimates by freezing point depression and vapor pressure deficit methods, Biophys Chem, 107 (2004) 317-323.

189. Wynne, C., Harvey, V., Schwabe, C., Waaka, D., McIntyre, C., and Bittner, B. Comparison of Subcutaneous and Intravenous Administration of Trastuzumab: A Phase I/Ib Trial in Healthy Male Volunteers and Patients With HER2-Positive Breast Cancer. J Clin Pharmacol 53 (2013) 192-201.

190. Wynne, C.J., Ellis-Pegler, R.B., Waaka, D.S., Schwabe, C., Lehle, M., Heinzmann, D., Mangat, R., Li, C., Dick, A.E., Cranshaw, N.A., Lum, B.L., Comparative pharmacokinetics of subcutaneous trastuzumab administered via handheld syringe or proprietary single-use injection device in healthy males, Cancer Chemother Pharmacol, 72 (2013) 1079-1087.

191. Xia, Y., Callaghan, P.T., Study of Shear Thinning in High Polymer-Solution Using Dynamic Nmr Microscopy, Macromolecules, 24 (1991) 4777-4786.

192. Yadav, S., Laue, T.M., Kalonia, D.S., Singh, S.N., Shire, S.J., The influence of charge distribution on self-association and viscosity behavior of monoclonal antibody solutions, Mol Pharm, 9 (2012) 791-802.

193. Yadav, S., Liu, J., Shire, S.J., Kalonia, D.S., Specific interactions in high concentration antibody solutions resulting in high viscosity, J Pharm Sci, 99 (2010) 1152-1168.

194. Yadav, S., Scherer, T.M., Shire, S.J., Kalonia, D.S., Use of dynamic light scattering to determine second virial coefficient in a semidilute concentration regime, Anal Biochem, 411 (2011) 292-296.

195. Yadav, S., Shire, S.J., Kalonia, D.S., Factors Affecting the Viscosity in High Concentration Solutions of Different Monoclonal Antibodies, J Pharm Sci, 99 (2010) 4812-4829.

196. Yadav, S., Shire, S.J., Kalonia, D.S., Viscosity Analysis of High Concentration Bovine Serum Albumin Aqueous Solutions, Pharm Res, 28 (2011) 1973-1983.

197. Yadav, S., Shire, S.J., Kalonia, D.S., Viscosity behavior of high-concentration monoclonal antibody solutions: correlation with interaction parameter and electroviscous effects, J Pharm Sci, 101 (2012) 998-1011.

198. Yearley, E.J., Zarraga, I.E., Shire, S.J., Scherer, T.M., Gokarn, Y., Wagner, N.J., Liu, Y., Small-angle neutron scattering characterization of monoclonal antibody conformations and interactions at high concentrations, Biophys J, 105 (2013) 720-731.

199. Zarraga, I.E., Taing, R., Zarzar, J., Luoma, J., Hsiung, J., Patel, A., Lim, F.J., High shear rheology and anisotropy in concentrated solutions of monoclonal antibodies, J Pharm Sci, 102 (2013) 2538-2549.

200. Zhang, F.J., Skoda, M.W.A., Jacobs, R.M.J., Martin, R.A., Martin, C.M., Schreiber, F., Protein interactions studied by SAXS: Effect of ionic strength and protein concentration for BSA in aqueous solutions, J Phys Chem B, 111 (2007) 251-259.

201. Zhang, J., Burman, S., Gunturi, S., Foley, J.P., Method development and validation of capillary sodium dodecyl sulfate gel electrophoresis for the characterization of a monoclonal antibody, J Pharm Biomed Anal, 53 (2010) 1236-1243.

202. Zhao, S.S., Chen, D.D., Applications of capillary electrophoresis in characterizing recombinant protein therapeutics, Electrophoresis, 35 (2014) 96-108.

203. Zheng, Y., Tesar, D.B., Benincosa, L., Birnbock, H., Boswell, C.A., Bumbaca, D., Cowan, K.J., Danilenko, D.M., Daugherty, A.L., Fielder, P.J., Grimm, H.P., Joshi, A., Justies, N., Kolaitis, G., Lewin-Koh, N., Li, J., McVay, S., O'Mahony, J., Otteneder, M., Pantze, M., Putnam, W.S., Qiu, Z.J., Ruppel, J., Singer, T., Stauch, O., Theil, F.P., Visich, J., Yang, J., Ying, Y., Khawli, L.A., Richter, W.F., Minipig as a potential translatable model for monoclonal antibody pharmacokinetics after intravenous and subcutaneous administration, MAbs, 4 (2012) 243-255.

204. Zhou, J.X., Qiu, J.S., Jiang, G., Zhou, C., Bingham, N., Yeung, H., Dransart, B., Wadhwa, M.V., Tressel, T., Non-specific binding and saturation of Polysorbate-20 with aseptic filter membranes for drug substance and drug product during mAb production, J Membr Sci, 325 (2008) 735-741.

Curriculum Vitae

Publication and Conferences

**CURRICULUM
VITAE**

ANDREA ALLMENDINGER

APOTHEKERIN

PERSONAL DETAILS

DATE AND
PLACE OF BIRTH

JAN 25TH 1986
LUDWIGSBURG (GERMANY)

NATIONALITY
GENDER

GERMAN
FEMALE

JULY 2014

PROFESSIONAL CAREER AND ACADEMIC EDUCATION

Since Oct 2013	**Group leader** in late-stage formulation and processing development, Hoffmann-La Roche, Basel
Since Feb 2011	**PhD student** in pharmaceutical technology at the University of Basel in cooperation with Hoffmann-La Roche, Basel (supervision: Prof. J. Huwyler)
Dec 2010	**Approbation** as a pharmacist
Nov 2010	**3rd state examination**
May 2010 − Oct 2010	**Postgraduate education** as a pharmacist at Early-stage formulation development, Hoffmann-La Roche, Basel
Oct 2009 − Apr 2010	**Postgraduate education** as a pharmacist at Hof-Apotheke Heidelberg
Oct 2005 − Oct 2009	**Pharmacy student at Ruprecht-Karls-Universität Heidelberg**, Institute of Pharmacy and Molecular Biotechnology • Oct 2009: 2nd state examination (grade 1.8) • Oct 2007: 1st state examination (grade 1.6)
Jun 2008 − Sept 2008	**ERASMUS semester at the University College of London**: Research group Dr. Deniz Tasdemir, School of Pharmacy (Pharmacognosy - Pharmaceutical and Biological Chemistry)
Mar 2006 − Oct 2009	Scholarship of the German National Academic Foundation **(Studienstiftung des Deutschen Volkes)**
Mar 2008	**Internship Research Group Prof. Dr. Mall, University Heidelberg** on chronic respiratory diseases investigated in a mouse model
Mar 2007	**Internship at Abbott Ludwigshafen (Quality control for biologics)**
Aug 2006	**Internship at Sicherer'schen Apotheke Heilbronn**
Mar 2006	**Internship at St. Vincent's Hospital in Melbourne, Australia**
1996 – 2005	A-LEVELS Justinus-Kerner-Gymansium Heilbronn (1.0; best in class)
2002 - 2005	**Young Student at the University of Music Karlsruhe** (Prof. N. Erlich, main subject violin)

PUBLICATIONS AND CONFERENCES

PUBLICATIONS

2014
(within this work)

Rheological characterization and injection forces of concentrated protein formulations: An alternative predictive model for non-Newtonian solutions.
Allmendinger A, Fischer S, Huwyler J, Mahler HC, Schwarb E, Zarraga IE, Mueller R.
Eur J Pharm Biopharm. 2014 Jul;87(2):318-28.

2014
(within this work)

High-throughput viscosity measurement using capillary electrophoresis instrumentation and its application to protein formulation
Allmendinger A, Dieu LH, Fischer S, Mueller R, Mahler HC, Huwyler J
Accepted in 2014 for publication in J Pharm Biomed Anal.

2014
(within this work)

Factors influencing sterile filtration of highly concentrated protein formulations: a closer look into formulation composition, viscosity, protein concentration, and filter material
Allmendinger A, Fischer S, Huwyler J, Mahler HC, Mueller R.
Submitted to Pharm Res, 2014.

2014
(within this work)

Measuring tissue backpressure – *in vivo* injection forces during subcutaneous injection
Allmendinger A, Mueller R, Schwarb E, Chippefield M, Huwyler J, Mahler HC, Fischer S.
Submitted to J Pharm Sci, 2014.

2013

Assessment of dual life stage antiplasmodial activity of british seaweeds.
*Spavieri J, **Allmendinger A**, Kaiser M, Itoe MA, Blunden G, Mota MM, Tasdemir D.*
Mar Drugs. 2013 Oct 22;11(10):4019-34.

2011

Antiprotozoal, antitubercular and cytotoxic potential of cyanobacterial (blue-green algal) extracts from Ireland.
*Broniatowska B, **Allmendinger A**, Kaiser M, Montamat-Sicotte D, Hingley-Wilson S, Lalvani A, Guiry M, Blunden G, Tasdemir D.*
Nat Prod Commun. 2011 May;6(5):689-94.

2010

Antiprotozoal and cytotoxic potential of British and Irish red algae
Allmendinger A, Spavieri J, Kaiser M, Guiry M, Blunden G, Tasdemir D.
Planta Medica, 2010. 76(12): p. 1296-1297.

2010

Antimycobacterial, antiprotozoal and cytotoxic potential of twenty-one brown algae (Phaeophyceae) from British and Irish waters.
*Spavieri J, **Allmendinger A**, Kaiser M, Casey R, Hingley-Wilson S, Lalvani A, Guiry MD, Blunden G, Tasdemir D.*
Phytother Res. 2010 Nov;24(11):1724-9.

2010

Antiprotozoal, antimycobacterial and cytotoxic potential of twenty-three British and Irish red algae.
Allmendinger A, Spavieri J, Kaiser M, Casey R, Hingley-Wilson S, Lalvani A, Guiry M, Blunden G, Tasdemir D.
Phytother Res. 2010 Jul;24(7):1099-103.

CONFERENCES

ORAL PRESENTATION

May 2014	**Pharma Technical Development summit Roche Europe-Genentech, Santa Cruz (California, USA)** (In vivo characterization of tissue backpressure during subcutaneous injection in *Göttingen* minipigs)
Nov 2013	**PDA Universe of Pre-filled syringes and Injection Devices, Basel** (Injection forces during subcutaneous drug administration)
Jul 2013	**National Pharmaceutical Technology-Biotechnology Meeting of Switzerland, Geneva** (Highly concentrated protein formulations: Rheological characterization and its impact on injection forces)
Jun 2013	**PhD Retreat University of Basel, Interlaken** (Injection forces during subcutaneous drug administration; 2nd price for best oral presentation)
Mar 2013	**All Scientist meeting PTDE-P Roche, Munzingen** (Rheological characterization of highly concentrated protein formulations and its impact on injection forces)

POSTER PRESENTATION

Oct 2013	**Pharma Technical Development Summit Europe, Oberstdorf**
Feb 2013, 2012, 2011	**Annual Research meeting University of Basel, Basel**
Sept 2012	**MipTec & BioValley Life Sciences Week, Basel**
Jun 2012	**APV Conference on Protein Formulation, Munich**
Apr 2012, 2014	**Meeting on Innovation and New Technologies of Roche, Basel**
Mar 2012	**8th World Meeting on Pharmaceutics, Biopharmaceutics, and Pharmaceutical Technology, Istanbul (Turkey)**
Jul 2011	**Conference on Protein stability, Breckenridge (Colorado, USA)**

POSTER TITLES:
1. Rheological behavior of a monoclonal antibody mAb1
2. Enabling the Delivery of High mAb Doses through Protein Process and Device Engineering
3. Estimation of Injection Forces of Non-Newtonian Liquids using Cone/plate Viscosity data: Theory and Experimental Verification
4. Injection forces of highly concentrated protein formulations
5. *In vivo* characterization of tissue backpressure during subcutaneous injection in Göttingen minipigs

Ich erkläre, dass ich die Dissertation 'Rheological investigation of manufacturability and injectability of highly concentrated monoclonal antibody formulations' nur mit der darin angegebenen Hilfe verfasst und bei keiner anderen Universität und keiner anderen Fakultät der Universität Basel eingereicht habe.

August 2014, Andrea Allmendinger

Prüfungsvorsitz:	Prof. Dr. Tilman Schirmer
Fakultätsvertreter/ Dissertationsleiter:	Prof. Dr. Jörg Huwyler
Korreferent:	Prof Dr. Wolfgang Friess
Externer Gutachter:	PD Dr. Hanns-Christian Mahler